LIQUID METAL FLOW IN HORIZONTAL RODS

by

LYLE CAMPBELL MACAULAY

B.A.Sc. (Met. Eng.), University of British Columbia, 1966

A THESIS SUBMITTED IN PARTIAL FULFILMENT OF

THE REQUIREMENTS FOR THE DEGREE OF

DOCTOR OF PHILOSOPHY

in the Department

of

METALLURGY

We accept this thesis as conforming to the

required standard

THE UNIVERSITY OF BRITISH COLUMBIA

June, 1972

In presenting this thesis in partial fulfilment of the requirements for an advanced degree at the University of British Columbia, I agree that the Library shall make it freely available for reference and study. I further agree that permission for extensive copying of this thesis for scholarly purposes may be granted by the Head of my Department or by his representatives. It is understood that copying or publication of this thesis for financial gain shall not be allowed without my written permission.

Department of Metallurgy

The University of British Columbia
Vancouver 8, Canada

Date July 17, 1972

ABSTRACT

Radioactive tracer techniques have been developed which allow direct in situ observation of the nature of fluid flow in liquid tin contained in a long shallow covered horizontal boat. Extensive series of experiments have been conducted in order to confirm the acceptability and accuracy of the techniques employed.

The findings of the investigation establish the dependence of flow velocity on temperature difference across the melt, average melt temperature and total melt length. The flow velocity was observed to increase linearly with the average temperature gradient between the hot and cold ends of the melt. An increase in flow velocity with increasing average melt temperature was also observed. Flow was observed to occur at very small temperature gradients. When the temperature gradient was zero at any point between the hot and cold ends of the melt, two flow cells developed. Convective mass transfer did not occur between these two cells.

Autoradiography of quenched specimens showed the flow pattern to be a laminar unicellular longitudinal flow upon which a traverse double cell flow is superimposed.

The results of the flow pattern and flow velocity experiments are compared to a modification of Batchelor's solution of thermal convection in a rectangular enclosure. In general, the agreement between the experimental results and the modified solution is good.

A separate investigation of the macrosegregation associated with casting structure controlled by forced convection is also presented.

ACKNOWLEDGEMENT

The author gratefully acknowledges the advice and encouragement given by his research director, Dr. Fred Weinberg. Thanks are also due to fellow graduate students and members of the Faculty for many helpful discussions. The assistance of the technical staff, throughout the experimental program, has been greatly appreciated.

The financial assistance provided by the National Reseach Council and an Alcan Fellowship are gratefully acknowledged.

TABLE OF CONTENTS

LIST OF FIGURES

LIST OF TABLES

PART I - THERMAL CONVECTION IN HORIZONTAL RODS OF MOLTEN TIN

1 - INTRODUCTION

During the solidification of metals, solute redistribution can lead to macro and micro segregation which in turn can markedly influence the mechanical properties of the resulting solid metal. In solidification of binary alloys the extent of mixing in the liquid metal greatly influences the solute redistribution. The two limiting cases are:

(1) Complete mixing in the liquid during solidification which results in a solute distribution given by[1]:

$$C_s = k_o C_o (1 - f)^{k_o - 1} \qquad (1.1)$$

(2) No mixing in the liquid, that is, solute transport in the liquid is by diffusion only. The resulting solute distribution in the initially solidified portion of the melt is given by[2]:

$$C_s = C_o \{(1 - k_o)[1 - \exp(-\frac{k_o\ Rx}{D})] + k_o\} \qquad (1.2)$$

where: C_o is the average composition of the starting liquid

C_s is the composition of the resulting solid

C_L is the composition of the liquid in equilibrium with solid of composition C_s

$k_o = C_s/C_L$ = equilibrium distribution coefficient.

f is the fraction solidified

R is the freezing rate

D is the diffusion coefficient for solute in the liquid

x is the distance from the start of unidirectional solidification.

In arriving at Equations (1.1) and (1.2) it was assumed that the solid-liquid interface remained planar, that no solute diffusion occurred in the solid and that equilibrium conditions existed at the interface during solidification. Figure 1 illustrates the solute redistribution that arises as a result of varying the extent of mixing in the liquid.

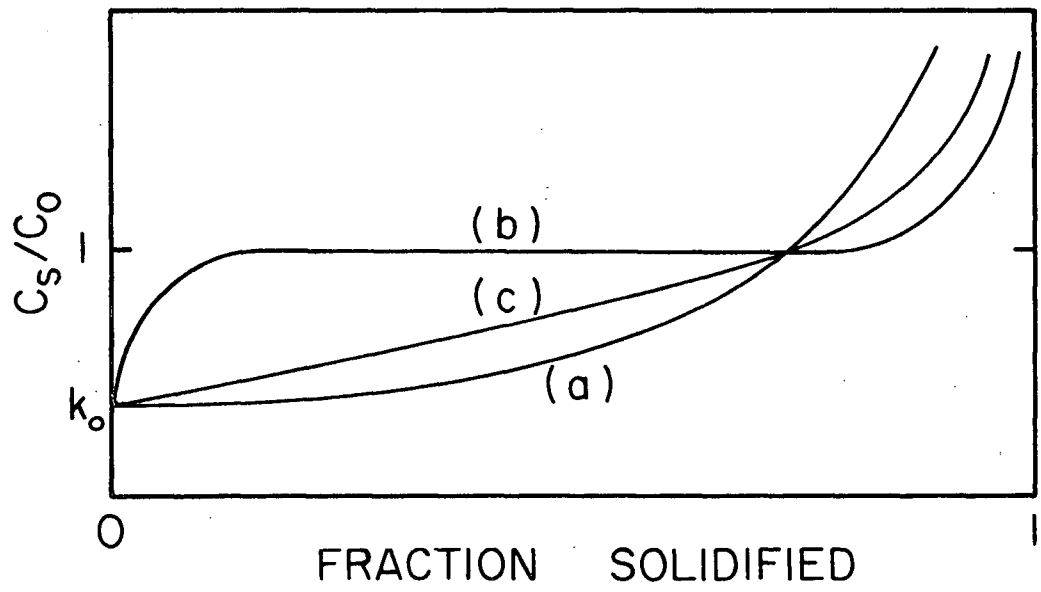

Figure 1. Segregation resulting from (a) complete mixing, (b) no mixing and (c) partial mixing in the liquid.

From Figure 1 it is apparent that complete mixing in the liquid, curve (a), causes long range compositional variations (macrosegregation) whereas no mixing, (b), yields a uniform solute distribution (except for the initial and terminal transients). The intermediate case of partial mixing, (c), can be represented by [2]:

$$C_s = k_e C_o (1 - f)^{k_o - 1} \tag{1.3}$$

where k_e, the effective distribution coefficient, is defined to be C_s/C_o and is given by[2]:

$$k_e = \frac{k_o}{k_o + (1 - k_o) \exp\left(-\frac{R\delta}{D}\right)} \tag{1.4}$$

where δ is the thickness of the diffusion boundary layer which exists at the interface. The magnitude of k_e (assuming $k_o < 1$) ranges from a minimum of k_o for complete mixing to a maximum of 1 for no mixing in the liquid. It is apparent from Equation (1.4) that an increase in δ results in an increase in k_e. The boundary layer thickness is largely dependent on the extent of liquid mixing. Maximum values of δ occur when no mixing is present and minimum values arise under conditions of extensive mixing. Thus, control of mixing in a solidifying liquid can afford control over the solute redistribution in the solidified product.

Mixing in the liquid may arise from one or more of several sources. Fluid flow may result from natural convection. This is examined in Part I of this thesis. Flow may also result from forced convection. Part II considers the solute segregation which occurs as a result of controlling ingot grain structure by forced convection.

Natural convection occurring during solidification can be divided into two main categories, solute convection and thermal convection. Solute convection may occur when concentration differences, arising from solute rejection at a solid-liquid interface, cause the appearance of density gradients in the liquid metal. Wagner[3] has studied the interaction of solute convection with the diffusion boundary layer and has developed equations to describe the resulting solute redistribution.

An evaluation of the effect of mixing in the liquid on solute distribution along unidirectionally solidified horizontal rods of dilute silver in tin alloys has been made by Weinberg[4]. He varied the fluid flow in a qualitative way by varying the diameter of the rods being solidified. Weinberg found that, based on the distribution of silver in the solidified rods, extensive mixing occurred in the liquid during solidification of all rods of diameter greater than 2mm. Suggested causes for this mixing were (a) thermal convection (b) convective currents set up by volume changes during freezing, and (c) solute convection. Evidence was presented that causes (b) and (c) were not primarily responsible for solute mixing. This conclusion led to several extensive studies on thermal convection in horizontal melts.

Thermal convection will occur when the melt is subjected to a horizontal temperature gradient. The explanation of this phenomenon is quite simple. Because the density of most liquid metals decreases with increasing temperature, the horizontal temperature gradient results in a horizontal density gradient. The system is unstable and the liquid can be expected to flow in a fashion similar to that shown in Figure 2.

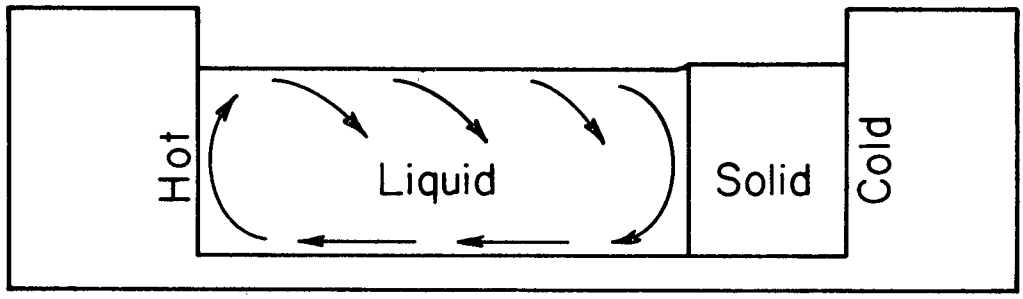

Figure 2. Convective flow pattern arising from horizontal temperature gradient.

During investigations to determine solidification conditions necessary to eliminate macrosegregation and intercellular segregation, Cole[5] found that one of the most important parameters in controlling these features was the temperature gradient in the liquid G_L. Consequently, in early experiments, sensitive thermocouples were placed in direct contact with the liquid in order to measure G_L. It was found that the temperature in the liquid fluctuated in a random manner.

Although temperature fluctuations had been observed during solidification experiments by Jackson and Chalmers[6] and Bolling and Kramer[7], Cole found that the presence of the solid-liquid interface had no bearing on the appearance of the fluctuations. Thus, experiments were designed to study the character of temperature fluctuations in a completely liquid system.

From these experiments Cole concluded that temperature fluctuations occurred when the longitudinal temperature gradient G_L exceeded a critical value G_L^c. The amplitude and frequency of temperature

fluctuations were found to decrease (a) as G_L decreased, (b) as the angle of heating was decreased from the horizontal (with the cold end of the liquid being the lowest point of the system) and (c) as the height of the liquid in the system decreased. It was also found that the relationship - (Height of Melt)^3 G_L^c = constant described the conditions necessary for the onset of temperature fluctuations. The greater the melt height, the greater the instability of the systems with respect to thermal convection.

Cole further concluded that the presence of temperature fluctuations resulted from the existence of natural thermal convection in the liquid metal and therefore natural thermal convection could be detected by sensitive thermocouples placed in the liquid. It was suggested that convection could be eliminated by suitably controlling the temperature distribution in the liquid.

Subsequent experiments by Cole investigated fluid flow during solidification. As a result of the interaction of thermal convective flow with the solid-liquid interface a "thermal boundary layer" was found to exist. This was described by the parameter δ_T. Proceeding away from the interface, the flow is first laminar, a buffer or transition region follows and for distances away from the interface greater than δ_T the flow is essentially turbulent. The thickness of the thermal boundary layer, as a function of the fluid properties of the liquid metal and the growth variables, was found to be given by the expression[5]:

$$\delta_T = H^{1/5} \left[\frac{203\alpha^2}{g\beta G_L^o} \left(1 + 1.58\ Pr - \frac{R\delta_T}{\alpha}\right) \right.$$

$$\left. + \frac{203R^2L^2}{C_p^2 g\beta (G_L^o)^3} + \frac{406RL\alpha}{C_p g\beta (G_L^o)^2} \left(1 - \frac{R\delta_T}{2\alpha}\right) \right]^{1/5} \qquad (1.5)$$

where: L is latent heat of fusion

g is the acceleration due to gravity

β is the coefficient of volume expansion

α is the thermal diffusivity

Pr is the Prandtl number

H is the height of the solid-liquid interface

G_L^o is the temperature gradient at the interface

C_p is the specific heat

R is the growth rate

Using this experession δ_T was calculated for the experimental conditions employed ($0.001 < R$ cm/sec. < 0.005, $10 < G_L^o$ °C/cm < 20) giving values of the order of 1 cm. These values were in good agreement with the experimentally observed boundary layer thicknesses.

In order to estimate the effect of thermal convection on macrosegregation a theory was developed which accounted for the interaction of convection with the solute boundary layer δ_s which exists at the solid-liquid interface of a solidifying alloy. The relationship formulated to determine the magnitude of δ_s was:

$$\delta_s^5 - 4\delta_T\delta_s^4 + 5\delta_T^2\delta_s^3 + \frac{80\delta_T^5 (R\delta_s - 2D)}{53.3\ H \left[\alpha + R\left(\frac{L}{C_p G_L^o} - \frac{\delta_T}{2}\right)\right]} \qquad (1.6)$$

where D is the diffusion coefficient of the solute in liquid solvent.

To obtain the solute distributions during horizontal solidification the following procedure was utilized:

(1) Substitute appropriate values of fluid flow parameters and G_L^o and R into Equation (1.5) and thus calculate δ_T.

(2) Substitute this value of δ_T into Equation (1.6) and solve for δ_s.

(3) Substitute this value of δ_s into the equation:

$$k_e = \frac{k_o}{1 - \frac{(1 - k_o)\,\delta_s R}{2D}} \qquad (1.7)$$

and obtain the value of k_e.

When the growth parameters are such that the value of k_e=1, a solidified product which has uniform composition over most of its length (Figure 1, curve b) should be obtained (providing constitutional supercooling does not occur and cause the planar to cellular interface transition).

Cole also obtained an expression for calculating the maximum velocity of fluid flow parallel to the interface:

$$u_m = \frac{53.3\,H}{\delta_T^2}\left[\alpha + R\left(\frac{L}{C_p G_L^o} - \frac{\delta_T}{2}\right)\right] \qquad (1.8)$$

from (1.8) and (1.5) it would be expected that u_m increases as the height of the melt increases and as the temperature gradient G_L^o increases. Equation (1.8) shows that u_m should increase with increasing H. This is consistent with the finding that the critical horizontal gradient G_L^o necessary for the onset of temperature fluctuations decreases as H increases. That is, increasing the melt height decreases the stability of the melt with respect to convective flow.

For a stationary system (R = 0) the expression for u_m becomes:

$$u_m = 53.3\ \alpha\ H^{3/5} \left[\frac{g\beta G_L^o}{203\alpha^2\ (1 + 1.58\ Pr)} \right]^{2/5} \qquad (1.9)$$

or, for a given melt height and average melt temperature:

$$u_m \propto (G_L^o)^{0.4}$$

Clearly then, for any non-zero horizontal temperature gradient one would expect convective flow, that is, $u_m \neq 0$. This indicates that the detection of temperature fluctuations at some critical gradient $G_L^c > 0$ does not indicate the onset of fluid flow. The Cole technique then is not sufficiently sensitive to detect fluid flow at $G_L < G_L^c$. No attempt was made to measure flow velocities and thus validate the expression for u_m.

Müller and Wiehelm[8] have also demonstrated the existence of temperature fluctuations in the melt during the growth of metal and semiconductor crystals by the horizontal normal freeze, and zone melting techniques. Correlation of the periodic variation in temperature with

the spacing of concentration striae in crystals of InSb was established. Experiments showed that for melts between 10 and 30 cm long the amplitude and frequency of the observed temperature fluctuations were independent of the melt length provided that the temperature and temperature gradient were kept constant at the measuring point.

The first direct measurements of flow velocities in liquid metals contained in horizontal boats were carried out by Utech[9]. In studies of thermal convection in molten tin the observation was made that a sequence of temperature fluctuations recorded by a thermocouple inserted into the melt was repeated a short time later by a second thermocouple located down stream. By measuring the time required for the temperature fluctuation to travel a known distance downstream, an indication of mean flow velocity could be obtained. Utech found (in agreement with Cole) that a critical horizontal temperature gradient was necessary to produce temperature fluctuations. Evidence that flow occurred at gradients below G_L^c was obtained by observing that as the horizontal temperature gradient increased from zero a corresponding increase in vertical temperature gradient (hot liquid above cold) appeared. Suppression of convective flow by a magnetic field and the resultant disappearance of the vertical gradient showed conclusively that the vertical temperature gradient was a direct consequence of convective flow.

The results of the investigation of Utech for convective flow in a horizontal boat with an open top can be summarized as follows. At small horizontal temperature gradients circulation of liquid begins, causing a vertical temperature gradient to appear. This convective flow may be considered laminar in as much as the temperature at any point in

the system remains constant, once steady state conditions have been attained. The flow pattern under these conditions could not be determined directly. Utech inferred the pattern would be similar to that observed in low viscosity oil, that is, a narrow stream along the bottom flowing from the cold end to the hot end of the boat, a rising column of liquid at the hot end of the boat with the hot liquid which had been carried to the top falling more or less uniformly along the entire length, Figure 2.

As the horizontal gradient is increased, this uniform flow breaks down and a number of cells of circulating liquid appear along the length of the boat. Their presence is manifested by the fluctuations in temperature as measured by a thermocouple located at any point in the system. The resulting "turbulence" becomes increasingly severe as the temperature gradient is increased. When the liquid tin is approximately 1 cm deep and the gradient in the liquid is about 12°C/cm, mean velocities in the liquid of the order of 1 cm/second are observed. The flow velocities measured by Utech are approximately an order of magnitude less than would be predicted by the Cole analysis.

Utech employed the boundary layer analysis of Eckert and Drake[10] for flow past a vertical plate with surface temperature T_w, immersed in a fluid at uniform temperature T_o, to obtain the expression for maximum flow velocity:

$$u_m = 0.766\nu \, (0.952 + Pr) \left(\frac{g\beta\Delta Tx}{\nu^2} \right)^{1/2} \qquad (1.11)$$

where: ν is the kinematic viscosity

x is the vertical distance from the leading end of the vertical wall

T is the temperature difference across the boundary layer.

According to Utech (although it is not evident from an examination of his results[9]) Equation (1.11) agrees reasonably well with his velocity measurements.

A NaCl melt (transparent) was used in order to verify this velocity determination technique and to directly observe the flow pattern associated with a horizontal temperature gradient across a melt[11]. The flow pattern observed in NaCl appears in Figure 3. Superimposed on the generally steady flow along the bottom and top of the boat is a pattern of cells that result in upward and downward vertical currents along the entire length of the boat.

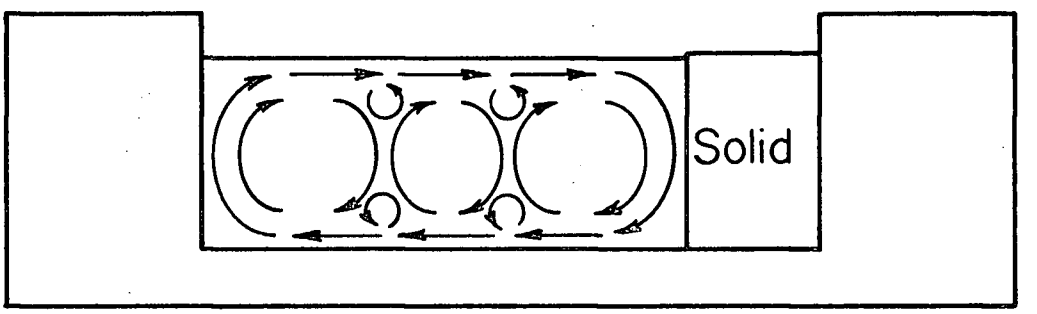

Figure 3. Representation of the flow pattern in the horizontal boat.

This pattern of cells changed with time. Only at the cold and hot ends was the vertical flow always in the same direction. Since the Prandtl number (a dimensionless parameter classifying the convective behaviour of fluids) of molten NaCl (Pr = 0.13) approaches those of liquid metals (typically 0.1 - 0.01) it was assumed that flow patterns in liquid metals would resemble those observed in molten NaCl.

The fact that liquid NaCl is transparent suggests that heat transfer by radiation is appreciable and therefore the convective heat transfer for NaCl and a liquid metal, constrained by the same thermal environment, would be appreciably different. If the heat transfer modes were dissimilar the flow patterns would also be dissimilar.

Observations by Hurle[12] that the mode of temperature fluctuations could be changed by quite small movements of the thermocouple or by inserting a 50 μ diameter wire vertically into the melt clearly indicated that the presence of any obstruction in the melt, including the thermocouple, had a profound effect on the temperature oscillations. This observation suggested that the temperature fluctuations reported earlier (5,6,7,8,9) were probably not characteristic of the melts themselves. It was subsequently found that, provided the thermocouples were inserted to a depth of less than 0.04 cm, oscillations could still be recorded and these oscillations were not affected by moving the thermocouples. Hurle also observed that above a critical horizontal temperature gradient temperature oscillations appeared. This critical gradient was found to increase with decreasing melt length. (At a boat length of 4 cm it was 5.0 °C/cm and at 2.6 cm it was 7.5 °C/cm).

Davis and Fryzuk[13] studied thermal convective mixing in horizontal melts with known initial solute distributions. Results showed that observable convective mixing (in rods 2 mm in diameter) occurs at horizontal temperature gradients greater than 5°C/cm and that extensive solute redistribution occurs for temperature gradients 15°C/cm or greater. Cole and Winegard's formulation[5], $H^3 G_L^c = 3.1$, predicts that temperature fluctuations (indicative of the onset of turbulent thermal convection) would not appear until a temperature gradient of approximately 400°C/cm was attained. Obviously then, the occurrence of temperature fluctuations in the melt is not sufficiently sensitive to detect the presence of extensive thermal convection.

Carruthers and Winegard[14] employed yet another technique for determining the extent of convectivemixing in horizontal melts. In their experiments a solid horizontal rod of pure lead was melted by moving a tube furnace along the rod. The liquid in contact with the solid lead contained approximately 10% thallium. After steady state melting had been achieved over 5 to 10 cm, the liquid was solidified by removing the furnace. Since the distribution coefficient of thallium in lead is close to unity, very little solute redistribution occurred during freezing. Concentration profiles resulting from boundary layer flow at the interface were revealed by a suitable etching technique. The variation of boundary layer thickness and shape was then taken as a measure of the extent of convective flow. The following conclusions were obtained:

(1) Convective mixing increases with increasing horizontal temperature gradient and also with increasing radial heat transfer.

(2) Increasing the length of the melt promotes more vigorous thermal convection.

(3) The liquid height exerts very little effect on either the extent or the configuration of mixing due to thermal convection.

(4) The effect of introducing thermocouples into the melt is to cause increased convective mixing.

Another important conclusion of the work of Carruthers[15] is that the onset of temperature oscillations seen by Cole corresponds to a flow transition from laminar boundary layer to turbulent boundary layer flow. Thus, it is again apparent that appreciable fluid flow may be present at gradients well below those necessary for the onset of temperature fluctuations.

Of the techniques described above not one is capable of measuring flow velocities in melts subjected to horizontal temperature gradients below G_L^c, the gradient associated with the onset of temperature fluctuation. Nor is it possible to accept the flow patterns observed in nonmetallic melts[9,11] as being typical of the convective flow patterns which occur in liquid metals. However, any theory attempting to predict the solute distribution in a solidified metal requires information concerning the extent of fluid flow in the liquid metal during solidification. In the absence of such information it becomes necessary to make assumptions about the fluid flow present in the melt.

Accordingly, the present investigation was undertaken to

obtain direct in situ measurements of fluid flow velocities and to observe fluid flow patterns in liquid metals. This was accomplished by the use of radioactive tracers. Stewart and Weinberg[16] have employed radioactive tracer techniques to observe flow velocities and flow patterns in thin cells with length to height ratio of approximately 1. However, for the purpose of the present investigation a horizontal rod configuration (length to height ratios between 40 and 70) was selected since this is the geometry adopted in most fundamental examinations of solute segregation during solidification. Also the boat used to contain the melt was provided with a cover to reduce asymmetric heat losses from the system and to simulate conditions required for growth of crystals of a specified size. Although this geometry provides a simple configuration for solidification studies it presents a complex and as yet unsolved problem from the thermal convection and fluid dynamics points of view.

2 - DETERMINATION OF FLOW VELOCITIES IN HORIZONTAL RODS OF MOLTEN TIN

2.1. Flow Velocity Determination by Manually Monitoring the Movement of Radioactive Tracer

As outlined in the introduction, one of the purposes of the present investigation was to develop a technique that would permit direct measurement of flow velocities in horizontal rods of molten metal. It was considered essential that the measurement technique employed should not perturb the liquid metal system. Specifically, the velocity observed should be due only to the fluid properties of the system and the experimentally imposed conditions. It was decided that a method involving the external monitoring of radioactive tracer as it flowed along with the melt would best satisfy the condition of not interfering with the fluid flow that would normally occur. The development of such a technique is presented below.

2.1.1. General Experimental Apparatus and Procedure

The apparatus employed for the first series of experiments is shown in Figure 4. The molten metal (pure tin) was contained in a graphite boat which was equipped with a device for introducing the radioactive tracer. The boat was inserted into a 45 mm O.D. Vycor tube surrounded by an 18 inch long tube furnace. The furnace was constructed in the following way. An 18 inch length of 2 inch diameter copper tube was

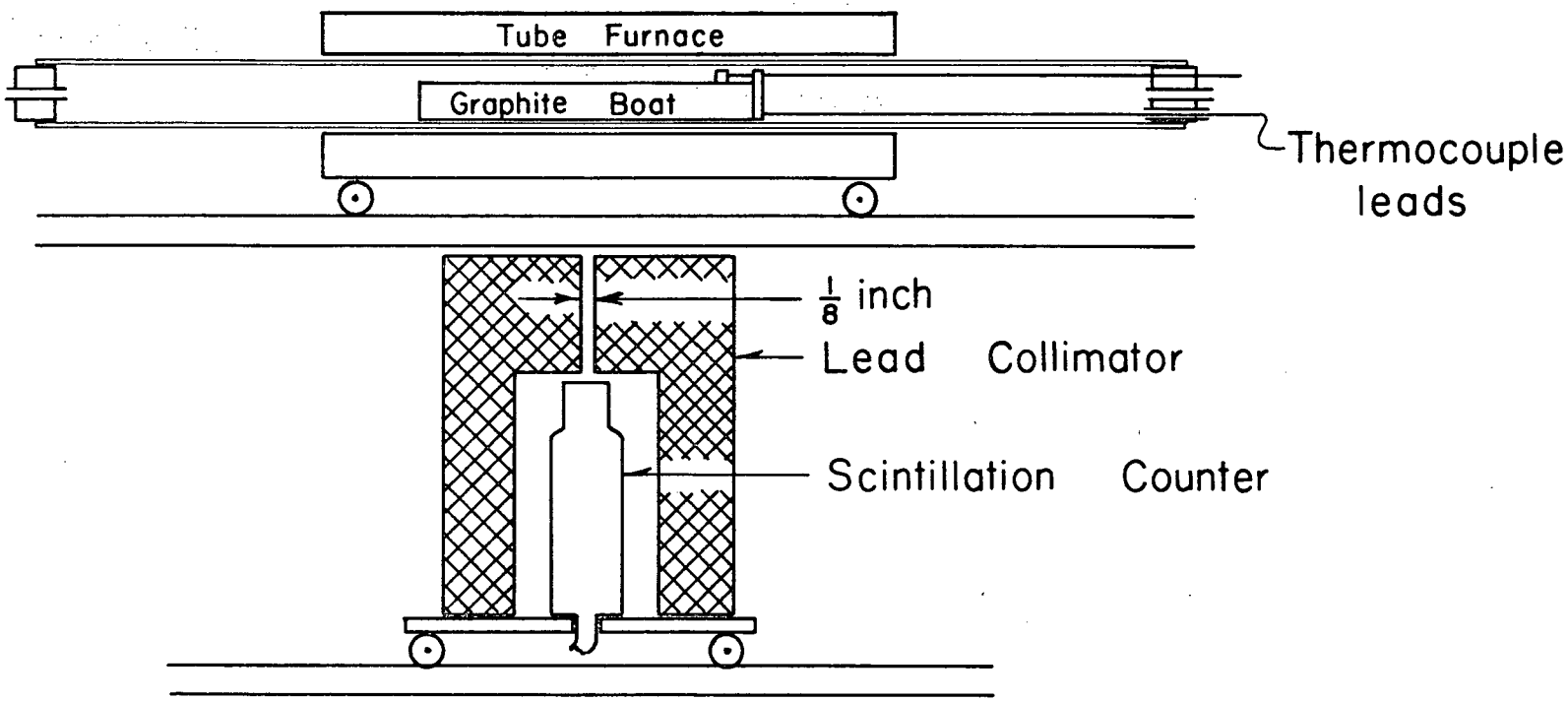

Figure 4. The apparatus employed for initial series of experiments.

wrapped with a layer of 1/16 inch thick asbestos cloth. Four resistance windings (26 gauge nichrome) each 4 inches long, separated by 1/2 inch, and having separate power terminals were wound on to the asbestos. The resistance of each winding was approximately 120 ohms. Each winding was coated with Sairset refractory cement. The wound tube was surrounded by glass wool and placed in an aluminum container. The container was mounted on a set of wheels so that the entire furnace assembly could be moved. This facilitated changing the thermal environment of the melt without physically disturbing the melt itself. The inner two windings were connected in series to a 0 to 130 volt, 10 ampere, variac. The outer windings were similarly connected to a second variac. The Vycor tube and tube furnace were supported by a Handy Angle framework.

A scintilation counter surrounded by a lead collimator (constructed from lead bricks) and mounted on a moveable carriage was located below the graphite boat, Vycor tube and furnace assembly. A locating device was attached to the side of the carriage rail to allow fixing the position of the scintilation counter-lead collimator assembly at any desired position. The arrival of radioactive trace isotope above a given collimator slit position would be detected by a rapid increase in the activity reaching the scintillation counter through the collimator slit. The velocity of fluid flow in the melt above could then be measured by determining the time difference for the movement of radioactive tracer from one position to a position a known distance away.

The activity passing through the collimator was measured with a Quantum Electronics Q-6A, video scalar using a sodium iodide scintillation counter. To establish the optimum operating voltage for the counter, a radioactive source was placed above the counter and the activity was measured as a function of applied voltage, in 25 volt steps. The optimum operating voltage was taken as the voltage in the center of the plateau obtained on the activity versus applied voltage curve.

Radioactive trace isotopes used during the course of this investigation were Ag^{110}, Sn^{124} and Tl^{204}. Table 1 lists the pertinent properties of these isotopes. Non-radioactive Ag, Sn, Sb and Tl of 59's or better quality was sent to either A.E.C.L. at Chalk River, Canada,or to Radioactive Materials Corporation, Buffalo, New York, for irradiation. Trace alloys of varying composition were prepared from the resulting isotopes. The alloy was melted in a resistance wound vertical tube furnace and mixed frequently (by vigorous shaking) for at least 15 minutes to insure homogeneous dispersal of the radioactive isotope throughout the trace alloy. The alloy was then cast into a graphite mold and the resulting casting was cut into conveniently sized pieces (2-4 gms in weight), packaged, labelled and then stored in a lead castle until needed.

Throughout the following presentation the density of trace alloys will be given relative to the density of pure molten tin at a similar temperature. The relative densities of the trace alloys, calculated on the assumption of independent behaviour of the species alloyed, were determined by the relation:

TABLE 1

Properties of Radioisotopes[50]

Isotope	Half Life	Type of Radiation and Energy (Mev)
Ag^{110}	270d	β^- (.53), γ (.66 - 2.0)
Sn^{113}	112d	X-ray, γ (.26)
Sb^{124}	60d	β^- (2.31), γ (.60-2.11)
Tl^{204}	4.1y	β^- (.76)

$$\rho_{alloy} = \left(\frac{100\ \rho_I}{(\text{wt \%Sn})\ \rho_I + (100 - \text{wt \%Sn})\ \rho Sn} \right) \rho Sn$$

where ρ_I is the density of the trace isotope.

The major problem associated with the measurement of flow velocity by a radioactive tracer technique lies in discovering a way to introduce the tracer without disturbing the melts. The observations and results obtained from an extensive series of experiments undertaken to develop a suitable tracer introduction technique are presented sequentially in Sections 2.1.2. to 2.1.8.

2.1.2. Tracer Introduction by Melting Back Through a Region Containing Radioactive Material

2.1.2.1. Experimental Apparatus and Procedure

The graphite boat used for the initial attempt to study the extent of convective flow in horizontal rods of molten tin is shown in Figure 5. The boat had two channels which were covered for approximately 90% of the channel length with a short uncovered section at each end. In the covered section the melt cross section was 0.64 cm wide and 0.64 cm high. The height of metal in the uncovered reservoirs was approximately 1 cm. Thermocouples (30 gauge iron-constantan, insulated by 2 hole-1/16 inch O.D. mullite tubing) were positioned at 3 cm intervals along one of the channels with the thermocouple beads situated in the centre of the channel. Thus, the temperature distribution could be measured in one channel while study of the fluid flow, unimpeded by temperature measuring devices, could be carried out in the other channel. It was assumed that the two channels had identical temperature distributions.

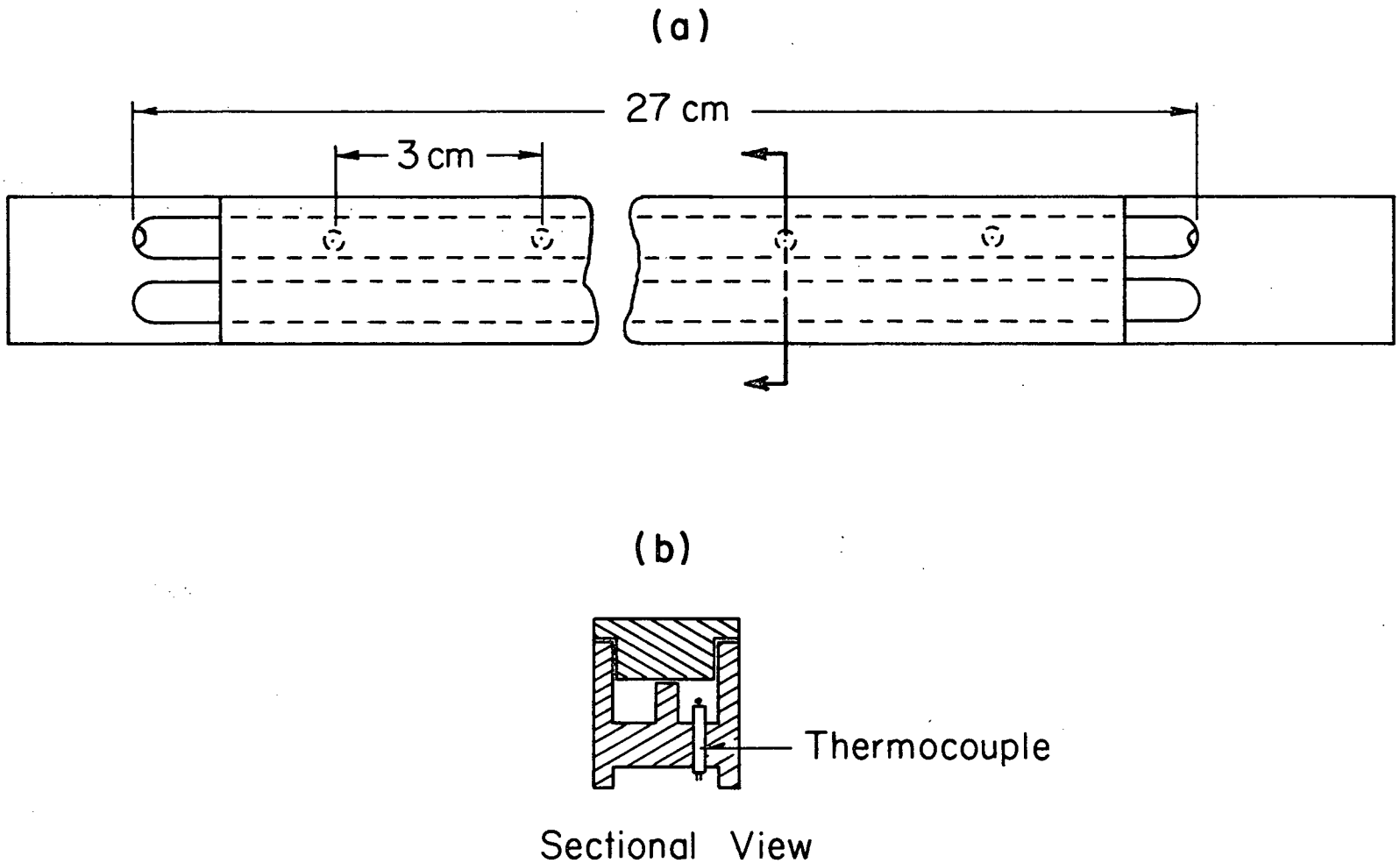

Figure 5. The graphite boat used for initial studies of convective flow in horizontal rods of molten tin.

The boat was filled with 59's tin (supplied by Vulcan Metals) and allowed to solidify. Approximately 3 gms of tin was removed from one end of the "clear" channel and in its place was cast radioactive tracer, a Sn-0.2 wt % Ag^{110} alloy. Ag^{110} was chosen as the trace isotope since it is a strong gamma emitter capable of penetrating the Vycor tube and furnace assembly and thus its presence over the collimator slit is easily detected. The loaded boat was then placed in the Vycor tube and the thermocouple leads were connected through a Leeds and Northrup multi-point switch to a Honeywell Electronik 194 recorder. An ice water bath was employed as the cold junction and the thermocouples were periodically calibrated against the freezing point of pure tin. Temperatures measured were believed to be correct within ± 0.1 °C.

The distribution of activity along the length of the channel was determined prior to melting with the moveable collimator-scintillation counter described earlier. The furnace was switched on and the tin melted. When the thermocouple adjacent to the radioactive tracer indicated the tracer was molten, monitoring of tracer movement began. This was accomplished by equal time interval counting at various positions along the length of the channel. Any movement of tracer would be accompanied by a change in the observed distribution of activity along the boat.

In order to evaluate the capability of the collimator to accurately determine the distribution of activity along the boat the following test was devised. Following the procedure outlined above,

the distribution of tracer was determined some time after melting had occured. The melt was then quenched (by filling the Vycor tube with water) and, with the boat still in the same position, the distribution of tracer was again monitored. The boat was taken from the furnace and the solidified tin was removed from the clear channel of the boat. The distribution of tracer along the tin was determined by sectioning it into 1/4 inch pieces, weighing each piece, and measuring its activity by fixed geometry counting with a Tracerlab Inc. scintillation counter and ampliscalar.

2.1.2.2. Results and Discussion

Results of the test to evaluate the accuracy of the collimated counting procedure appear in Figure 6. The open squares are from the in situ monitoring after quenching and the filled circles from the sectioning and counting procedure. The activities have been normalized to facilitate comparison of the results. Both sets of data can be represented by one curve. Accordingly, the activity versus position profile determined by the collimator-scintillation counter arrangement can be taken as an accurate representation of the horizontal distribution of radioactive tracer along the melt length.

Figures 7, 8, and 9 show results typical of those obtained from preliminary experiments to determine the amount of fluid flow associated with small horizontal temperature gradients along the liquid tin. Figure 7(a) shows the temperature distribution along the tin melt 1/2 hour, 1 hour and 4 hours after melting had occured. Although the average temperature of the melt changes, the temperature distri-

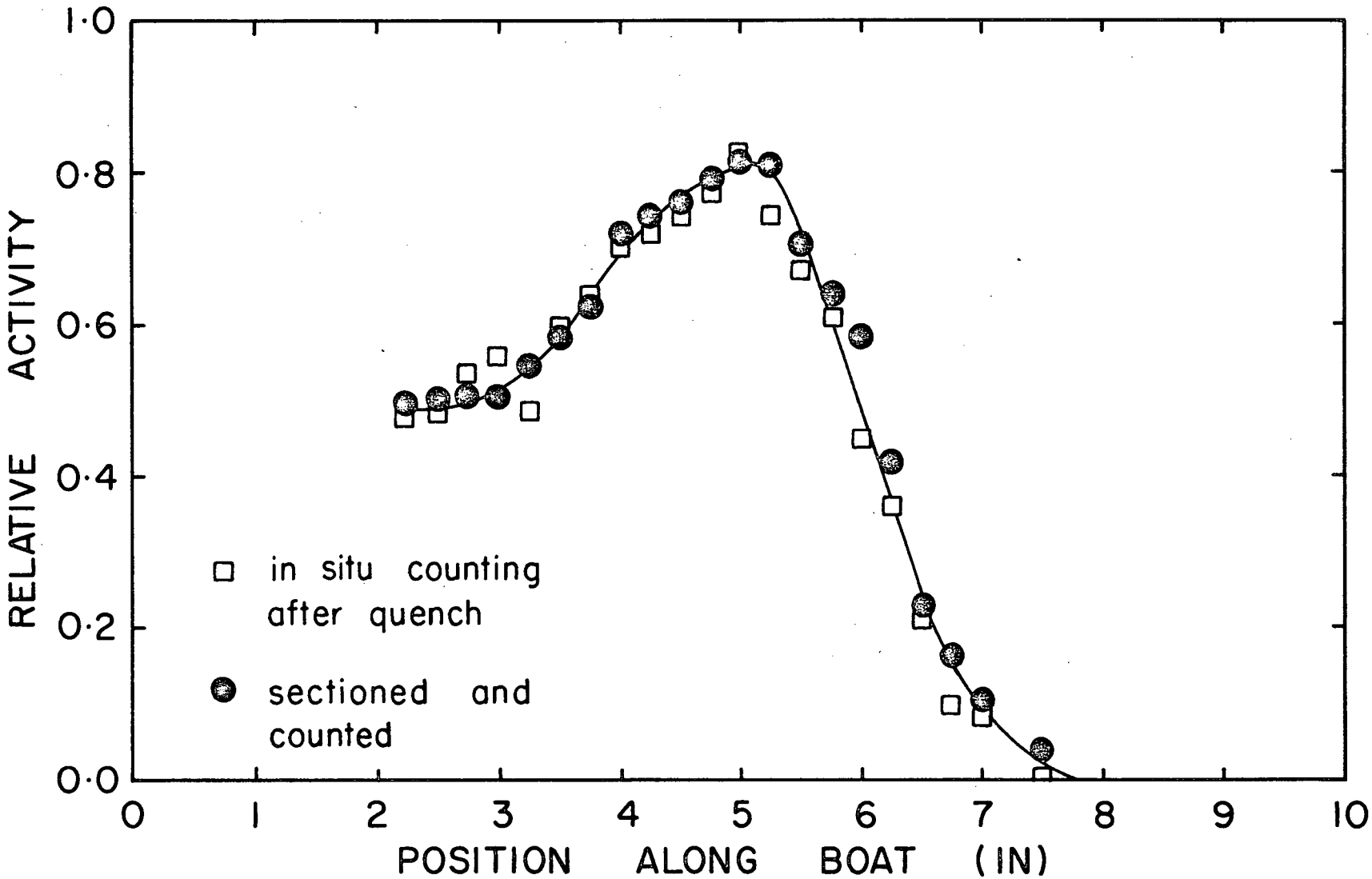

Figure 6. Results of the test to evaluate the accuracy of the collimated counting procedure.

bution across the melt remains essentially the same for the 4 hour period. Figure 7(b) shows the distribution of tracer before melting and at approximately 1/2 hour, 1 hour and 4 hours after melting. The tracer has moved approximately half the length of the melt in the first 1/2 hour but very little movement occurs over the subsequent 3½ hours. A gradual leveling of the tracer distribution in the first half of the melt was observed over the 4 hours. Comparison of Figures 7(a) and 7(b) indicates that the position of furthest advance of tracer and the position of zero temperature gradient are approximately coincident. To establish whether the stoppage of flow was uniquely determined by the position of the zero temperature gradient the tube furnace was moved, thus changing the temperature distribution in the melt. Figure 8(a) shows the temperature distribution 5, 10 and 20 minutes after moving the tube furnace. Figure 8(b) shows the effect of the temperature changes on the distribution of tracer along the melt.

The coincidence of tracer redistribution with movement along the boat of the zero gradient is made more obvious by comparing Figures 8(a) and 9. Figure 9 is a plot of activity at a particular position along the boat at various times after melting. As can be seen from Figure 8, positions at 8.5, 11 and 13.5 cm are on one side of the zero gradient whereas those at 18.5 and 21 cm are on the other side. Very little change in the activity observed at each position occurred between 1 hour after melting and 4 hours after melting. Significant changes occur shortly after the furnace is moved. Figure 8(a) indicates that at between 5 minutes after and 10 minutes after

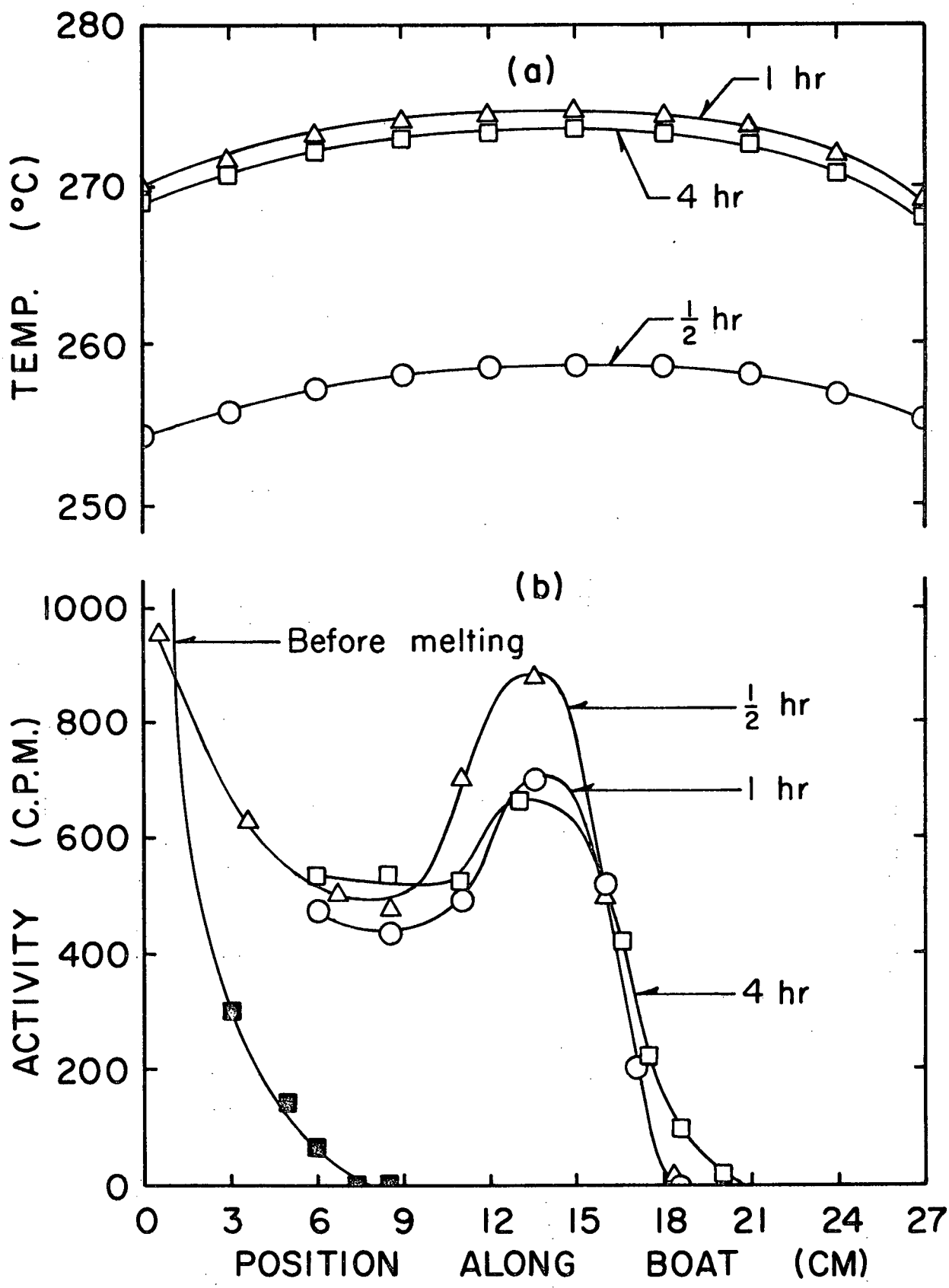

Figure 7. (a) The temperature profiles at the indicated times after the tracer had melted. (b) The distribution of tracer at the indicated times after melting.

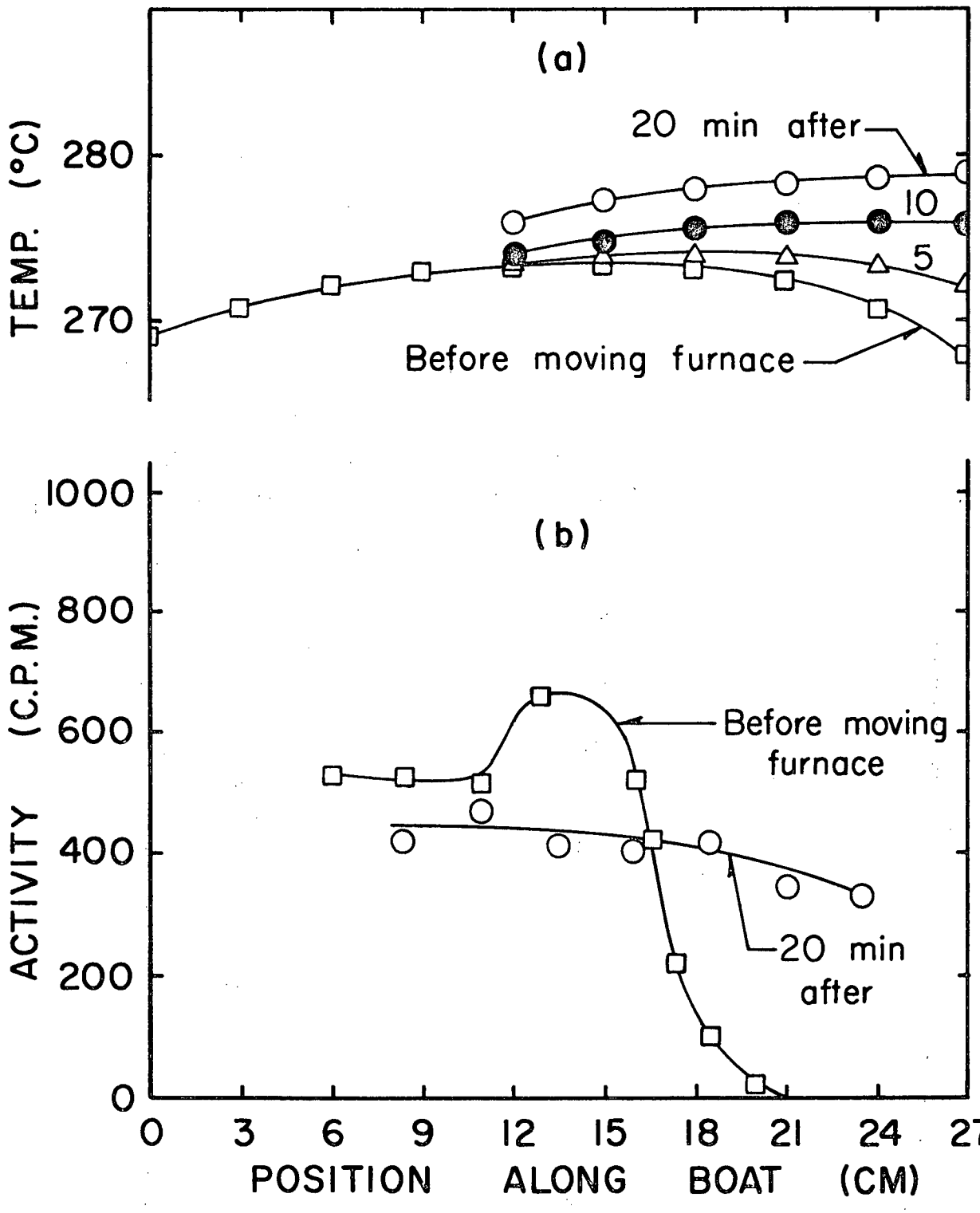

Figure 8. (a) The temperature profiles at the indicated times. (b) The distribution of tracer before and after moving the furnace.

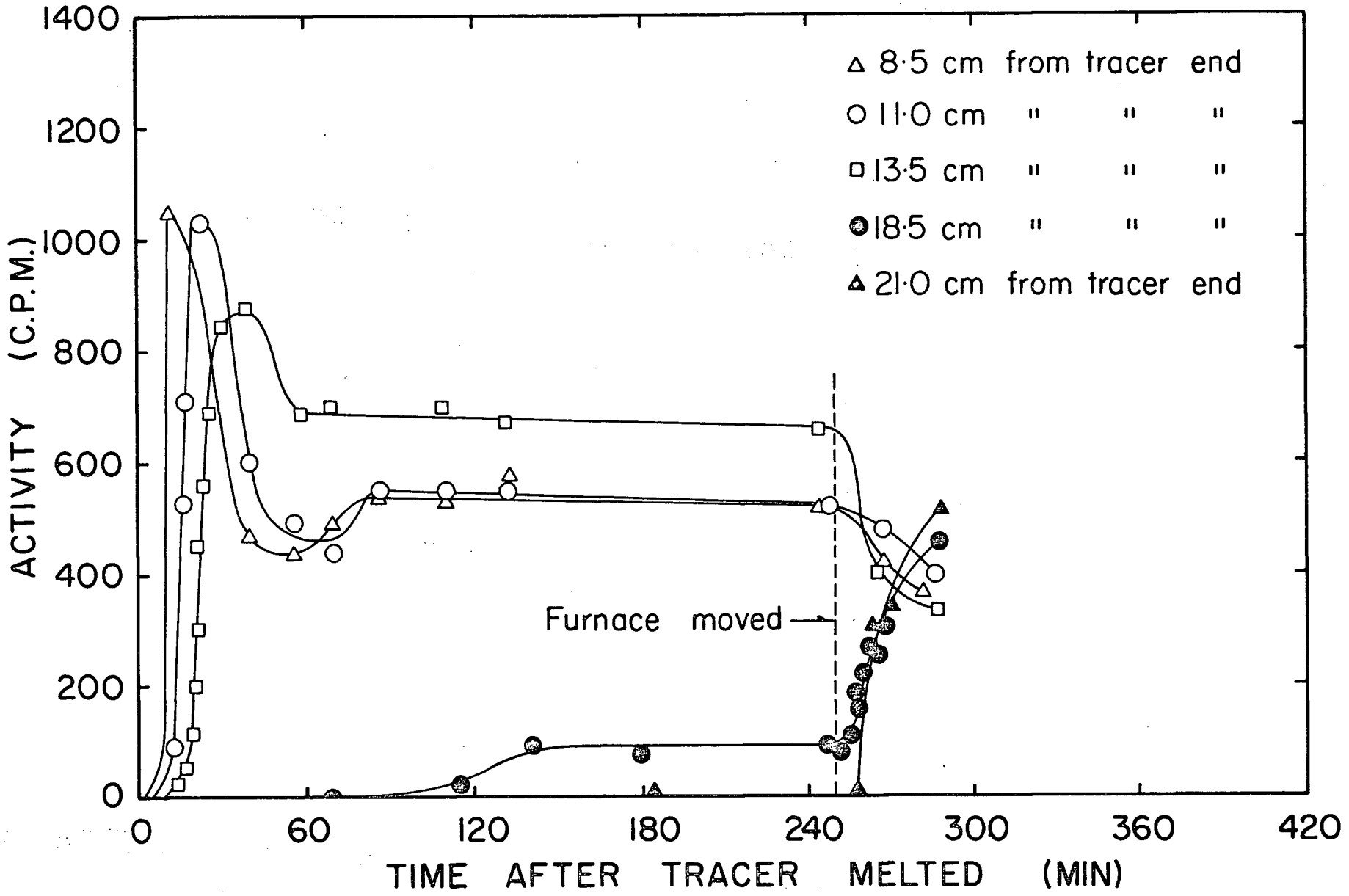

Figure 9. The change in activity with time at various positions along the melt.

moving the furnace the zero gradient has moved past the 18.5 cm position. Correspondingly the 18.5 cm plot on Figure 9 shows that tracer starts moving past this position approximately 6 minutes after moving the furnace. Similarly the zero gradient moves past the 21 cm position about 10 minutes after furnace movement and Figure 9 indicates tracer movement past this position at approximately the same time. These results clearly show that:

(1) The region of zero horizontal temperature gradient is not permeable to thermal convective flow.

(2) An extremely small horizontal temperature difference, apparently any gradient greater than zero, provides sufficient driving force for thermal convective flow.

The conclusion that thermal convective mixing will not pass through a region of zero horizontal temperature gradient is in agreement with the findings of Davis and Fryzuk[13] who studied the redistribution of a radioactive solute along 2 mm diameter horizontal melts. However, they were unable to detect convective mixing at temperature gradients below 5 °C/cm.

Evidence that convective mixing occurs on both sides of the region of zero gradient is presented in Figure 10. The initial distribution was achieved, by allowing tracer to move down the boat to a region of zero gradient (at approximately 21 cm), waiting until the tracer distribution in the first 21 cm became homogeneous and then quenching. The boat was removed from the furnace and a new piece of Sn-0.2 % Ag^{110} was cast into the end of the boat. Figure 10(a) shows

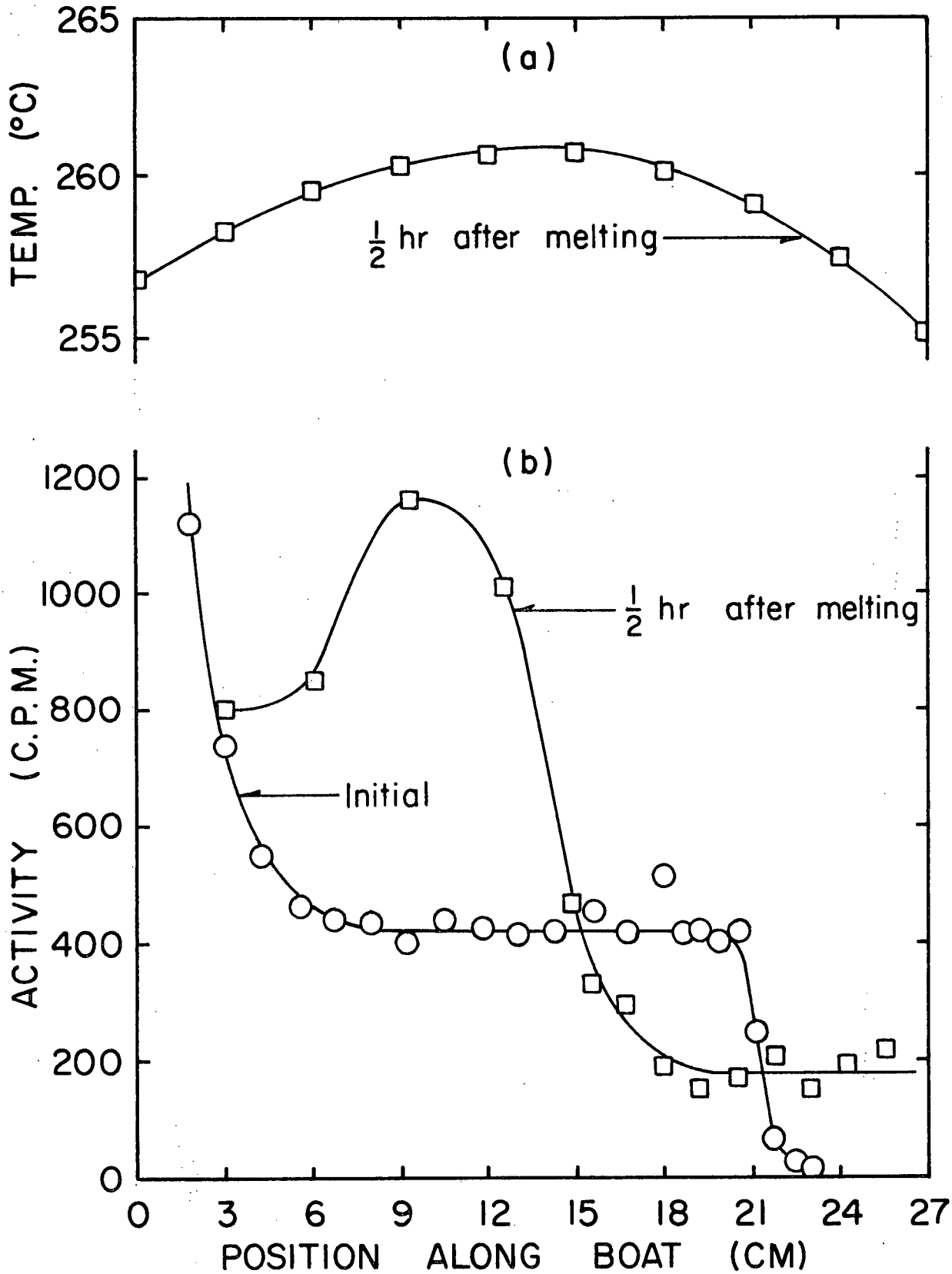

Figure 10. (a) The temperature profile 1/2 hour after the tracer melted. (b) The distribution of tracer before and after melting.

that a zero gradient occurred approximately 15 cm along the boat. Correspondingly there was movement of tracer up to, but not past the 15 cm mark. Also, the distribution of tracer to the right of the 15 cm mark had evened out. Thus, thermal convective mixing was taking place on both sides of the zero gradient, but the presence of the zero gradient prevented mixing along the entire length of the boat. This result suggests the existence of a quiescent zone in the region of zero gradient. Figure 11 illustrates the type of flow pattern which would be expected under the experimental condition employed here. The zero gradient functions as a valve in that convection occurs on both sides of the zero gradient but there is no mass transport between the two cells. Stewart's autoradiography[17] of double cell flow has now provided visual confirmation of the existence of a quiescent zone in a zero gradient region.

2.1.2.3. Evaluation of Technique

Although the tracer introduction technique just described was rather unsophisticated, it did show that detectable thermal convective flow occurs at any horizontal gradient greater than zero. This flow could not have been detected by temperature oscillation techniques. Unfortunately it was not possible to determine the contribution of volume changes on melting to the observed flow. The major shortcoming of this tracer introduction technique is the lack of control over the time at which the tracer was introduced into the melt. A much more desirable technique would allow introduction of tracer at any specified time, for example, after achieving a stable temperature

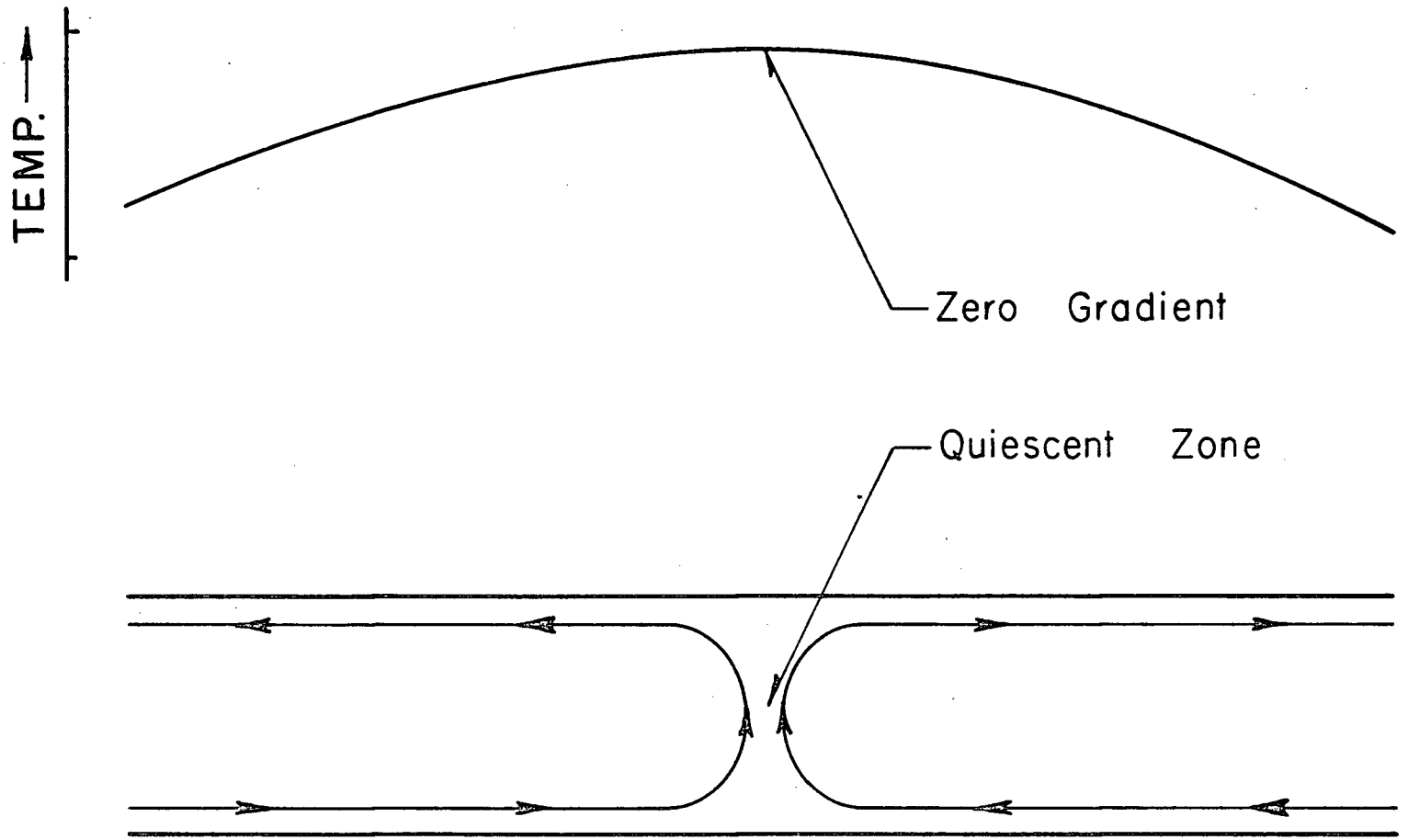

Figure 11. The expected flow pattern when a zero gradient is present.

distribution in the melt.

2.1.3. Tracer Introduction by Rotating a Vertical Cylinder Located at the End of the Graphite Boat

2.1.3.1. Experimental Apparatus and Procedure

The graphite boat used for this section of the investigation is shown in Figure 12. It is the same boat as was used in the previous section but with one modification; one end of the clear channel has been fitted with a hollow cylinder which is opened on one side, Figure 12(b). The cylinder was loaded with tracer in the tracer loading block shown in Figure 12(c).

The block was heated with a Bunsen Burner until the tracer melted and flowed into the introducing cylinder. The cylinder was then rotated such that the cylinder opening was not in line with the channel to the tracer reservoir. Following solidification of the tracer, the introducing cylinder was removed from the loading block and placed in the graphite boat such that the cylinder opening was not aligned with the channel. Introduction of tracer into the melt was achieved, at any desired time after melting, by rotating the cylinder until the channel and cylinder opening were coincident. The movement of tracer along the melt was monitored by the method described earlier.

2.1.3.2. Results and Discussion

In order to determine the extent of mixing associated with tracer introduction, experiments were carried out in which there was a zero horizontal temperature gradient in the melt just ahead of the

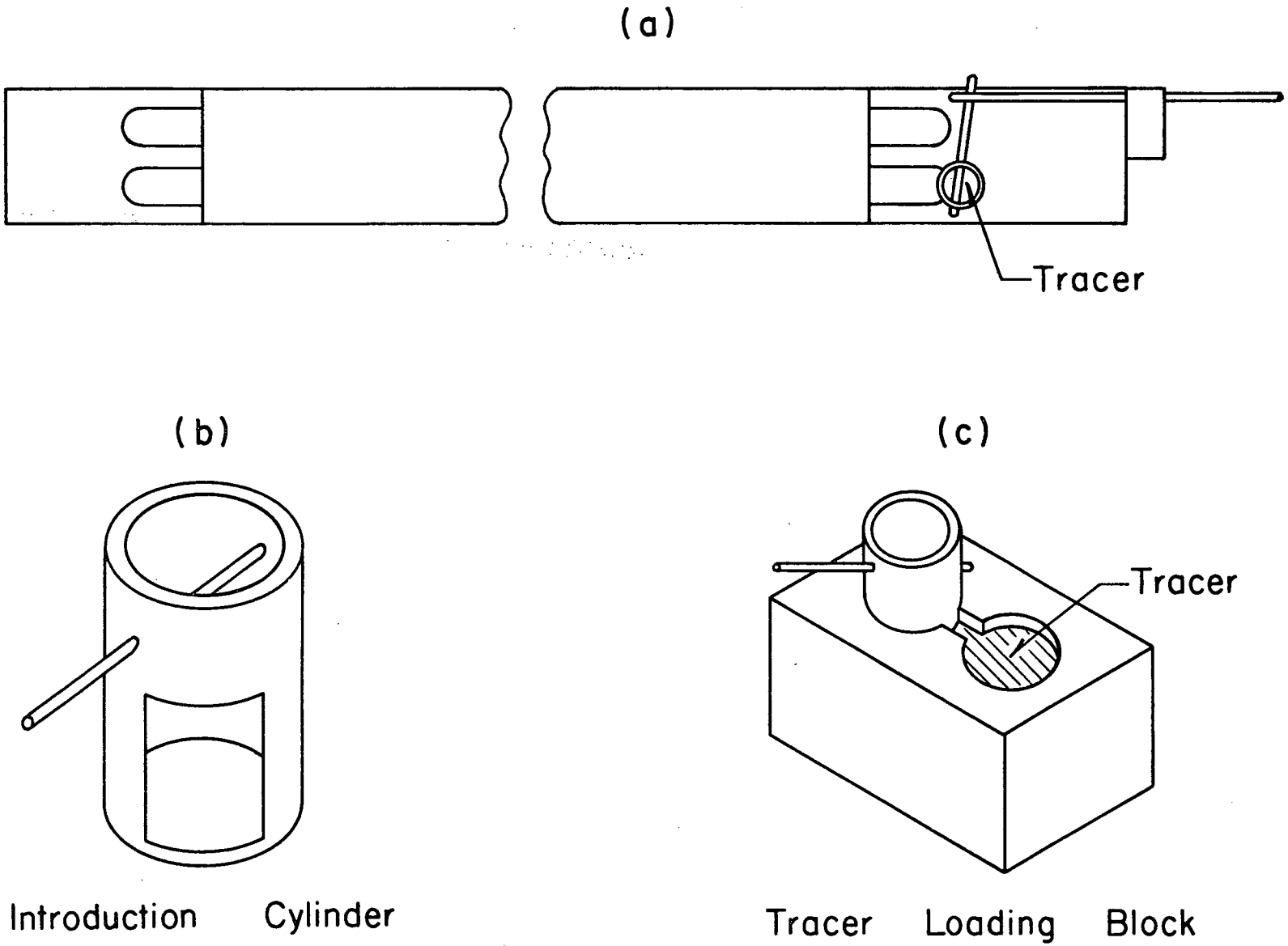

Figure 12. (a) Top view of graphite boat with tracer introduction cylinder in place. (b) Introduction cylinder. (c) Tracer loading block.

tracer introducer. Figure 13 shows results of such an experiment. From Figure 13(a) it can be seen that there is a region of zero gradient approximately 3 cm ahead of the tracer introducer. Movement of tracer past the region of zero gradient is clearly shown in Figure 13(b). It is evident that there is some additional driving force for the movement of tracer along the melt. This flow may arise from solute convection, since the Sn-0.2 wt % Ag^{110} alloy is more dense than pure tin, (1.0005 ρ_{Sn}) or from some mechanical disturbance associated with tracer introduction, or from a combination of both.

To eliminate the effect of mixing associated with introduction, experiments were conducted in which tracer was introduced into a melt which had a zero gradient approximately 6 to 10 cm ahead of the tracer introducer. With the zero gradient further down the melt than was the case in the experiment shown in Figure 13 mixing associated with introduction was not sufficient to carry the tracer past the region of zero gradient. After initial flow along the melt had stopped the temperature distribution in the melt was changed by passing argon through the Vycor tube. The temperature gradients at various positions along the boat appear in Figure 14(a) and the tracer distribution in Figure 14(b). The "initial" gradient distribution represents the conditions under which tracer was introduced and flow along the melt stopped. One and one half hours after introduction the stable tracer distribution marked "initial" was observed. The times shown on Figure 14 are times after turning on the argon. Comparison of Figures 14(a) and 14(b) show that increasing the gradient above zero results in flow along the boat.

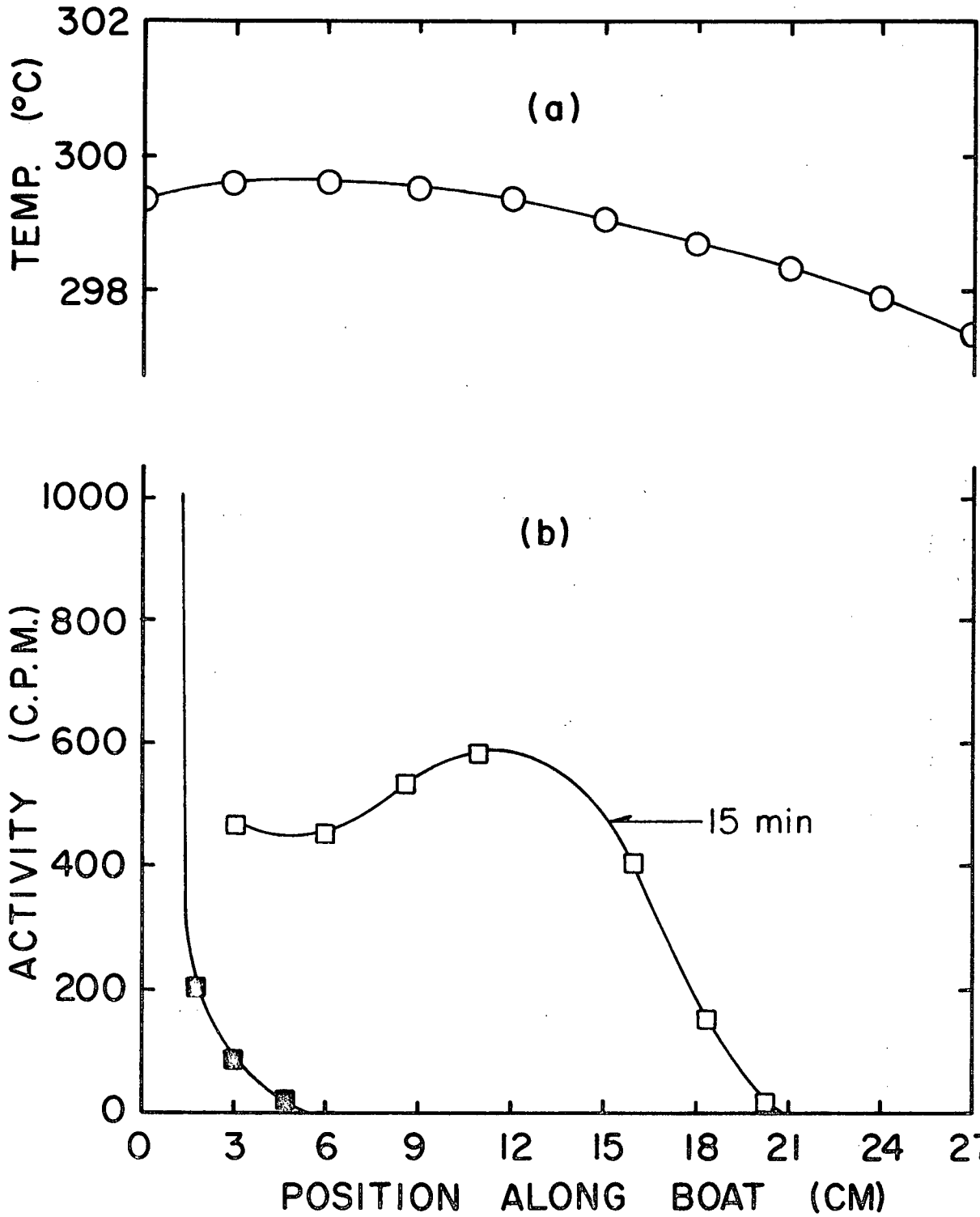

Figure 13. (a) The temperature profile along the melt at the time of tracer introduction. (b) The distribution of tracer before and 15 minutes after introduction.

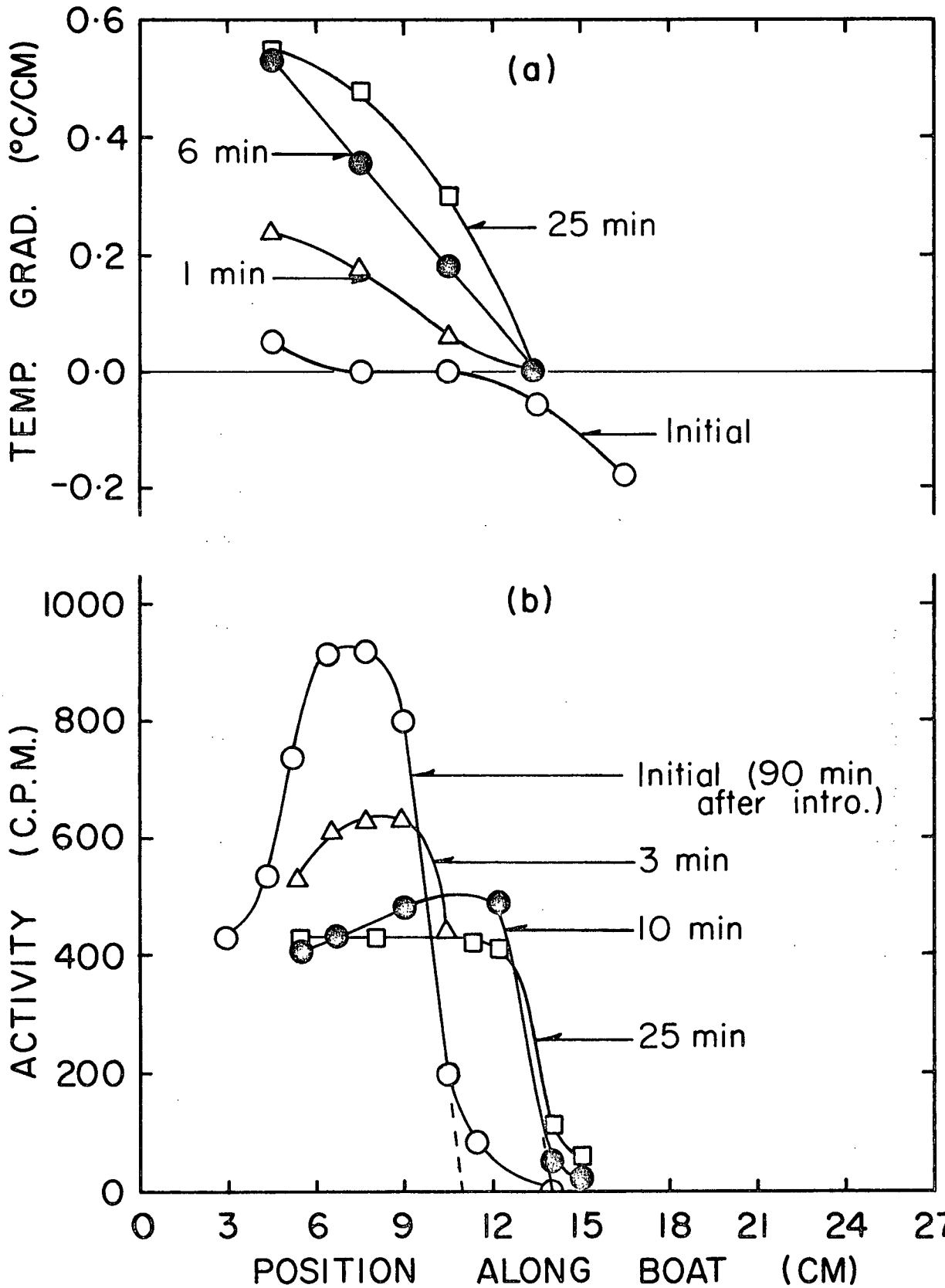

Figure 14. (a) The temperature gradients along the melt. (b) The distribution of tracer before and after passing argon.

In the experiments described in the previous section the temperature distribution was changed by moving the furnace whereas during this series of tests argon flow was employed to alter the temperature along the melt. Since the furnace is inductively wound it could be speculated that electromagnetic stirring effects were responsible for the flow which occurred after moving the furnace. The results of the experiments using argon to alter the temperature gradient along the melt agree with those obtained in the previous section. Thus, it can be concluded that it is the thermal driving force that causes the fluid flow. The average flow velocity estimated from the rate of advance of the points of intersection with the abscissa of a tangent drawn along the leading edge of the activity versus position curve (Figure 14(b))was 5×10^{-3} cm/sec.

During the course of experimentation to evaluate the extent and cause of mixing associated with tracer introduction occasional anomalous results of the type shown in Figure 15 occurred. The temperature profile 25 minutes after turning on the argon (Figure 15(a))would, from previous results, be considered extremely favourable for fluid flow. However, Figure 15(b) shows that no flow occurred. Apparently under some conditions there is no mixing between the uncovered reservoir where tracer is introduced and the covered section of the boat.

2.1.3.3. Evaluation of Technique

The estimate of flow velocity obtained above is of limited value since the temperature gradient along the melt was continually changing during the velocity measurement. In order to determine the

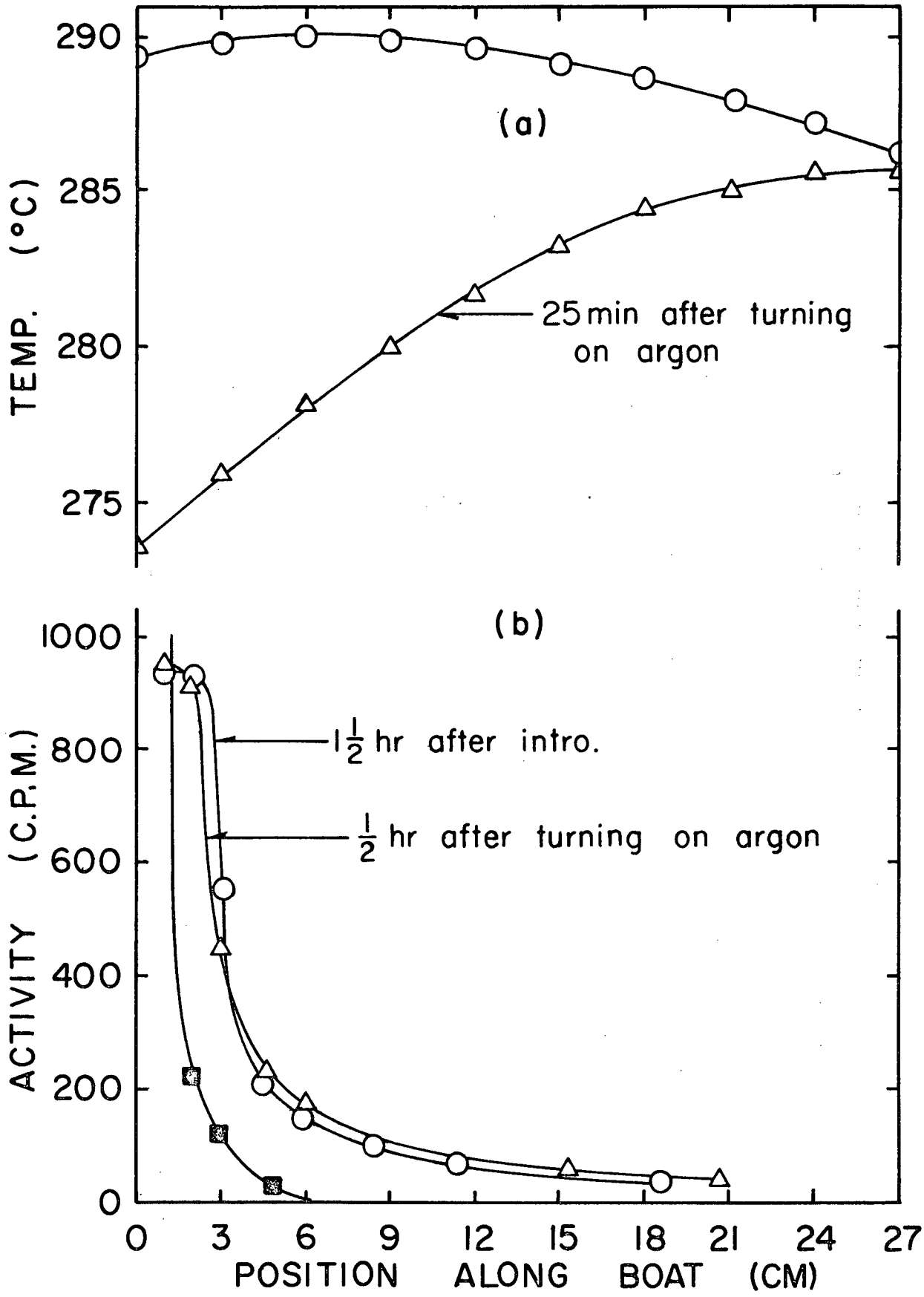

Figure 15. (a) The temperature profiles before and after passing argon.
(b) The distribution of tracer at the times indicated.

relationship between temperature gradient and flow velocity it is necessary to introduce the tracer into the melt after a steady state temperature distribution has been attained. Although the amount of mixing associated with tracer introduction may be small compared to flow velocities which would occur at higher temperature gradients, the anomalous phenomenon displayed in Figure 15 necessitated that subsequents attempts at tracer introduction be carried out in the covered section of the boat.

2.1.4. Tracer Introduction by Rotating a Vertical Cylinder Situated in the Covered Section of the Graphite Boat

2.1.4.1. Experimental Apparatus and Procedure

Introduction of tracer into the covered section of the boat was accomplished using the apparatus shown in Figure 16. The graphite boat was essentially the same as that used previously, that is, two channels and an overall melt length of 27 cm. Modifications included the addition of a graphite heating block and a copper cooling block, (coated with a graphite suspension, Aquadag). The heat source for the heating block was a resistance winding powered by a Variac. Argon flow through the cooling block was measured and controlled by a Victrometer model 0158 flowmeter. The tracer was loaded into the introduction cylinder in the same way as described in Section 2.1.3.1. Introduction of tracer into the melt was accomplished by rotating the introduction cylinder, Figure 16(b), until the square hole in the cylinder and the clear channel were aligned. Stainless steel guides and stops (not shown in the diagram) were employed to insure that the cylinder could be manipulated to the fully opened or fully closed positions remotely. Overall

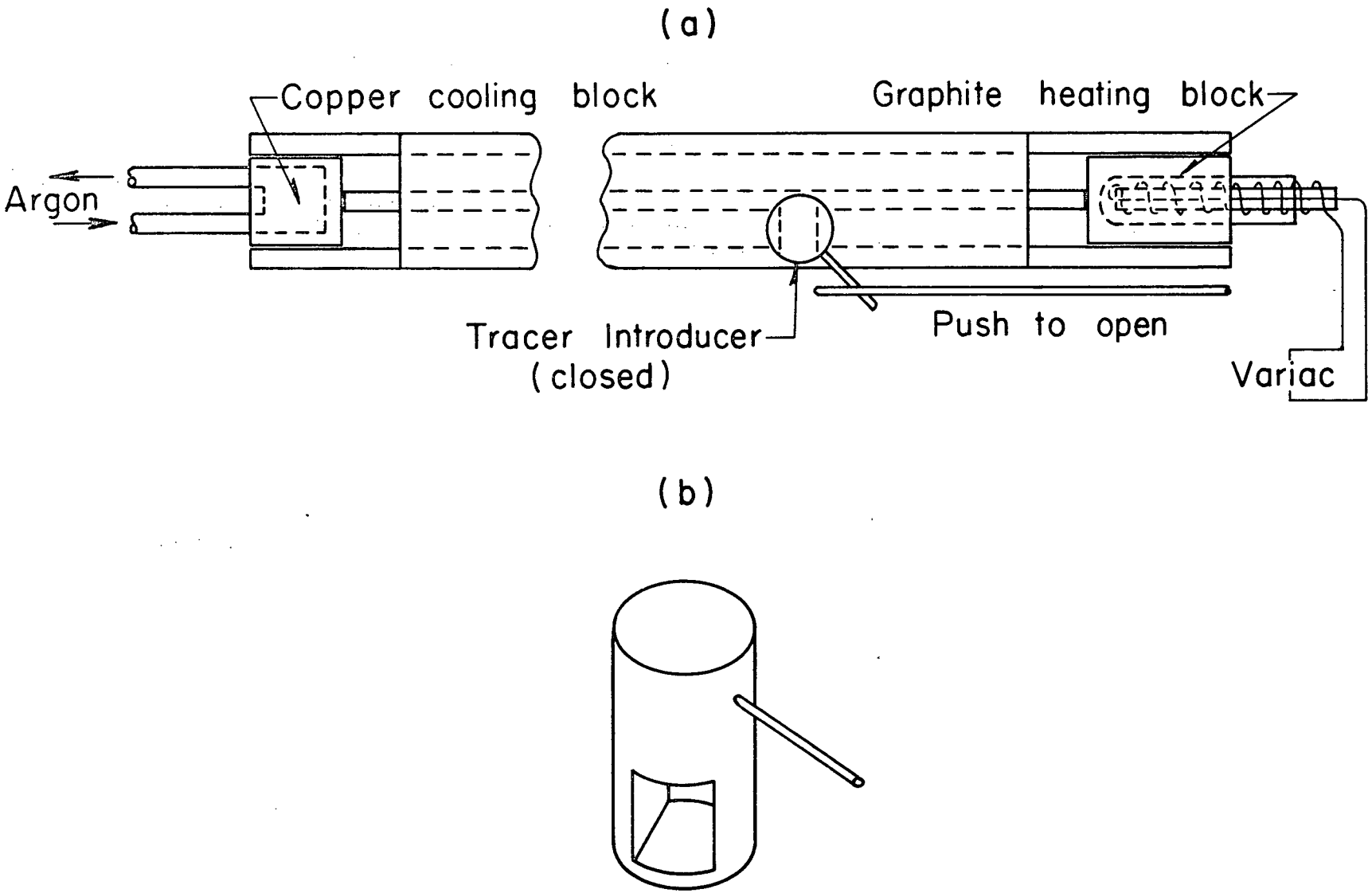

Figure 16. (a) Details of the graphite boat employed for experiments in which the tracer was introduced in the covered section of the melt. (b) Tracer introduction cylinder.

experimental set-up and monitoring techniques were the same as described earlier.

2.1.4.2. Results and Discussion

To determine the amount of flow associated with this introduction technique tracer was introduced when the melt had a stable zero temperature gradient along its entire length. Sn^{113} was used as the trace isotope to remove the possibility of solute convection. Figure 17(a) shows the results of introducing Sn^{113} tracer into a melt having zero gradient. Appreciable flow has accompanied tracer introduction as the tracer has moved approximately 10 cm in 40 minutes. To ascertain whether or not the mixing on introduction was due solely to rotating the cylinder (and possibly disturbing the boat) an experiment was undertaken in which the tracer introducer was placed in the fully opened position prior to melting and the temperature was gradually raised (maintaining a flat temperature distribution) until melting occurred. The results of this experiment are shown in Figure 17(b). The movement of tracer along the boat was almost as far as occurred in Figure 17(a). This indicated that the rotation of the cylinder to effect tracer introduction was not the major cause of the fluid flow associated with the introduction of tracer.

2.1.4.3. Evaluation of Technique

The results shown in Figure 17 indicated that rotation of the cylinder was not a major cause of flow associated with introduction; they also clearly showed that flow did occur under thermal conditions which

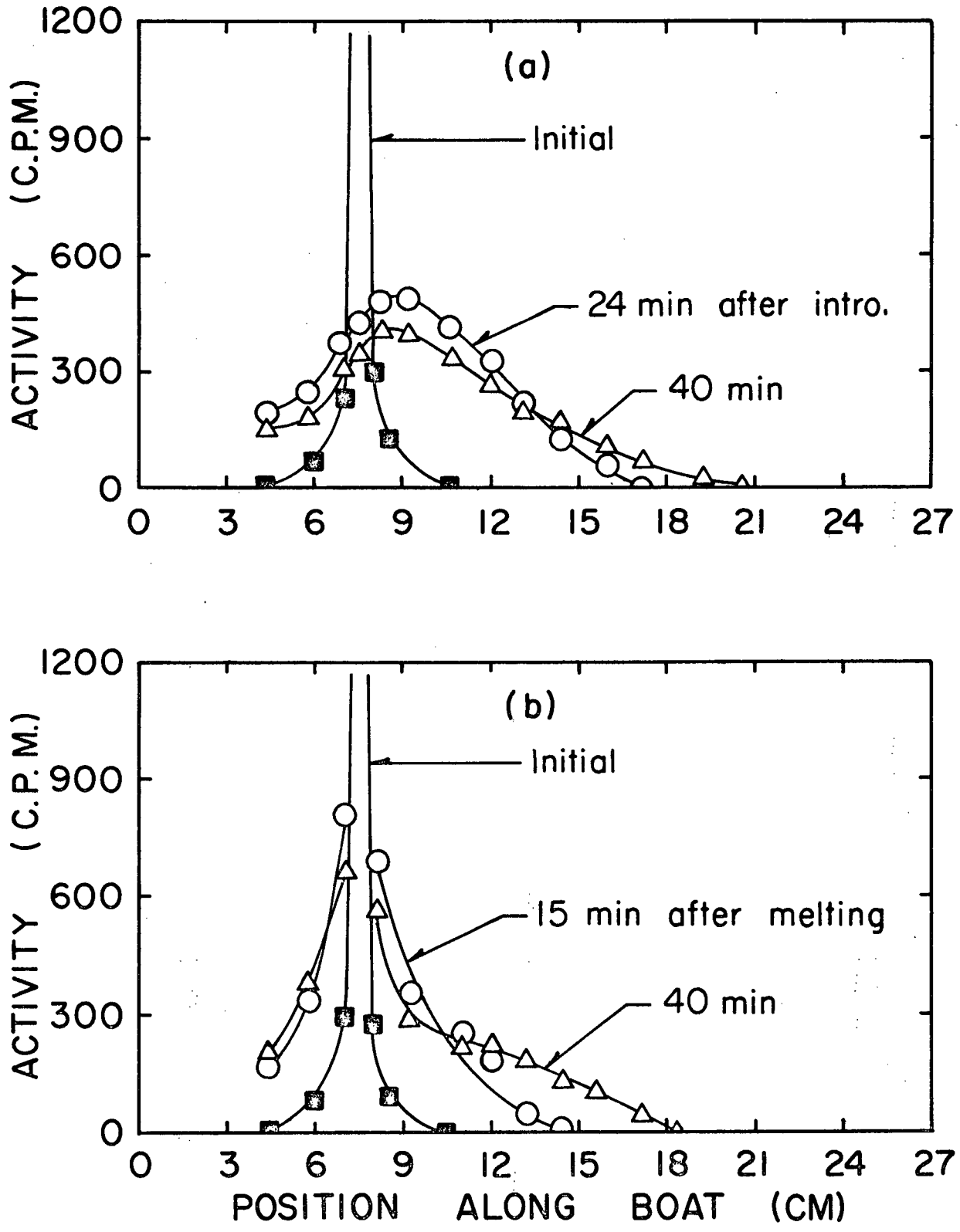

Figure 17. The distribution of Sn^{113} (in a pure Sn melt having zero horizontal temperature gradient) before and after (a) tracer introduction and (b) melting with the introduction cylinder in the open positions.

have heretofore been shown to be unfavourable. Therefore, this technique was temporarily abandoned in hopes of developing a method of introduction which would in no way alter the fluid flow that was occurring prior to tracer introduction.

2.1.5. Tracer Introduction by Rotating a Horizontal Cylinder Located in the Cover of the Graphite Boat.

2.1.5.1. Experimental Apparatus and Procedure

The only difference between the graphite boat used for this section of the investigation and the one shown in Figure 16 is the method of tracer introduction. Details of the introduction technique are shown in Figure 18. In order to prevent any interaction between the tracer introducer and the melt the introduction cylinder was placed in the boat cover. To introduce tracer the cylinder opening was rotated into alignment with the hole in the cover. Flow past the hole should then draw tracer out into the melt. The movement of tracer, due to the fluid flow present, could then be monitored by the procedure described earlier.

2.1.5.2. Results and Discussion

Three different trace isotopes, Sn^{113}, Ag^{110} and Tl^{204} were used to evaluate the effectiveness of the tracer introduction technique shown in Figure 18. Initial experiments were conducted using Sn^{113} as the trace isotope, therefore, there would be no solute convection to interfere with the thermal convection. When the tracer introducer or "gate" was opened to the melt under conditions of zero horizontal

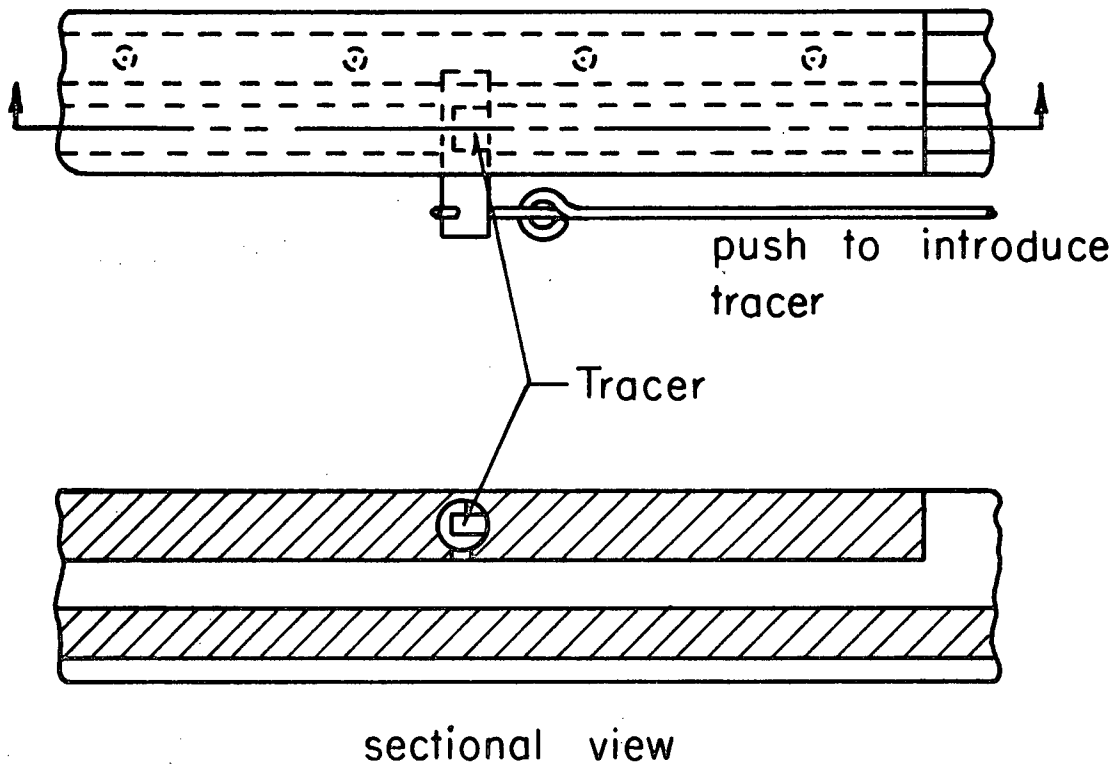

Figure 18. Details of tracer introduction from the boat cover.

temperature gradient no detectable change in the tracer distribution occurred over a half hour period. The gate was then closed and the gradient in the melt was changed such that thermal convection would be expected. The gate was then reopened. Even under conditions favourable for flow no change in the tracer distribution along the boat was observed. The tracer had not entered the melt.

To assist introduction of tracer into the melt a 30 wt % Tl^{204} in Sn alloy was used in a subsequent experiment. Since Tl^{204} is a soft β-emmitter, the relatively high weight per cent of Tl^{204} in the trace alloy was necessary to facilitate monitoring. This alloy was then appreciably more dense than the pure tin melt (1.133 ρSn) and would be expected to enter the melt by solute convection after opening the gate. This was confirmed experimentally as the tracer profile became uniform approximately 4 minutes after opening the gate, Figure 19(b). With the temperature distribution shown in Figure 19(a) one would expect tracer movement to be predominantly to the left of its original position as this would follow the thermal convective flow pattern expected. That is, the more dense fluid moving from the cold end to the hot end along the bottom of the channel. Autoradiography of the quenched melt clearly showed that the trace alloy had fallen to the bottom of the channel and spread in both directions. Solute convection must then have overcome the thermal convective flow.

To reduce the density of the trace alloy but still maintain a high enough specific activity an alloy of 0.5 wt % Ag^{110} in Sn was prepared. This alloy had a specific activity high enough to facilitate monitoring and it was slightly more dense than the pure tin (1.0013 ρSn) thus

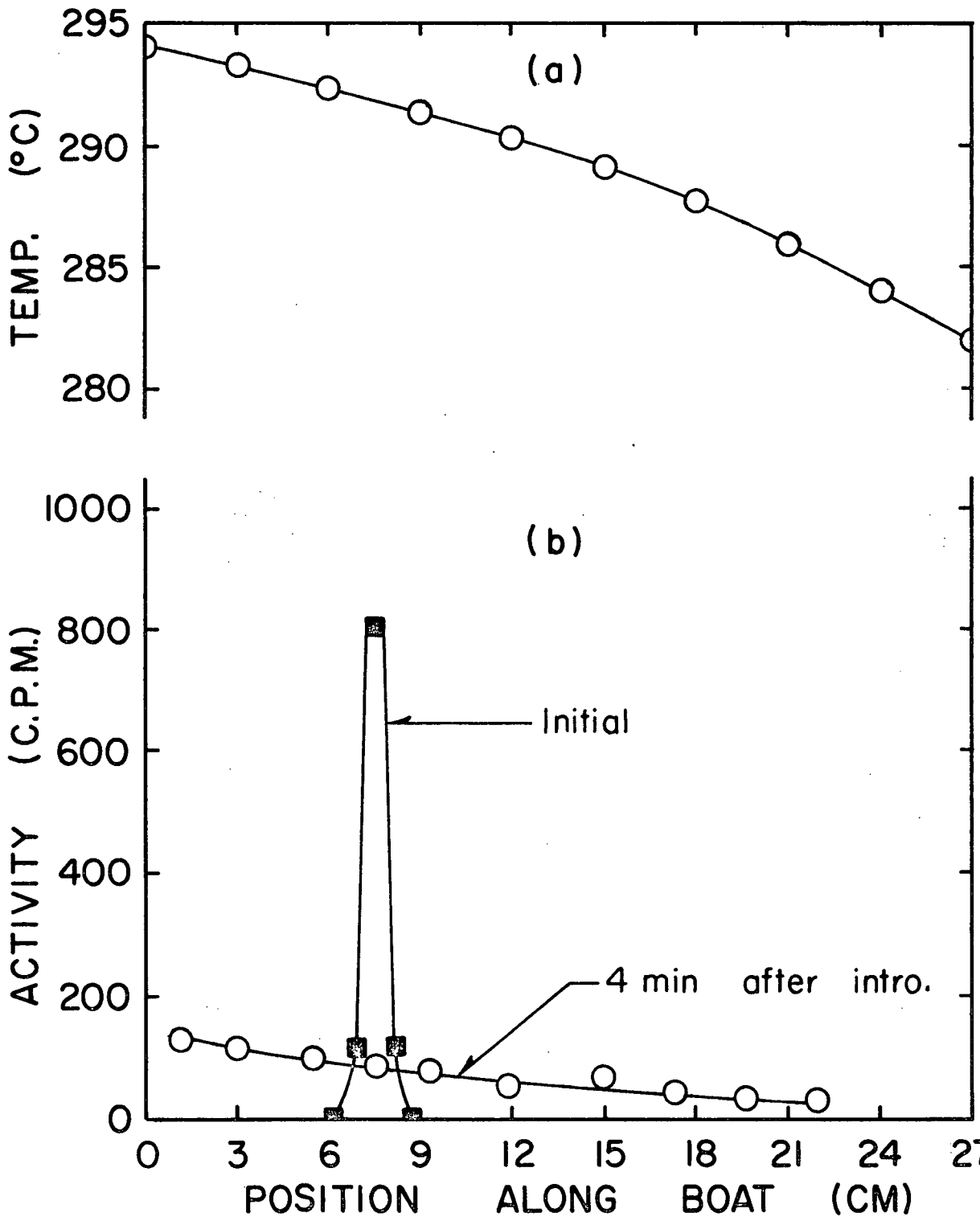

Figure 19. (a) The temperature profile along the melt. (b) The distribution of Tl^{204} before and after tracer introduction.

aiding introduction into the melt. Opening the gate with a zero gradient along the melt produced negligible flow along the channel over a 20 minute interval. The gate was closed and the temperature distribution adjusted to that shown in Figure 20(a). Figure 20(b) shows the resulting movement of tracer. As expected the more dense trace alloy moved to the left of the place of introduction.

2.1.5.3. Evaluation of Technique

Experiments using Sn^{113} showed that this tracer introduction technique depends on solute convection for entry of trace alloy into the melt. That is, the tracer must be more dense than the melt. If the tracer is too dense, as was the case with the 30 wt % Tl^{204} in Sn alloy, it interfered with or overcame the thermal convective flow present. Even the reasonably successful experiment with the 0.5 wt % Ag^{110} in Sn trace alloy requires that the slightly more dense tracer drop from the top to the bottom of the melt in order to follow the thermal convective flow. How this interferes with the thermal convection is not known. Also, this method of tracer introduction leads to continuous dilution of the tracer even as the tracer is being introduced thus making detection of the passage of tracer over a given collimator position more difficult. A far more desirable technique would allow introduction of a concentrated amount of tracer into a small area within a short period of time. Such a technique is described in the following section.

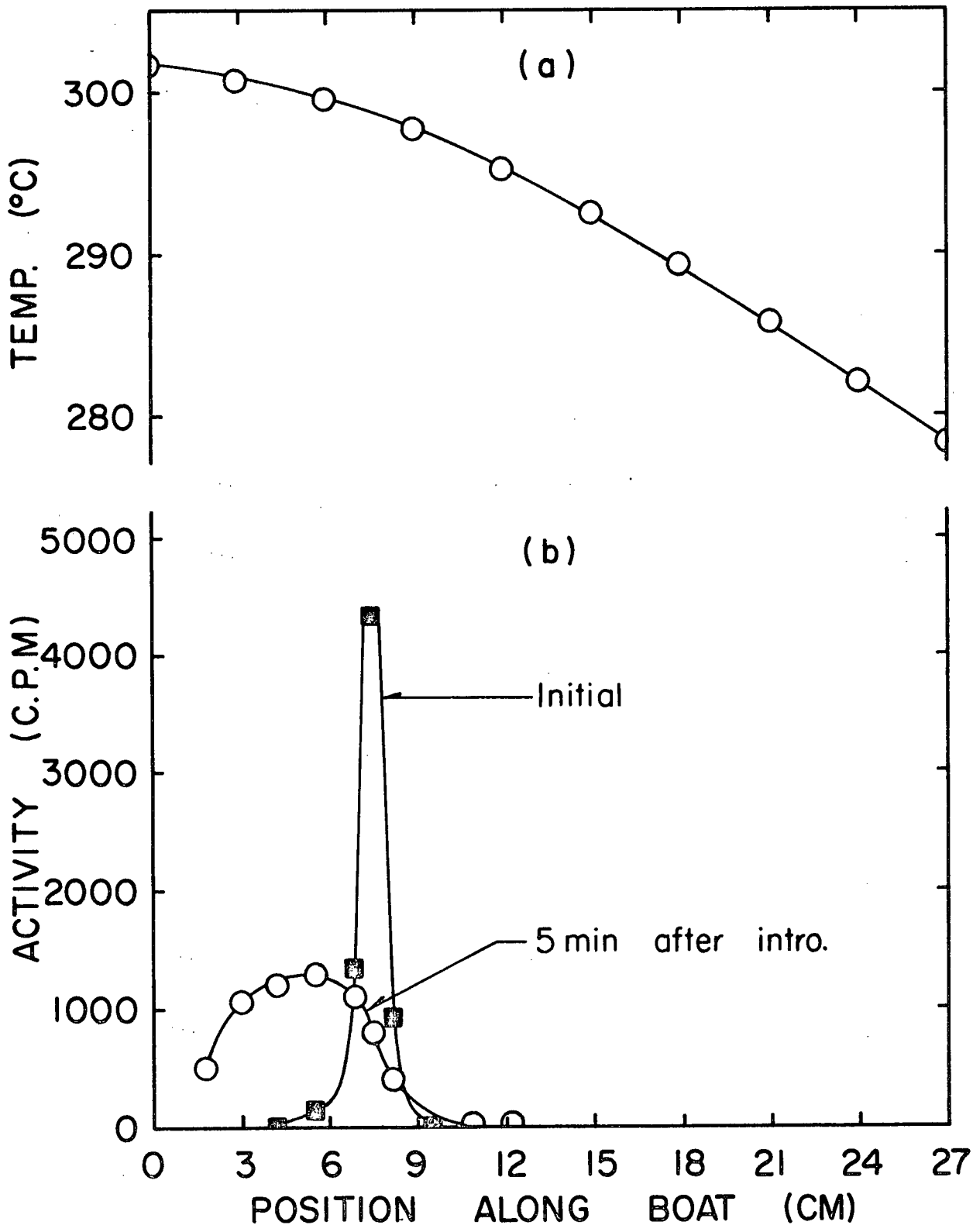

Figure 20. (a) The temperature profile along the melt. (b) The distribution of Ag^{110} before and after tracer introduction.

2.1.6. Tracer Introduction by Rotating a Horizontal Cylinder Located in the Cover of the Boat and then Gently Pushing Tracer into the Melt.

2.1.6.1. Experimental Apparatus and Procedure

Figure 21 shows the modifications that were made to the introduction technique illustrated in Figure 18. A piston arrangement has been added to facilitate rapid introduction of tracer into the melt and thus avoid the tracer dilution problem discussed in the previous section. Tracer introduction was accomplished by rotating the gate to the open position and then gently forcing the tracer into the melt with the piston mechanism shown in Figure 21(b).

Detection of tracer movement was carried out as described previously. Data typical of that obtained employing the new introduction technique appears in Figure 22. The two curves represent the change in activity observed above two collimator positions "downstream" from the place of introduction. The monitoring positions were 6.3 cm apart. The first position was approximately 3 cm away from the gate to reduce the effects on the observed flow velocity, of transients associated with introduction. Activities plotted are average count rates over a 30 second time interval. The time required for movement of tracer between the two collimator positions was determined by measuring the time difference between the intersections of the extrapolations of the activity-time curve and the abscissa. Justification of this method of analysis is presented later in the thesis. Observed flow velocity was then calculated by dividing the known separation of 6.3 cm by the measured time difference.

The variation in observed flow velocity with temperature

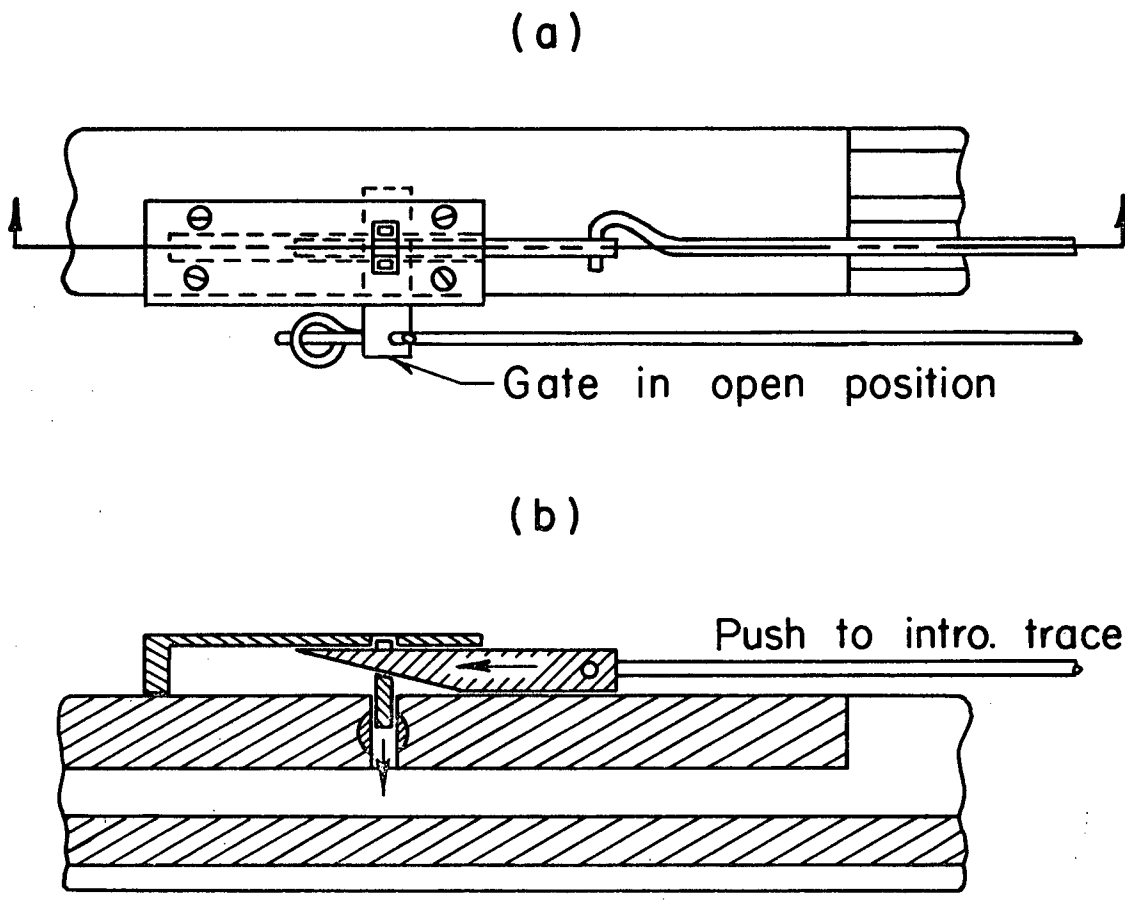

Figure 21. Details of mechanism used to facilitate tracer introduction from the boat cover. (a) Top view (b) Side sectional view.

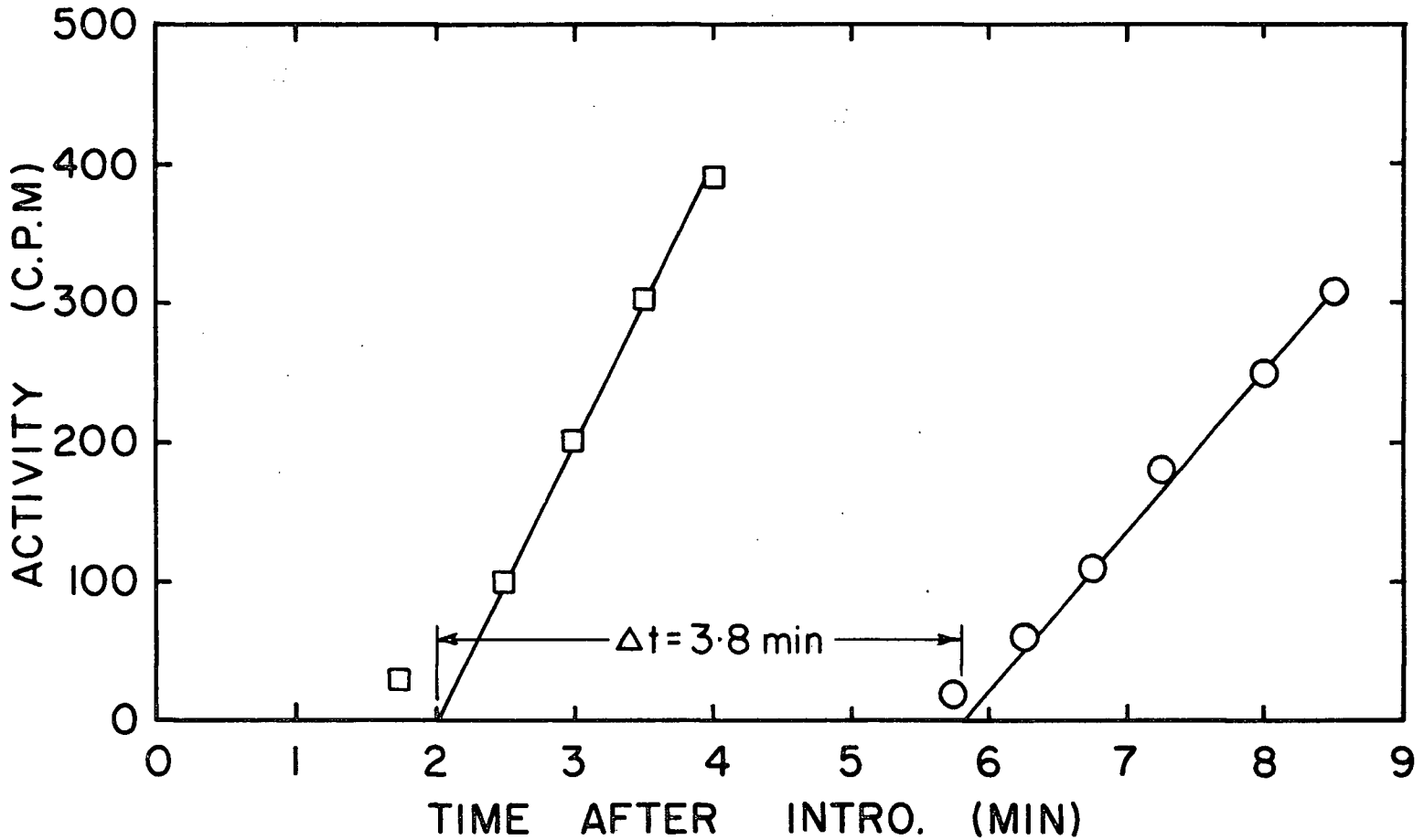

Figure 22. Typical activity versus time data for experiments employing forced tracer introduction from the boat cover.

difference between the hot and cold ends was studied using a 1% Sb^{124} in pure Sn trace alloy. Sb^{124} was chosen as the trace isotope as it is a strong γ - emmitter of high specific activity and because it is slightly less dense than pure Sn (0.9993 ρSn). Since the tracer is less dense than the tin, it should tend to remain near the top of the melt in moving from the hot end to the cold end. Thus, motion of tracer from the top to the bottom of the melt by solute convection will not occur as it did with the more dense Ag^{110} and Tl^{204} alloys. Sn^{113} is not a suitable isotope for velocity measurements since flow along the boat causes dilution of the isotope, which has a low specific activity relative to Sb^{124}, and makes detection of its presence above a given collimator position difficult.

Although Sn^{113} is not a good trace isotope for the collimated monitoring system used to determine flow velocities, its low energy radiation makes it an acceptable tracer for autoradiography experiments. For this reason Sn^{113} trace alloys were used to determine flow patterns in the melt and to evaluate the tracer introduction technique. A series of specimens to be autoradiographed was prepared by quenching the melt (by filling the Vycor tube with water) at various times after tracer introduction and with different temperature distributions. Autoradiographs were obtained by placing the quenched specimens on double emulsion X-ray film in light tight boxes. Areas of the film adjacent to regions of tracer appear darkened on developing. All autoradiographs which appear in the thesis have been printed such that dark regions indicate the presence of tracer.

2.1.6.2. Results and Discussion

2.1.6.2.1. Flow Velocity Measurements

The variation of flow velocity with temperature difference between the hot and cold ends of the boat is shown in Figure 23. The increase in flow velocity with increasing temperature difference across the melt was expected, however, the large degree of scatter made it impossible to determine the form of the relationship between these two variables.

2.1.6.2.2. Autoradiography

The extent of flow associated with tracer introduction was evaluated by introducing tracer into a melt having zero horizontal temperature gradient and then quenching the resulting tracer distribution. The possibility of solute convection was avoided by employing Sn^{113} as the trace isotope. Autoradiographs of specimens quenched 0.5, 1 and 10 minutes after introduction of the tracer are shown in Figure 24. It is evident that appreciable mixing accompanies introduction of tracer. What is more significant is that the tracer has not only spread through the melt, under conditions where convective flow would not be expected, but has also spread in a nonreproducible and unexpected manner. One might expect a slight amount of tracer dispersion to be associated with the forcing of the tracer into the melt via the piston mechanism. This is shown to be so in the specimen which was quenched 0.5 minutes after introduction, Figure 24(a). Since the horizontal gradient in the melt was zero and the trace alloy the same density as the melt, specimens

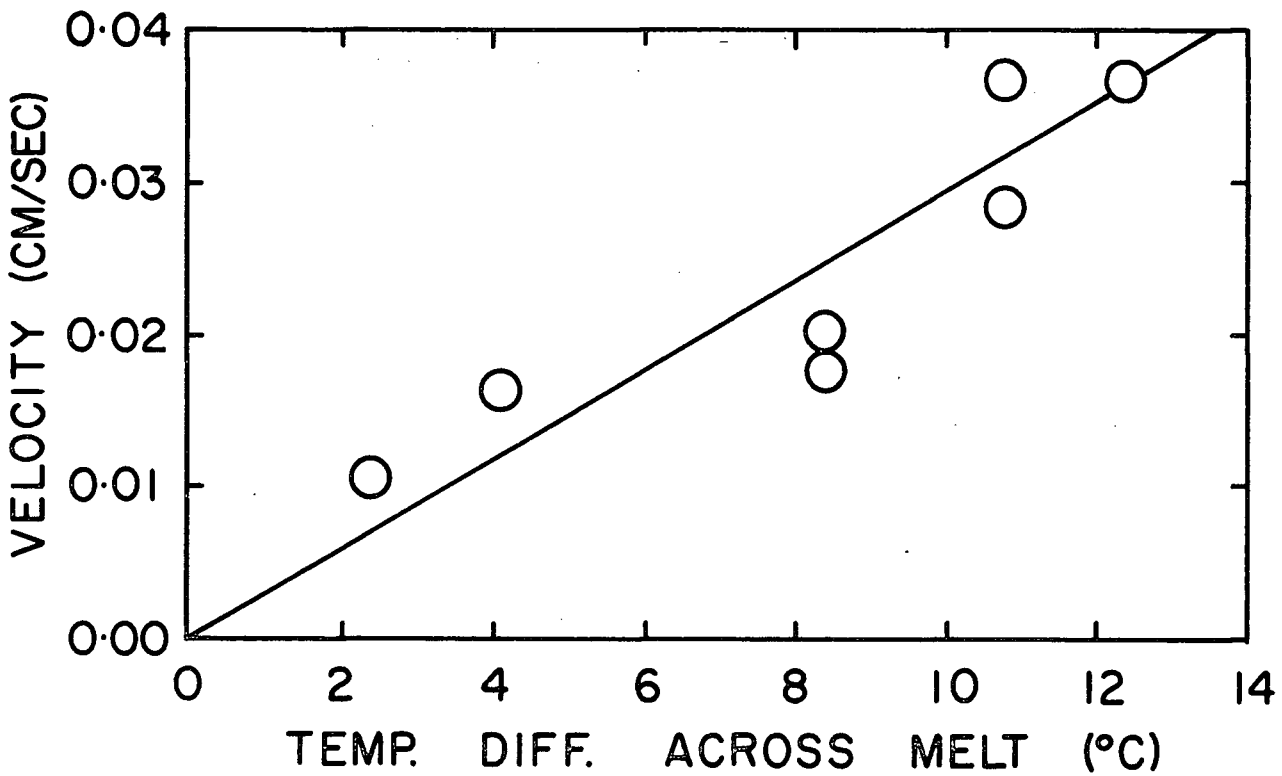

Figure 23. The dependence of flow velocity on the temperature difference between the hot and the cold ends of the melt.

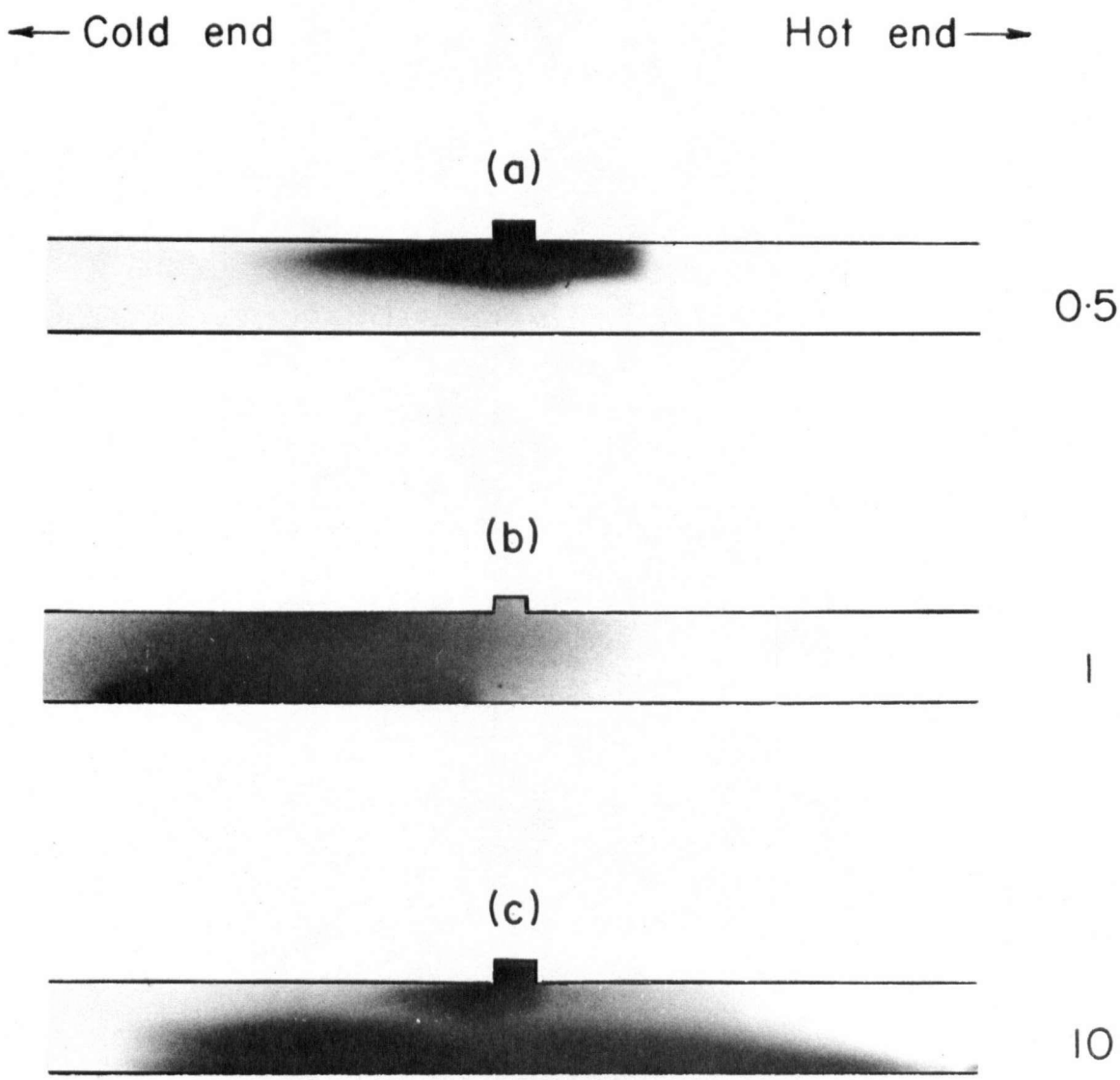

Figure 24. Longitudinal section autoradiographs of specimens quenched (a) 0.5 minutes (b) 1 minute and (c) 10 minutes after tracer introduction into a melt having zero horizontal temperature gradient.

quenched at times greater than 0.5 minutes after introduction should show no further redistribution of tracer. However, Figure 24(b) shows movement of tracer towards the cold reservoir and to the bottom of the channel. The specimen quenced 10 minutes after introduction of tracer again shows movement of tracer to the bottom of the channel but in this case the redistribution about the point of introduction is quite uniform.

Figure 25 contains transverse section autoradiographs of a specimen quenched one minute after introduction of tracer into a melt having zero horizontal temperature gradient. These autoradiographs show a double cell flow pattern in the transverse direction. This suggests that the tracer must be more dense than the melt. Even with a 70 °C temperature difference between the hot and cold ends the transverse flow pattern maintains its double cell appearance, Figure 26. Since the average time required to quench the melt was of the order of 15 seconds it was questioned whether flow patterns observed reflected the flow patterns that existed prior to quenching, or, whether the double cell appearance was a quench effect. In order to study the effect of the quench on the observed flow pattern a series of experiments was carried out in which the quench was initiated from the top side of the melt. (Recall, that to this time quenching was accomplished by filling the Vycor tube with water, therefore, the quench was initiated at the bottom of the melt). Any major change in the observed flow pattern for a given set of experimental conditions would then illustrate the presence of a quench effect. A spray tube over the covered section of the boat was employed to facilitate quenching. Both opened reservoirs were covered with stainless steel caps and sealed with Sairset cement to pre-

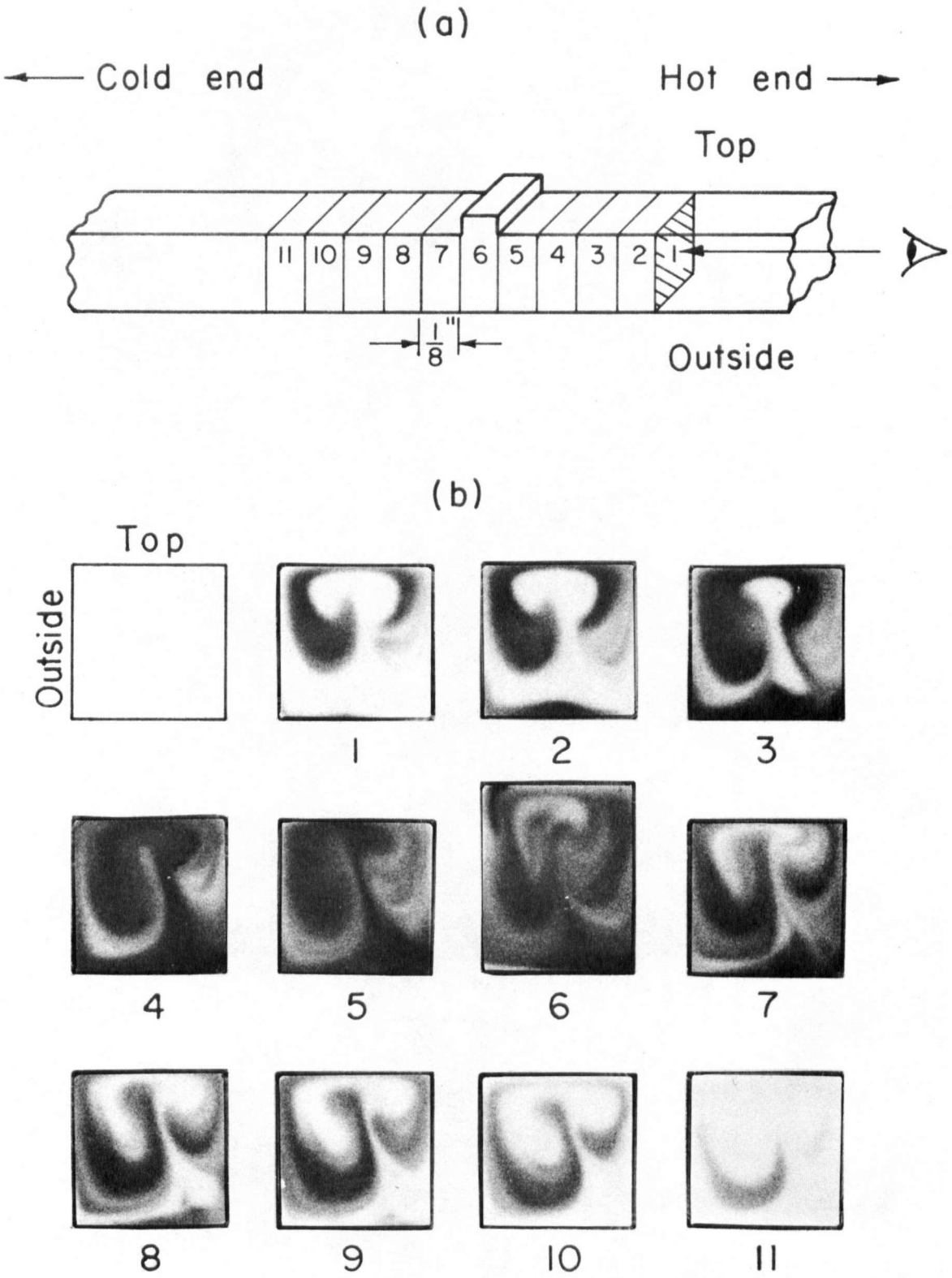

Figure 25. (a) Position from which autoradiographs were obtained. (b) Transverse section autoradiographs (from positions indicated in (a)) of a specimen quenched 1 minute after tracer introduction into a melt having zero horizontal temperature gradient.

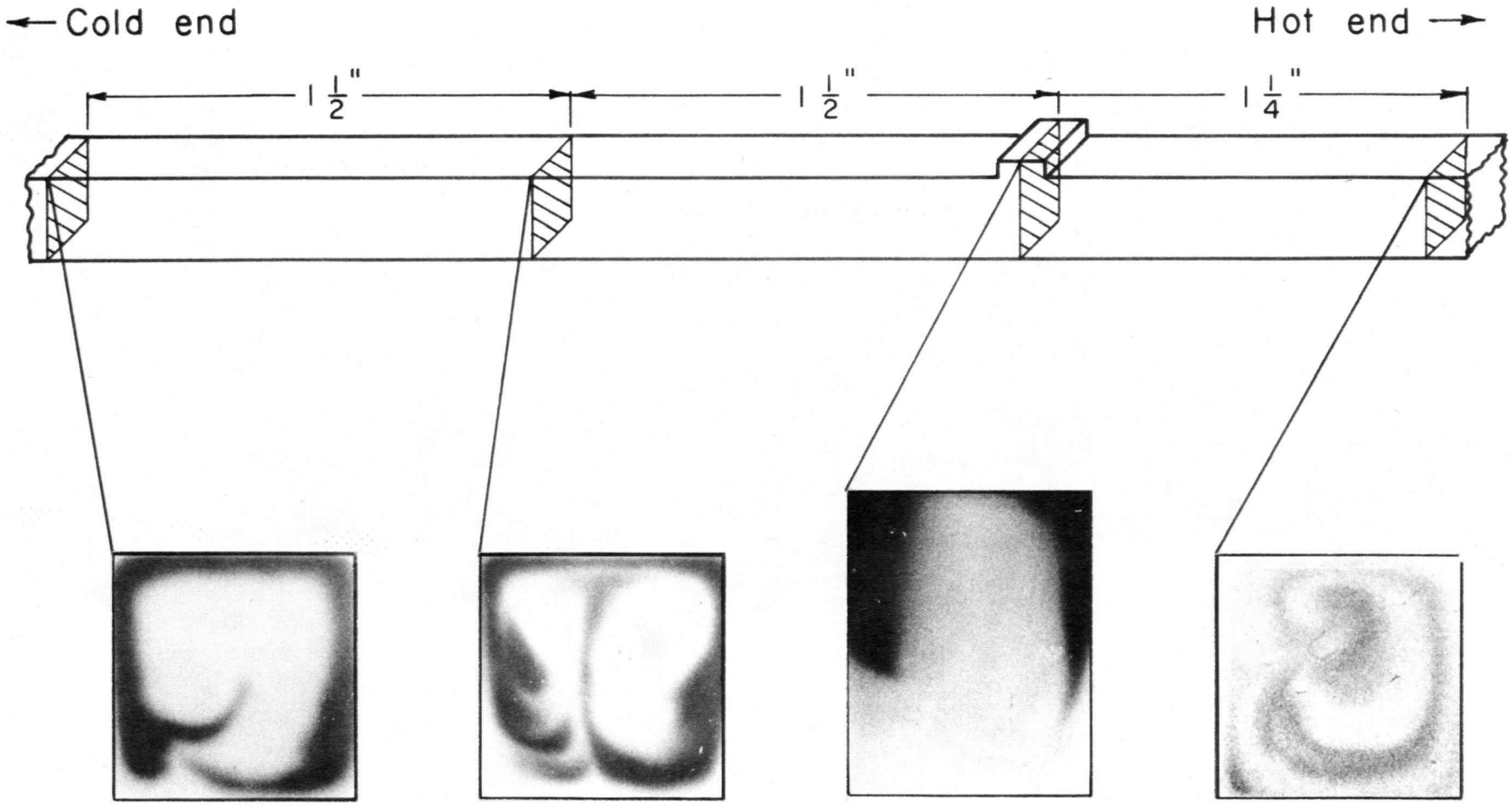

Figure 26. Transverse section autoradiographs (from the positions indicated) of a specimen quenched 1 minute after introduction of tracer into a melt having a 70 °C temperature difference between the hot and cold ends.

vent quench water contacting the molten tin. The top quench tests proved to be unsuccessful as it was impossible to prevent water from seeping into the melt. This resulted in radioactive tin being sprayed throughout the Vycor tube yielding an obviously unrepresentative flow pattern. In order to reduce the quench time a different type of boat was developed and the results of autoradiography studies using this boat will be discussed in Section 3.

2.1.6.3. Evaluation of Technique

Although it was not possible to confirm the accuracy of the autoradiographs obtained, it was apparent that the tracer was more dense than the melt. Quenching from the bottom first (normal procedure) should create an initial condition of cooler liquid below warmer liquid and therefore one would not expect the double cell pattern observed to be a result of such quenching. Since the melt and trace alloy were of identical chemical composition, that is, pure tin and pure tin containing radioactive tin, the possibility of solute convection must be ruled out. The higher density of the tracer must reflect the fact that the tracer is at a lower temperature than the melt into which it is introduced. Since the tracer is originally located in the cover of the boat and the tracer introduction mechanism extends approximately 5/16 inch above the cover (and could thus be effected more by air convection in the Vycor tube), it is not unreasonable that the tracer could be slightly cooler than the melt below it. This would account for the double cell flow pattern observed in the transverse section autoradiographs. From Figure 24(b) it was apparent that this tracer introduction

technique can cause a net flow of tracer in one direction rather than a uniform spread about the point of introduction. Flow due to forcing the tracer into the melt was probably the main cause of the scatter observed in Figure 23 and therefore this introduction technique was abandoned.

2.1.7. Return to Introduction by Rotating a Vertical Cylinder Located in the Covered Section of the Channel

2.1.7.1. Experimental Apparatus and Procedure

Research to this point in the investigation has shown that:

(1) Tracer must be introduced in the covered section of the boat to avoid the anomalous results caused by the convective currents in the uncovered reservoirs at the end of the graphite boat (Section 2.1.3.).

(2) Tracer cannot be held in the boat cover as this causes the tracer to be cooler than the melt (Section 2.1.6.2.2.). This results in the formation of a double cell flow pattern in transverse section and thus interferes with the convective flow that would normally occur under similar experimental conditions.

Of the five introduction techniques studied introduction of tracer by rotating a vertical cylinder located in the covered section of the boat appears most satisfactory. Therefore, the introduction technique discussed in Section 2.1.4.1. and illustrated in Figure 16 was readopted. In order to facilitate greater flexibility in the establish-

ment and control of experimental temperature distributions the following modifications were made to the furnace and furnace power supply. A 0 to 92 ohms rheostat was placed in series with one of the end furnace windings to enable establishment of steeper temperature gradients along the furnace, Figure 27(a). The Variac power supplies were replaced by the dual zone power supply and temperature controller shown in Figure 27(b). The control thermocouple was located between the two central furnace windings. The temperature gradient along the furnace could then be adjusted by manipulation of the central and end windings power discriminators and the 0 to 92 ohm rheostat. Average furnace temperature was adjusted and maintained with the thermocouple bucking potentials and Honeywell controller. As before, the temperature difference across the melt could be further adjusted by the heating coil and cooling block shown in Figure 16.

Flow velocity measurements were carried out in the following way. The furnace power, heating coil power and argon flow rate through the cooling block were adjusted to give a desired temperature distribution along the melt. This temperature profile, as monitored by the Honeywell Electronic 194 recorder, was maintained for approximately one hour to insure steady state heat transfer through the boat and melt. The tracer was then introduced into the melt and the movement of tracer resulting from the convective flow present was monitored by the moveable collimator-scintillation counter assembly described earlier. As in Section 2.1.6., the first collimator position was approximately 3 cm away (towards the cold end) from the place of introduction. Once it was apparent that the tracer had passed this position the collimator was moved 6.3 cm "down-

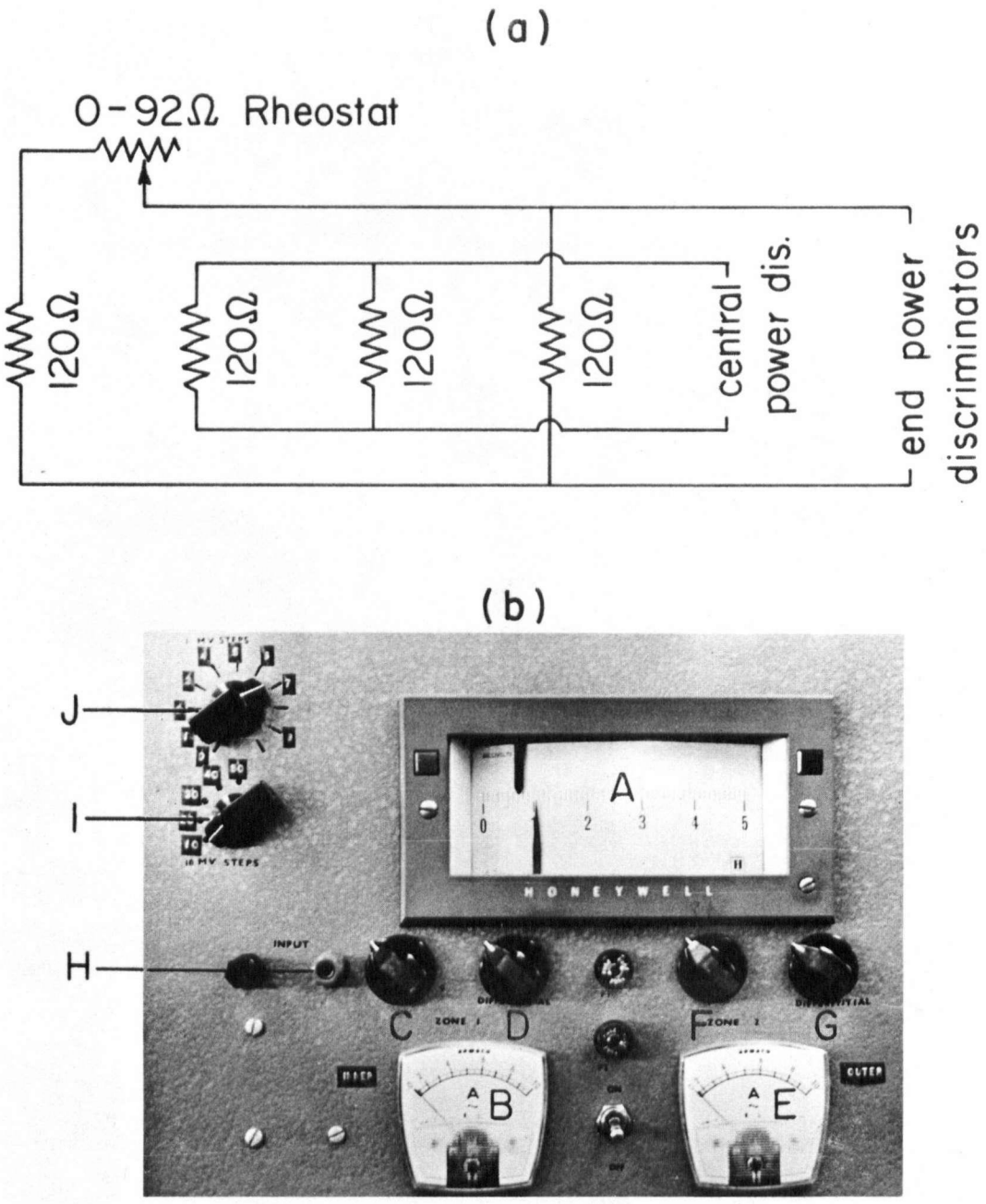

Figure 27. Tube furnace wiring diagram. (b) Details of furnace temperature controller.

A 0-5 mv Honeywell Controller
B Ammeter for center windings
C&D Power discriminators for center windings
E Ammeter for end windings
F&G Power discriminator for end windings
H Control thermocouple input
I 0-50 mv (10 mv steps) backing potential
J 0-10 mv (1 mv steps) backing potential

stream" and counting was continued until the tracer was observed to pass. Figure 28 shows a typical activity-time curve; the activities plotted are average count rates over a 15 second time interval. As before, the time required for flow of tracer from one collimator position to another was determined by measuring the time difference between the intersection of the extrapolation of the activity-time curves and the abscissa. Experiments were conducted to determine:-

(1) The variation of flow velocity with temperature difference between the hot and cold ends of the melt. Sb^{124} was used as the trace isotope for reasons similar to those presented in Section 2.1.6. The trace alloy was 0.46 wt % Sb^{124} in pure tin. Average temperature across the melt was maintained at approximately 312 °C, with 309 °C minimum and 320 °C maximum.

(2) The effect on the observed flow velocity of allowing the average temperature to be outside the limits set above. This was accomplished by conducting velocity determination experiments at 300 °C and 325 °C and then comparing these values with the results obtained in (1).

(3) The effect on observed flow velocity of varying the density difference between trace alloy and melt. To evaluate this effect five experiments were undertaken in which the trace alloy and melt were of the same density. This was accomplished by making the melt composition the same as that of the trace alloy, namely 0.46 wt % Sb in Sn (Sb used in the melt was nonradioactive). The melt was prepared under an argon atmosphere and was stirred periodically for appoximately one half hour to insure homogeniety. Further comparison of flow velocity with trace alloy density was provided by increasing the amount of Sb in the trace alloy to

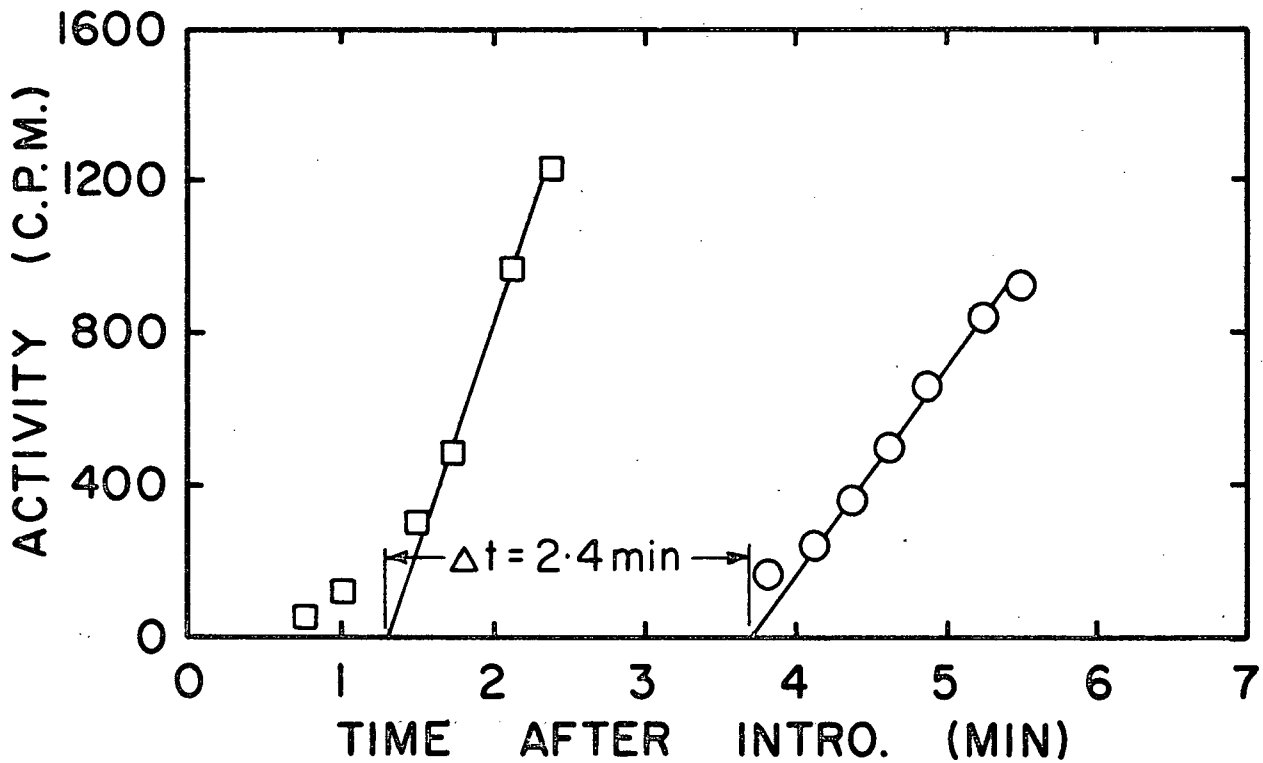

Figure 28. Typical activity versus time data for experiments employing tracer introduction by rotating a vertical cylinder located in the covered section of the melt.

3.0 wt % (by adding nonradioactive Sb), thus making the trace alloy appreciably less dense than the 0.46 wt % Sb^{124} used above.

2.1.7.2. Results and Discussion

2.1.7.2.1. Variation of Flow Velocity with Temperature Difference Across the Melt

The results of experiments to determine the variation of flow velocity with temperature difference between the hot and cold ends of the 27 cm long melt are tabulated in Table 2 and plotted in Figure 29. As expected flow velocity increases with increasing temperature difference along the melt. Furthermore, the results show flow velocity increases linearly with temperature difference over the range of experimental conditions investigated.

2.1.7.2.2. Effect of Varying Average Melt Temperature

To evaluate the effect (on observed flow velocity) of varying the average melt temperature, the results of experiments carried out with average melt temperature of 300 °C and 325 °C have been plotted, Figure 30, for comparison to the results shown in Figure 29. The line which appears in Figure 30 is that which was determined from the data plotted in Figure 29. The minimum and maximum average melt temperatures of the results which determined the relationship obtained in Figure 29 were 309 °C and 320 °C. If average melt temperature had any major effect on the flow velocity one might expect, due to the temperature dependence of viscosity (Table 6), to see the results of the experiment conducted with $\overline{T}$ = 300 °C to lie below the line and those from the test at $\overline{T}$ = 325 °C to lie above the line. Since both points are above the line, it must be concluded that variation in average melt temperature, over the range des-

TABLE 2

Flow Velocity Results

Experiment Number	Average Temp. °C.	Δ Temperature °C	Velocity cm/sec.
1	312	5.5	0.014
2	309	7.1	0.018
3	309	14.5	0.042
4	312	17.6	0.047
5	311	20.2	0.052
6	311	22.7	0.060
7	312	24.2	0.083
8	310	27.2	0.075
9	314	33.2	0.080
10	320	41.8	0.111
11	313	55.5	0.140
12	310	60.8	0.167
13	311	61.6	0.162

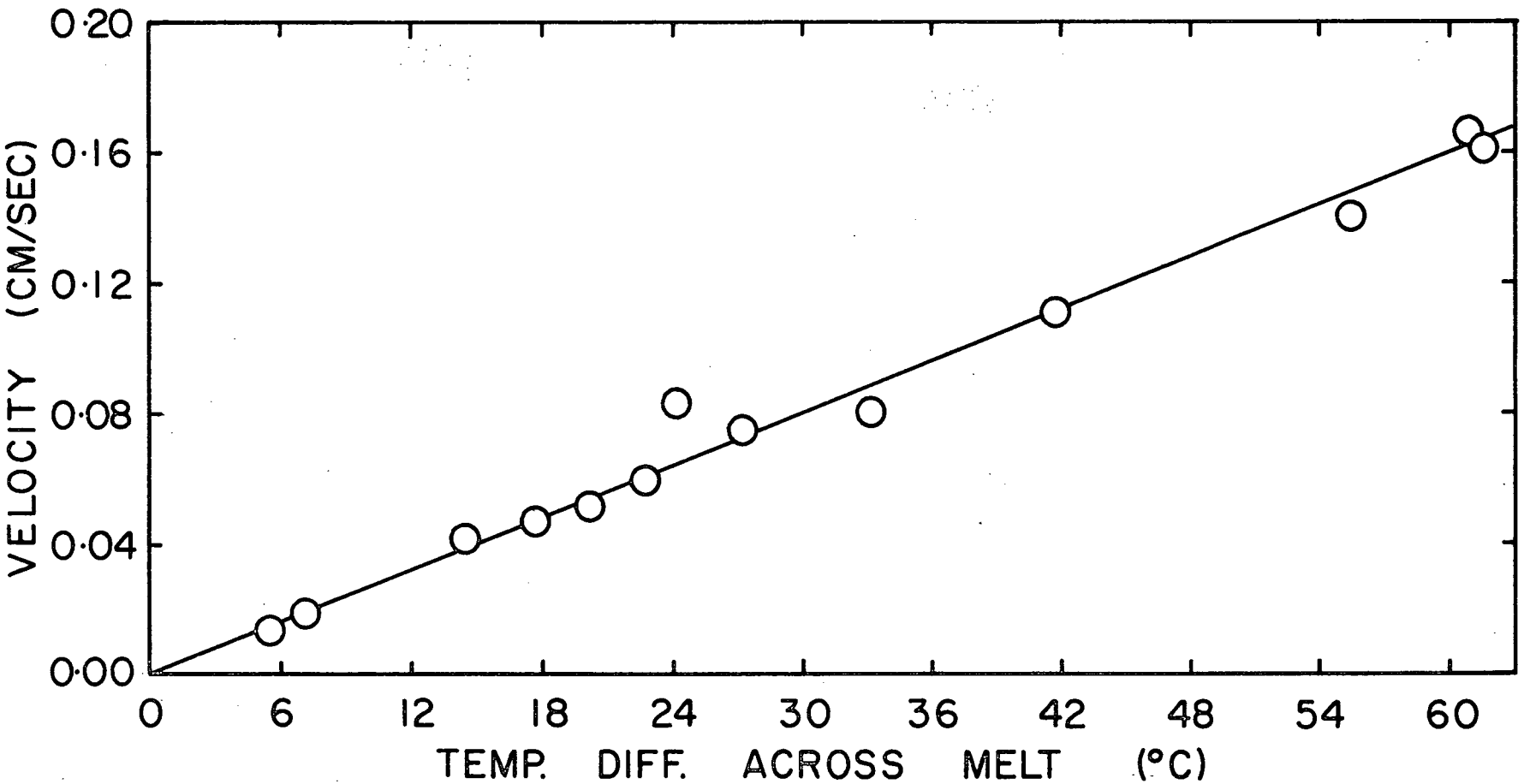

Figure 29. The dependence of flow velocity on the temperature difference between the hot and the cold ends of the melt.

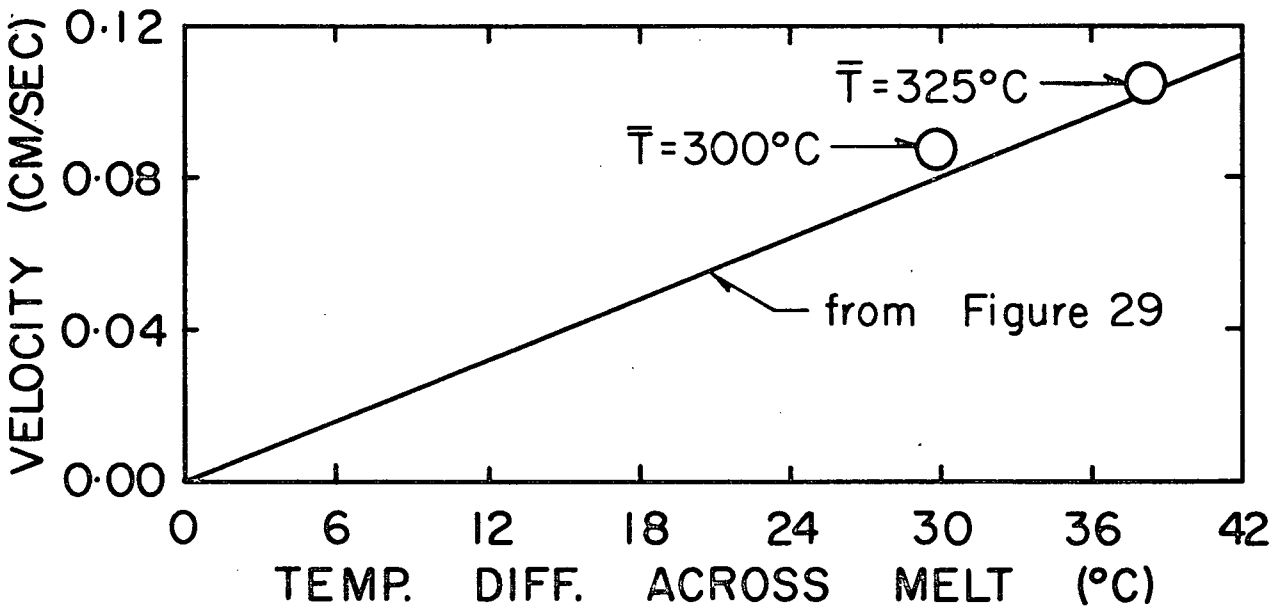

Figure 30. The effect on the flow velocity of varying the average melt temperature.

cribed for these experiments, has no effect on the flow velocity measured by the presently employed monitoring technique. Points which do not fall on the line must then do so because of normal experimental scatter inherent in the tracer introduction and velocity determination techniques.

2.1.7.2.3. Effect of Varying Trace Alloy and Melt Density

Since the trace alloy, 0.46 % Sb^{124} in Sn, used to obtain the results plotted in Figure 29 is less dense than the melt (0.9997 ρSn) it was necessary to determine what effect this density difference might have on the observed flow velocity. Figure 31 shows the results of experiments in which the melt and tracer were of the same composition, namely, 0.46 % Sb in pure Sn.

As in Figure 30, the results are plotted along with the linear relationship obtained in Figure 29. There is excellent agreement between four of the five experimental points and the line. There was no apparent reason for the large deviation displayed by the one point. The results of Figure 31 clearly show that no discrepancy in observed flow velocity occurs as a result of the trace alloy being slightly less dense than the melt. Further evidence of the absence of any major tracer density effect on observed flow velocity is presented in Figure 32. Activity-time curves for three different tracer-melt combinations are plotted:

1) Tracer and melt same density (both 0.46 wt % Sb in Sn)

2) Tracer slightly less dense (0.9997 ρSn) than the melt (tracer 0.46 wt % Sb in Sn, melt pure Sn).

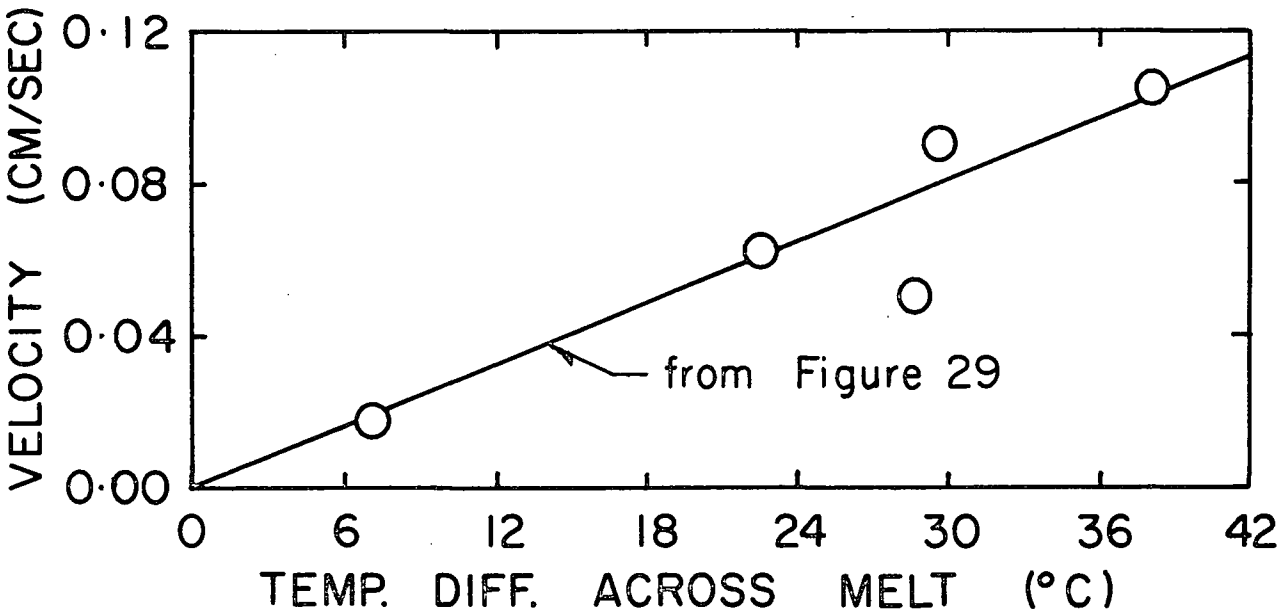

Figure 31. The effect on the flow velocity of having identical trace alloy and melt densities.

3) Tracer appreciably less dense (0.9978 ρ_{Sn}) than the melt (tracer 3.0 wt % Sb in Sn, melt pure Sn).

The temperature difference for all three experiments was approximately 30 °C and the separation between monitoring positions was 10 cm.

To simplify comparison of the curves the time scale of each test has been adjusted so that the time of arrival of tracer at the first monitoring position is coincident. Examination of the points representing the increase in activity at the second monitoring position shows that the time for movement of tracer between the two monitoring positions is essentially the same. The flow velocities in the three cases are therefore the same, from which it may be concluded that trace alloys containing up to 3.0 wt % Sb can be introduced into pure tin melts without solute density differences affecting the flow velocity.

2.1.7.2.4. Evaluation of Technique

The small scatter of the results plotted in Figure 29 indicates that this technique for introducing tracer is acceptably reproducible. Although previous investigations of this technique (Section 2.1.4.) had shown that some fluid flow was associated with tracer introduction the magnitude of the flow must be negligibly small when compared with the velocities which result from thermal convection. This conclusion arises from the fact that the data plotted in Figure 29 lies on a line which passes through zero velocity when zero thermal driving force is present. When the velocities obtained in Section 2.1.6.2.1. are plotted along with those of Figure 29 it becomes apparent that introduction of

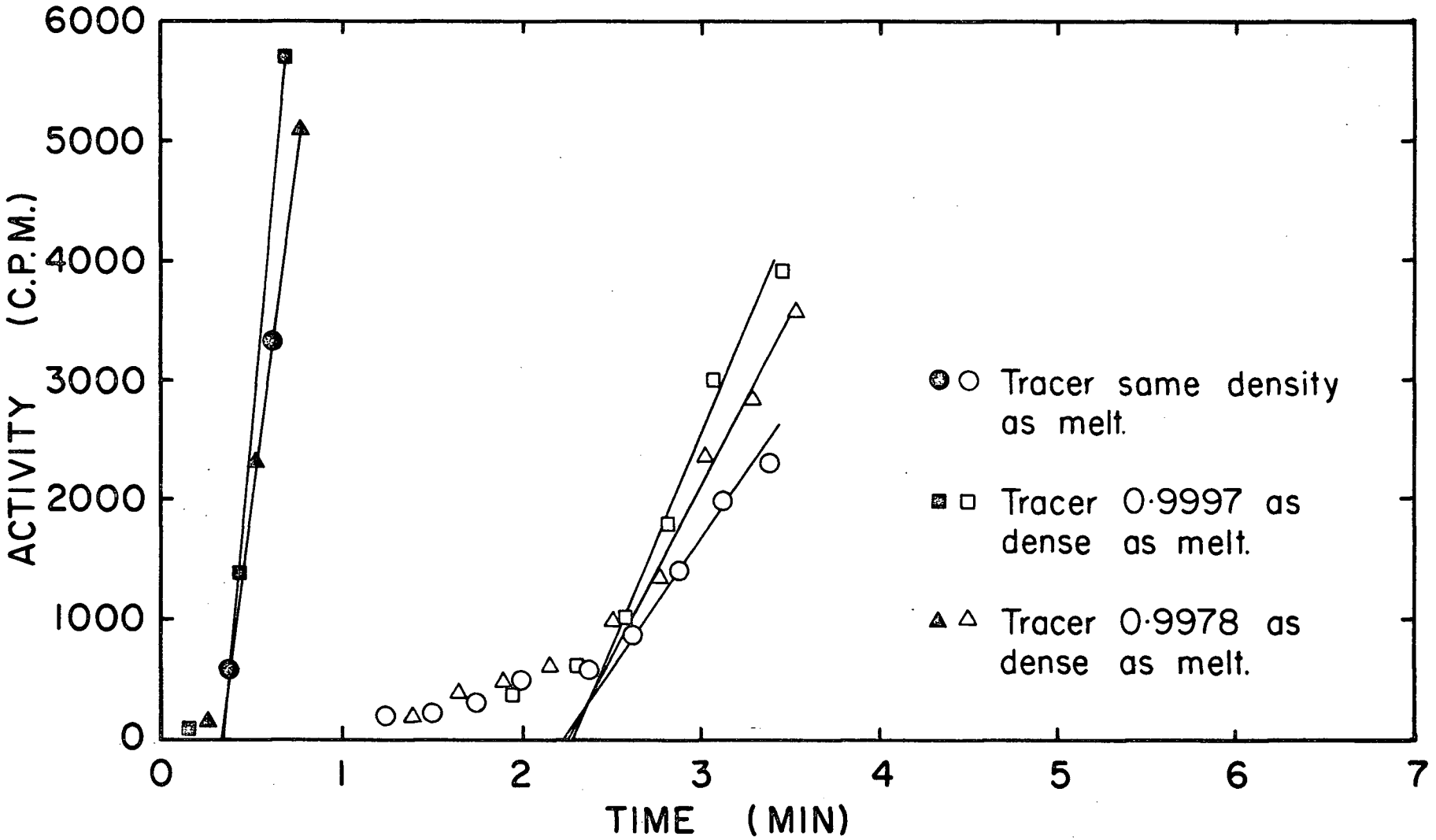

Figure 32. The effect on the flow velocity of varying the density difference between the trace alloy and the melt.

tracer by a piston mechanism has more mechanical mixing associated with it than does the technique just employed. This comparison appears in Figure 33, the filled in circles are from Figure 29 and the open circles which display slightly larger scatter are the results obtained when tracer was introduced by the piston mechanism. The tracer introduction technique of revolving a vertical cylinder located in the covered section of the boat was therefore permanently readopted and employed for all subsequent velocity measurement and autoradiography experiments.

2.1.8. Single Aluminum Channel Supported by Graphite Reservoirs

Although a satisfactory tracer introduction technique has been developed the preliminary autoradiography results presented in Section 2.1.6.2.2. indicated that melts contained in the two channel graphite boat could not be quenched rapidly enough. To decrease the quench time the graphite boat was replaced by a boat constructed of a single aluminum channel with both ends held in graphite reservoirs. The single channel boat was designed primarily to facilitate rapid quenching but was also used for velocity measurement experiments since it was anticipated that the lateral temperature gradients in the aluminum boat might differ significantly from the larger cross-section graphite boat.

2.1.8.1. Experimental Apparatus and Procedure

The new boat is shown schematically in Figure 34. The aluminum channel was 0.64 cm square (inside dimensions) and the overall melt length was 37.5 cm, approximately 10 cm longer than that used in previous

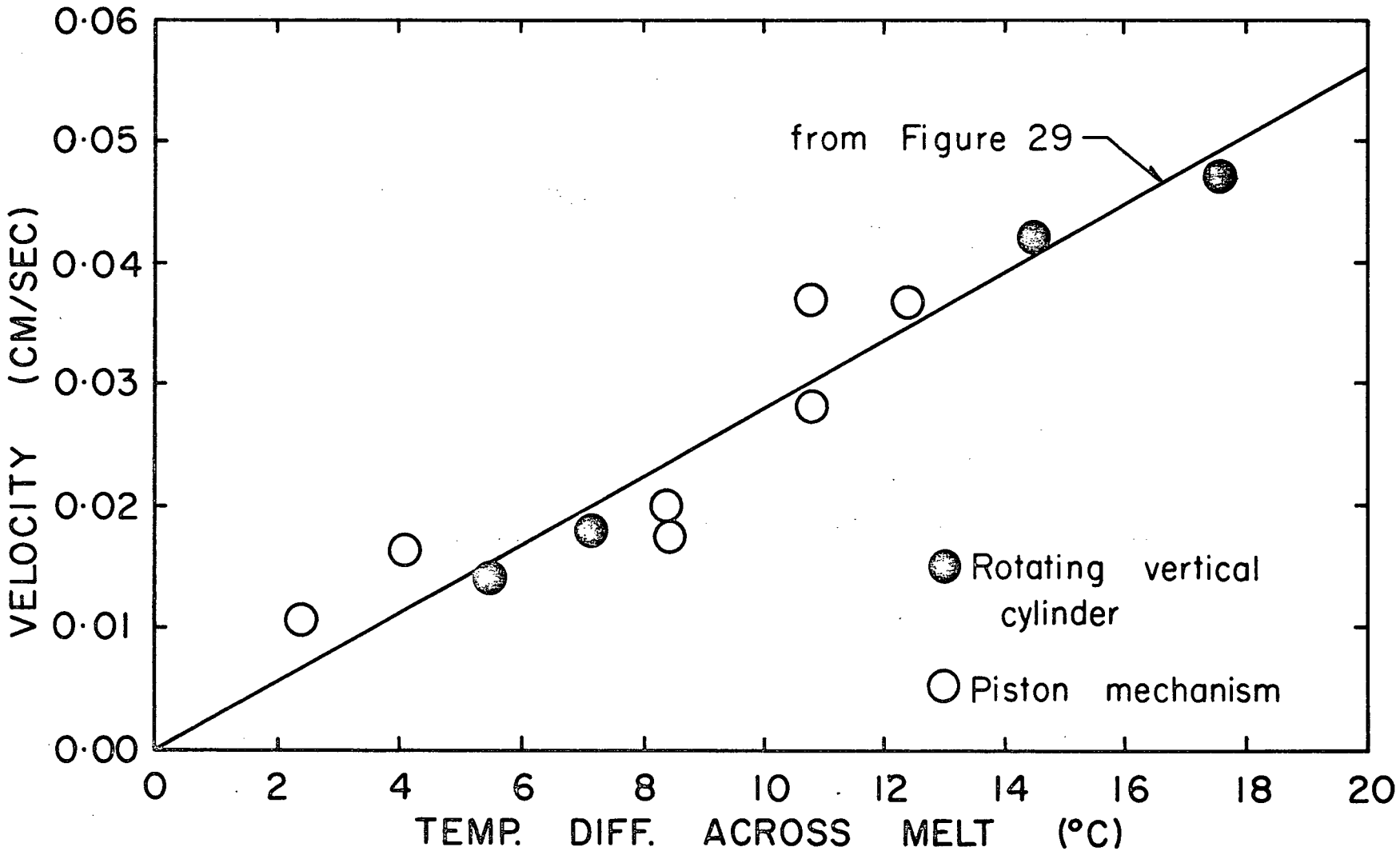

Figure 33. Comparison of the flow velocity measurements obtained employing the rotated vertical cylinder and piston mechanism introduction techniques.

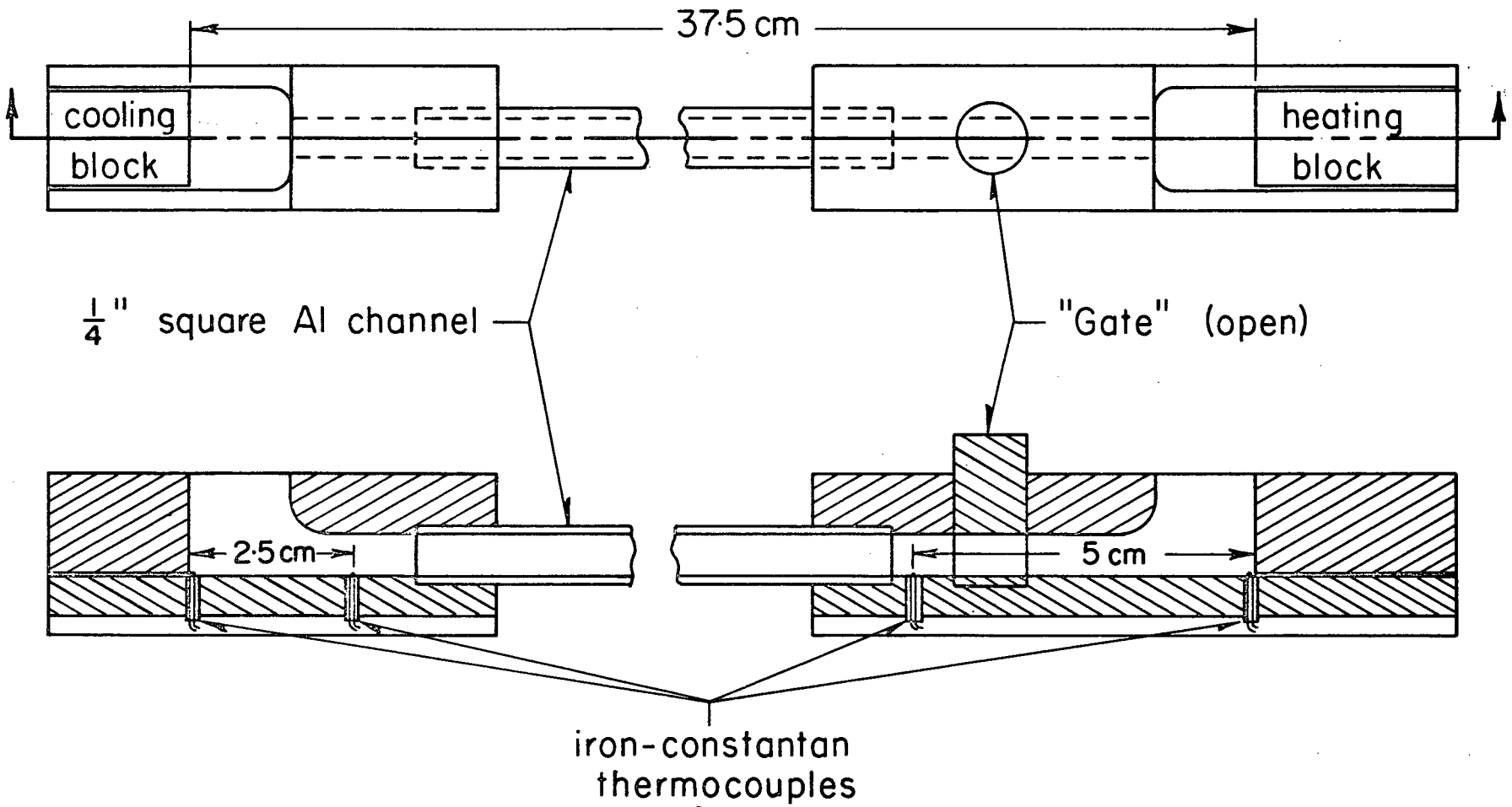

Figure 34. Details of the graphite end supported single aluminum channel boat.

experiments. The channel was constructed by wiring a 0.05 inch thick strip of aluminum over the top of a length of 3 sided aluminum U-channel having a wall thickness of 0.06 inches.

Thermocouples (30 gauge iron-constantan insulated by 2 hole, 1/16 inch O.D. mullite tubing) were inserted in the graphite reservoirs at the positions shown in Figure 34. Four additional thermocouples were fixed along the aluminum channel. These thermocouples were attached to the aluminum channel by drilling 1/8 inch long, 0.02 inch diameter holes up the sidewalls of the channel, inserting the thermocouple wire, and then hammering the hole shut around the wire. Selection and control of the temperature difference along the melt and introduction of tracer were carried out in the same way as described in Section 2.1.7.1. The first collimator position was approximately 5 cm downstream (towards the cold end) from the place of introduction and the second positon was 20 cm beyond the first.

2.1.8.2. Results and Discussions

The results of velocity determination experiments are tabulated in Table 3 and plotted in Figure 35. It is clearly evident from Figure 35 that the experimental results fit a linear relationship between observed flow velocity and temperature difference between the hot and cold ends of the melt. The slope of the line obtained for the 37.5 cm single alumium channel boat is less than that obtained for the 27 cm long two channel graphite boat used earlier. Possible causes for this difference in slope are:

TABLE 3

Flow Velocity Results

Experiment Number	Average Temp. °C.	Δ Temperature °C	Velocity cm/sec.
1	306	20	0.04
2	310	43	0.07
3	310	56	0.12
4	300	85	0.16
5	303	135	0.21
6	322	177	0.32
7	325	182	0.33

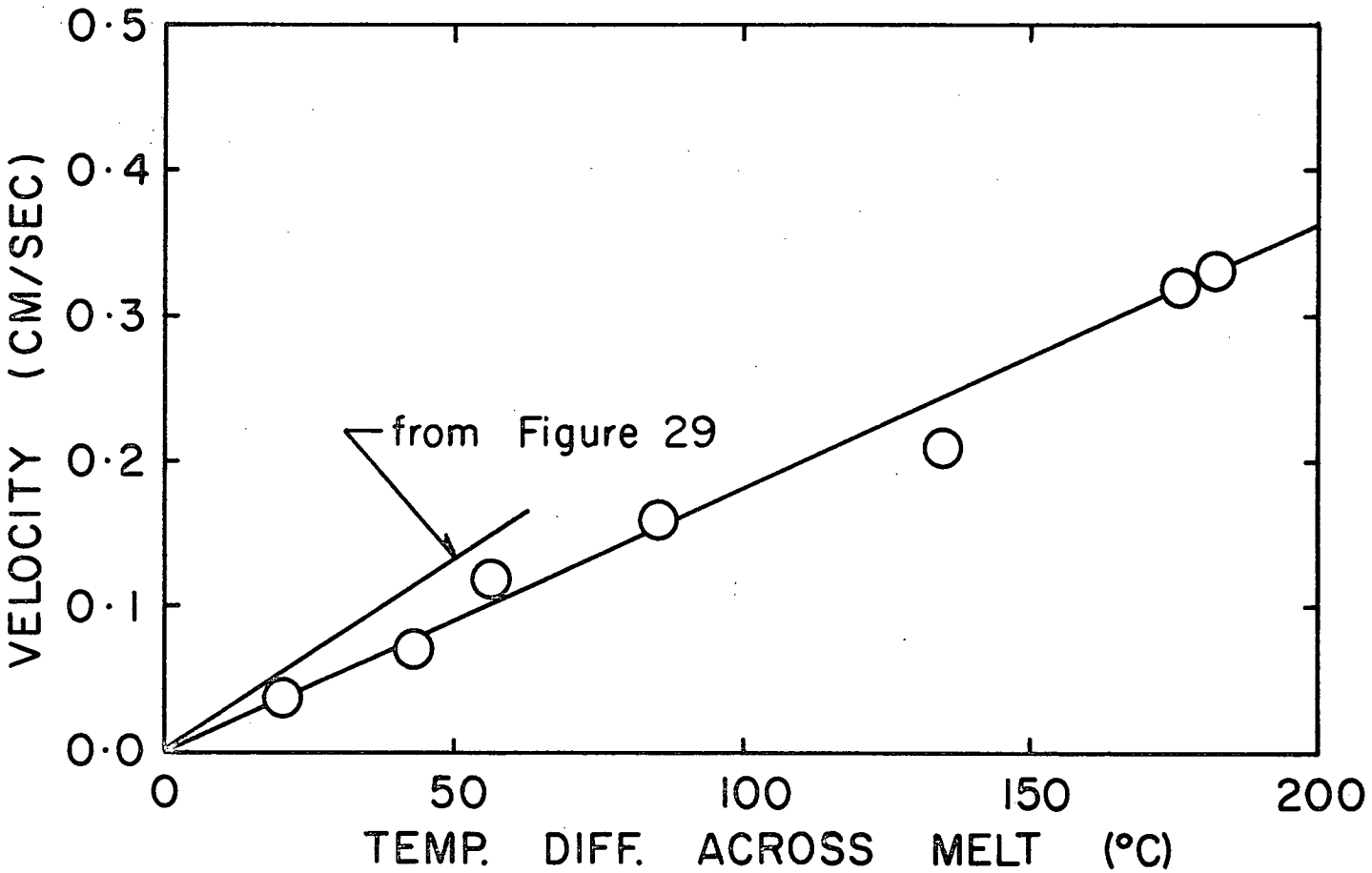

Figure 35. Comparison of the flow velocity measurements obtained employing the two channel graphite boat (Figure 29) and the single aluminum channel boat.

(1) A difference in the lateral temperature gradients in the two boats.

(2) A variation of flow velocity with total melt length.

The effect of melt length on flow velocity will be discussed below when more experimental results are available.

2.1.8.3. Evaluation of Technique

The acceptability of the tracer introduction technique has been established. However, measurement of flow velocities by the manual collection of activity versus time data is extremely difficult when the flow velocity exceeds 0.5 cm/second. Even with the larger monitoring interval used in this last series of experiments (20 cm as opposed to the 6.3 cm and 10 cm intervals used earlier) there is not sufficient time (less than 40 seconds) to collect data that will accurately determine the time of arrival of tracer above a given collimator position. Furthermore, for flow velocities exceeding 0.5 cm/sec a counting interval of 15 seconds is far too long to yield sufficiently sensitive data for accurate determination of tracer arrival. It is, however, extremely difficult to manually collect data with count time intervals appreciably less than 15 seconds. The necessity to move the collimator from one position to the next further decreased the time available for monitoring the increase in activity over the second collimator position. Improvement in the sensitivity of the tracer monitoring system was necessary before investigation of the variation of flow velocity with thermal driving force could continue,to flow velocities above 0.5 cm/second. These improvements and the results from

them are discussed in the next section.

2.2. Flow Velocity Determination by Dual Monitoring

2.2.1. Experimental Apparatus and Procedure

To facilitate measurement of higher flow velocities two collimator slits were used and the activity of radiation passing through the slits was monitored continuously with two separate Quantum Electronic Q6-A scintillation counters. This arrangement is shown schematically in Figure 36. The collimator separation was 20 cm. In a typical experiment the single channel aluminum boat shown in Figure 34 was placed in the tube furnace and a desired temperature profile along the melt was established and maintained for about one hour. When the temperature profile had stabilised, the trace alloy (0.85 wt % Sb^{124} in Sn) was introduced into the tin melt. The visual display on the two scalers plus the visual display from a Hamner NT-15F-1 timer was photographed on 35 mm film at 5 second intervals. The field of view of the camera is shown in Figure 37(a) and some typical data in Figure 37(b). Analysis of the data collected is discussed below.

2.2.2. Analysis of Activity Versus Time Data

As active material approaches and passes through the section of liquid subtended by the collimator slit the activity detected by the counter initially increases slowly and then rapidly. To establish whether the shape of the activity-time curves is entirely due to a corresponding increase in activity in the liquid above the collimator slip or partly due to the collimating procedure used the following ex-

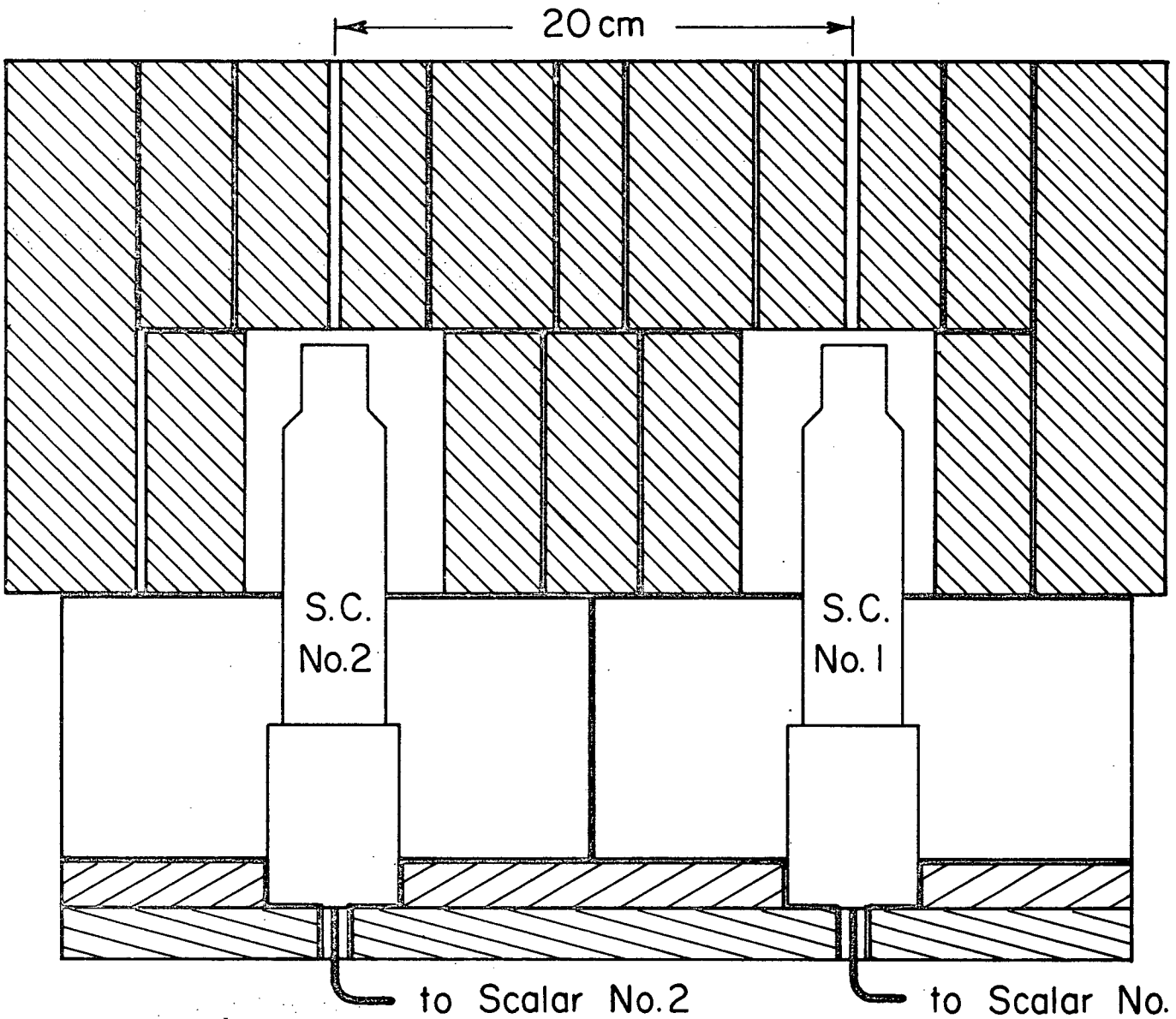

Figure 36. Sectional view of the double slit collimator with two scintillation counters.

(a)

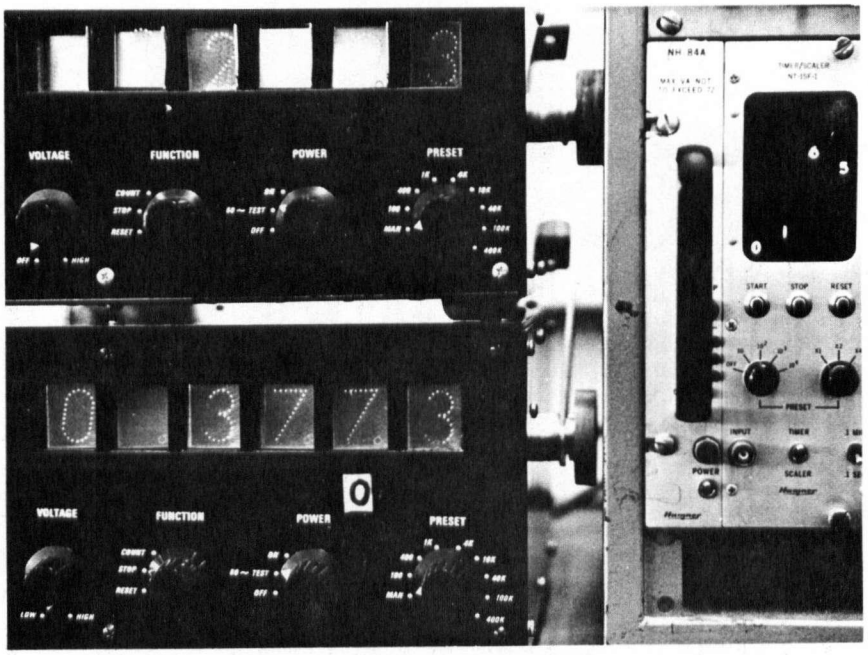

(b)

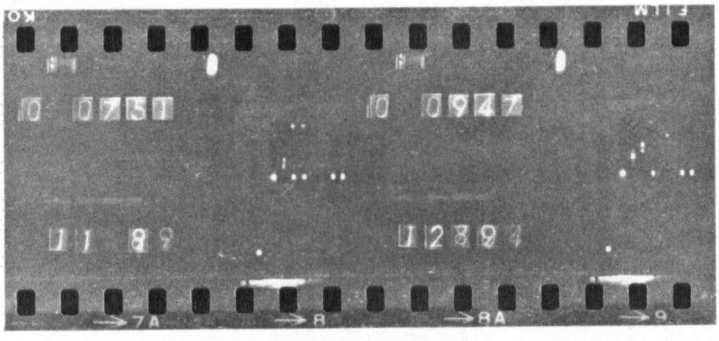

Figure 37. (a) Field of view of 35 mm camera employed to collect activity versus time data. (b) A section of the 35 mm film showing some typical data.

periment was carried out. A 0.6 cm square by 16 cm long rod of tin containing 100 ppm of Sb^{124} was positioned along the Vycor tube at various distances away from the region intersected by the collimator slit and the activity reaching the scintillation counter was monitored for a 15 second interval. The results of this test are shown in Figure 38. The most important characteristics of this plot are:

(1) There is a marked increase in the activity seen by the scintillation counters as the radioactive source approaches the collimator slots.

(2) The rapid increase in activity as the radioactive source moves over the collimator slot is spread over an interval of approximately 1 cm.

(3) The count rate observed through collimator no.1 is less than that observed through no.2.

The collimators clearly do not exhibit a step function response to the movement of a radioactive source past them. The fact that the rapid increase in activity occurs over a 1 cm interval can be readily understood by examining Figure 39. The collimator slit is 1/8 inch wide by 4 inches long and the distance between the top of the collimator slot and the plane along which the radioactive source passes is 3 inches. From Figure 39 it can be seen that under these circumstances the scintillation counter sees an interval approximately 1 cm long at the plane of the radioactive source. Therefore, the rapid increase in activity will begin before the source is directly over the collimator slit. The gradual increase in activity reaching the scintillation counter which occurs as the source approaches the

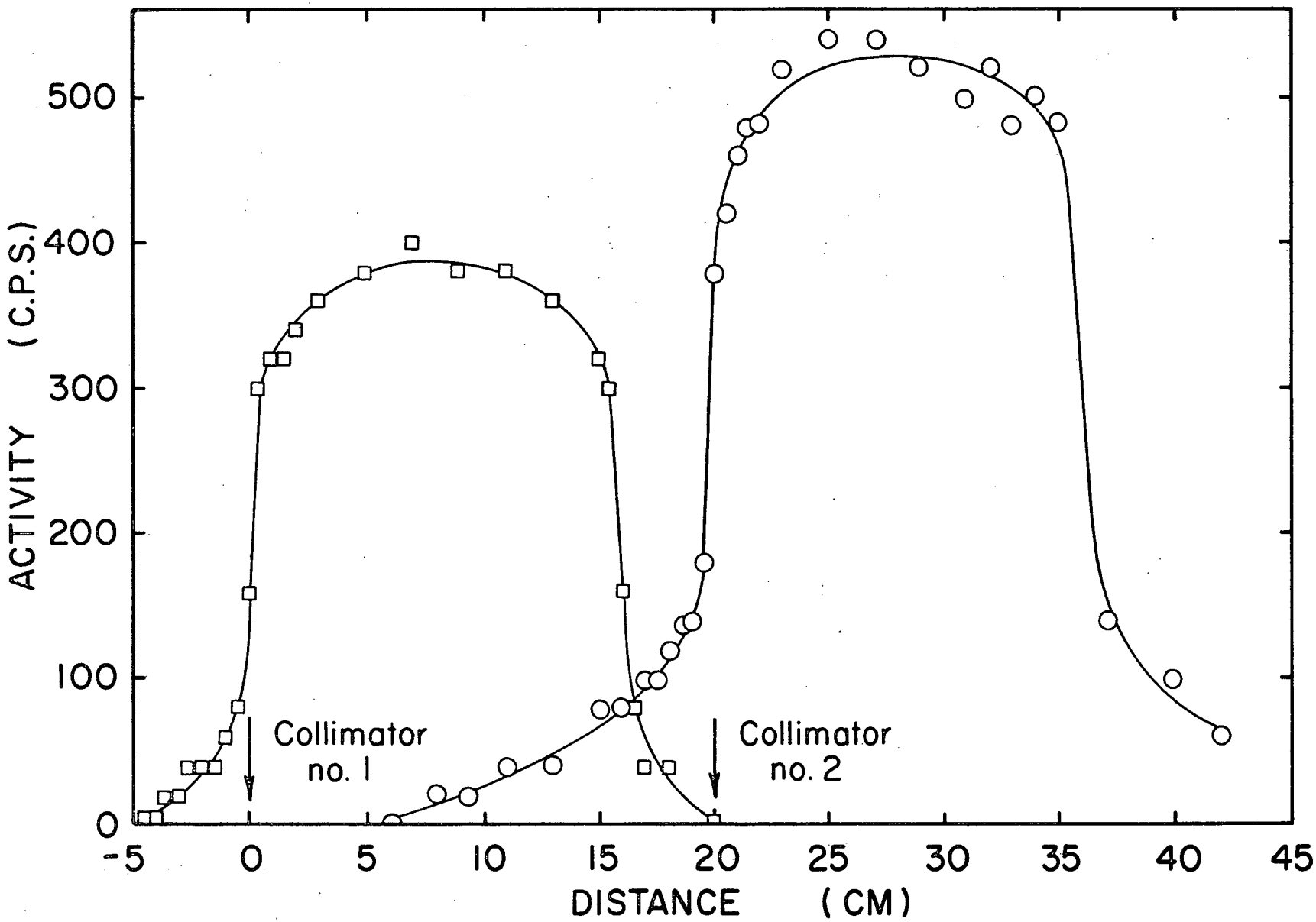

Figure 38. The counting characteristics of the double slit collimator-scintillation counter arrangement.

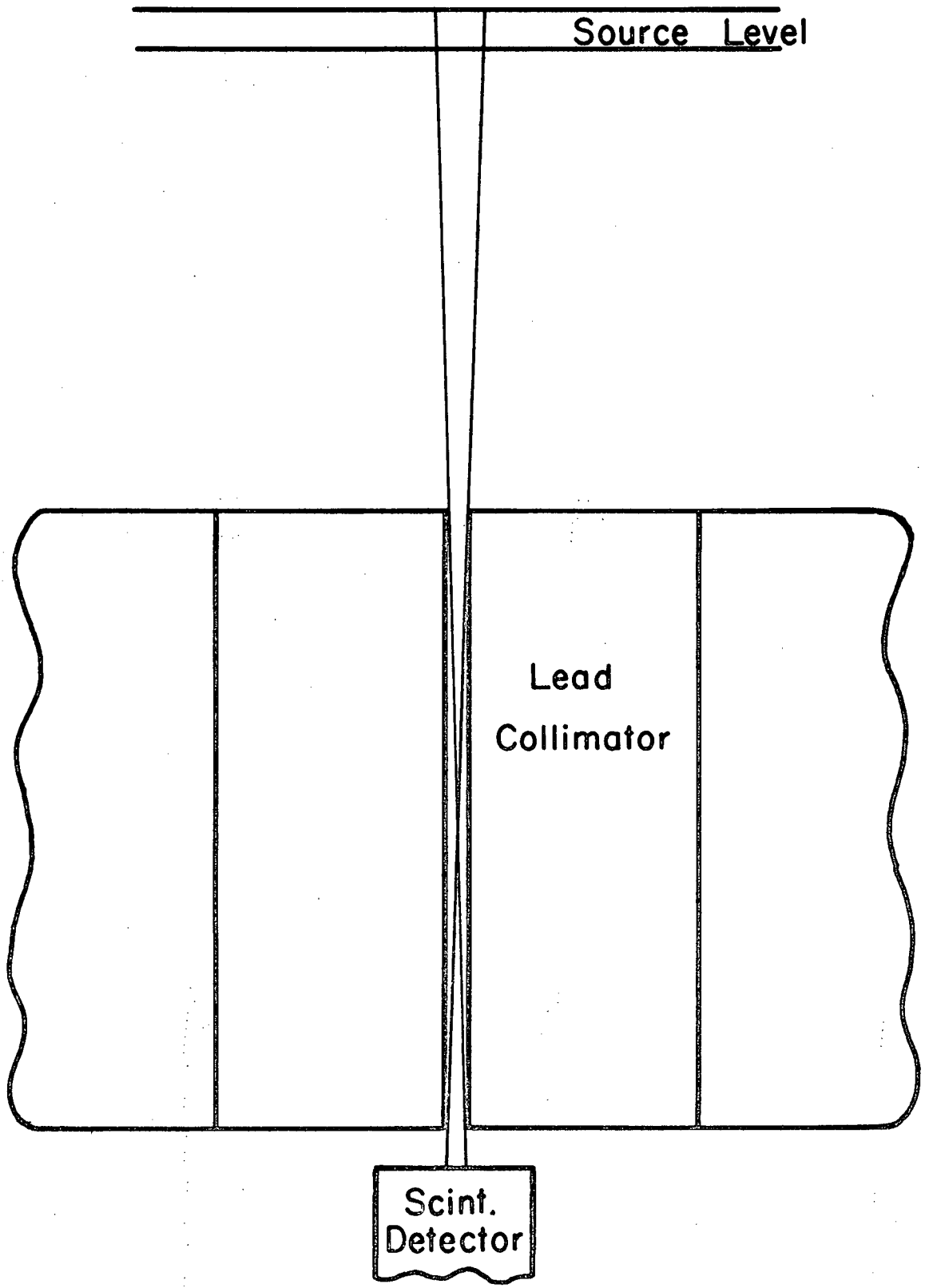

Figure 39. Full size schematic diagram showing the length of melt subtended by the scintillation detector.

the collimator slit is a result of :

(1) A decrease in distance between the source and detector.

(2) A decrease in the thickness of lead shield through which the radiation must pass.

The reason for the increased count rate observed through collimator no.2 is that the activity versus counter voltage plateau for detector no.2 occurred at a higher voltage than for no.1. This resulted in a higher count rate being recorded by scaler no.2.

To test the response of the collimator to a moving source, the 0.6 cm square by 16 cm long radioactive source was pulled through the Vycor tube at a constant velocity of 0.32 cm/second. The results of this test appear in Table 4 and are plotted in Figure 40. The timer and scaler readings appearing in Table 4 were read off the 35 mm film. Background radiation was determined by fixed count timing prior to movement of tracer.

In Figure 40 the average net count rate during the time interval has been plotted against the time at the end of the interval. It would be more correct to plot count rate versus the time at the middle of the interval, but, since all time intervals are five seconds and the difference in time between the increase in the activity at each collimator was the only measurement of interest this was not necessary. The most significant features of Figure 40 are:

(1) As expected there is a gradual increase in activity before the tracer appears over the collimator.

TABLE 4

Results of Dual Collimator Sensitivity Test

Time sec.	Collimator No.1 Background 58 cps		Collimator No.2 Background 30 cps	
	Scalar Reading	Net C.R. cps	Scalar Reading	Net C.R. cps
5.0	440			
10.0	695	0		
14.9	965	0		
19.9	1285	5		
25.0	1760	35		
29.8	2270	50	865	
34.9	3500	180	1025	0
39.9	6000	440	1200	5
45.0	8640	460	1410	10
50.1	11300	465	1600	5
55.0			1815	15
60.0			2070	20
65.0			2365	30
70.1			2690	35
75.1			3100	50
80.0			3600	75
85.0			4190	90
90.0			4830	100
95.0			5510	105
100.0			6670	200
104.9			8930	430
110.0			11880	550
115.0			14870	570
120.1			17930	570

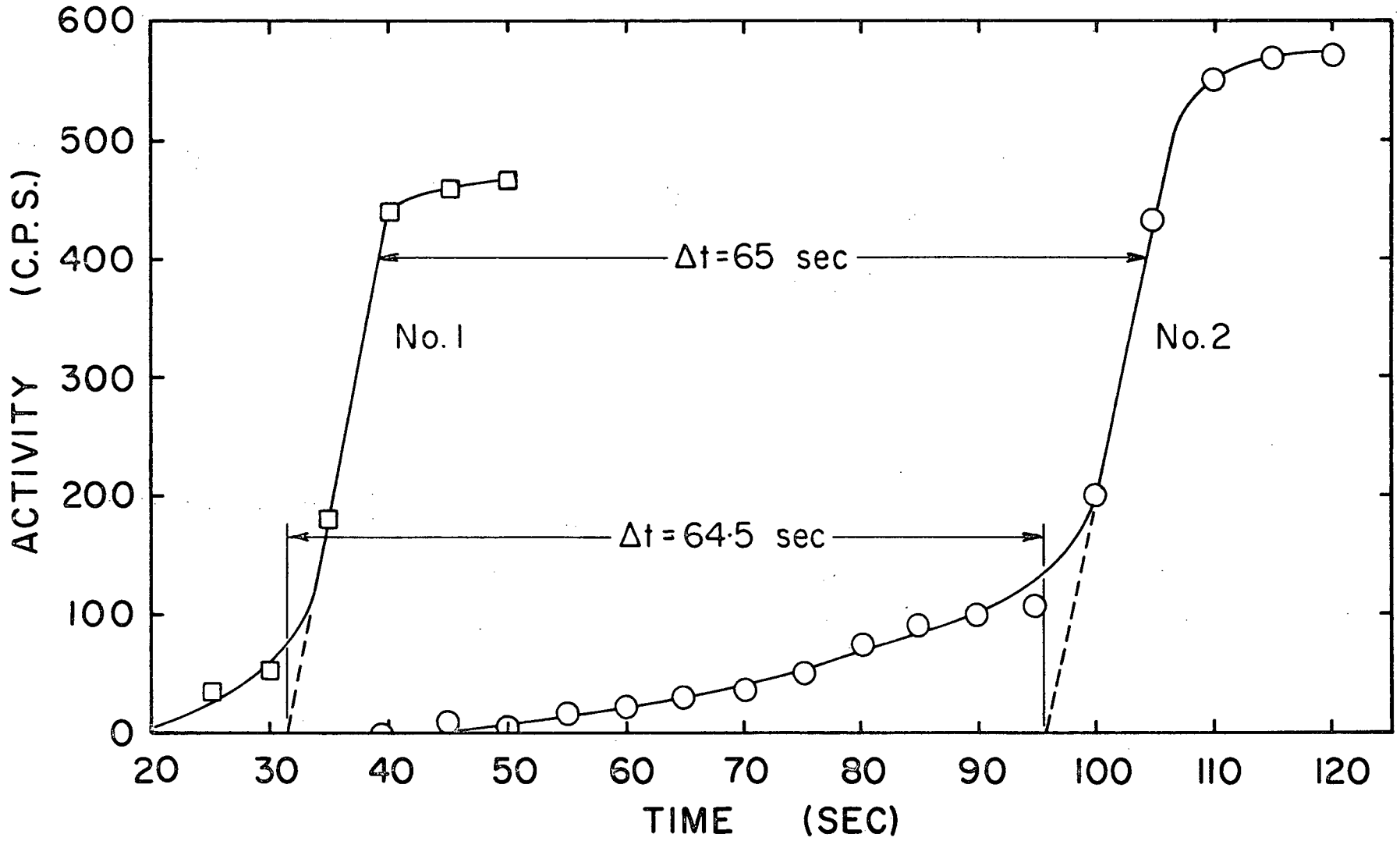

Figure 40. The response of the dual simultaneous counting to a constant activity source travelling at a known velocity.

(2) In the rapidly increasing portion of the curves the slopes are almost identical.

Since the tracer was of constant composition and travelling at constant speed, the time rate of change of activity as the tracer moved over each collimator should be the same, that is, the slopes in the rapidly increasing portion of the curves should be identical.

For the case of constant composition tracer moving at constant speed, velocity determination is simplified by the fact that the time difference between appearance of tracer over the two collimator slots may be obtained by taking the time difference at any average count rate, see Figure 40. The experimentally measured velocity of 0.31 cm/second agrees well with the "true" velocity of 0.32 cm/second.

During an actual experiment the tracer will be diluted as it moves through the melt. Even more important is the fact that the leading edge of the tracer is more dilute than the regions behind the leading edge. This is shown in the longitudinal section autoradiographs appearing in Figure 55 (Section 3.4.3.). It is apparent from Figure 55 that in moving from the cold end towards the hot end (place of tracer introduction) the average cross sectional composition of tracer increases. The net result of this will be that the slope of the linear portion of the collimator response curve will be lower for collimator no.2 than for collimator no.1. This effect is shown in Figure 41. If the collimators were capable of shielding the scintillation counters from all radiation other than that which reached them through the collimator slit itself, the activity versus time curves would probably be approximately linear

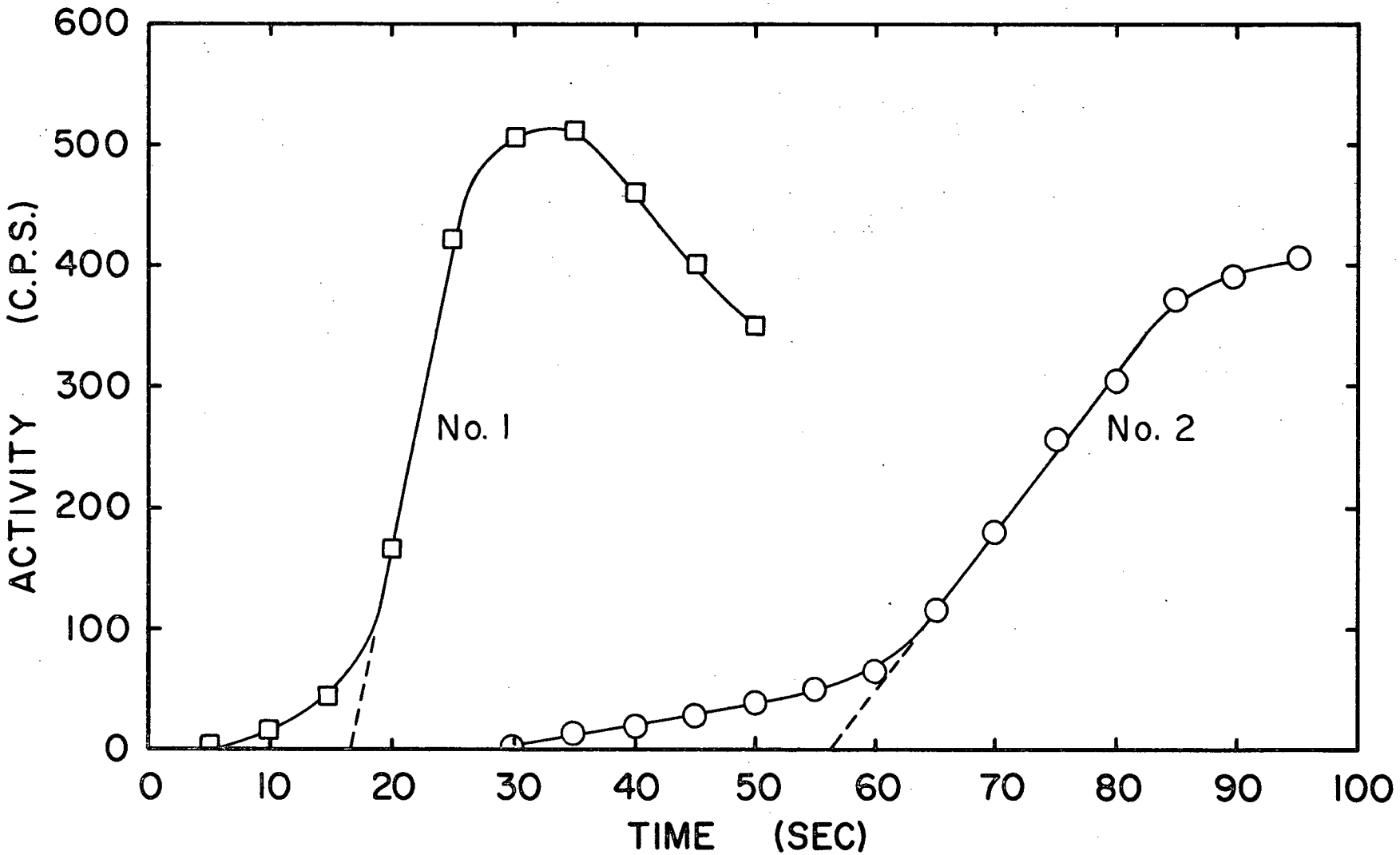

Figure 41. Typical activity versus time data obtained by the simultaneous dual monitoring.

starting from zero activity. Therefore, the intersection of the extrapolation of the rapidly increasing linear portion of the curve and the abscissa was taken to be the time at which the tracer first appeared over the collimator slit. The time difference at zero activity was used for all flow velocity measurements reported in this investigation.

2.2.3. Results and Discussion

2.2.3.1. Variation of Flow Velocity with Temperature Difference between the Hot and Cold Ends

Figure 42 shows the increase in flow velocity which occurs as a result of increasing the temperature difference between the hot and cold ends of the melt. Data plotted in Figure 42 appears in Table 5. As observed previously (Figures 23, 29 and 35), the relationship between flow velocity and temperature difference is linear. The line representing the data plotted in Figure 35 also appears in Figure 42. The same single aluminum channel boat was used for both series of experiments. Flow velocity measurements plotted in Figure 42 were obtained when the average melt temperature was approximately 400 °C (Table 4) whereas the average melt temperature for Figure 35 was 310 °C (Table 2). In Section 2.1.7.2.2. increasing the average melt temperature from 300 °C to 325 °C had no apparent effect on the observed flow velocity. As can be seen from Figure 42 an increase in average melt temperature from 310 °C to 400 °C leads to a 25% increase in flow velocity. This apparent disparity is discussed in the next section.

2.2.3.2. Variation of Flow Velocity with Average Melt Temperature

The dependence of flow velocity on average melt temperature is

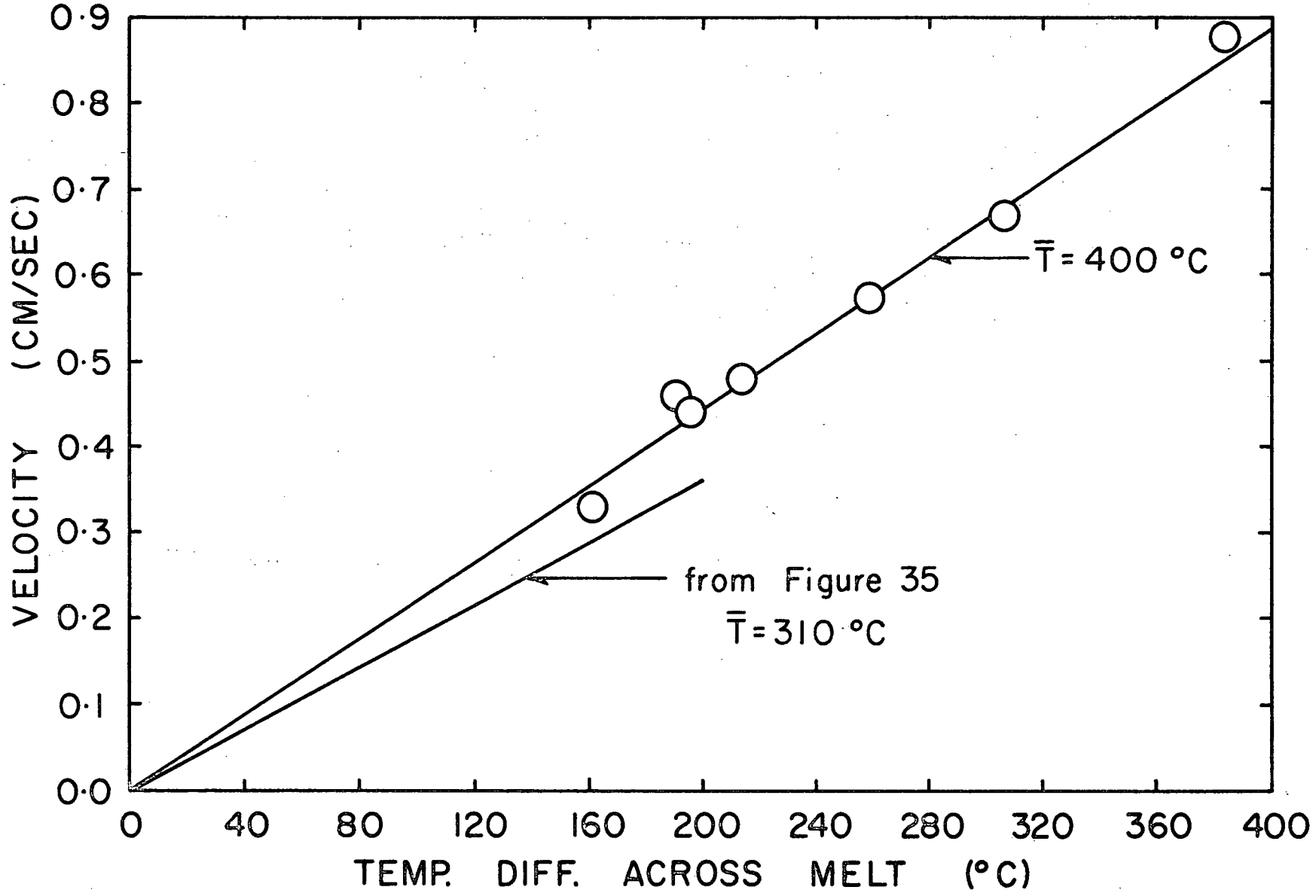

Figure 42. The dependence of flow velocity on the temperature difference between the hot and the cold ends of the melt.

TABLE 5

Flow Velocity Results

Experiment Number	Average Temp. °C.	Δ Temperature °C	Velocity cm/sec.
1	401	161	0.33
2	400	190	0.46
3	398	196	0.44
4	402	214	0.48
5	400	259	0.57
6	403	306	0.67
7	425	384	0.88

shown in Figure 43. The temperature difference across the melt was 214 °C for all three points. The increase in flow velocity with increasing average melt temperature might be anticipated since increasing the average melt temperature decreases the viscosity of the molten tin (Table 6). From Figure 43, one would expect about a 7% increase in flow velocity as a result of increasing the average melt temperature from 300 °C to 325 °C. Since this increase was not observed in Section 2.1.7.2.2., it must be concluded that manual collection of data from a single moveable collimator is less sensitive than simultaneous dual monitoring of the flow velocity.

2.2.3.3. Variation of Flow Velocity with Total Melt Length

The results of flow velocity measurements in melts of differing lengths appear in Figure 44 and Table 7. The average melt temperatures were approximately 400 °C. Decreasing the total melt length from 48.5 cm to 37.5 cm and then to 28.8 cm leads to an increase in the flow velocity observed for a given temperature difference between the hot and cold ends. If flow velocity is plotted against the average temperature gradient across the melt, Figure 45, it becomes apparent that velocity increases linearly with increasing average temperature gradient. In Figure 46 data from Table 5 (filled circles) has been plotted along with the data in Table 7. From Figure 46 it can be concluded that for covered liquid tin melts 0.64 cm high, ranging in length from approximately 25 to 50 cm and at an average temperature of 400 °C, the flow velocity is linearly dependent on the average temperature gradient across the melt such that Velocity (cm/sec) = 0.082 x Temperature gradient (°C/cm). This relation-

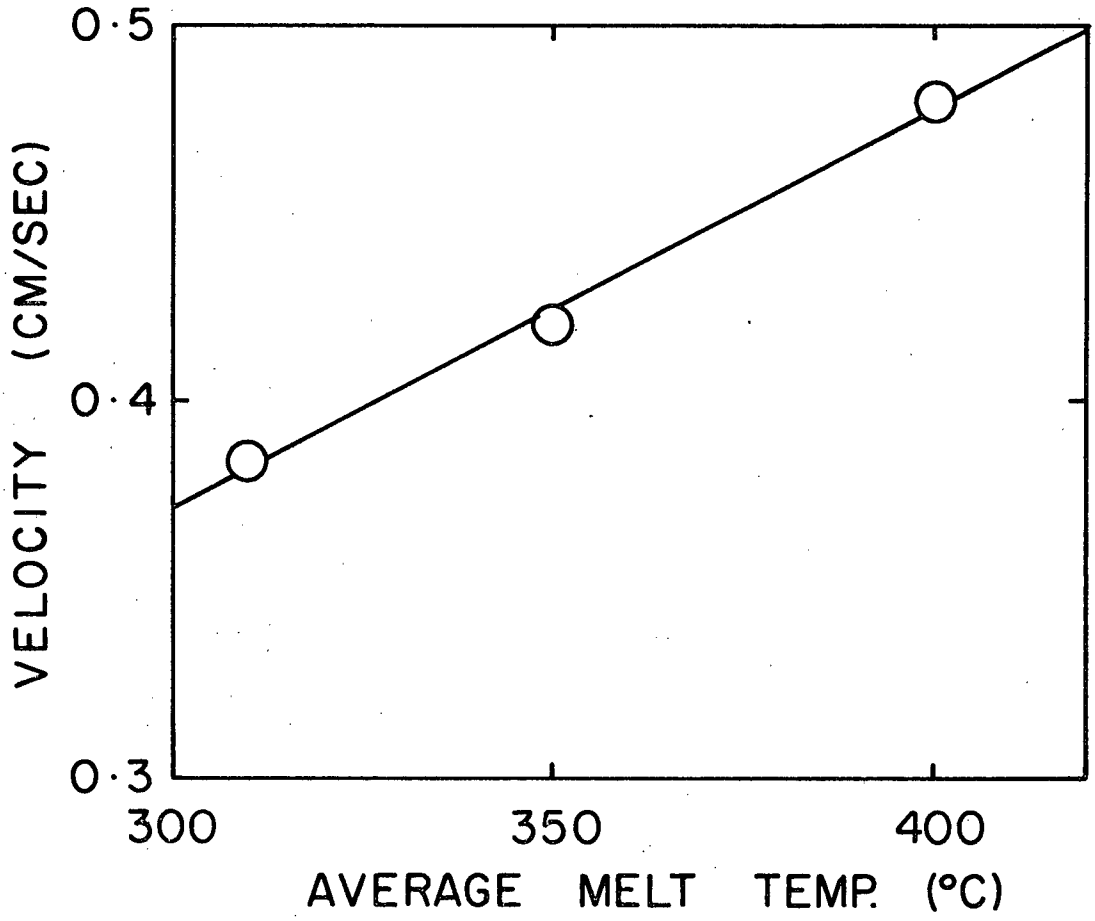

Figure 43. The effect on flow velocity of varying the average melt temperature (with a constant temperature difference across the melt of 214 °C).

TABLE 6

Properties of Molten Tin

Temperature °C	Viscosity (51) centipoise	Specific Heat (52) cal/gm°C	Thermal Conductivity (52) cal/cm sec °C	Coef. of Vol. Exp. (17) $1/°C \times 10^{-4}$	Density (53) gm/cm^3	Kinematic Viscosity $cm^2/sec \times 10^{-3}$	Thermal Diff. cm^2/sec
250	1.70			1.0229	6.961	2.44	0.203
300	1.53			1.0284	6.925	2.21	0.204
		0.0565	0.080				
400	1.29			1.0393	6.854	1.88	0.206
500	1.15			1.0502	6.783	1.70	0.207

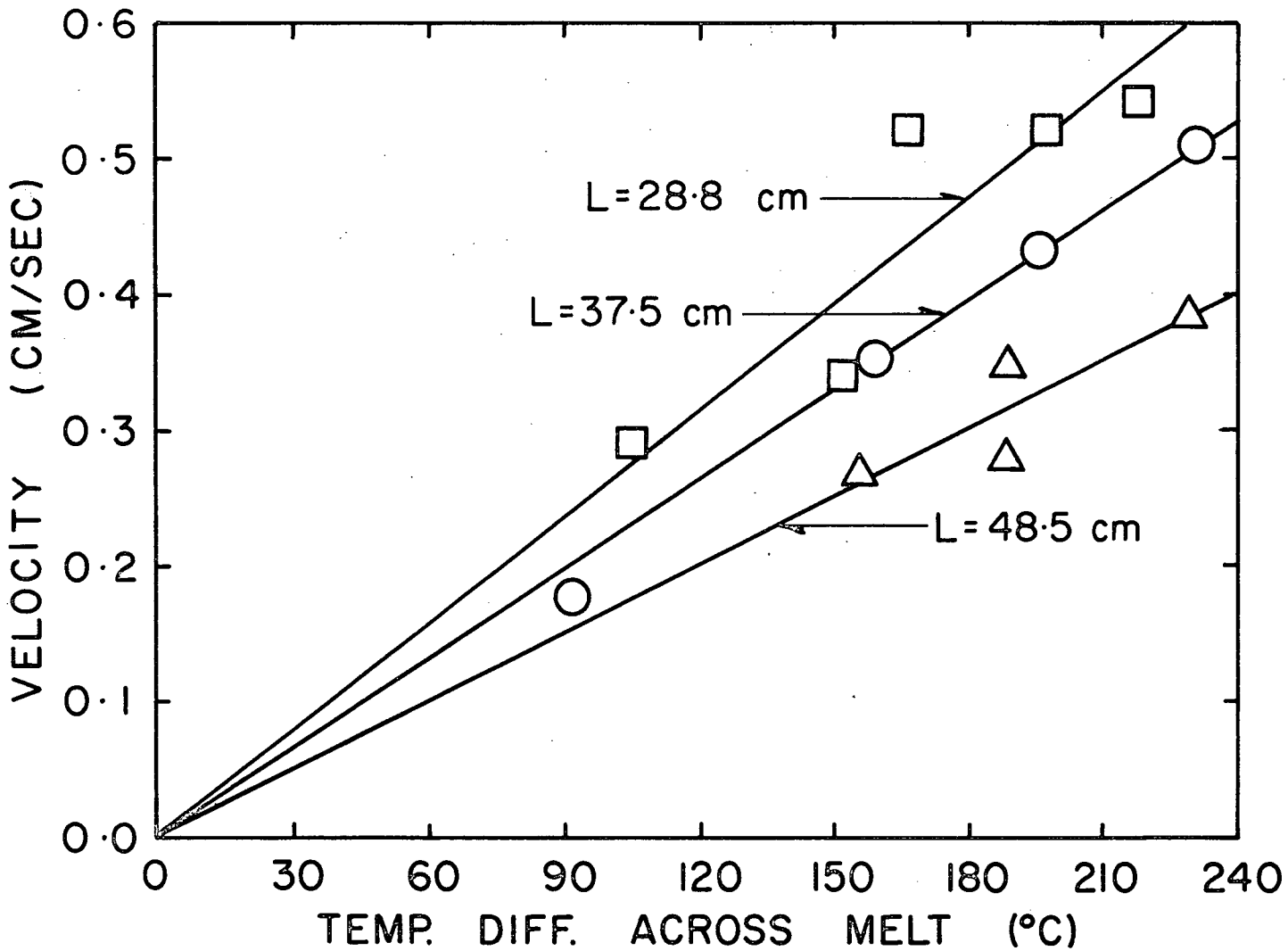

Figure 44. The dependence of flow velocity for three different melt lengths on temperature difference across the melt.

TABLE 7

Flow Velocity Results for Three Melt Lengths

Experiment Number	Melt Length	Δ Temperature °C	Temperature Grad. °C/cm	Velocity cm/sec.
1	48.5cm	156	3.22	.27
2		189	3.90	.28
3		189	3.90	.28 - .35
4		229	4.72	.39
5	37.5cm	92	2.46	.18
6		156	4.16	.36
7		158	4.22	.35
8		196	5.22	.43
9		231	6.17	.51
10	28.8cm	105	3.65	.29
11		153	5.31	.34
12		167	5.80	.52
13		198	6.88	.52
14		218	7.58	.54

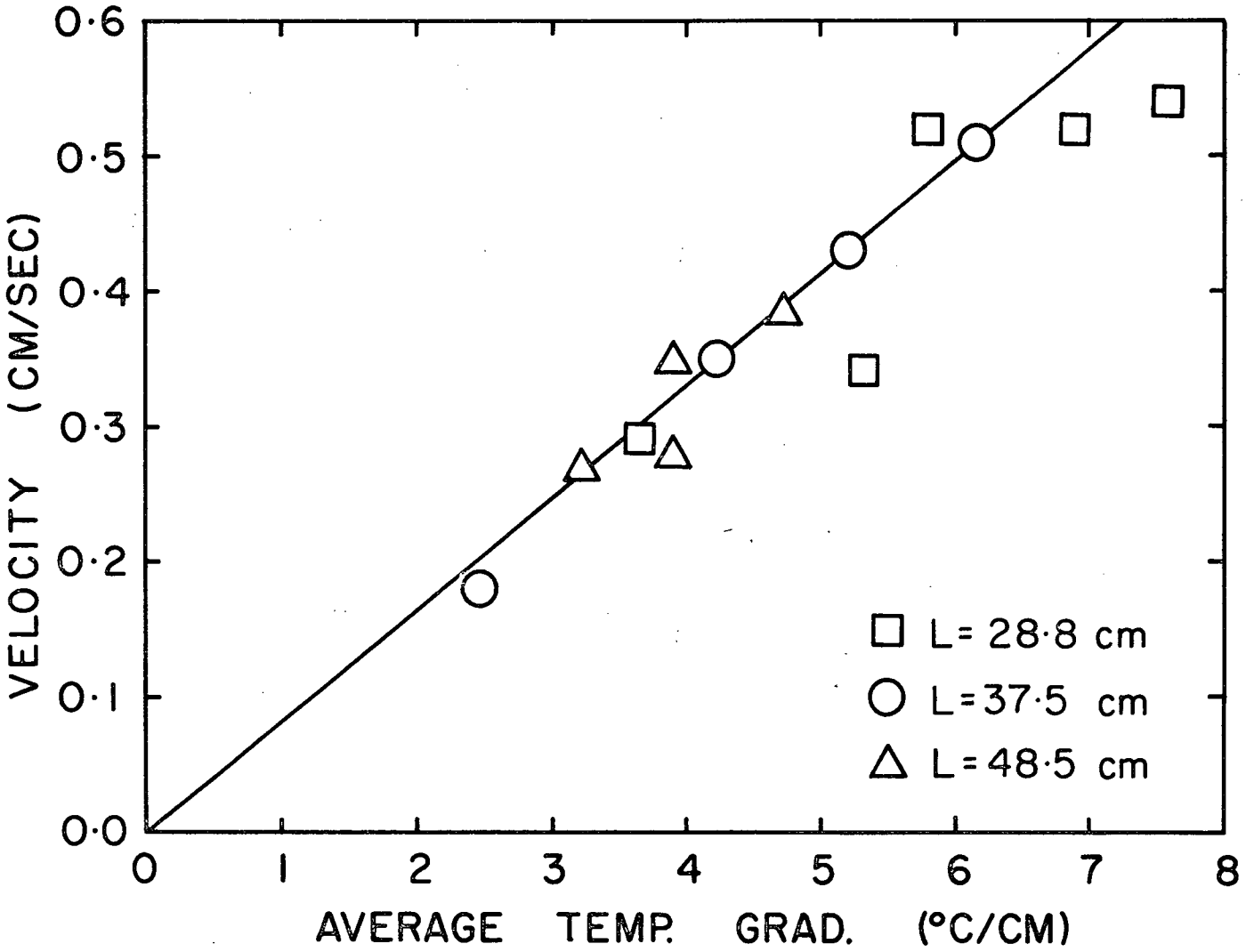

Figure 45. The dependence of flow velocity for three different melt lengths on the temperature gradient between the hot and cold ends of the melt.

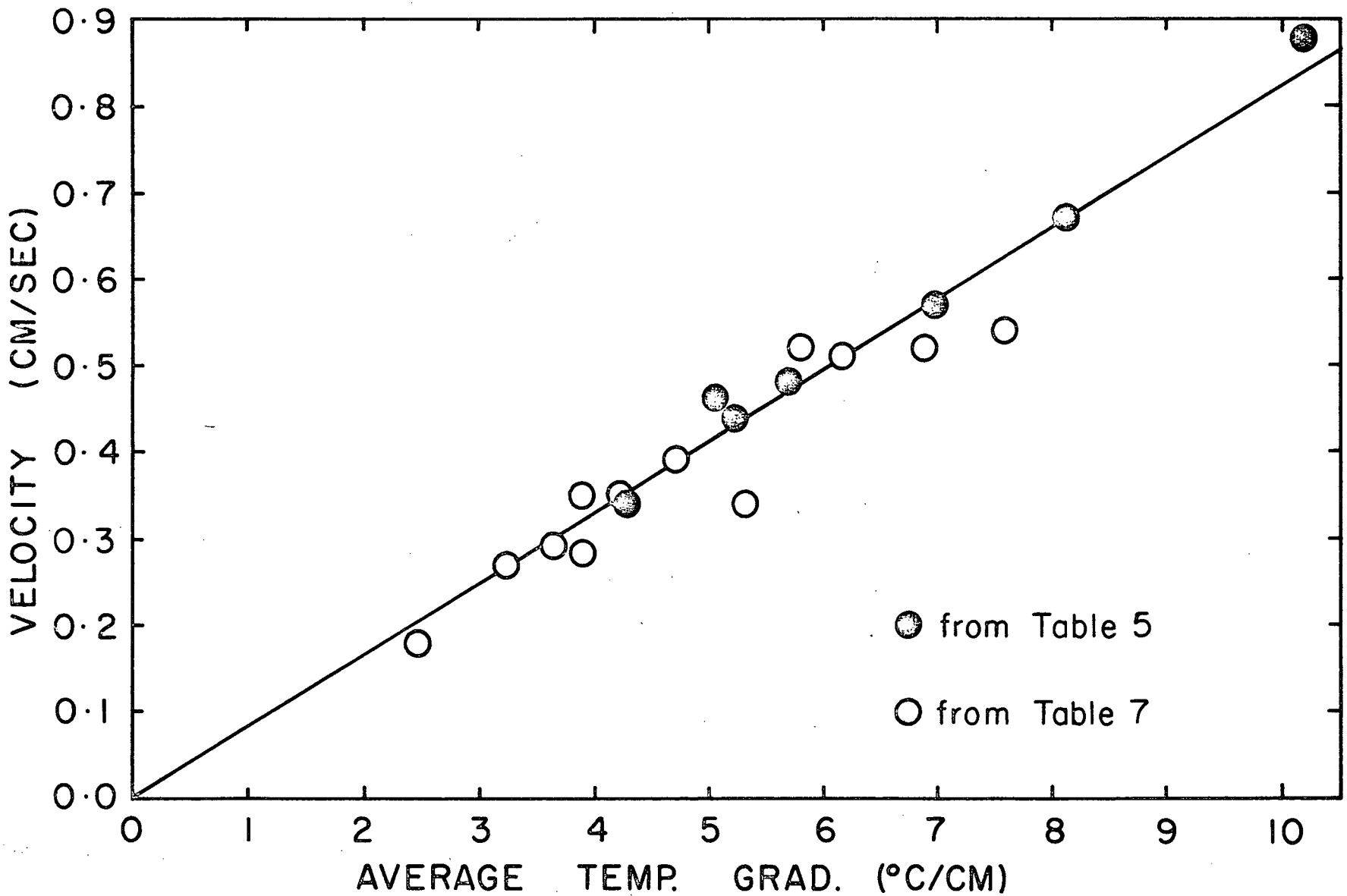

Figure 46. The dependence of flow velocity on the temperature gradient across the melt with an average melt temperature of 400 °C.

ship holds true up to average horizontal temperature gradients of at least 10 °C/cm.

In Section 2.1.8.2., Figure 35, it was observed that the slope of the line obtained for the 37.5 cm long single aluminum channel boat was less than that obtained for the 27 cm long two channel graphite boat. Two possible causes for this difference in slope were offered, namely, a difference in lateral gradients and/or a dependence of flow velocity on total melt length. When the flow velocities appearing in Figure 29 and 35 are plotted against average temperature gradient (as opposed to total temperature difference) across the melt, Figure 47, it becomes apparent that the slope difference observed in Figure 35 was a result of flow velocity dependence on total melt length. If there were different lateral gradients in the two channel graphite and single aluminum channel boats they did not significantly effect the longitudinal flow velocity observed. Figure 47 shows, in agreement with Figure 45, that flow velocity is linearly dependent on the average horizontal temperature gradient across the melt. The slope of the line in Figure 47 is less than that in Figure 45 since the average melt temperature was lower.

2.2.3.4. Evaluation of Technique

In order to evaluate the sensitivity of this flow velocity measurement technique a series of experiments was performed in which experimental procedures and parameters were varied from the norm. This was done to determine what effect inadvertent variations from normal experimental procedure would have on the observed flow velocity. Results

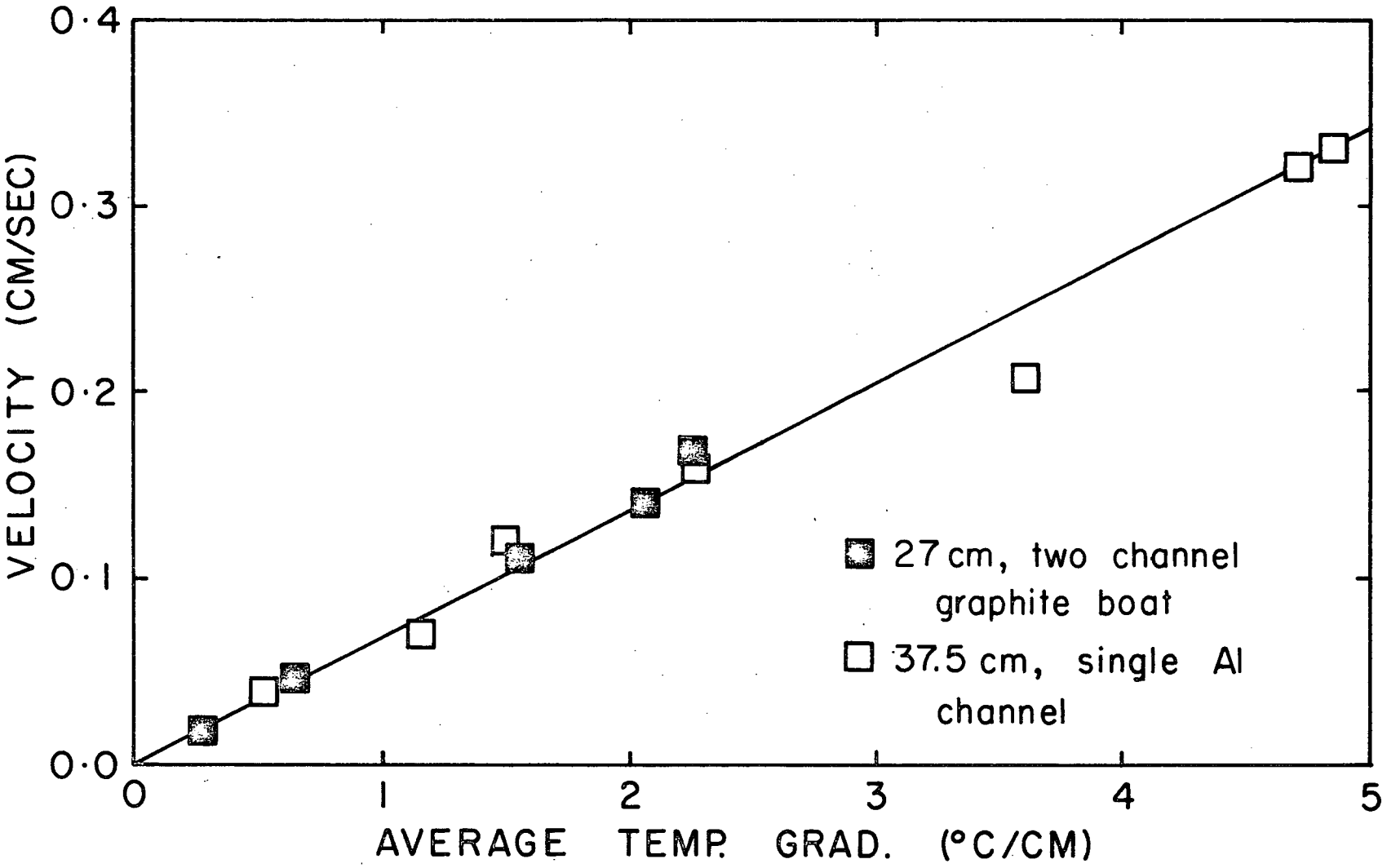

Figure 47. Comparison of the velocity versus temperature gradient results obtained using the two channel graphite boat and the single aluminum channel boat. Average melt temperature was approximately 310 °C.

of these tests appear below.

2.2.3.4.1. Effect on Flow Velocity of Varying the Nature of the Temperature Distribution

Figure 48 compares the temperature distribution imposed during two separate experiments designed to show that it is the average temperature gradient between the hot and cold ends of the melts, and not the average temperature gradient between the two collimator slots (monitoring interval) that determines the resultant flow velocity. As can be seen in Figure 48, the average temperature gradient across the monitoring interval is the same for both experiments. The average gradients between the hot and cold ends are however quite different. The flow velocities observed for the two tests were 0.39 cm/sec for the experiment with the lower gradient, 5.0 °C/cm, and 0.47 cm/sec when the average gradient between the ends of the melt was 5.8 °C/cm. When these results are compared, Figure 50, to the results of Figure 46 excellent agreement is found. Clearly then,the average gradient across the total melt length and not that in the monitoring interval is responsible for the flow velocity observed.

Also, from Figures 48 and 50 it can be concluded that the flow velocity is independent of the shape of the temperature profile, that is, whether the temperature distribution between the hot and cold ends is non-linear or nearly linear (as was generally the case) the same flow velocity will be observed when the average gradients are the same. The limiting case occurs when there is a maximum (or minimum) in the temperature profile between the hot and cold ends which stops fluid flow

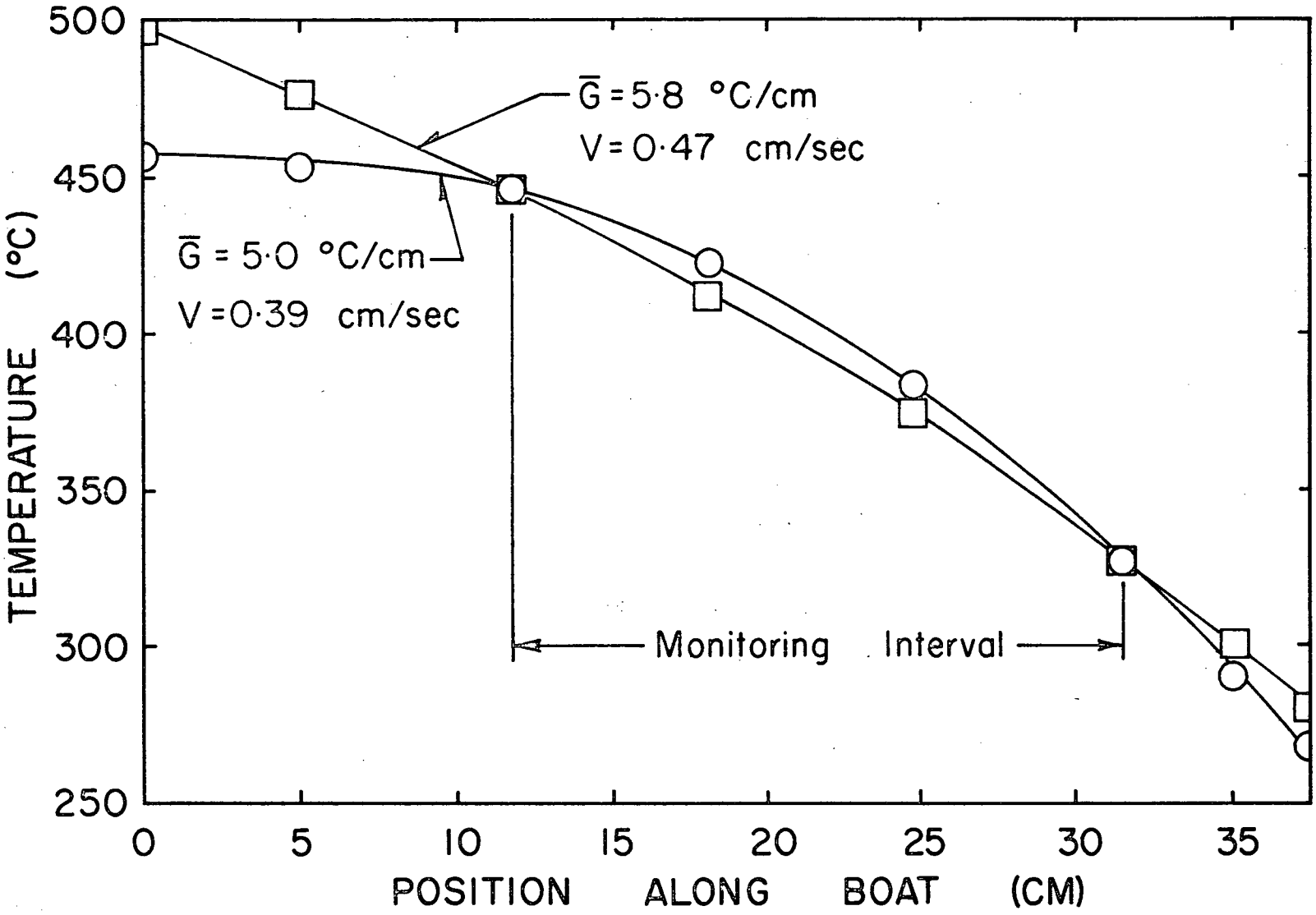

Figure 48. Temperature profiles from two experiments designed to show that the temperature gradient across the melt, and not the gradient across the monitoring interval, is the driving force for the observed velocity.

at that point (Section 2.1.3.).

2.2.3.4.2. Effect on Flow Velocity of Varying the Position of the Monitoring Interval

Although the position of the monitoring interval remained reasonably constant during a given series of experiments, experiments were conducted to determine whether changing the position of the monitoring interval would change the measured flow velocity. For these experiments a shorter interval of 13.8 cm was employed. The temperature profile shown in Figure 49 was established and for the first test the monitoring interval was between thermocouples A and C. The graphite boat was emptied and reloaded, the temperature profile of Figure 49 re-established, and the second experiment carried out with the monitoring interval between B and D. The average gradient across the melt was 5.1 °C/cm. The gradient between A and C was 4.3 °C/cm and that between B and D 6.0 °C/cm. Flow velocities determined from both intervals were approximately the same, 0.42 and 0.43 cm/sec respectively. If these velocities are plotted against the average temperature gradient between the hot and cold end, Figure 50, it is found that they are in excellent agreement with the results of Figure 46. Thus, it can be concluded that the position of the monitoring interval does not affect the flow velocity observed. However, it was necessary to keep the first collimator slit approximately 5 cm downstream of the place of tracer introduction and thus avoid any spurious effects which may be associated with introduction of tracer.

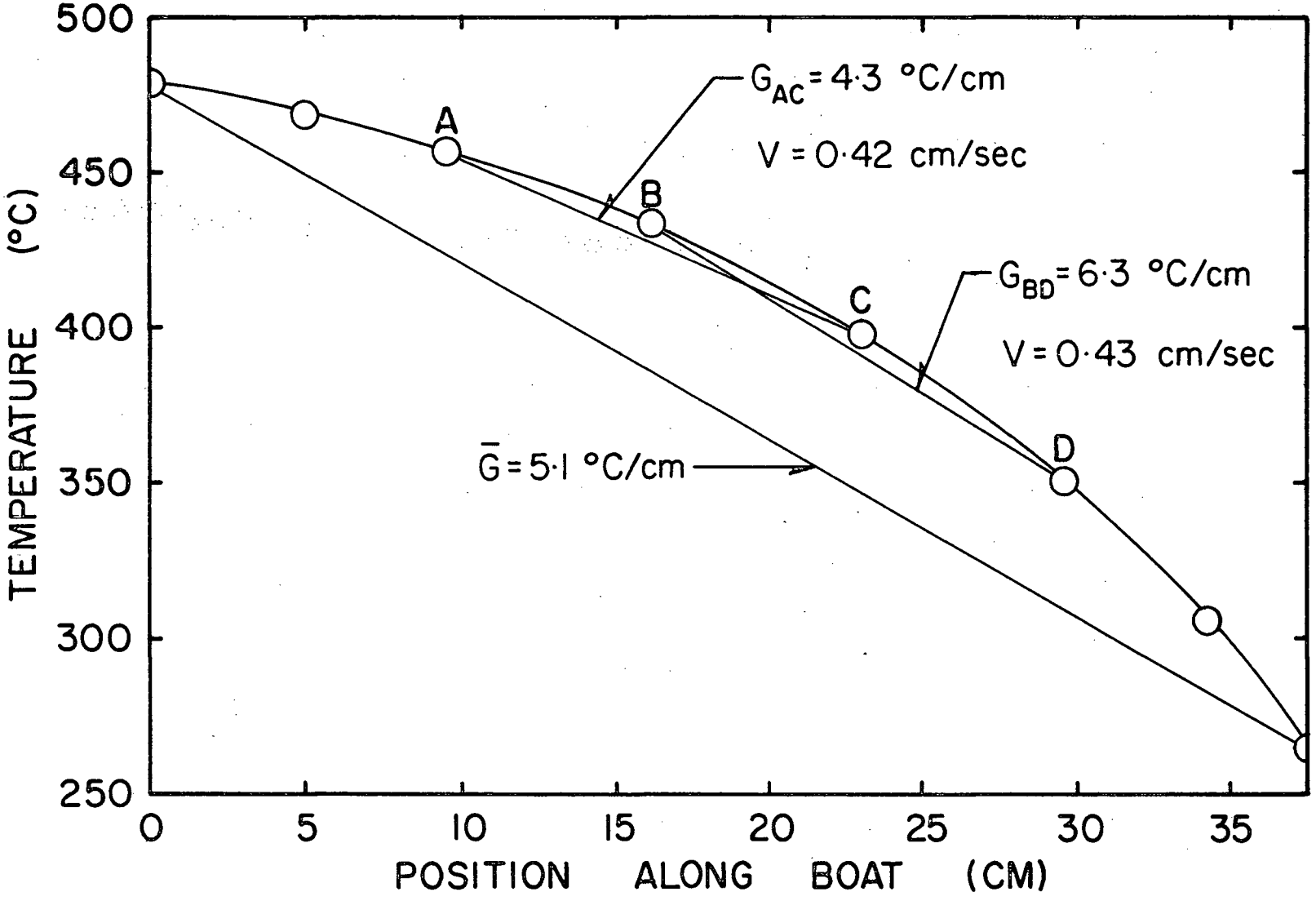

Figure 49. Temperature profile from an experiment undertaken to determine the effect on flow velocity of changing the position of the monitoring interval.

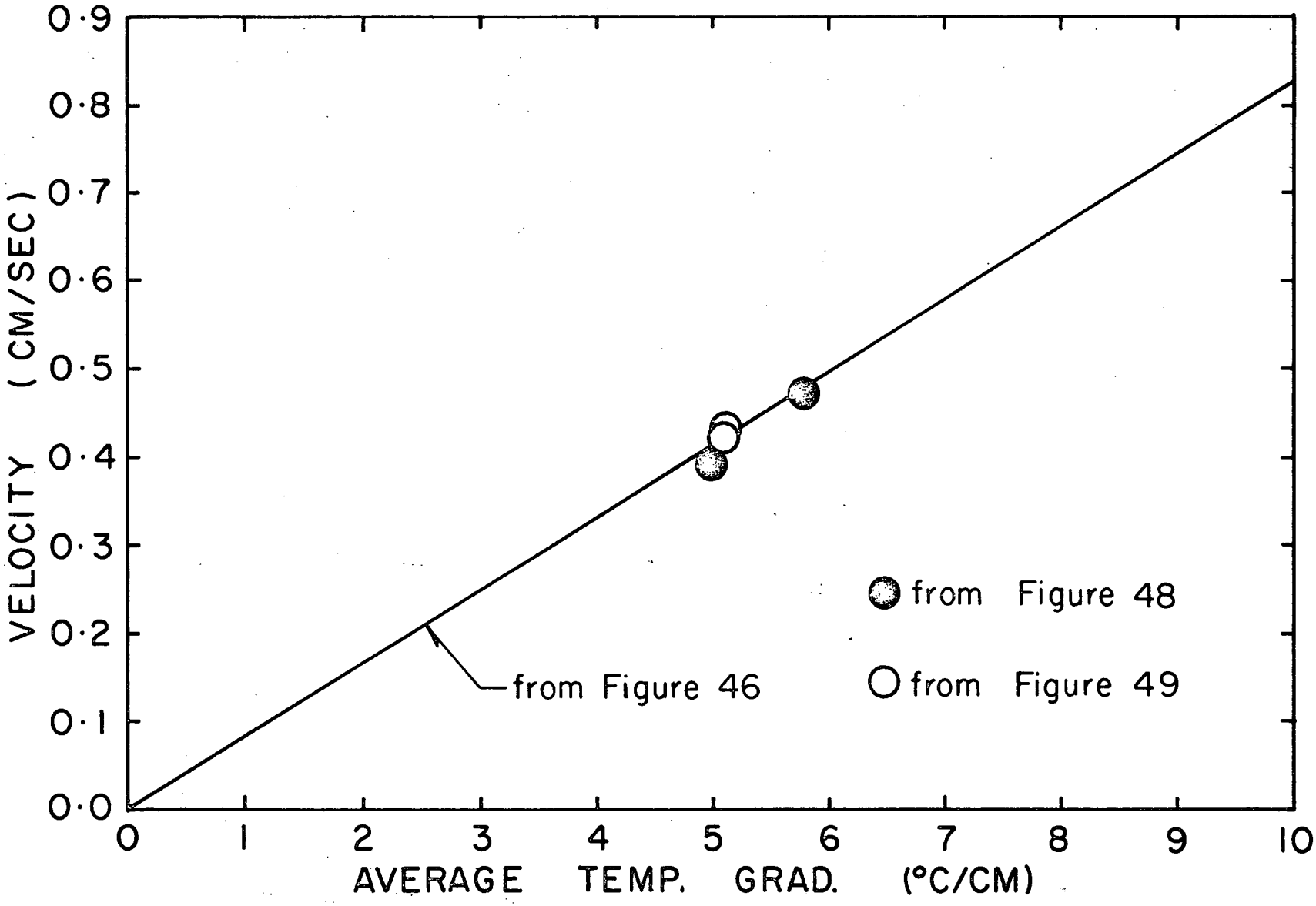

Figure 50. Comparison of the results of Figures 48 and 49 with results of Figure 46.

2.2.3.4.3. Effect on Flow Velocity of Varying the Height of Metal in the Reservoirs

Earlier in the thesis it was stated that the melt was covered for approximately 90% of its length with each end having an uncovered reservoir. The height of liquid metal in the covered portion was 0.64 cm while the melt was about 1 cm deep in both reservoirs. Since the height of liquid metal is a major parameter in any fluid dynamics analysis, experiments were conducted to determine the effect on flow velocity of varying the height of metal in the reservoirs. It was found that reducing the melt height in the reservoirs from 1 cm to 0.7 cm had no effect on the flow velocity. This is shown in Figure 51 were the velocity of 0.50 cm/second measured for the 0.7 cm height is plotted on the line from Figure 46, where the height of melt in the reservoir was 1.0 cm. Thus, it can be concluded that the height of melt in the reservoirs does not effect the observed flow velocity and, therefore, it is appropriate to use the height in the covered section, namely 0.64 cm, for the purpose of analyzing the horizontal melt system studied here.

Another variation in experimental procedure which may affect the observed flow velocity is a difference in height of metal in the two reservoirs. The tracer introducer is in the closed position (blocking the channel) when the boat is loaded with pure tin. It is quite possible then that the height of metal in one reservoir was different than in the other. Thus, when the tracer was introduced into the boat by rotating the cylinder there would be a head of liquid metal in one reservoir and this would most assuredly cause fluid motion through the channel. An experiment was conducted in which a 0.3 cm difference in liquid level in the hot and cold reservoirs was established prior to rotation of the

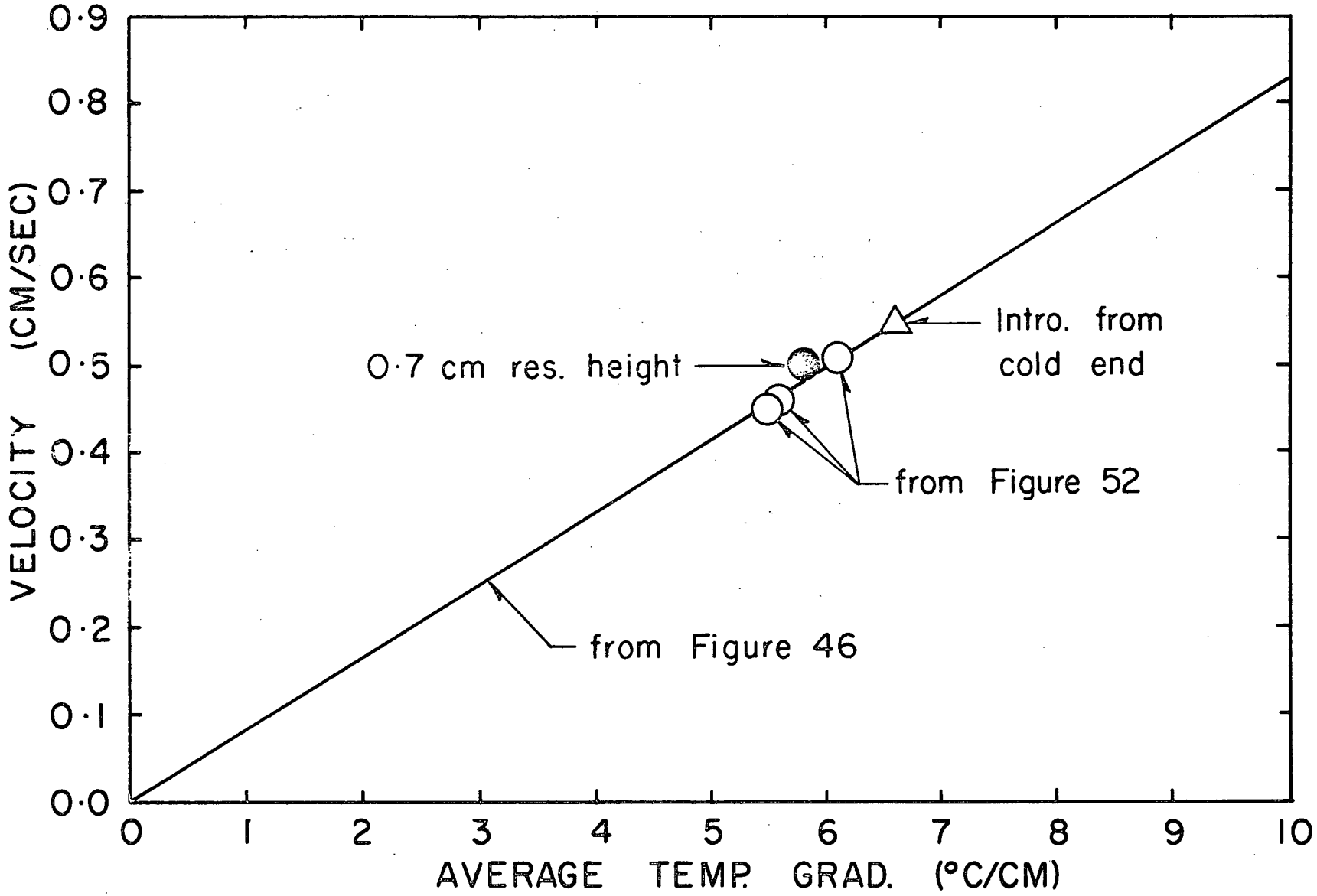

Figure 51. The effect on flow velocity of varying the liquid metal height in the reserviors and of introducing the tracer near the cold end.

tracer introducer. Visual observation of the melt following rotation of the cylinder to the open position showed a rapid rise in the liquid level in what had been the low level end. This was followed by oscillatory fluctuations in the reservoir levels. The oscillations disappeared within 10 to 15 seconds.

To determine the effect of liquid head in the reservoirs on the flow velocity a series of experiments was conducted in which there was:

(1) A 0.3 cm head in the hot reservoir, $\overline{G}$ = 5.5 °C/cm.

(2) Levels in hot and cold reservoirs equal, $\overline{G}$ = 6.1 °C/cm.

(3) A 0.3 cm head in the cold reservoir, $\overline{G}$ = 5.6 °C/cm.

The activity versus time curves for these three experiments are shown in Figures 52(a), 52(b) and 52(c) respectively. In going from Figure 52(a) to (c), there is an increase in the time required for tracer to reach the first collimator slit. (Recall that the tracer is introduced at the hot end). However, when the flow velocity is plotted versus average gradient (opened circles in Figure 51), the points coincide with the line taken from Figure 46. The initial leveling of the reservoirs causes a surge of tracer in the leveling direction, but apparently, the subsequent oscillatory motion has no net effect on the flow velocity. Since the 0.3 cm difference in reservoir level was much larger than that which could have normally occurred during a series of experiments it was concluded that differences in melt level in the reservoirs could not have effected the flow velocities observed.

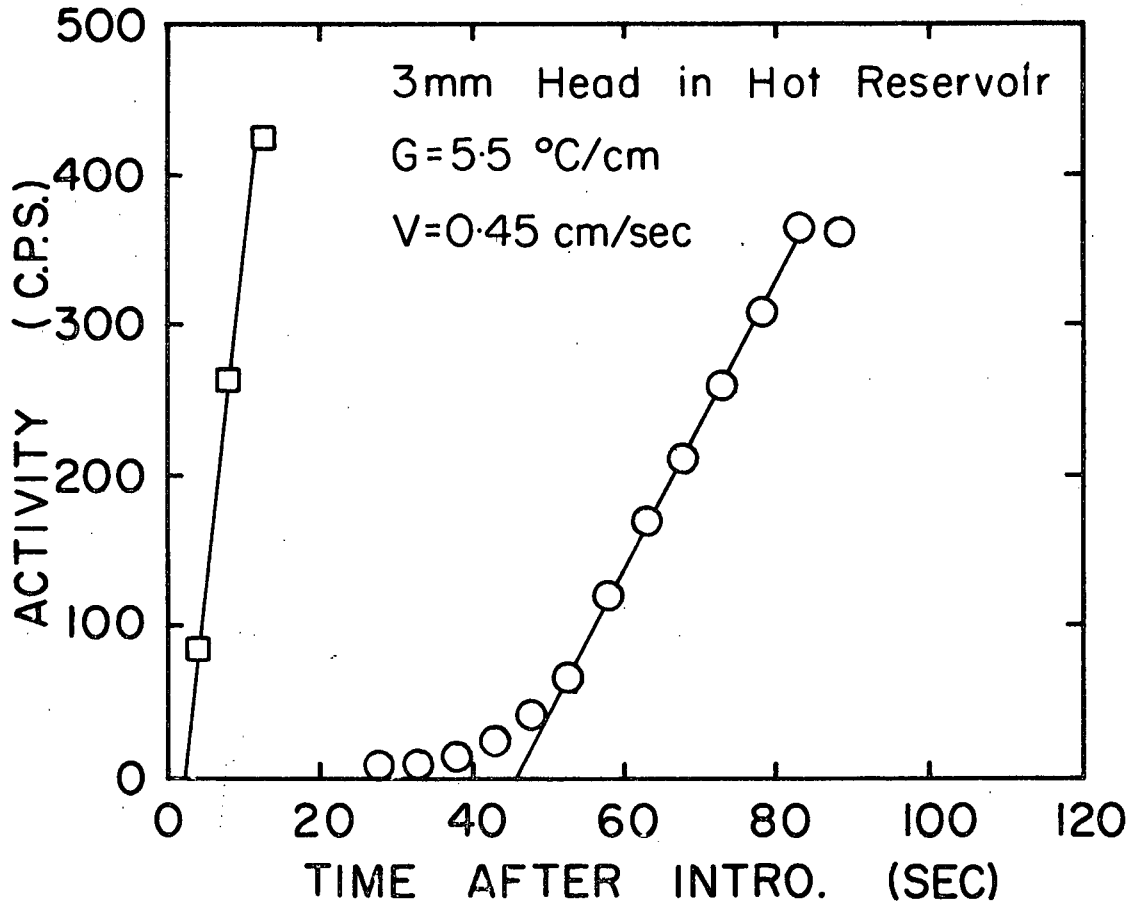

Figure 52(a). Activity versus time results when there was a 3 mm head of liquid tin in the hot reservoir.

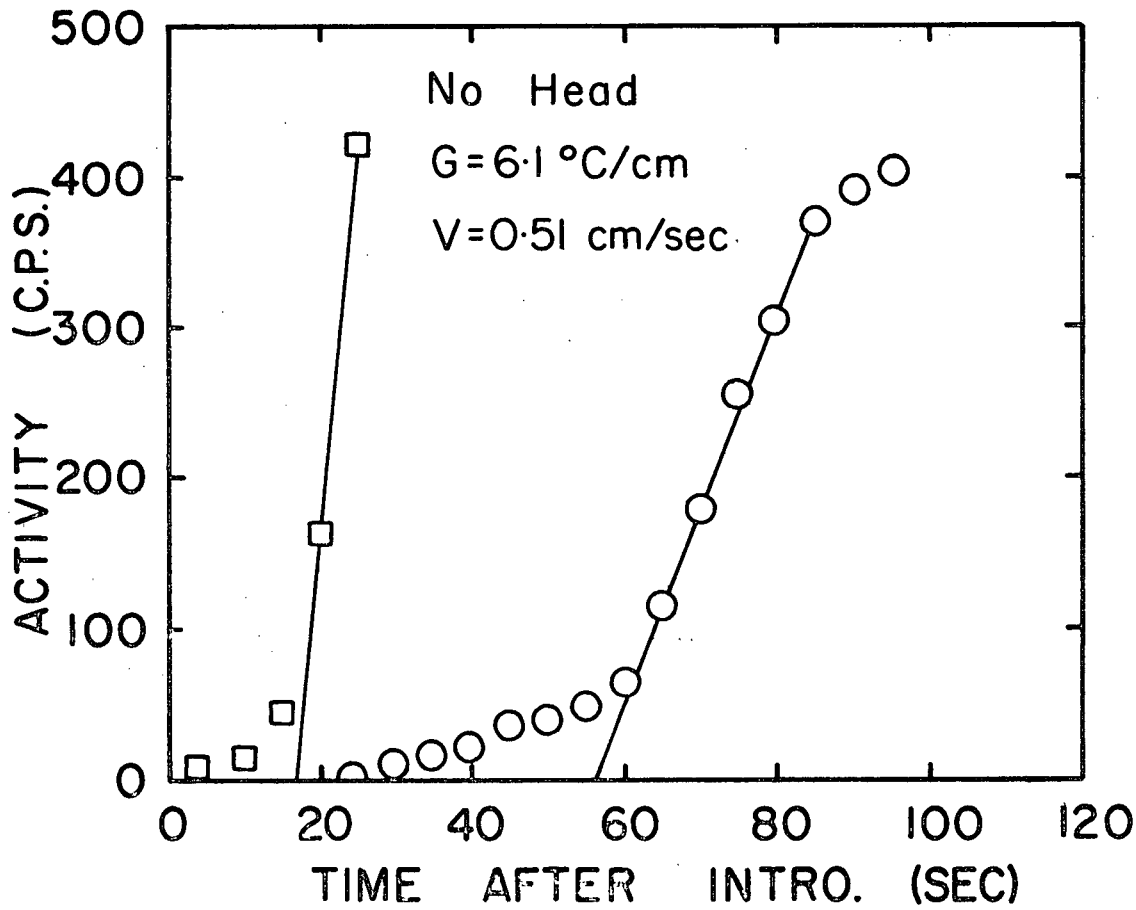

Figure 52(b). Activity versus time results when there was no difference in the liquid tin level in the hot and cold reservoirs.

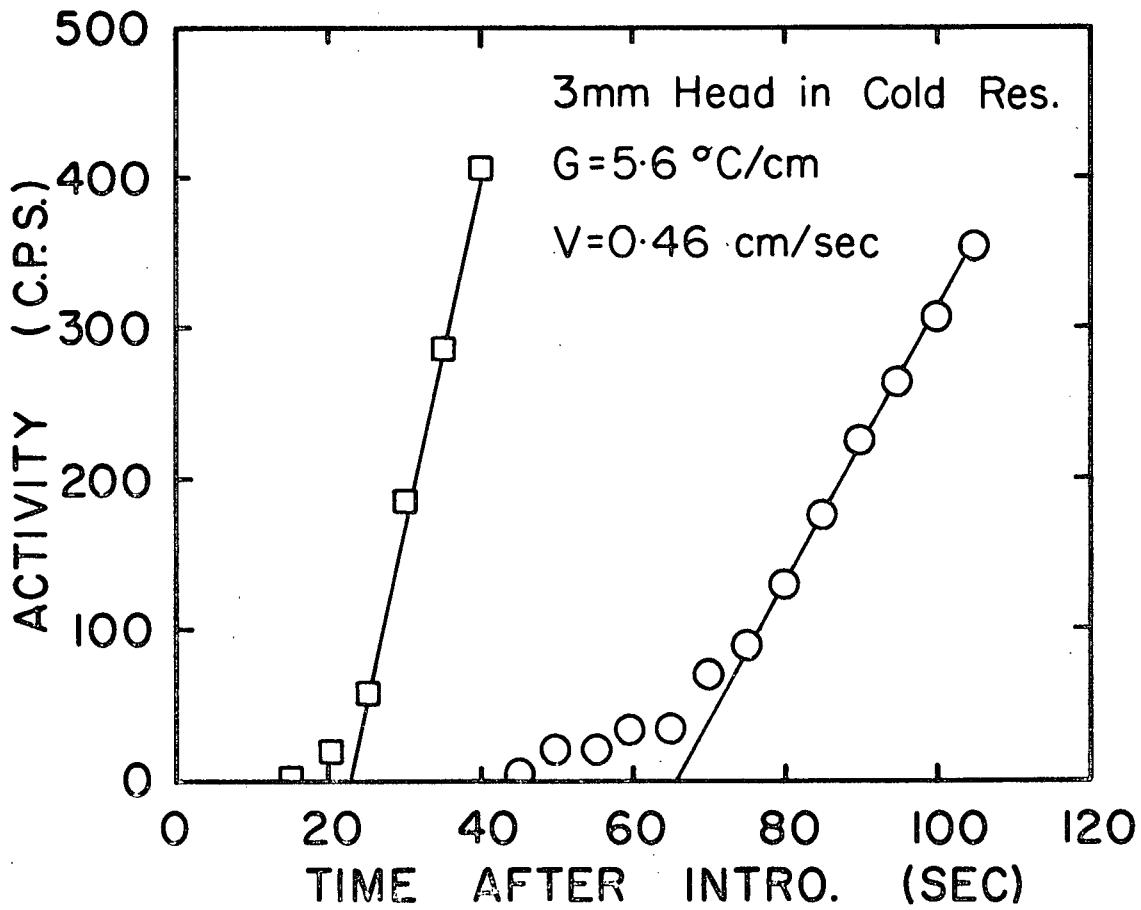

Figure 52(c). Activity versus time results when there was a 3 mm head of liquid tin in the cold reservoir.

2.2.3.4.4. Effect on Flow Velocity of Introducing Tracer in the Cold End of the Melt

In almost all the velocity measurement experiments tracer was introduced near the hot end of the melt. To determine whether addition near the hot end, as opposed to near the cold end, was significant an experiment was conducted in which tracer was introduced near the cold end. The results are plotted in Figure 51 (open triangle). The excellent agreement with the line taken from Figure 46 leads to the conclusion that the site of introduction, either near the hot end or cold end, has no bearing on the flow velocity measured by the present tracer monitoring technique.

2.2.3.4.5. Extent of Inductive Mixing

The fact that the tube furnace which surrounded the melt was inductively wound necessitated investigation of the extent of electromagnetic stirring. This was partially accomplished by conducting a series of"power off"experiments. In these experiments a desired temperature gradient was established, the furnace power was then turned off and introduction of tracer took place some time later. The solid circles appearing in Figure 53 are the results of four experiments in which the furnace power was turned off at 1, 3, 3 and 5½ minutes prior to tracer introduction. The scatter about the results of Figure 46 indicates that there is no significant inductive stirring in the longitudinal direction.

Further evidence of the absence of inductive mixing was obtained from the following experiments. The furnace power, heating block

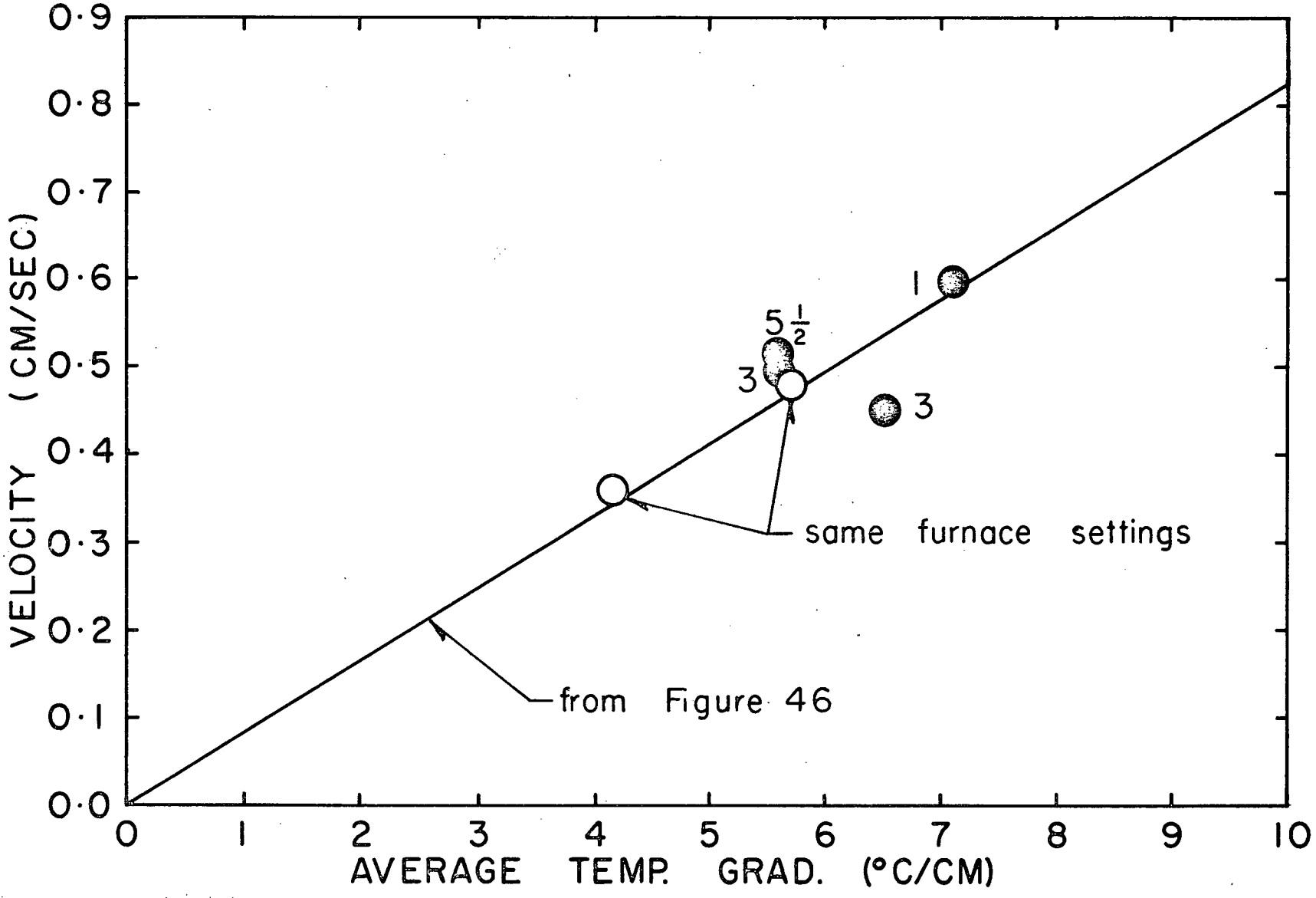

Figure 53. Results of the investigation of the extent of inductive mixing.

power and argon flow rate were adjusted to give a temperature gradient of approximately 6 °C/cm and the resulting flow velocity determined. Employing the same furnace power settings; the heating block power and argon flow rate were adjusted to give a gradient of approximately 4 °C/cm and the resulting velocity measured. The tube furnace windings are the only possible cause of electromagnetic stirring in the liquid metal. If induced flow due to the furnace windings contributes in a major way to the driving force of the observed flow, then, since the furnace power settings were identical for the two experiments just described, one would expect to observe similar flow velocities. The results of these experiments are the open circles plotted in Figure 53. The agreement between these results and the results of Figure 46 is very good. Clearly then, it is the average temperature gradient across the melt, that is, the thermal driving force, and not an electromagnetic driving force, which determines the velocity dependence obtained in Figure 46.

2.2.3.4.6. Reproducibility of Results

Most of the experiments presented in this "Evaluation of Technique" Section were conducted during different phases of the project The first stage of any series of experiments was to correlate the initial results to the results of Figure 46. It was found that as long as the average melt temperature was approximately 400 °C agreement between experiments to reconfirm the velocity versus average temperature gradient dependence and the results shown in Figure 46 was good. This occurred even when the appearance,that is, the slope of the rapidly increasing portion and maximum activity of the activity versus time curves changed. Changes

in the appearance of the activity versus time curves occcurred as a result of weakening of the tracer, due to radioactive decay, and as a result of slight irregularities accompanying tracer introduction.

2.2.3.4.7. Summary of Technique Evaluation

The dual collimator system with photography of the video scaler and timer outputs allows accurate and reproducible measurement of flow velocities up to approximately 1 cm/second. It has been established previously that the introduction technique of rotating a vertical cylinder located in the covered section of the melt causes less interference with normally occurring fluid flow than any of the other techniques investigated. Furthermore, the insensitivity of observed flow velocity with respect to slight variations in experimental procedure confirms the acceptability of the data analysis employed. Reproducibility of data has been excellent and the accuracy of the results, from Figure 46,appears to be of the order of ± 10% or better. The scatter of results about the line drawn in Figure 46 would probably have decreased had more care been taken in holding average melt temperature constant.

2.3. Summary of Flow Velocity Determination Results

A summary of all results obtained throughout the course of this investigation leads to the following important conclusions:

(1) Fluid flow arising from thermal convection will not cause mass transfer through a region of zero horizontal temperature gradient.

(2) An extremely small horizontal temperature gradient, apparently any non-zero gradient, provides sufficient thermal driving force for fluid flow.

(3) The flow velocities observed are the result of the presence of buoyancy forces created by the horizontal temperature difference across the melt. These velocities are not dependent on electro-magnetic stirring effects.

(4) The velocity of fluid flow increases with; increasing average melt temperature, increasing temperature difference across the melt, and decreasing total melt length (for a given temperature difference).

(5) For the covered horizontal rod configuration investigated herein the flow velocity is linearly dependent on the average temperature gradient between the hot and cold ends of the melt.

3 - FLOW PATTERNS IN HORIZONTAL RODS OF MOLTEN TIN

3.1. Introduction

To completely define fluid flow in liquid metals the flow pattern in the melt, as well as the flow velocities, must be specified. Preliminary autoradiography results presented in Section 2.1.6.2.2. indicated the presence of a transverse double cell flow pattern. There was no evidence of the longitudinal multi-cell flow patterns suggested by Utech et al[11] and Stewart[17]. However, it could not be established unambiguously that the flow patterns shown in Figure 25 and 26 were directly associated with the fluid flow and not partially due to quenching effects. The relatively long time (greater than 15 seconds) required for quenching plus the fact the tracer introduction was from the cover of the boat suggested that the flow patterns observed were not representative of the fluid flow in the melt. In order to appreciably reduce the quenching time the single channel thin walled aluminum boat was adopted for subsequent flow pattern observation experiments.

3.2. Experimental Apparatus and Procedure

The aluminum boat used to contain the melt is that shown previously in Figure 34. The square channel portion of the boat was surrounded by a 3/4 inch I.D. open ended copper quenching jacket. Quenching water was directed from the cold end towards the hot end. The water

supply to the quenching jacket was controlled by a pressure reducer and valve. In a typical experiment a desired temperature difference across the melt was established and maintained for approximately one hour, the tracer was then introduced into the melt and quenching took place at some specified time after introduction. The water pressure at the beginning of the quench was 5 psig and was quickly increased to about 15 psig once quenching had been initiated. Water pressure was kept low at the beginning of the quench to prevent any water surges from physically disturbing the boat. After quenching, the tin filled aluminum channel was cut from the graphite ends with a jewellers saw. The sample was then sectioned, mechanically polished, and placed on double emulsion X-ray film for a period of time sufficient to yield a satisfactory autoradiograph.

The autoradiograph results from the radiation received from a finite thickness of material adjacent to the photographic film. The thickness of this contributing layer increases with increasing energy of radiation, thus reducing the resolution obtained in the autoradiograph. Since the radiation from Sn^{113} (X-ray and gamma less than 0.4 Mev) is much less energetic than that from Sb^{124} (gamma up to 2 Mev), Sn^{113} was used for the flow pattern experiments. The trace alloy commonly used for the flow pattern experiments was 0.85% non-radioactive Sb in pure Sn with approximately 3.5% Sn^{113}. This alloy has the same density as the trace alloy used for the velocity determination measurements carried out in the previous section.

3.3. Results from Quenching Wired Top U-Channel

In initial experiments the square aluminum channel had been

constructed by wiring an aluminum cover over aluminum U-channel. All attempts to obtain suitable quenched specimens for autoradiography failed since quench water was able to seep under the cover and react violently with the liquid metal.

3.4. Autoradiography of Quenched Specimens Using a Completely Closed Square Aluminum Channel

3.4.1. Experimental Apparatus and Procedure

In order to avoid the disasterous results brought on by contact of quench water with the melt it became necessary to obtain totally enclosed square channel. It was not possible to obtain 1/4 inch square aluminum channel from commercial sources and therefore an approximately square channel was manufactured from 3/8 inch O.D., 0.038 inch wall thickness aluminum tubing. This was accomplished by forcing the tubing over a 1/4 inch square mandrel (with slightly rounded corners) followed by rolling in a horizontal rolling mill. The resulting channel was approximately 0.26 inches square with the corners having a radius of curvature of about 0.03 inches. The channel was cut to length such that the overall melt length was the same as that used in Section 2.1.8. and most of Section 2.2., namely 37.5 cm. The channel, surrounded by the quenching jacket, was inserted into the graphite reservoirs and the joints were sealed with Sairset cement. General experimental procedure for obtaining autoradiographs has already been described in Section 3.2.

3.4.2. Results from Square Aluminum Channel With No Water Shield

Even with the totally enclosed square aluminum channel quench-

ing of melts to provide specimens for subsequent autoradiography usually resulted in the spraying of melt out of the hot reservoir. This caused a decrease in the liquid metal level in the hot end of the channel and again resulted in specimens which were unacceptable for autoradiography. It appeared that quench water, which was directed from the cold and towards the hot end of the channel, was able to leak through the Sairset cemented aluminum channel-graphite reservoir joint and cause violent disruption of the melt at the hot end. Another possible cause could be that quench water hit the hot graphite reservoir creating a spray of water in the vicinity of the reservoir with some of the spray finding its way into the uncovered section of the reservoir.

3.4.3. Results and Discussion of Experiments Using Aluminum Channel with a Water Shield

To prevent water from leaking through the aluminum channel-graphite reservoir joint and to remove the possibility of water finding its way into the uncovered section of the reservoir a 3/32 inch thick, 3/4 inch O.D. aluminum water shield was welded around the aluminum channel at approximately 1/8 inch from the hot end support. As before, the channel, equipped with water shield and surrounded by the quench jacket, was cemented into the reservoirs. All autoradiographs which appear in this subsection were obtained from quenched melts which had an average temperature gradient of approximately 6 °C/cm. Figure 54 shows how most of the specimens were sectioned for autoradiography. Sections were taken perpendicular to the longitudinal axis of the rod at 0.5 cm intervals starting at 4 cm from the point of introduction. Several other specimens were sectioned paralled to the "outside" wall in order to

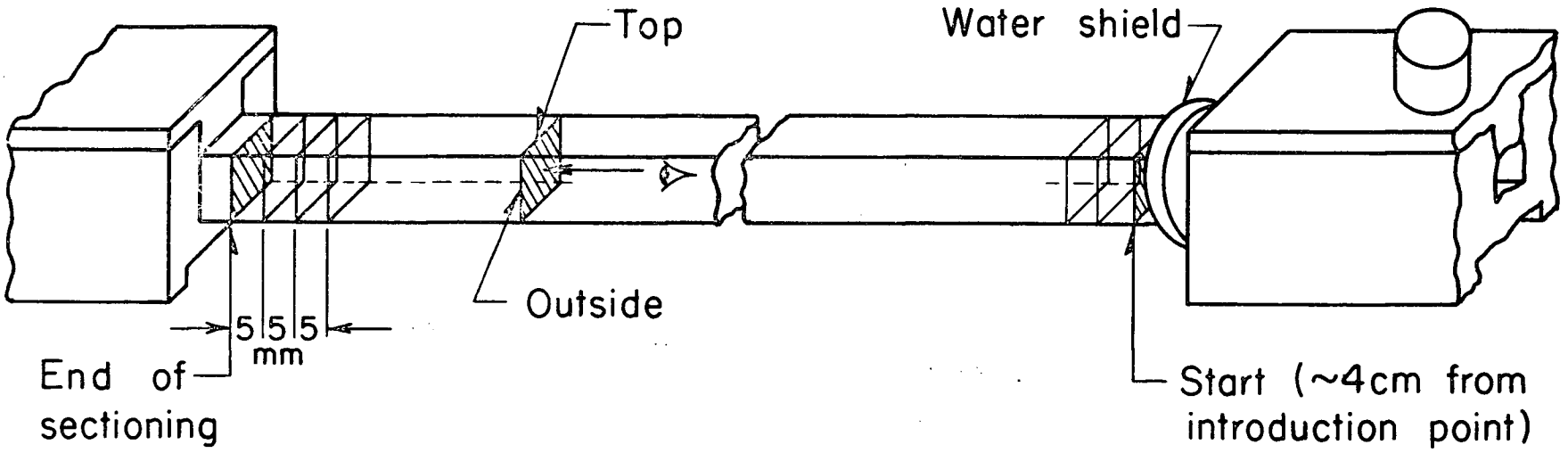

Figure 54. Schematic representation showing the positions at which the specimen was sectioned to obtain the transverse section autoradiographs.

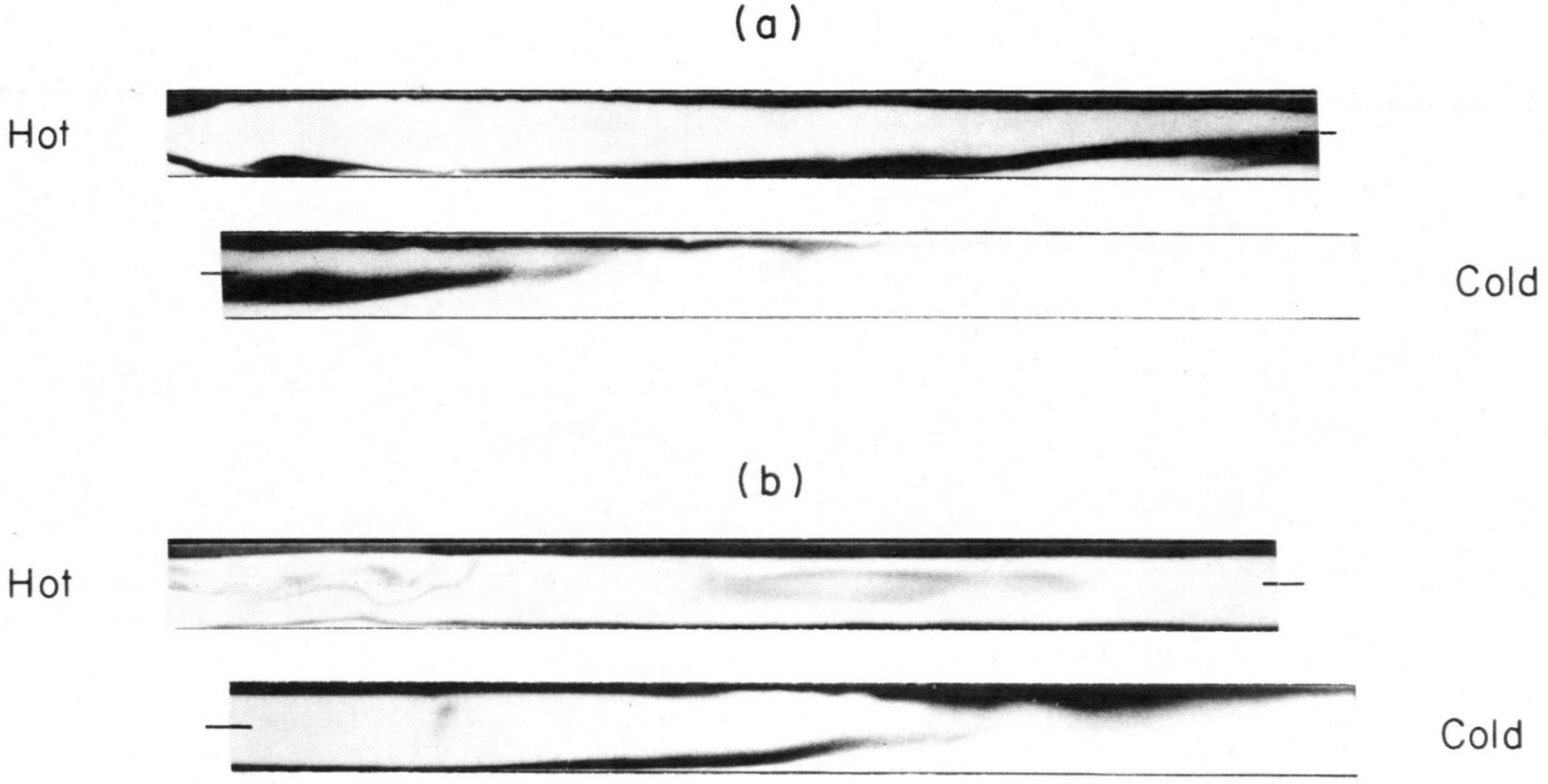

Figure 55. Longitudinal section autoradiographs of specimens quenched (a) 40 sec. and (b) 1 minute after introduction of trace alloy (0.85% Sb in pure Sn containing 3.5% Sn^{113}). Surface autoradiograph was 0.04 inches below outside surface (X2).

determine the flow pattern in the longitudinal direction.

Figure 55 shows autoradiographs of longitudinal sections of specimens which have been quenched 40 seconds (Figure 55(a)) and 1 minute (Figure 55(b)) after tracer introduction. The surface autoradiographed was approximately 0.04 inches below the outside surface of the tin. The distribution of tracer in both specimens is essentially identical and, as expected, the tracer has moved farther along the melt in the specimen that was quenched one minute after introduction, Figure 55(b), than in the specimen quenched 40 seconds after tracer introduction. There is no evidence of multi-cell flow. It appears that the longitudinal flow is unicellular with liquid moving from the hot end to the cold end along the top of the melt and returning from the cold end to the hot end along the bottom. This statement is not confirmed by the autoradiographs of Figure 55 since it is apparent that tracer has not reached the cold end of the melt and therefore the tracer which appears at the bottom of the melt did not arrive there as a result of unicellular longitudinal flow. The transverse section autoradiographs, Figure 56, of another specimen which was quenched 40 seconds after tracer introduction show that the tracer has been carried towards the bottom of the melt by a transverse flow which is superimposed on the unicellular longitudinal flow. The sections in Figure 56 are at 1 cm intervals along the rod starting at 4 cm from the point of introduction in the hot reservoir. Going from the hot end to the cold end of the melt the flow pattern becomes less complex but this is most probably due to the fact that as the tracer approaches the cold end it has spent less time at a given position and therefore the transverse flow has had less time to sweep the tracer with it in order to

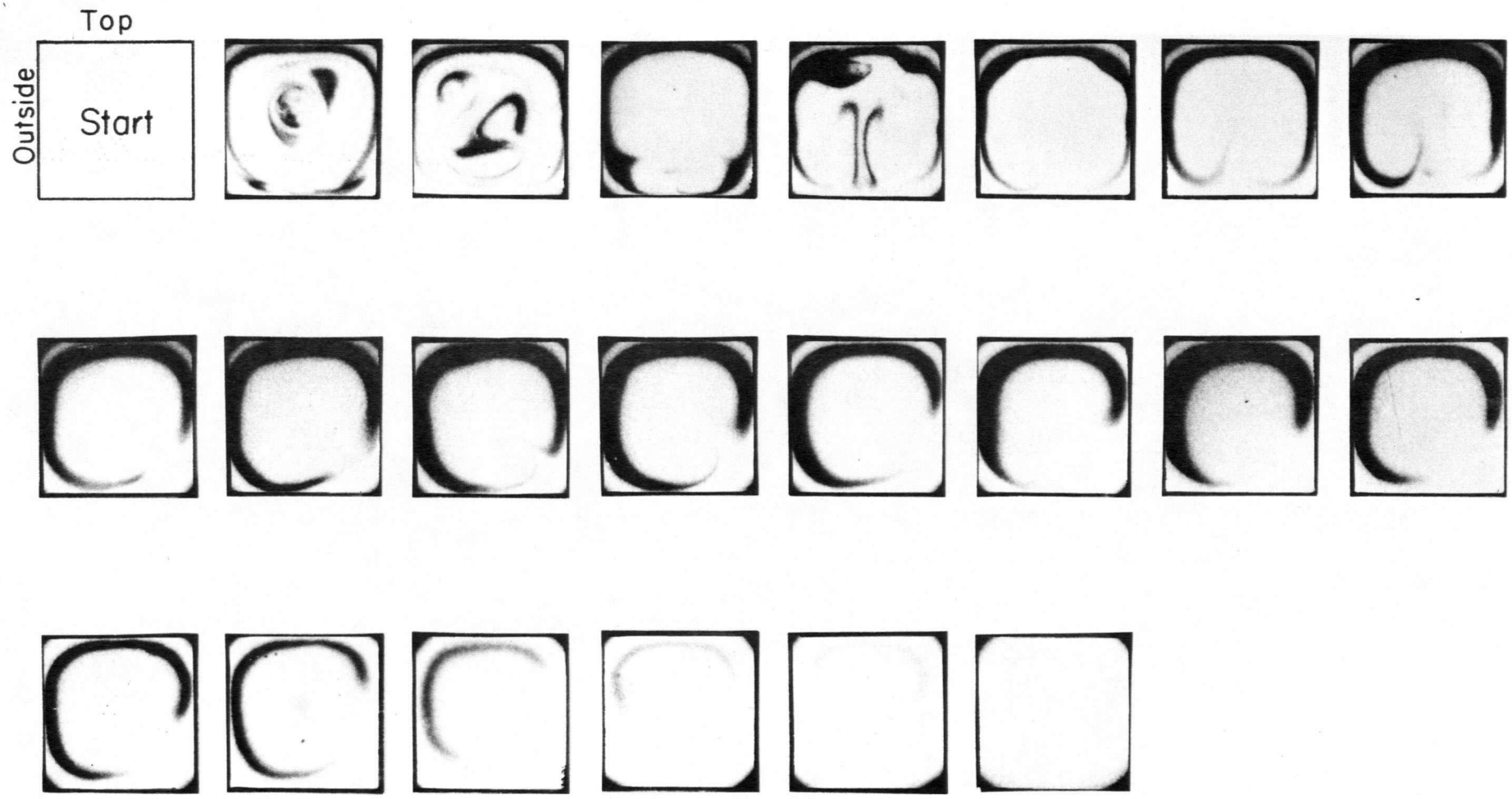

Figure 56. Transverse section autoradiographs of a specimen quenched 40 sec. after introduction of Sn^{113}-Sb-Sn tracer. Sections are at 1 cm intervals with the start (top left hand corner) 4 cm from point of introduction near the hot end (x 4).

outline the complete flow pattern.

In order to study the development of the transverse flow pattern, Figures 57 and 58 have been prepared so that a comparison can be made between the transverse flow observed 40 seconds, 1 minute, and 2 minutes after tracer introduction. The first, third and fifth rows of Figure 57 are transverse sections from the 40 second specimen and the second, fourth and sixth rows are from equivalent positions along the specimen quenched 1 minute after introduction of tracer. As expected, and in agreement with Figure 55, tracer has moved further along the specimen quenched 1 minute after introduction. Comparison of rows three and four shows that increased time before quenching has also allowed more extensive transverse flow of the tracer.

Figure 58 compares the specimens quenched 1 minute (rows one, three and five) and 2 minutes (rows two, four and six) after tracer introduction. There is no obvious difference in the transverse flow patterns observed at each point along the melt. The extra minute before quenching has no doubt allowed more extensive dilution of the tracer by the melt. This is reflected in the fact that the time required to obtained a suitable autoradiograph of the 2 minute specimen was 240 hours whereas only 24 hours was required for the 1 minute specimen. Since 1 minute was sufficient time for the tracer to travel from the place of introduction to the cold end of the aluminum channel, it would be expected that 2 minutes would be enough time for the tracer to pass through the cold reservior and, at the cold wall, move to the bottom of the boat and proceed along the bottom of the melt back towards the hot end. Thus, one would expect to observe tracer along the bottom of the transverse

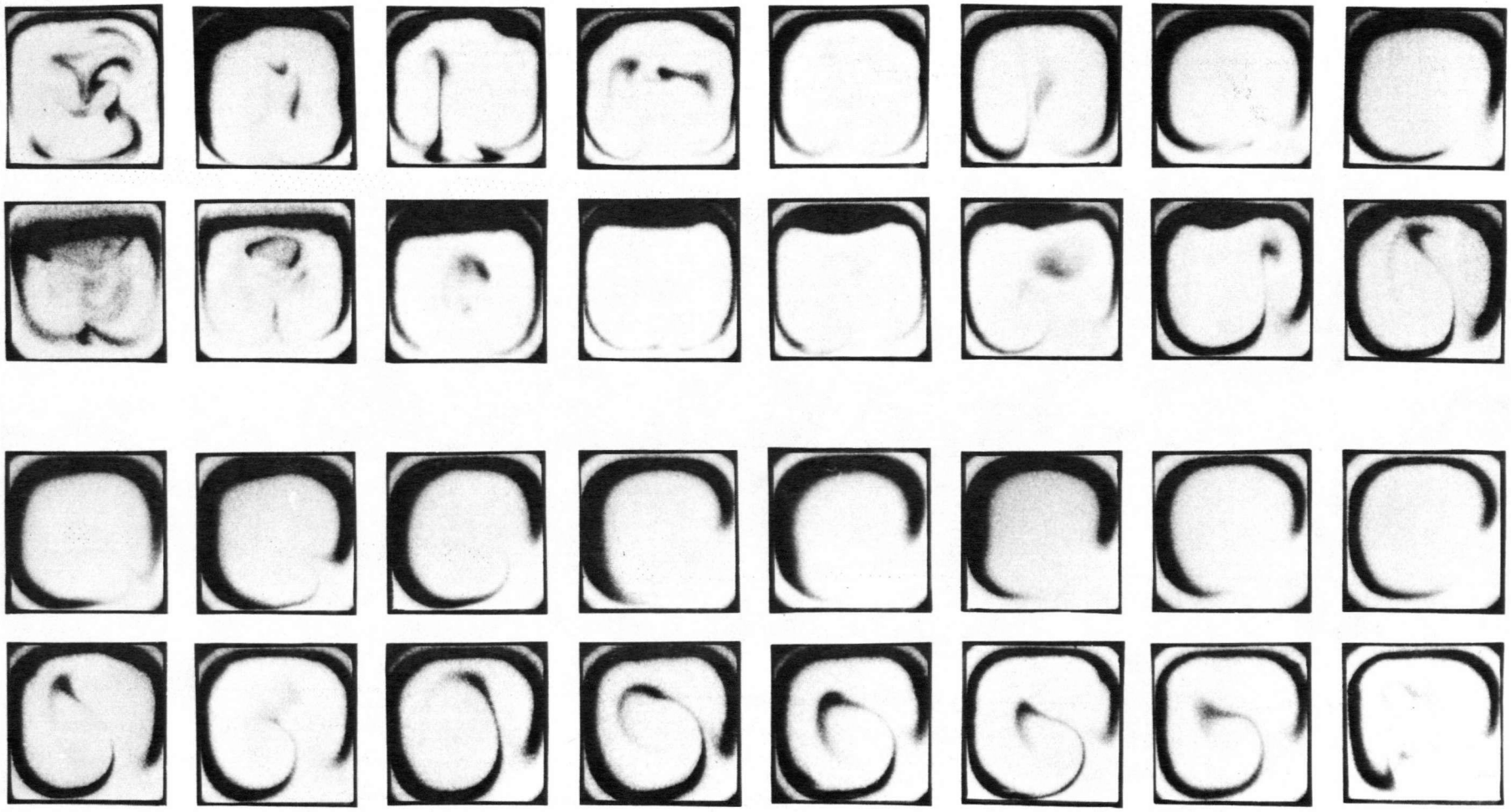

Figure 57. Comparison of transverse section autoradiographs from specimens quenched 40 seconds (first, third and fifth rows) and 1 minute (second, fourth and sixth rows) after introduction.

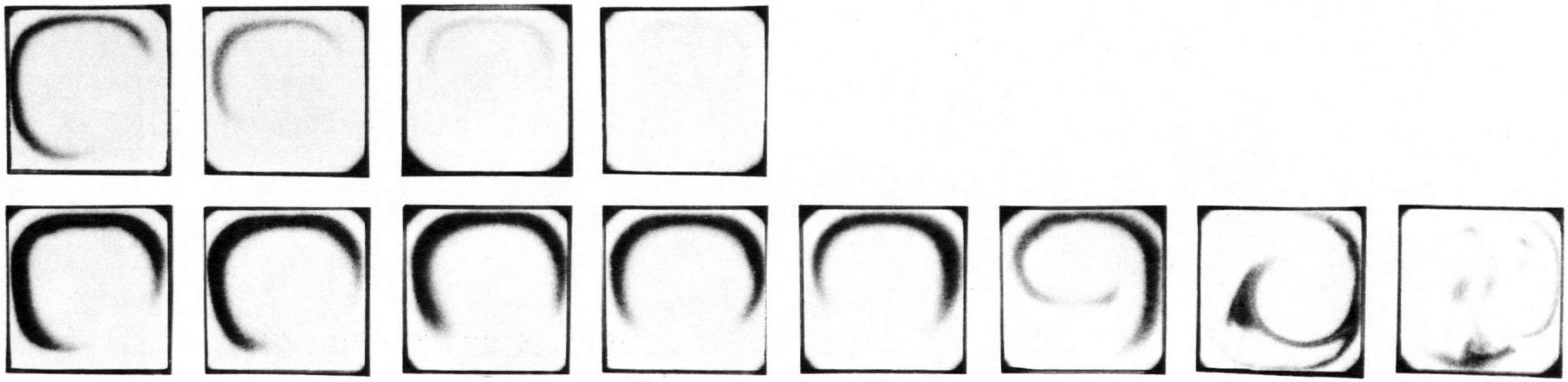

Figure 57 - Continued.

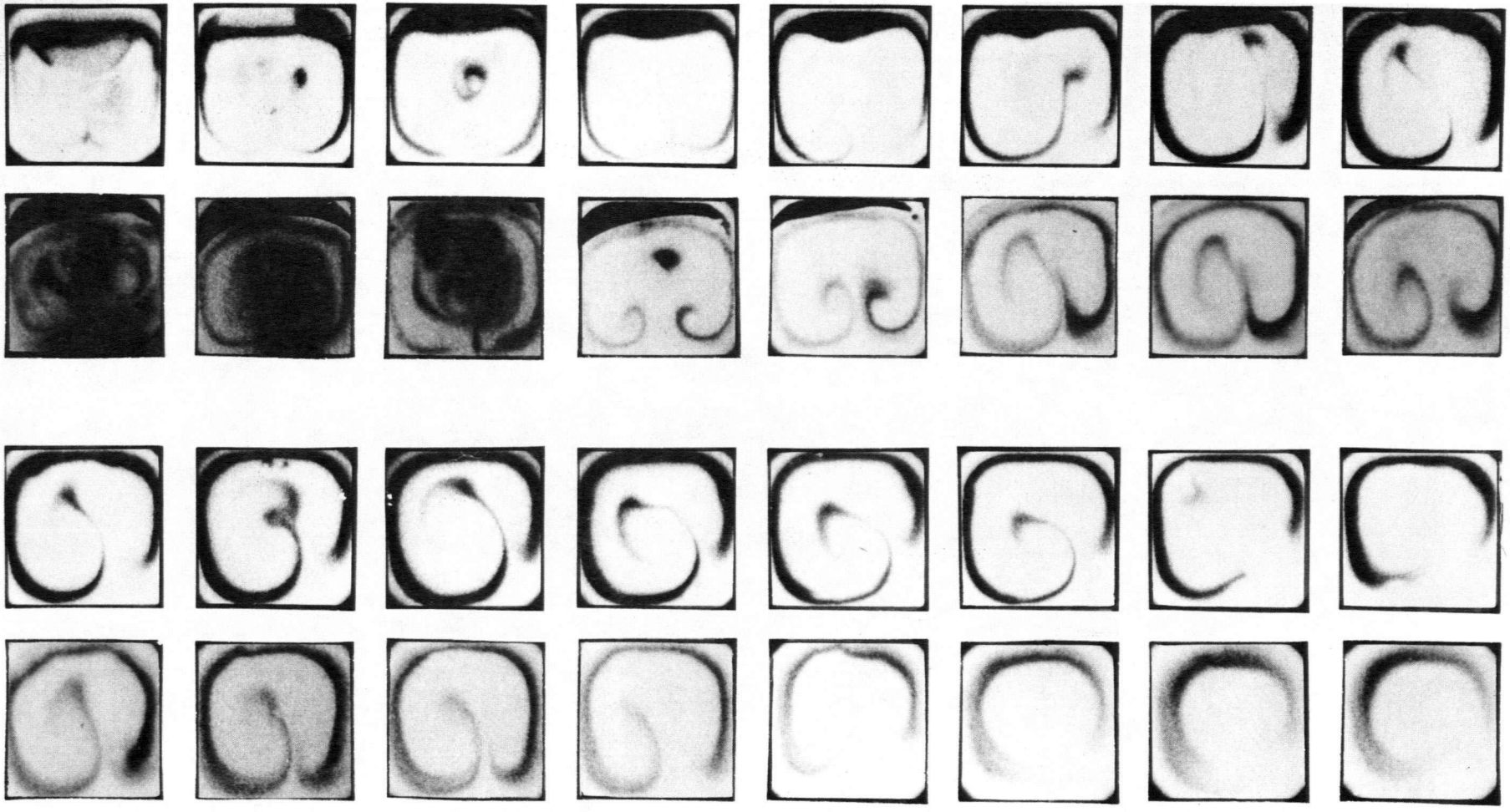

Figure 58. Comparison of transverse section autoradiographs from specimens quenched 1 minute (first, third and fifth rows) and 2 minutes (second, fourth and sixth rows) after introduction.

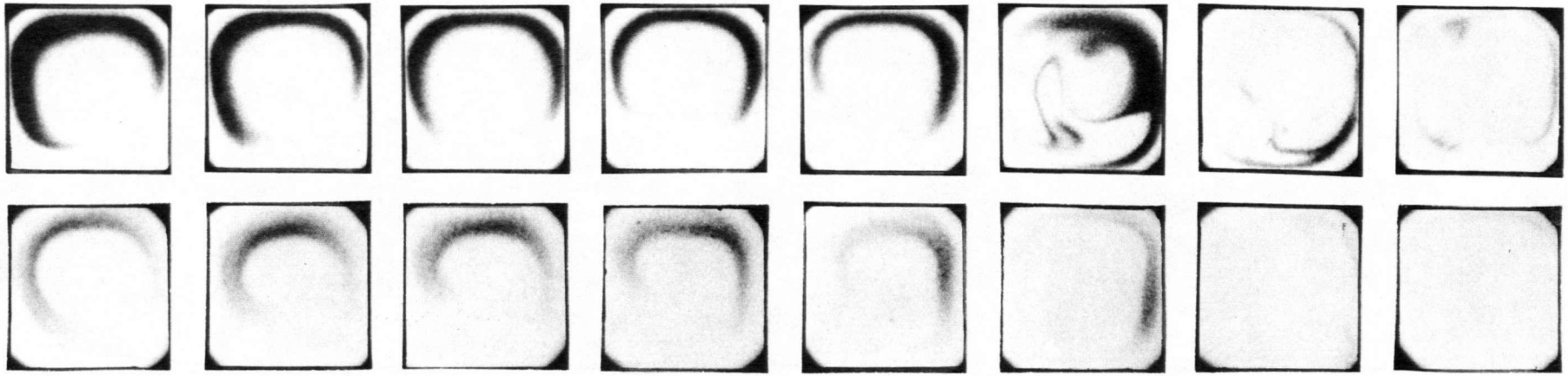

Figure 58 - Continued.

section autoradiographs of the melt which was quenched 2 minutes after tracer introduction. The fact that tracer is not observed along the bottom of these sections can be explained by recalling that extensive dilution of the tracer has occurred over the two minutes and therefore it is conceivable that by the time the tracer has moved to the bottom of the melt via the unicellular longitudinal flow it has become sufficiently diluted to be undetectable by autoradiographing for a reasonable length of time.

The effect of small variations in trace alloy density on the transverse flow pattern was also studied during this phase of the project. As outlined previously, the trace alloy used to obtain the autoradiographs shown in Figures 55-58 contained 0.85% Sb and was therefore slightly less dense (0.9994 ρSn) than the melt. Figures 59-61 show the transverse flow patterns observed one minute after introducing trace alloy which is of lower density (Figure 59), equal density (Figure 60) and greater density (Figure 61) than the melt. The trace alloy used to obtain Figure 59 was 0.85% Sb in pure Sn (with 3.5% Sn^{113}) and was 0.9994 times the density of the pure tin melt. A 3.5% Sn^{113} in pure tin was the equal density trace alloy and a 0.5% Tl^{204} in Sn trace alloy was prepared to observe the effect on the flow pattern of having the tracer more dense than the melt (1.0020 ρSn). Although these density differences due to alloying are small, they must be considered significant in comparison to the density changes arising from temperature differences. For a liquid the relative change in density due to a temperature difference is given by:

$$\frac{\rho T_2}{\rho T_1} = 1 - \beta (T_2 - T_1)$$

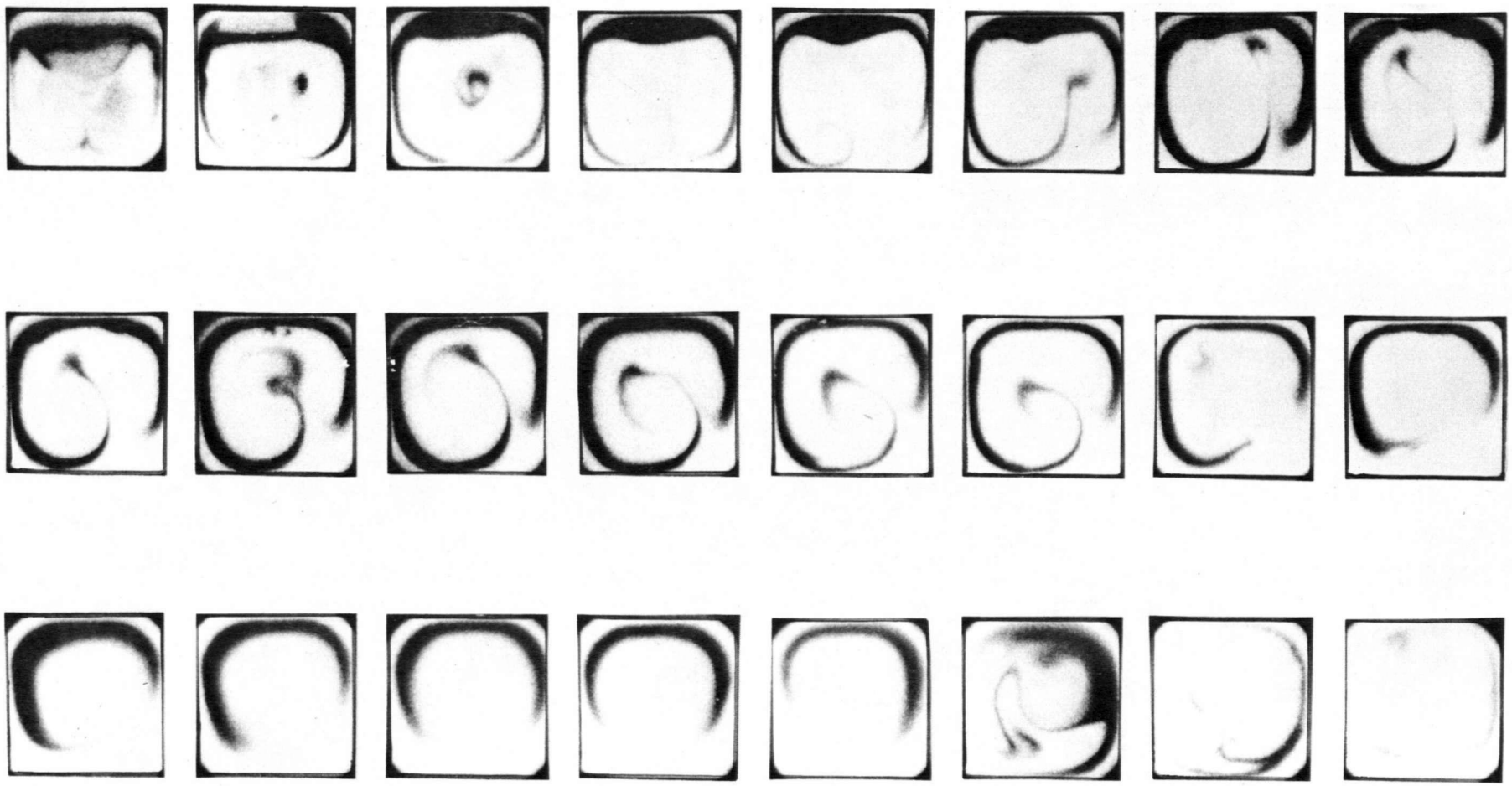

Figure 59. Transverse section autoradiographs of a specimen quenched 1 minute after introduction of a trace alloy containing 0.85% Sb in Sn^{113} with 3.5% Sn (0.9994 ρSn).

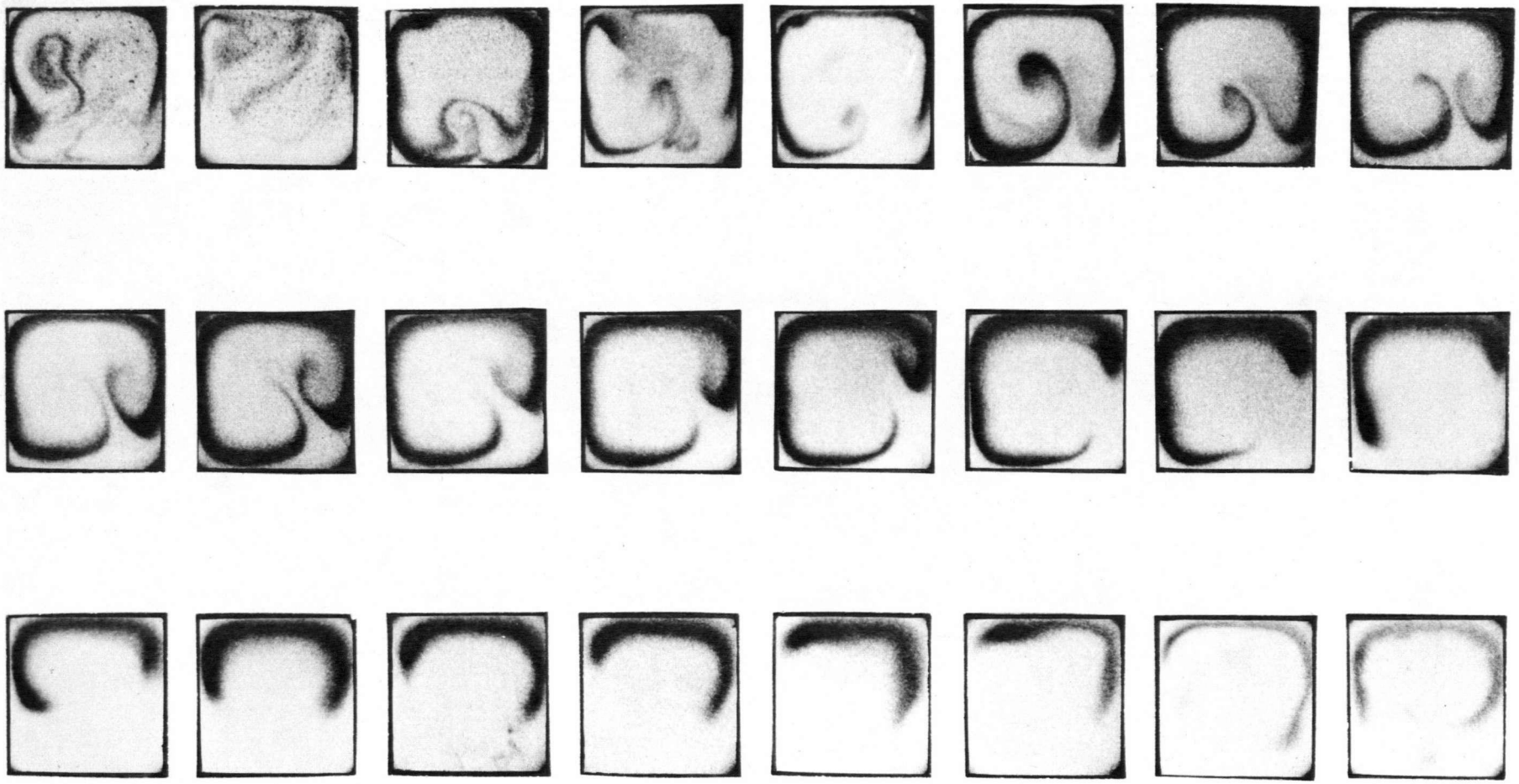

Figure 60. Transverse section autoradiographs of a specimen quenched 1 minute after introduction of a trace alloy containing 3.5% Sn^{113} in Sn (1.0000 ρSn).

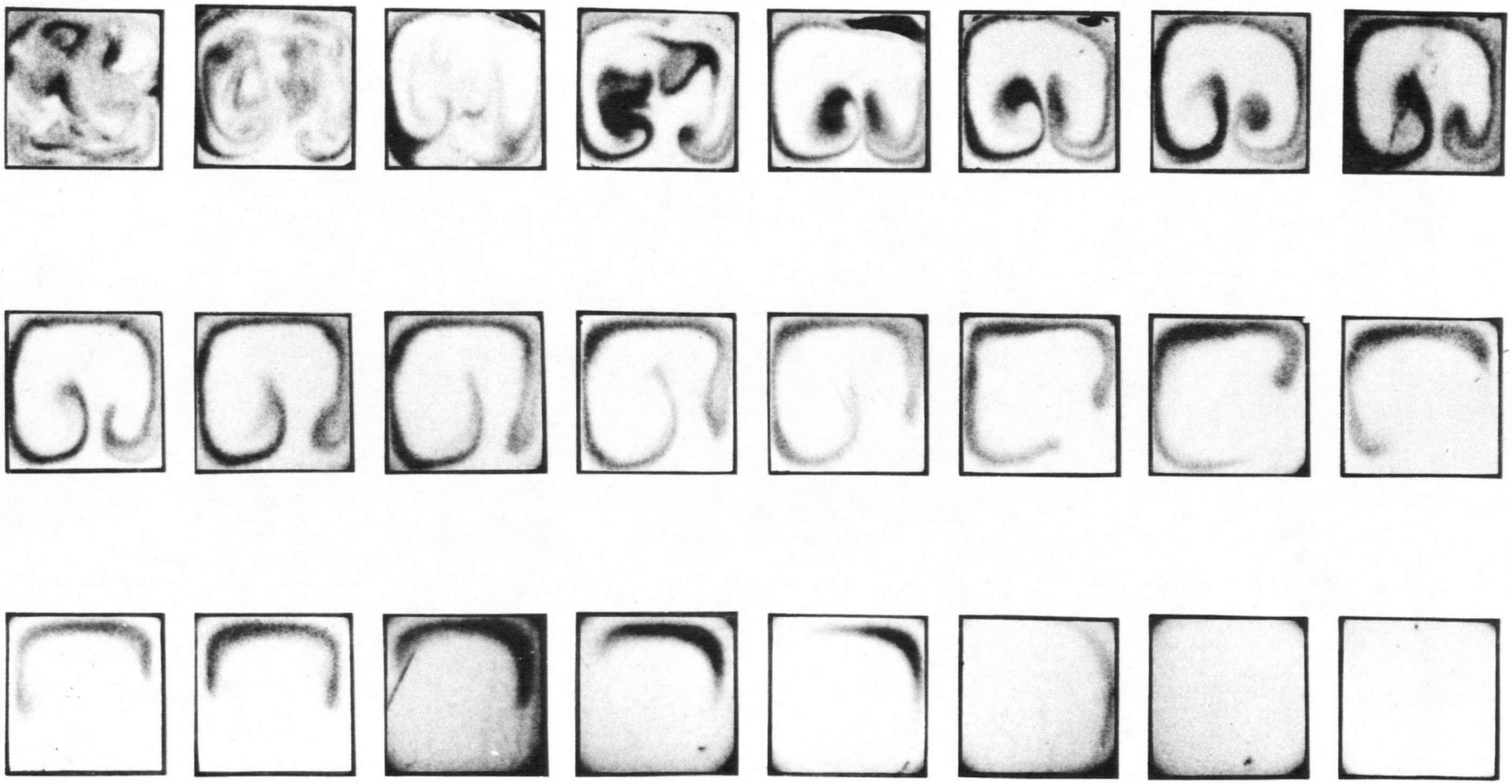

Figure 61. Transverse section autoradiographs of a specimen quenched 1 minute after introduction of a trace alloy containing 0.5% Tl^{204} in Sn (1.0020 ρSn).

where β is the volume coefficient of thermal expansion. Since β for molten tin is of the order of $10^{-4}/°C$ the change in density arising from small local temperature differences will be of the same order of magnitude as those caused by the addition of a small amount of alloying element. The flow pattern illustrated in Figures 59-61 are essentially identical and therefore it can be concluded that the thermal convective flow is sufficiently strong to overcome the solute convection which might be expected in view of the density difference between the trace alloys and the melt. In going from the less dense to the more dense trace alloy it might be expected that there would be an increased tendency for tracer to move via solute convection from the top to the bottom of melt. This was not observed.

To this point in the autoradiography studies, trace alloy has been introduced near the hot end of the melt and if it followed a unicellular longitudinal flow it would be expected to move along the top of the melt from the hot to cold end and then return along the bottom of the melt. A transverse autoradiograph of the unicellular flow would then look like Figure 62 (providing there had been sufficient time for tracer to make a complete circuit with the flow). Under the experimental condition of an average temperature gradient along the melt of approximately 6 °C/cm, 2 minutes should be sufficient time for tracer to outline the return flow (from cold to hot) along the bottom of the melt. Figure 58 (rows two, four and six) showed the 1 cm interval transverse sections from a specimen which had been quenched 2 minutes after tracer introduction and there was no evidence of a tracer rich region along the bottom of the melt. The fact that tracer did not appear along the bottom of melt has been ex-

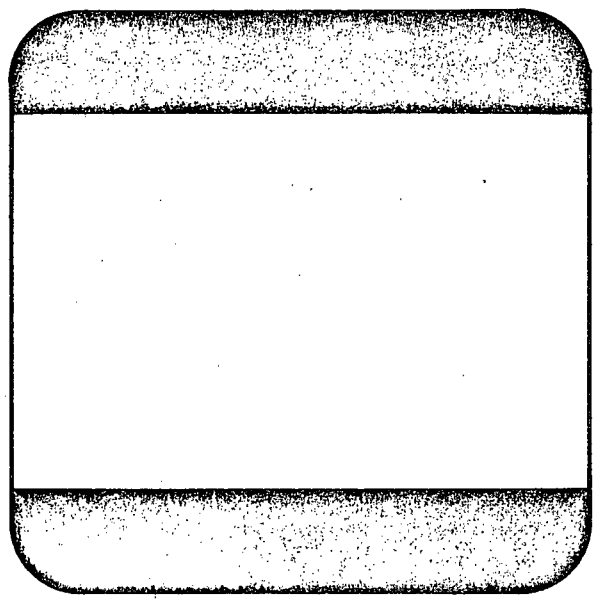

Figure 62. The expected appearance of a transverse section autoradiographs if only unicellular longitudinal flow were present (X12).

plained by assuming that the tracer became diluted to the extent that it was not detectable by autoradiographing (for a reasonable length of time).

To facilitate observation of flow along the bottom of the melt two experiments were conducted in which tracer was introduced in the cooler section of the melt. (This was accomplished by interchanging the heating and cooling blocks so that the graphite end support in which the introduction took place became the cold end). As before the average temperature gradient along the melt was 6 °C/cm. Quenching was initiated one minute after tracer introduction in both cases. Figure 63 shows the transverse section autoradiographs (the first being 4 cm from the place of introduction in the cold reservoir and subsequent sections at 1 cm intervals towards the hot end) obtained after introducing a 0.5% Tl^{204} in Sn tracer into the melt. As expected the tracer moves from the cold end to the hot end along the bottom of the melt. Approximately one-third of the way along the channel transverse flow is observed. Although the trace alloy is slightly more dense than the melt (1.0020 ρSn) the transverse flow is sufficiently strong to cause mixing of tracer throughout the cross section . The nature of the transverse flow is similar to that observed in Figures 56-61. The flow travels down the sides of the section and as it returns to the top, through the middle of the section, the radioactive tracer is drawn upwards by it. The transverse flow is greatly suppressed by using a dense (1.257 ρSn) trace alloy composed of 60% Pb in Sn containing 0.5% Tl^{204}, Figure 64.

In Figures 56-61 the apparent extent of transverse flow <u>decreases</u> with increasing distance from the point of introduction near the

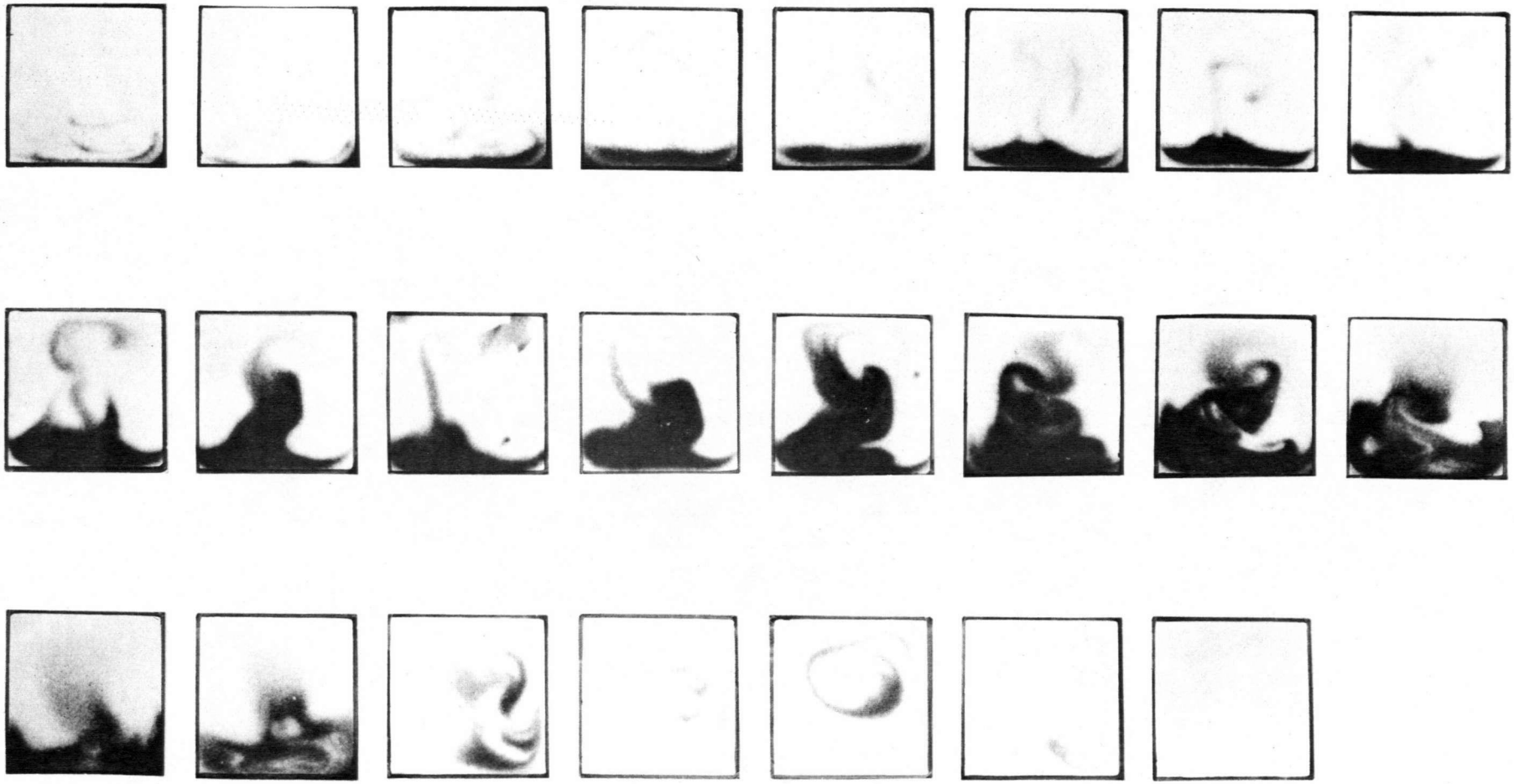

Figure 63. Transverse section autoradiographs of a specimen quenched 1 minute after introduction of a trace alloy containing 0.5% Tl^{204} in Sn. The first section (top left hand corner) is 4 cm from the point of introduction near the cold end.

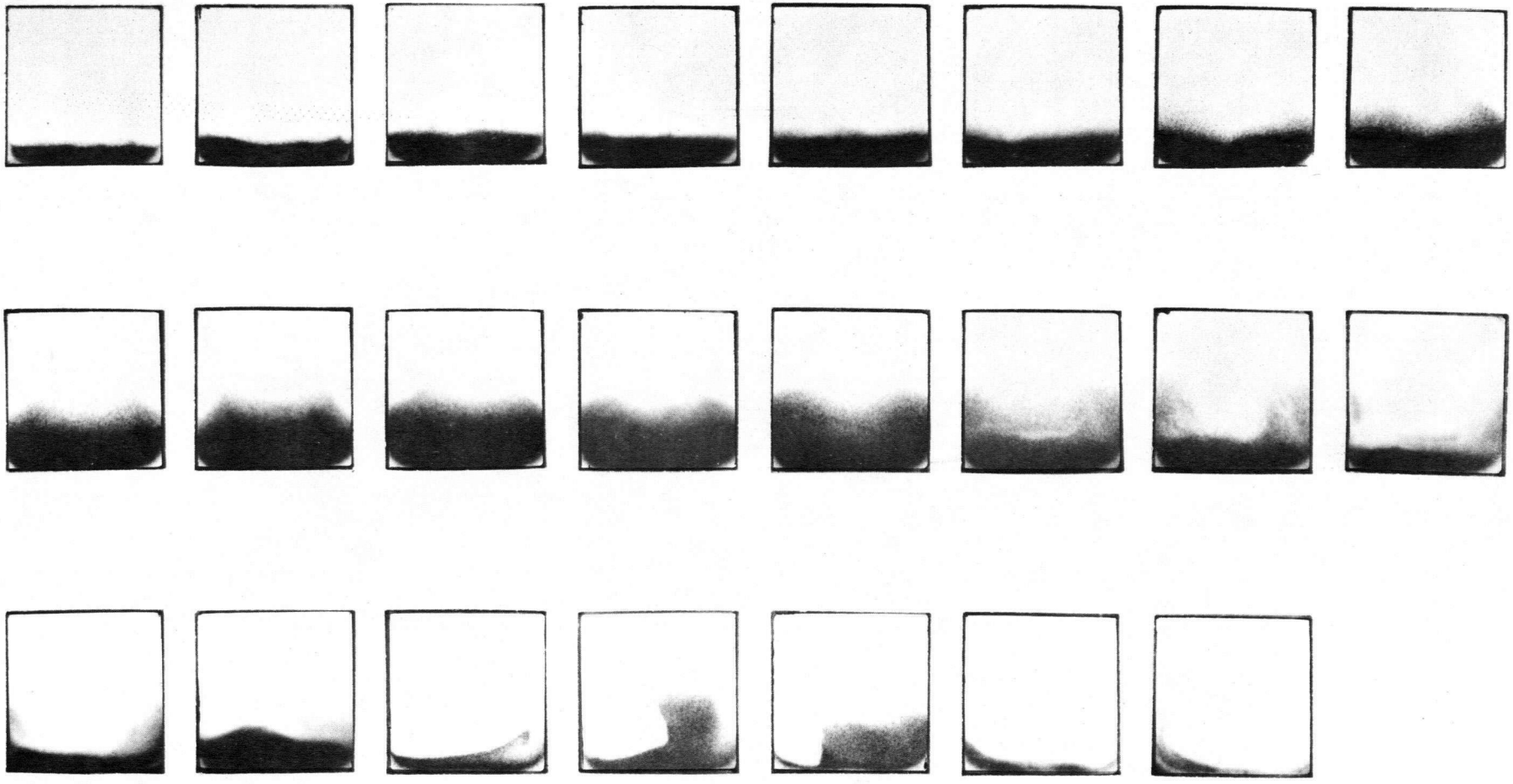

Figure 64. Transverse section autoradiographs of a specimen quenched 1 minute after introduction of a trace alloy composed of 60% Pb in Sn contained 0.5% Tl^{204}. Introduction took place near the cold end.

hot end. This has been explained by noting that as the distance from the introduction site increases the tracer has had continuously decreasing time in which to fully outline the transverse flow present. The net result is that one would observe move extensive transverse flow near the hot end (place of introduction)than near the cold end.

In Figures 63 and 64 it is observed that the extent of transverse flow increases with increasing distance from the place of introduction. This observation is not consistent with the explanation just offered. Recalling that Figures 56-61 were obtained by introducing tracer in the hot end whereas for Figures 63 and 64 introduction took place in the cold end (and the first section in each figure is approximately 4 cm from the place of introduction), it is apparent that transverse flow is more extensive near the hot end than the cold end. Since more heat must be removed from the hot end than the cold end of the melt during quenching it is possible that more time is required for solidification in the hot end and that during this additional time more extensive transverse flow may occur. Also, lateral temperature gradients which arise during quenching may cause transverse flow that is more extensive than was occurring prior to quench initiation. The results of quench time determination experiments and several other tests to attempt to confirm the validity of the observed flow patterns as well as the driving force for the transverse flow are discussed in the next section.

3.4.4. Results and Discussion of Attempts to Confirm the Validity of Observed Flow Patterns

3.4.4.1. Effect of Quench Cylinder on Observed Flow Velocity

In order to determine what, if any, effect the presence of

the quenching cylinder had on the flow taking place in the melt a velocity determination experiment was carried out in which the quench cylinder was in place. The results of this experiment were velocity equals 0.36 cm/sec for an average temperature gradient across the melt of 4.16 °C/cm. Figure 46 shows that for a gradient of 4.16 °C/cm one would expect to observe a flow velocity of 0.35 cm/sec. From this it can be assumed that the quench cylinder does not affect the longitudinal flow.

3.4.4.2. Quench Time Determination

The time required for complete solidification was determined at both the hot and cold ends of the square aluminum channel. The thermocouples (30 gauge iron-constantan insulated by 1/16" O.D. mullite tubing) were inserted through the top of the channel such that the beads were located in the cross sectional centre of the melt. The hot end thermocouple was positioned 5 mm downstream from the water shield and the cold end thermocouple was 5 mm ahead of the cold end support. The thermocouples were connected through a multipoint switch to the Honeywell recorder. Results of typical quench time determination tests are shown in Figure 65. On the basis of six tests the average time for total solidification at the hot end was 2¼ seconds and at the cold end was 4¼ seconds. At first glance a somewhat surprising result.

The latent heat of fusion of tin is 14.5 cal/gm and the heat capacity of liquid tin at 350 °C is approximately 0.06 cal/gm °C. If the hot end of the melt was 200 °C higher than the cold end the amount of heat that would have to be removed from the hot end would be roughly 1.2 cal/gm more than that removed from the cold end. Since this is less

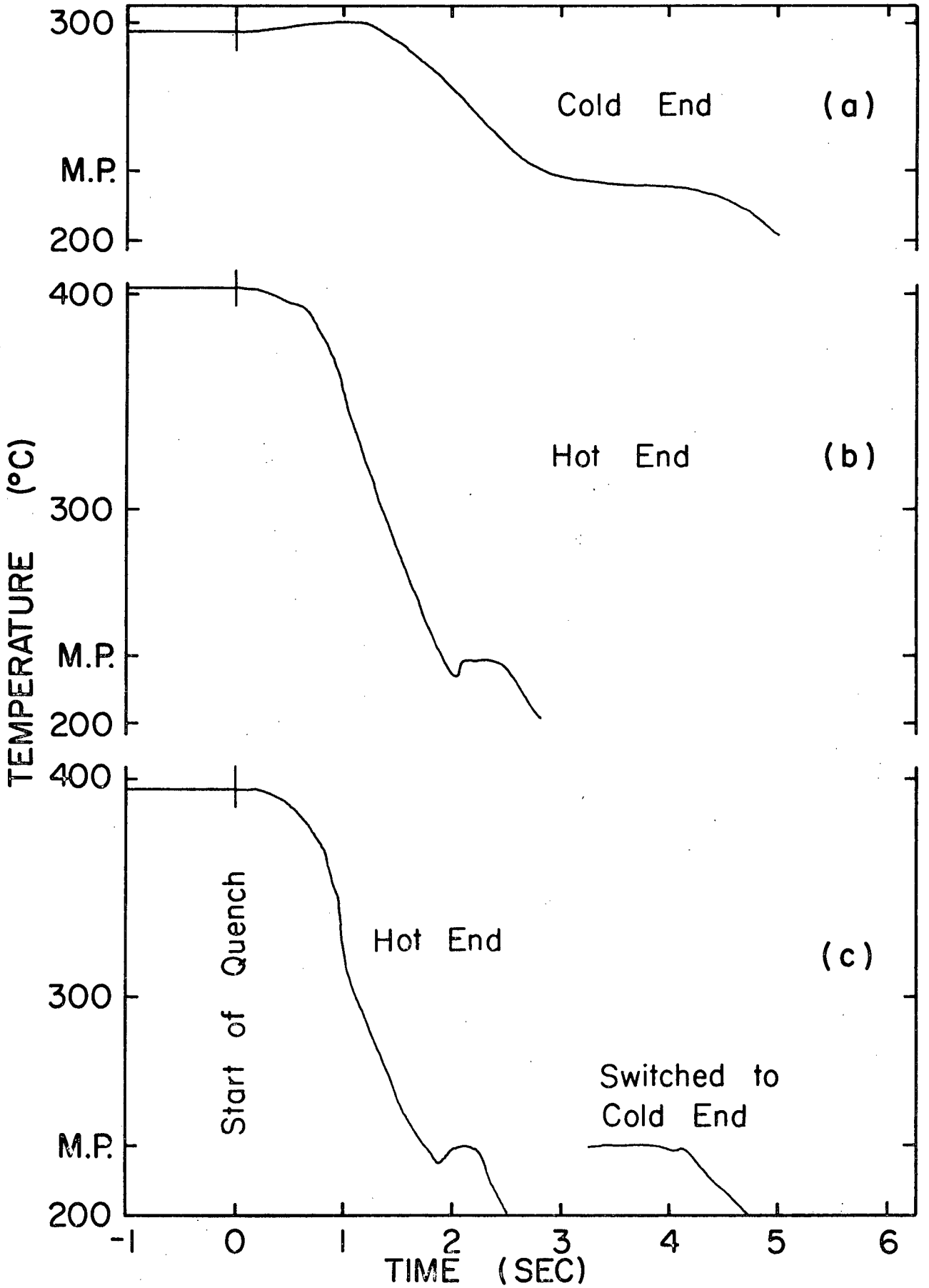

Figure 65. Typical results of quench time determination experiments.

than 10% of the heat of fusion it would not be unreasonable for the hot and cold ends to solidify in approximately the same length of time. Also, since the quench water enters the chamber 3 cm ahead of the cold reservoir and the stream is directed towards the water shield at the hot end, the observation that the hot end of the channel solidifies 2 seconds before the cold end is understandable. In any case, the quench time tests conclusively show that the hot end does not take longer to solidify than the cold end. The possibility that the more extensive transverse flow in the hot end results from delayed quenching in this region must be ruled out.

3.4.4.3. Quenching in a Prearranged Tracer Distribution

The possibility that the quenching operation was the prime driving force for the development of the observed transverse flow pattern was further investigated by conduction experiments which involved quenching a melt which had a prearranged and thus known tracer distribution. The prearranged tracer distribution is shown in Figure 66. This distribution was achieved by the following technique. A 0.04 inch thick, 0.24 inch wide by 11 inch long layer of 0.5% Sn^{113} in Sn was placed along the bottom of a square aluminum channel which was an inch longer than the usual channel length. The graphite ends were attached and the boat placed in the furnace. A furnace temperature of 200 °C(30 °C below the melting point of pure tin) was established and maintained. When the temperature along the boat was 200 °C lead-tin eutectic (m.p. 183 °C) at approximately 210 °C was poured into the boat. Upon solidification of the eutectic the boat was removed from the furnace and the channel

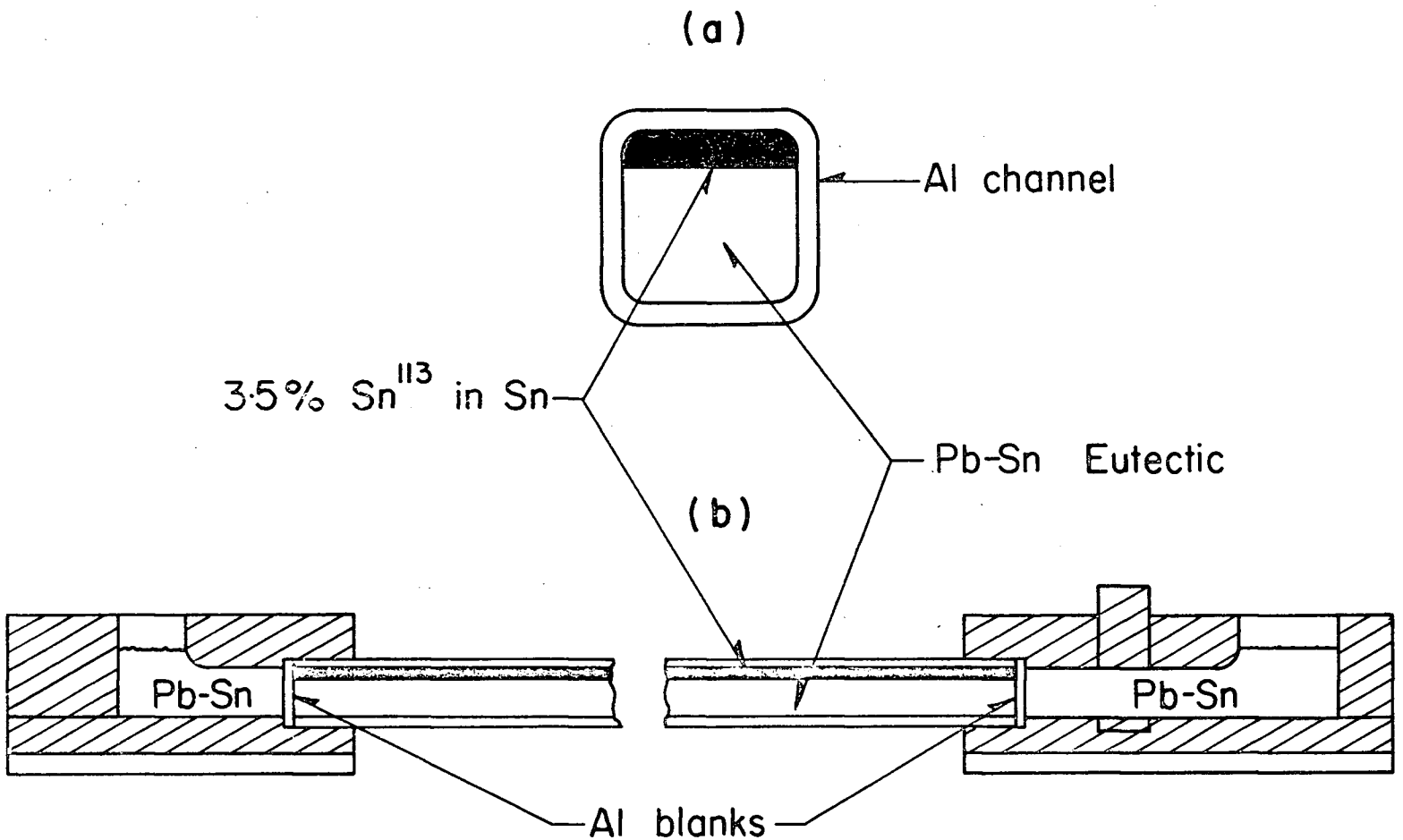

Figure 66. Schematic representation of the prearranged tracer distribution (a) transverse section and (b) longitudinal section.

which now had lead-tin eutectic over the 3.5% Sn^{113} in Sn layer was removed with a jewellers saw. The reservoirs were reheated to remove the eutectic and the ends of the aluminum channel which were left after sawing. The channel was then inverted so that the Sn^{113} layer was above the eutectic, the boat was reassembled and the reservoirs refilled. The aluminum blanks were placed across each end of the channel to insure that, once molten, no movement of the melt (due to differences in head between the hot and cold reservoirs or due to physical disturbance) could occur through the channel and thus change the tracer distribution.

In the first test the boat, with the tracer distribution just described, was gradually heated to approximately 285 °C to give a superheat of about 100 °C. This superheat was chosen so as to reproduce the conditions of earlier quenching experiments where the average superheat was of the order of 100 °C. During the melting and superheating all possible care was taken to maintain a zero horizontal temperature gradient along the melt and thus avoid the possibility of thermal convection. Solute convection should not occur since the configuration of the less dense tin layer over the more dense eutectic (1.257 ρSn) should be stable. Since neither solute nor thermal convection is expected,the quenched specimen should yield transverse section autoradiographs which are similar to Figure 66(a). Results of this first test showed a completely uniform distribution of tracer. This showed that mixing had either occurred during the superheating period (approximately 3/4 hour) or as a result of the quench. The idea that the quench (which from previous tests is known to take less than 5 seconds) was solely responsible for this complete mixing is totally unacceptable. It was not possible

to maintain a perfectly flat temperature profile during the superheating and therefore some thermal convection must have occurred.

The second test was conducted in a similar manner but this time quenching was started shortly after the melting point of tin (232 °C) was passed. The total time from the melting of the eutectic to the time of quenching was 12 minutes. The results of this test are shown in Figure 67. The sections are at 1 cm intervals. Although some mixing of Sn^{113} into the eutectic has occurred, there is no evidence of the transverse flow observed in previous autoradiographs. The conclusion that the quench technique is not responsible for the transverse flow observed would now appear valid.

3.4.4.4. Extent of Inductive Mixing

In Section 2.2.2.5. evidence was presented to show that inductive mixing is not the driving force for the longitudinal flow of the liquid tin. The extent to which inductive mixing effects the transverse flow pattern was determined by introducing tracer (3.5 % Sn^{113}) into the melt two minutes after the furnace power had been turned off. The gradient across the melt was 6 °C/cm and quenching took place one minute after tracer introduction. Rows two, four and six of Figure 68 show the results of the power off test. The results of a test with the same temperature gradient and tracer but with the furnace power on (normal procedure) are shown in rows one, three and five. Comparison of rows one and two, and three and four shows the transverse flow patterns in the power on and power off experiments to be virtually identical. The only apparent difference between the two being that the power off

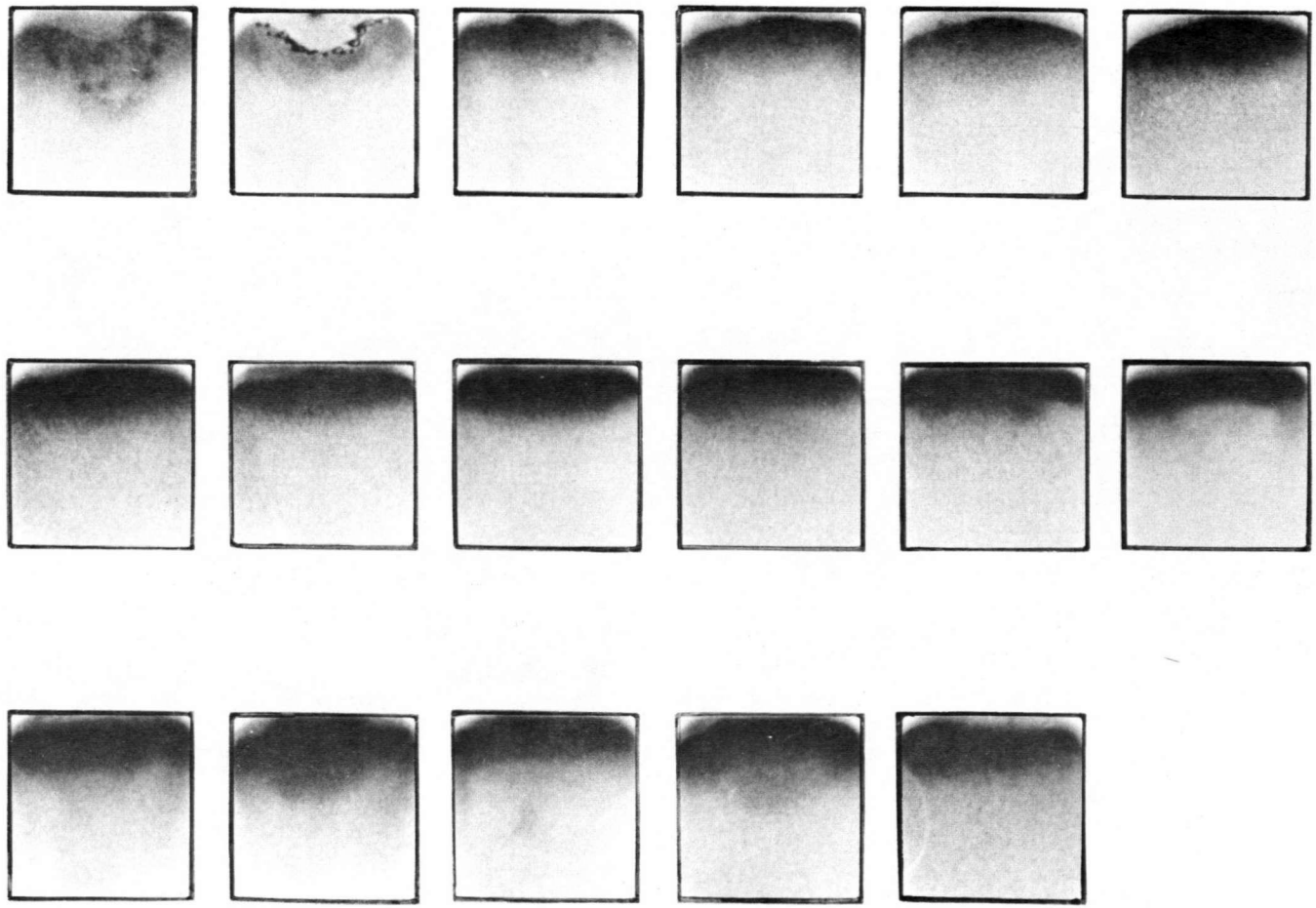

Figure 67. Transverse section autoradiographs of the specimen which had the prearranged tracer distribution shown in Figure 66.

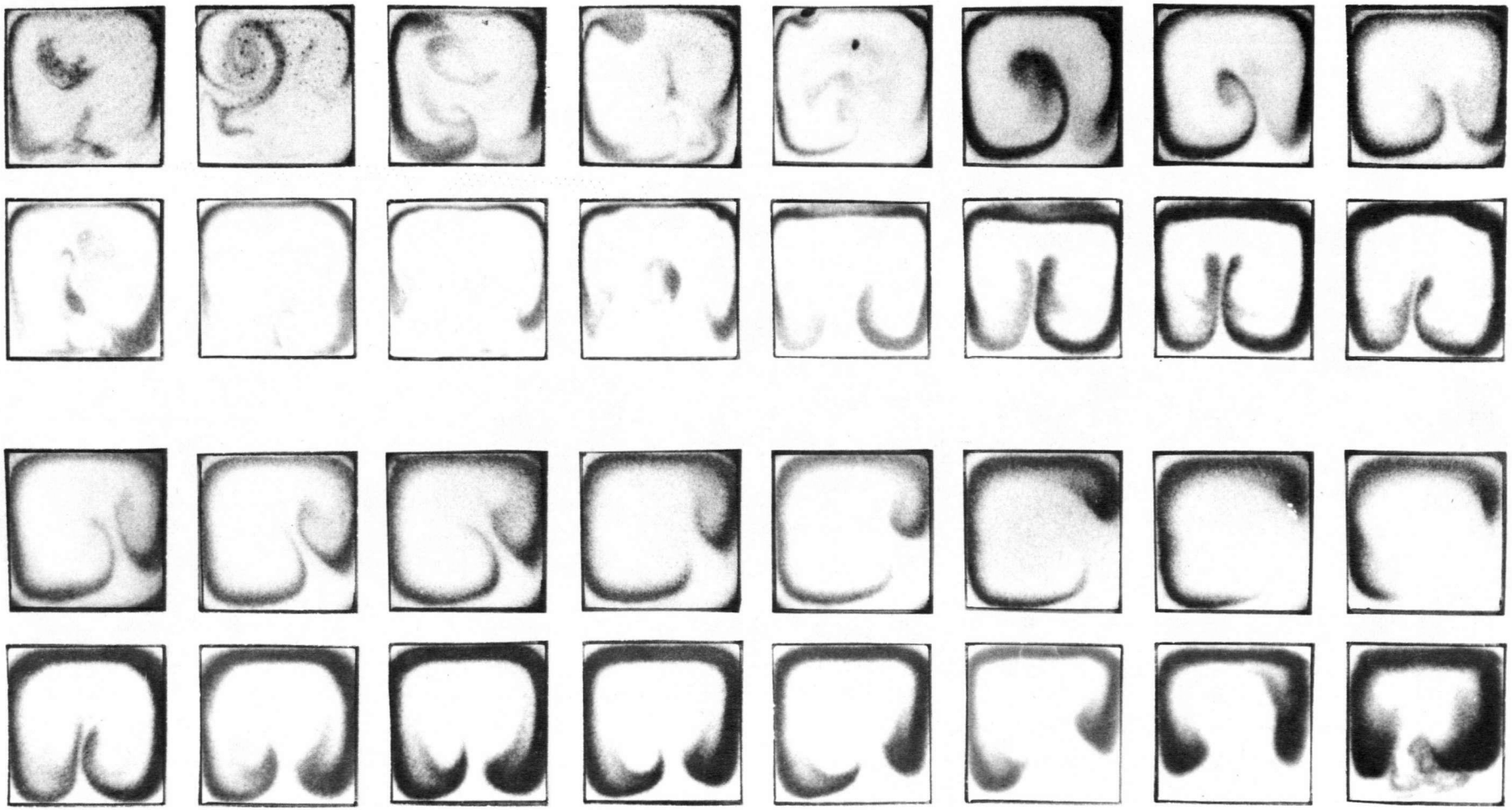

Figure 68. Comparison of transverse section autoradiographs of specimens quenched 1 minute after introduction of 3.5% Sn^{113} in Sn tracer into the melt; while the furnace power was on (first, third and fifth rows) and 2 minutes after the furnace power had been turned off (second, fourth and sixth rows).

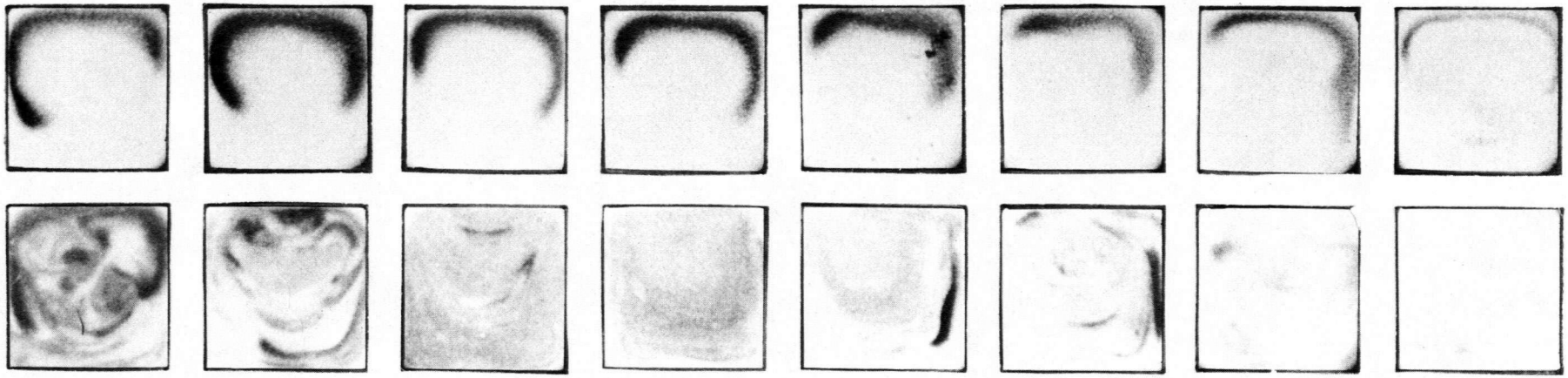

Figure 68 - Continued.

flow seems to be somewhat more diffuse. There is considerably more transverse mixing towards the cold end in the power off test (comparing rows five and six) and this coupled with the fact that the flow in this test is generally more diffuse suggests a slight increase in the driving force for transverse flow when the power is off. The probable source of this driving force would be an increase in transverse temperature gradients which arise after turning off the furnace power.

3.4.4.5. Determination of Transverse Temperature Gradients

Measurements were made of the temperature distribution on planes transverse to the boat axis using the apparatus illustrated in Figure 69. This apparatus allowed complete freedom of two dimensional movement of the thermocouple bead in a given transverse plane. One moveable thermocouple was chosen over a series of fixed thermocouples so that accurate relative temperature diffences could be measured without having to be concerned about thermocouple calibration corrections. The boat in which the transverse gradients were measured was the two channel graphite boat used in Section 2.1.6.. This boat was chosen since it was much easier to adapt the moveable thermocouple in this case than it would have been for the single channel aluminum boat. Since the transverse flow patterns observed in the two channel graphite boat (Figures 25 and 26) are similar to ones observed in the single channel aluminum boat it was assumed that transverse temperature gradients would also be similar (especially so in the graphite end supports used on the single channel aluminum boat).

Figure 69(a) is a top view of the boat showing the wedging mechanism used to move the thermocouple from one side of the channel

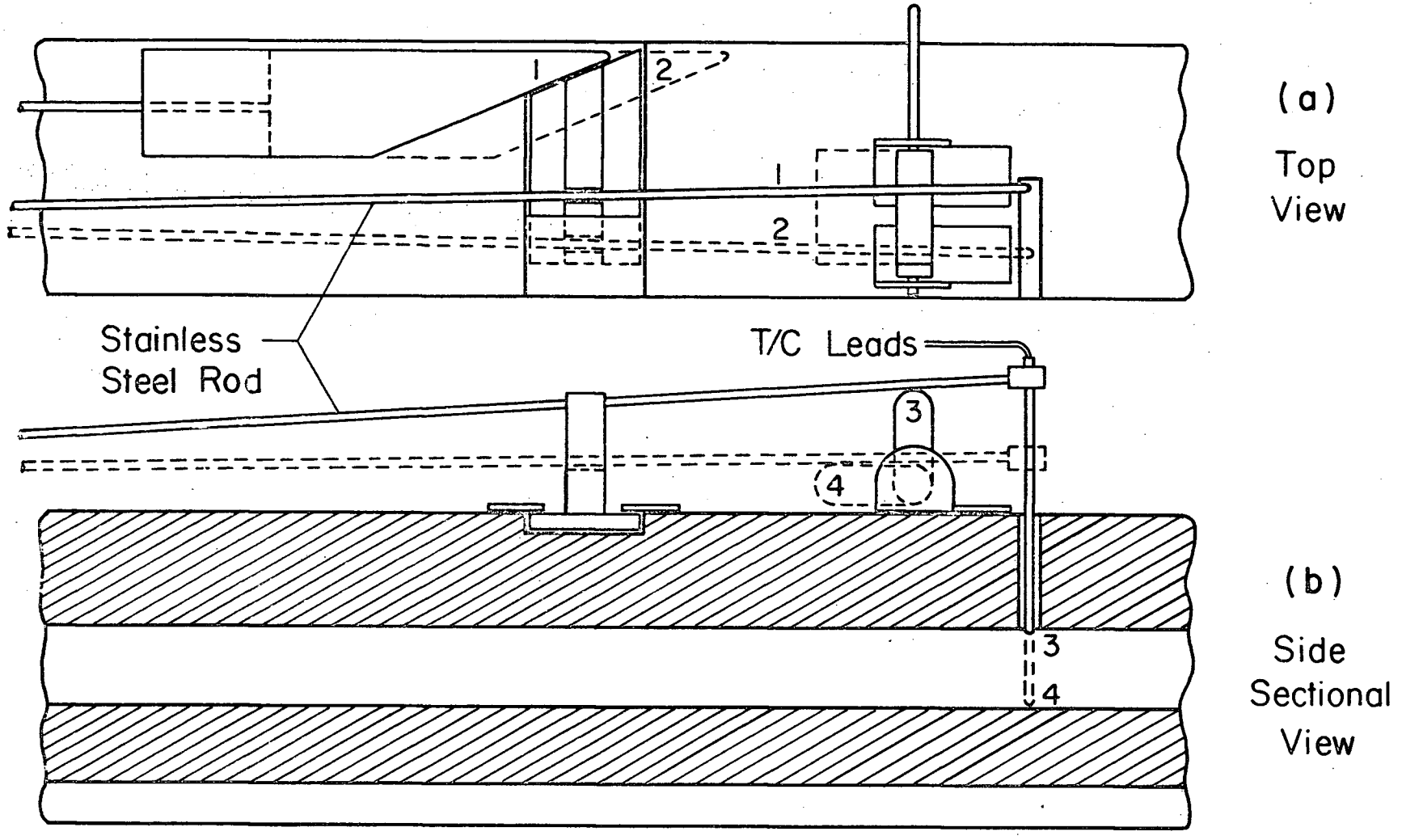

Figure 69. Schematic representation of apparatus used to measure transverse temperature gradients (x2).

to the other. The stainless steel rod was fastened on to the boat at the cold end and had sufficient elasticity to cause it to return to its original position (1) when the wedge was withdrawn. A cam mechanism, which could be operated remotely by a lever system, was employed to raise and lower the thermocouple, Figure 69(b). The stainless steel rod would return to the low position due to its own elasticity. The thermocouple was connected to the end of the stainless steel rod such that it was self aligning (in the plane of Figure 69(b)) with the slot in the boat cover. The thermocouple was 38 gauge chromel-alumel wire and was insulated by two hole 1/32 inch O.D. mullite tubing. To strengthen the thermocouple probe the mullite was surrounded for approximately 90% of its length (2 cm) by stainless steel tubing which had been produced by drilling out a 0.050 inch O.D. hypodermic needle on a jewellers lathe.

The temperature traverse of the cross section was done while the average temperature gradient across the melt was 4 °C/cm. Figure 70 shows the numbering system which will be used to describe the results of the traverse. During the traverse the Honeywell recorder was on the 0.1 mv full scale span (for the chromel-alumel thermocouple employed this represents a full scale span of less than 2.5 °C). It was not possible to determine the absolute temperature at each point shown on Figure 70 since temperature variations associated with cyclic furnace temperature controlling were present in the melt. The technique adopted was to move the thermocouple bead to a bottom position (1,4, or 7) and then move the bead up and down between this bottom and the corresponding top position at 2 second intervals. After about 3 cycles the temperature difference between the upper and lower positions decreased indicating the probe was causing some mixing. The temperature

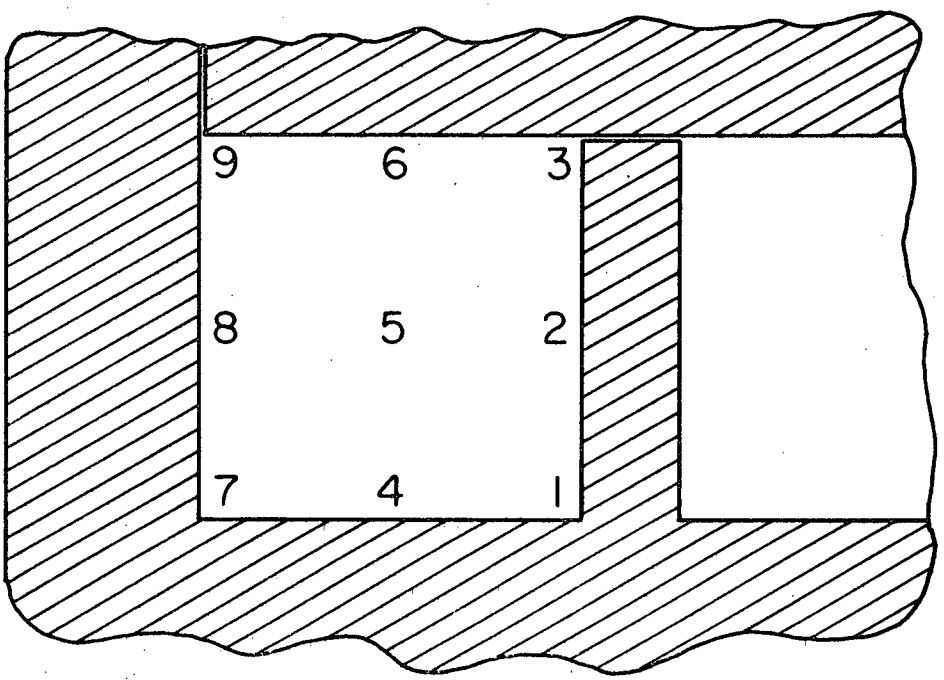

Figure 70. The numbering systems for locating positions on the temperature traverse.

differences stated below are the average values after 3 cycles between the top and bottom positions. The results of the traverse were:

(a) Position 3 is colder than position 1 by approximately 0.25 °C.

(b) Position 6 is colder than position 4 by approximately 0.25 °C.

(c) Position 9 is colder than position 7 by approximately 0.1 °C.

No differences in temperature were detected in the horizontal direction. The results show that the top of the melt is slightly cooler than the bottom. This is a direct contradiction of the findings of Utech[9]. The results Utech obtained for the increase in vertical temperature gradient (hot liquid above cold) with increasing horizontal (longitudinal) temperature gradient are shown in Figure 71. According to Figure 71 the vertical and horizontal temperature gradients are nearly equal. Utech demonstrated that the vertical temperature arose as a direct consequence of convection. This was accomplished by suppressing convection with a magnetic field and observing that the vertical gradient went to zero. It must be pointed out that the experiments of Utech were conducted in an open top boat with a melt depth of 0.94 cm whereas the experiments presented in this thesis were carried out in closed top boat with a melt depth of 0.64 cm. A difference in the nature of the flow is understandable. First, the melt whose depth is 0.64 cm would be more stable with respect to fluid flow than a melt 0.94 cm deep. Secondly, the closed top graphite boat, a good thermal conductor, might prevent the establishment of a vertical gradient in the melt.

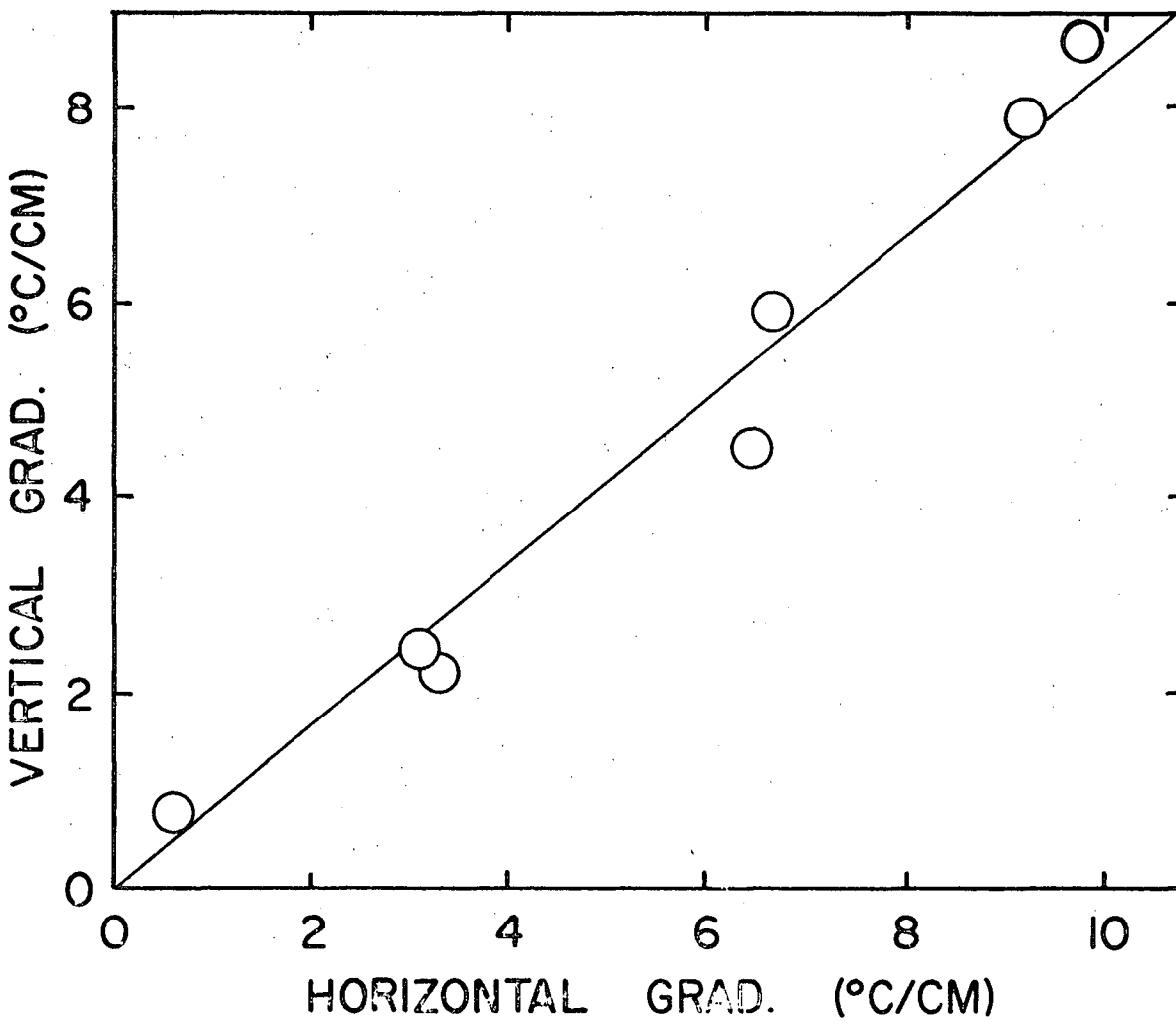

Figure 71. The relation between the horizontal and vertical temperature gradients for an uncovered tin melt of depth 0.94 cm (after Utech).

Cole, in a literature review of convection[18], stated that recent investigations in a rectangular cavity bounded by vertical plates indicate that a weak unicellular motion is generated for all non-zero temperature differences. Furthermore, the heat transported by this flow is negligible, except for small contributions near the corners of the walls.

The numerical analysis of thermal convection in liquid by Stewart[17] showed that large flow rates may be developed in a melt while the thermal profile is still unaltered from the pure conduction form. This is in total agreement with the results of the present work. At a horizontal temperature gradient of 4 °C/cm Figure 46 shows that a flow velocity of greater than 0.3 cm/sec would be observed. At this horizontal gradient the temperature traverse has shown that heat transport in the melt must be almost completely conductive. In fact, the vertical gradient measured here is opposite to that which would be expected, that is, the temperature traverse has shown a very small vertical gradient (less than 0.3 °C/cm) in which the cold liquid is above the hot liquid. This gradient may result from the fact that the bottom of the graphite boat is in contact with the Vycor tube whereas the top surface of the boat may be cooled by the convective air currents within the Vycor tube. The transverse flow observed is the type of flow one would expect in a cell which is heated from below and cooled from above, namely, a double cell flow pattern with cooler liquid from the top moving down the cell walls, being heated at the bottom and then rising in the middle of the cell. For the case of the square aluminum channel supported by the graphite ends it would be expected that the most extensive flow would occur in the vicinity of the graphite ends. This is especially apparent in the autoradiographs shown in rows one and five

of Figure 58. It is also observable in rows two and six of Figure 58, but to a lesser degree, probably due to the fact that this specimen was quenched 2 minutes after introduction (specimen in rows one, three and five was quenched at 1 minute) and therefore the tracer becomes much more dilute. The observation that transverse flow in the vicinity of the hot reservoir is more extensive than the transverse flow near the cold reservoir must reflect the fact that the adverse vertical gradient in the hot reservoir is greater than that present in the cold reservoir.

3.5. Interaction of Unicellar Flow with a Moving Solid Liquid Interface

Fluid flow across a solid-liquid interface at which solute segregation is taking place is prime of importance in determining the solute distribution that appears in the resultant solid. During solidification of an alloy, solute build-up (assuming k_o is less than 1) will occur at the interface and this in turn can lead to constitutional supercooling. Following the onset of constitutional supercooling the morphology of the interface will change from planar to cellular and then possibly to dendritic (provided the growth rate and temperature gradient are favourable for such a transition). A general observation in experiments used to determine the growth criteria for the planar to cellular transition is that breakdown occurs first at the melt-container interface. Examples of this are shown in Figures 72 and 73. Both figures are from unpublished work by F. Weinberg. Figure 72 is an autoradiograph of a transverse (to the growth direction) section of a 1/4 inch square rod. The rod was produced by directionally solidifying a melt of pure tin containing 500 ppm of Tl^{204}. The autoradiographs of

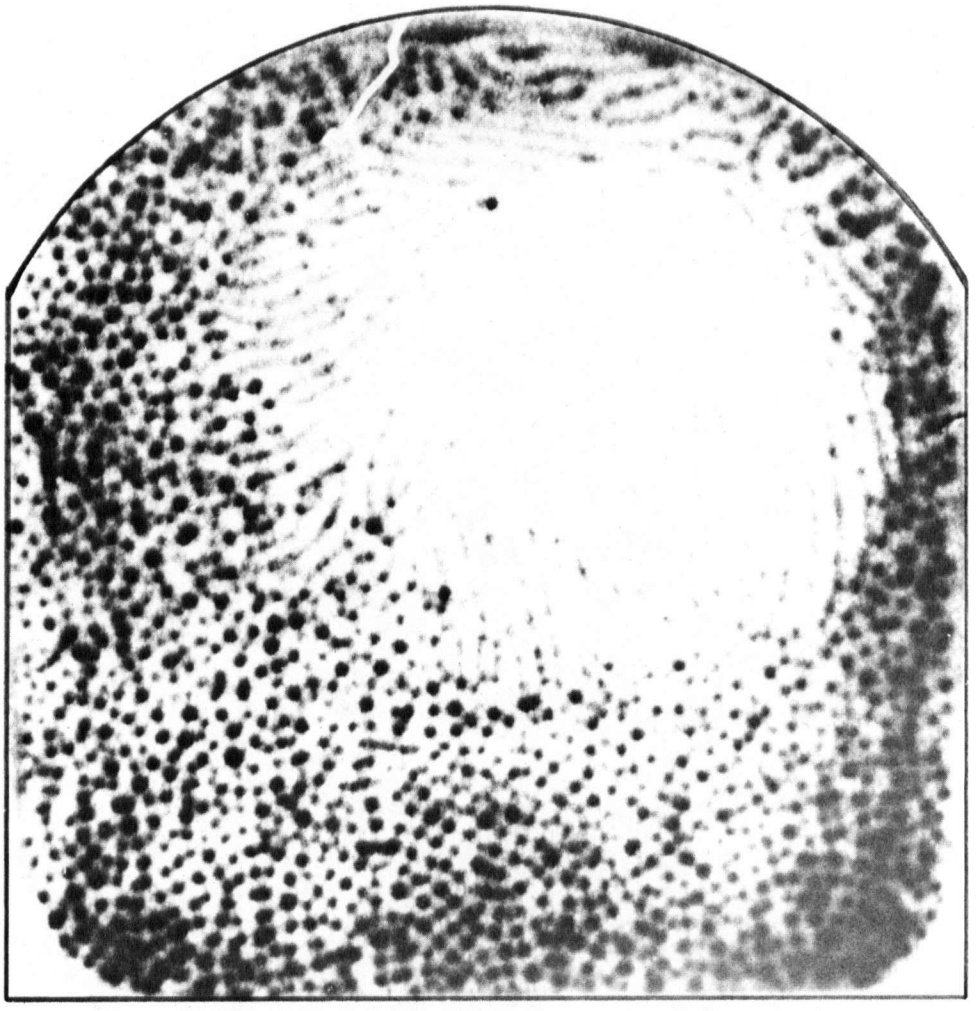

Figure 72. Transverse section autoradiograpy of a directionally solidified tin melt containing 500 ppm Tl^{204} (X20).

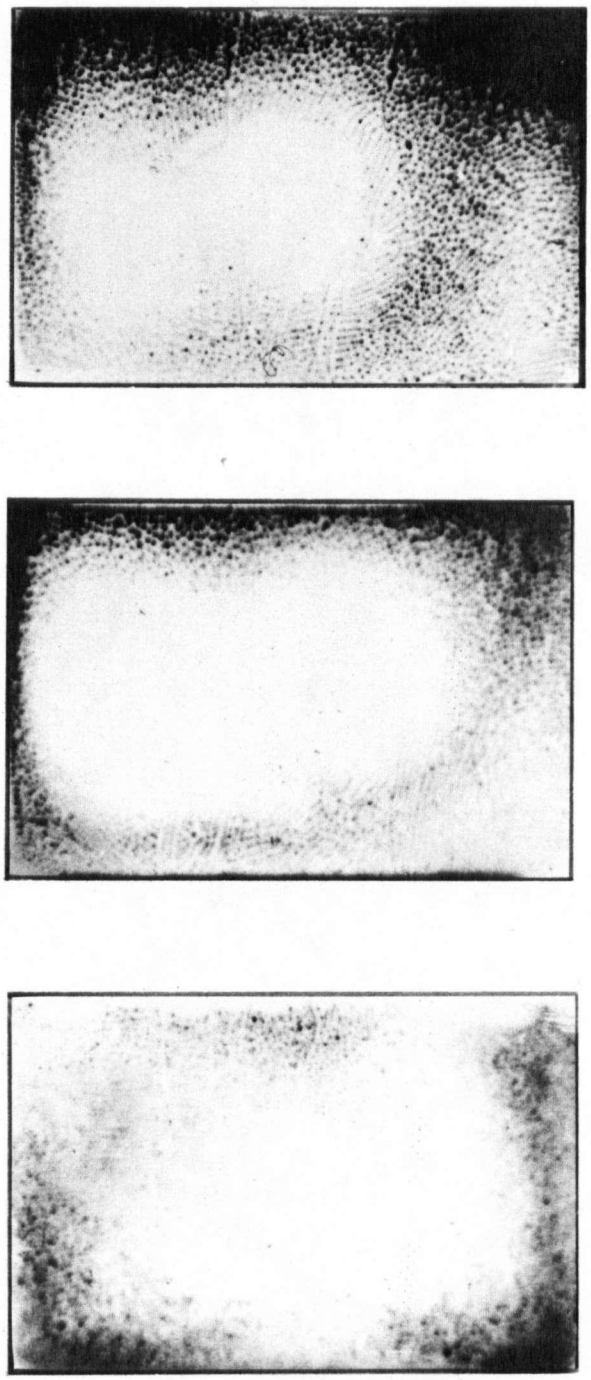

Figure 73. Transverse section autoradiographs of a directionally solidified tin melt containing 100 ppm Tl^{204} (X6).

Figure 73 are from 3 different transverse sections of a directionally solidified pure tin plus 100 ppm Tl^{204} melt. The cross-sectional dimensions of this rod are 1/2 inch wide by 1/4 inch high. The growth rate in both cases was approximately 2×10^{-3} cm/sec and the temperature gradient in the melt was of the order of 0.5 °C/cm.

The most widely accepted mechanism for preferential breakdown of the planar interface near the container walls invokes the concept of an enlarged solute rich boundary layer (δ_s- layer) in this region. That is, thermal convection is reasonably effective in removing rejected solute (in this case Tl^{204}) from the central region of the solid-liquid interface, but is much less effective in removing rejected solute from regions where the interface and container meet. The reason for this is that liquids metals with their low Prandtl numbers (typically of the order of 10^{-2}) tend to maintain circular flow paths rather than conform to the shape of the container in which they are flowing[17]. Therefore, the extent of convective mixing in the interface-container region will be small in comparison to the mixing which occurs at the central region of the interface. This will result in the build-up of a much larger solute rich layer ahead of the periphery of the interface. The net result is that conditions suitable for constitutional supercooling and thus planar to cellular breakdown will occur first in regions where the interface and container meet.

The main objection to this mechanism is that the size of the δ_s- layer required to produce as pronounced an effect as is shown in Figures 72 and 73 is much larger than is normally observed in liquid metal systems. (δ_s- layer sizes are generally considered to range from a low

10μ for complete mixing to 1000μ when no mixing is present[2]). The type of convective flow described in the previous sections, that is, unicellular longitudinal flow with a superimposed transverse double cell flow would certainly encourage the onset of interface breakdown to occur near the interface container junction. The transverse flow would tend to distribute solute, which had been picked up by the unicellular longitudinal flow, around the outside edges of the melt. Although the transverse double cell flow would bring solute into central region of the melt, this solute would not be seen by the interface since the longitudinal flow is constantly sweeping the central region of the interface. The result is that the interface would be growing into a melt which had greater portion of the rejected solute distributed around the outer edges, that is, adjacent to the melt container walls. As before, the net result would be preferential breakdown of the planar interface in this region.

The classical mechanism requires the establishment of an unrealistically large solute layer at the container walls. The fact that the δ_s- layer around the periphery is larger than that which exists at the central portion of the interface cannot be denied. It would appear that the most acceptable mechanism for the preferential onset of the planar to cellular transition near the melt container walls must be a combination of the classical mechanism and the mechanism just proposed.

3.6. Summary

The flow which occurs in the horizontal melt system studied here is an unicellular longitudinal flow in which the liquid moves from the hot end to the cold end along the top of the melt and returns from

the cold end to the hot end along the bottom. This mode of flow has been suggested but not observed by Carruthers[15]. However, Carruthers made no mention of the possibility of transverse flow. Additional movement of fluid from the top to the bottom of the cell has been herein observed to occur by a double cell transverse flow which is superimposed on the longitudinal motion. The driving force for the transverse flow is an adverse vertical temperature gradient (cold liquid above hot).

The driving force for the longitudinal unicellular flow is the imposed horizontal temperature gradient. The heat transferred by this flow is negligible. Although the heat transferred by the flow is negligible, the flow velocities and the resulting convective mixing must be considered important in the solidification process.

4 - ANALYSIS OF RESULTS

4.1. Introduction

In order to analyse the flow velocity results obtained during this investigation it is first necessary to determine the exact physical nature of the velocity measured. In particular, is the flow which gives rise to the observed velocity simply a superposition of a transverse double cell flow on a longitundinal unicellular flow or could it be more accurately defined as a double spiral flow of the type observed during forced convection through a cylindrical tube[19], Figure 74. The broken lines in Figure 74(a) show the path that would be followed by a particle as it moved along with the spiral flow. If tracer was injected into this system, the rotational flow would cause transverse section autoradiographs to have the appearance of Figure 74(b). Since the autoradiographs appearing in Figures 56-64 do not, for the most part, display fully outlined transverse double cell flow, it may be concluded that the concept of spiral flow does not accurately describe the flow system investigated herein. It is possible, however, that the flow could be described as a slow spiral flow (rather than a strictly transverse flow) superimposed on the more dominant unicellular longitudinal motion. In any case, the major contribution to the observed velocity comes from the longitudinal flow.

The longitudinal flow velocity close to the top and bottom of the enclosed melt must be much greater than the velocities in the cen-

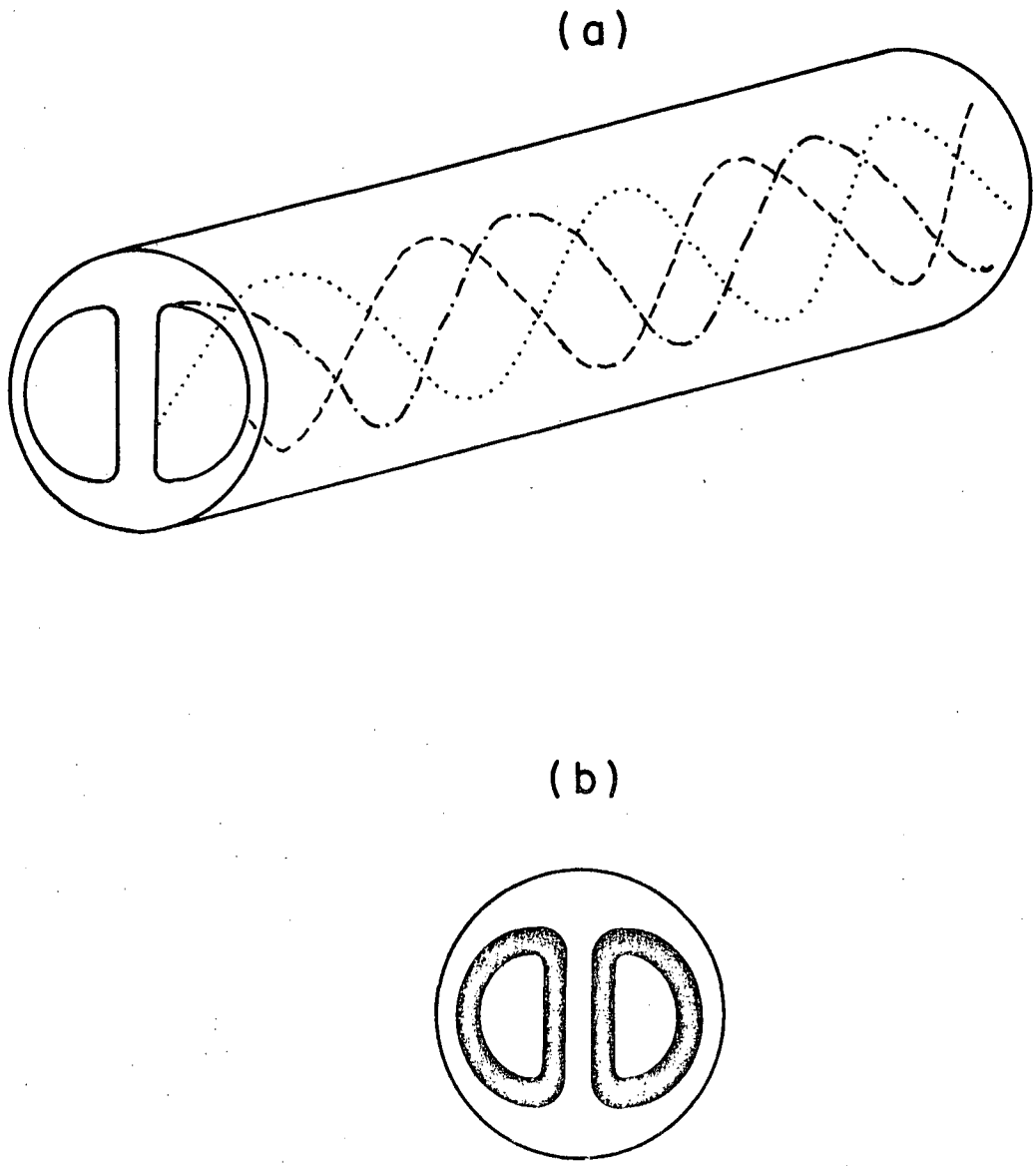

Figure 74. (a) Schematic representation of the double spiral flow observed during forced convection through a tube .(b) Expected appearance of transverse section autoradiographs if double spiral flow were present.

tral region. This conclusion results from a consideration of the tracer introduction technique employed. Essentially, tracer introduction involves placing a 0.64 cm cube of trace alloy in the covered channel. If the longitudinal velocity did not vary significantly with vertical position in the melt one would not expect to observe (as is shown by the autoradiographs) the tracer to be concentrated in the top and bottom layers of the melt. The observed predominance of flow close to the top and bottom surfaces of the melt suggests that it may be appropriate to apply boundary layer theory to analyse the flow velocity results obtained in Section 2.

The ratio of the buoyancy forces generated as a result of temperature differences in the fluid to the viscous force in the fluid, is given qualitatively by the dimensionless Grashof number. For a rectangular enclosure with heated and cooled vertical walls the Grashof number is generally written as:

$$Gr = \frac{g\beta\Delta TL^3}{\nu^2} \qquad (4.1)$$

where: Gr is the Grashof number

g is the acceleration of gravity

β is the coefficient of volume expansion

ΔT is the temperature difference between the hot and cold walls

L is the distance between the hot and cold walls

ν is the kinematic viscosity

α is the thermal diffusivity

In order that the buoyancy force be consistent with the results of the present investigation, it is necessary to redefine the

Grashof number. It has been established above that the driving force for the observed flow is the average temperature gradient between the hot and cold ends of the melt. If the Grashof number as presently defined is slightly modified to allow incorporation of the average horizontal temperature gradient across the melt, $\overline{G}_L$, it becomes:

$$Gr = \frac{g\beta L^4 \overline{G}_L}{\nu^2} \qquad (4.2)$$

Thus the buoyancy force, which is the driving force for the observed flow, would appear to be strongly dependent on the melt length for a given average gradient. This grossly contradicts the experimental results which clearly show (for two different boat designs and 4 melt lengths ranging from 27 to 48.8 cm) that flow velocity is independent of total melt length, provided the average gradient across the melt remains constant. When the Grashof number is further modified to remove the melt length dependence it becomes:

$$Gr = \frac{g\beta H^4 \overline{G}_L}{\nu^2} \qquad (4.3)$$

where the melt height H has replaced the length L. This Grashof number now has the experimentally determined properties of linear dependence on average gradient and is independent of total melt length.

This modification is similar to that employed by Cole[20] to describe the dependence of the critical horizontal temperature gradient required for the onset of thermocouple oscillation, G_L^c, on the melt height. Cole redefined the Rayleigh number (Grashof x Prandtl) for a liquid heated

from below, namely:

$$Ra = \frac{g\beta H^4 G_{vertical}}{\alpha\nu} \qquad (4.4)$$

by assuming that H x G (vertical) could be replaced by L x G (horizontal). The new Rayleigh number then became:

$$Ra = \frac{g\beta H^3 L G_L}{\alpha\nu} \qquad (4.5)$$

from which can be obtained the expression:

$$H^3 G_L = \frac{Ra\alpha\nu}{g\beta L} \qquad (4.6)$$

Cole established experimentally that $H^3 G_L^c = 3.1$ (cgs units) where G_L^c is the critical horizontal gradient required for the onset of thermocouple fluctuations which in turn were taken to be indicative of the onset of turbulent convection. Using this result, an expression for the critical Rayleigh number Ra^c necessary for the onset of turbulent convection was obtained:

$$Ra^c = \frac{(3.1)\ g\beta L}{\alpha\nu} \qquad (4.7)$$

Thus it would appear that Ra^c is a function of the melt length L. Cole did not determine whether in fact Ra^c varied with melt length. However, since Ra^c is a dimensionless parameter of dynamic similarity it is reasonable to assume that it should not vary with melt length. Therefore, since g is a constant and α, β and ν remain essentially constant, provided

the average melt temperature does not vary greatly, the product $H^3 L G_L^c$ must also remain constant. For a melt of height H it follows that thermocouple fluctuations should be observed once the appropriate value (that which makes $Ra > Ra^c$) of the product $G_L L$ exceeds a constant $G_L^c L$. Hurle's[12] results noted in Section 1.1. showed that for a melt length of 4.0 cm, $G_L^c = 5.0$ °C/cm and for L = 2.6 cm, $G_L^c = 7.5$ °C/cm. The values of $G_L^c L$ for these two experiments are 20°C and 19.5°C respectively. Thus it becomes apparent that whereas flow velocities are dependent on the average temperature gradient (independent of melt length) across the melt, the onset of turbulent convection is determined by a critical temperature difference (again independent of melt length) between the hot and cold ends of the melt.

The results of Müller and Wiehelm[8] indirectly support the finding that flow velocities are independent of melt length for a given horizontal temperature gradient. They found that for melts between 10 and 30 cm long the observed temperature fluctuations were independent of melt length provided the temperature and temperature gradient remain constant at the measuring point. If the amplitude and frequency of the temperature fluctuations can be taken as being repreeentative of the extent of convective flow and thus an indirect measure of flow velocities, then the results of Müller and Wiehelm are in agreement with those of the present investigation. Therefore, for this investigation the buoyancy driving force, as represented by a Grashof number, will be given by Equation (4.3).

In Section 2.2.3.4.3. it was shown that varying the height of liquid metal in the open reservoirs had negligible effect on the flow

velocity. It should, therefore, be possible to consider the system as being covered for the entire melt length.

In summary one obtains the following picture of fluid flow in a covered horizontal rod of liquid metal:

(1) The flow which gives rise to the observed velocity is laminar longitudinal unicellular flow confined to the outer extremeties of the melt, Figure 75. The transverse flow will be neglected thus reducing the mathematical analysis to a 2-dimensional problem. The assumption that the transverse flow can be neglected is based on autoradiography experiments which show that the transverse flow does not make a significant contribution to the longitudinal flow.

(2) The buoyancy forces which generate the longitudinal flow can be represented by a modified Grashof number of the form:

$$Gr = \frac{g\beta H^4 \overline{G}_L}{\nu^2}$$

(3) The covered horizontal rod with the two small open reservoirs can be considered to be a totally enclosed rectangular system as shown in Figure 75.

Successful mathematical analysis of the simplified two dimensional problem must predict:

(1) A linear relationship between flow velocity and average temperature gradient across the melt.

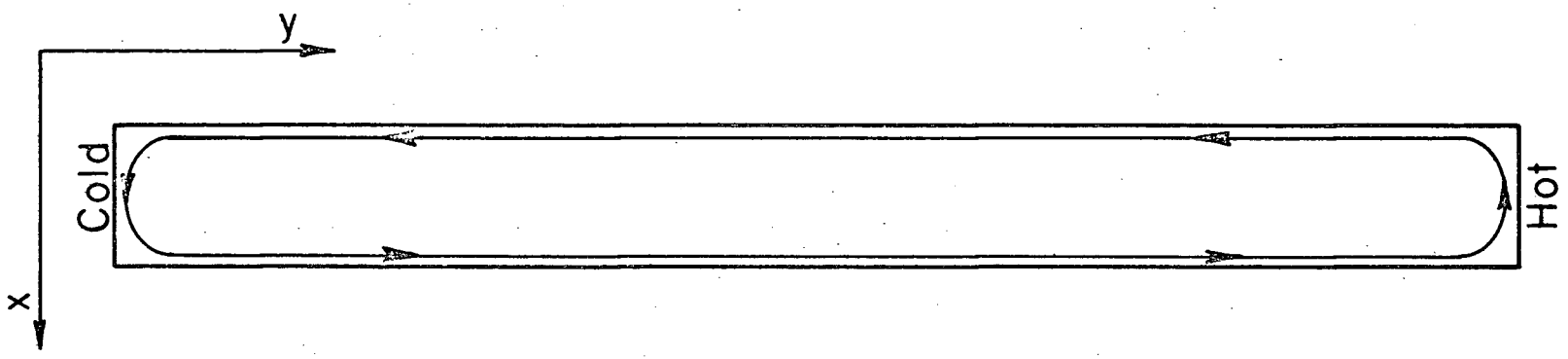

Figure 75. The simplified flow system in the long shallow retangular enclosure.

(2) A lack of velocity dependence on total length.

(3) A dependence of flow velocity on average melt temperature.

4.2. Previous Investigations

Hydrodynamic analysis of natural thermal convective flow in liquid metals having the horizontal rod configuration investigated here has received little attention in the literature. The vast majority of existing solutions have been primarily concerned with the heat transferred via convection, rather than the magnitude of the flow velocities. Although heat transfer is a integral part of the solidification process, the purpose of the present investigation was to study flow patterns and flow velocities.

Attempts that have been made to analyse fluid flow in a liquid metal contained in a horizontal boat[5,9] and thus predict flow velocities have suffered from a lack of accurate reproducible results with which to confirm or dispute the mathematical solution. The analyses of Utech[9] and Cole[5] which were outlined briefly in Section 1.1. will now be reviewed and discussed with respect to the results obtained in the present investigation.

4.2.1. Solution of Utech[9]

The solution used by Utech was developed by Eckert and Drake[10] for laminar flow along a vertical plate at a temperature T_W immersed in a fluid at temperature T_o. The momentum equation for the boundary layer adjacent to the wall is:

$$\frac{d}{dx}\int_o^{\delta} u^2 dy = g\beta \int_o^{\delta} \Theta dy - \nu \left(\frac{du}{dy}\right)_{wall} \qquad (4.8)$$

The heat flow equation is:

$$\frac{d}{dx}\int_o^{\delta} u\Theta dy = -\alpha \left(\frac{d\Theta}{dy}\right)_{wall} \qquad (4.9)$$

where: x is the distance along the wall

y is the distance perpendicular to the wall

* δ is the boundary layer thickness

u is the velocity in the x direction

$\Theta = T - T_o$

T is the temperature at some y position inside the boundary layer

---

* Merks[21] has shown that the thermal and hydrodynamic boundary layers are equal for free convection in liquids metals, so that $\delta_{thermal} = \delta_{hydro} = \delta$.

By assuming a temperature distribution in the boundary layer of:

$$\Theta = (T_W - T_o)\ (1 - \frac{y}{\delta})^2 \tag{4.10}$$

and a velocity profile of the form:

$$u = u_1\ \frac{y}{\delta}\ (1 - \frac{y}{\delta})^2 \tag{4.11}$$

where u_1 is an arbitrary function with the dimension of velocity, Equations (4.8)and (4.9) assume the form:

$$\frac{1}{105}\ \frac{d}{dx}\ (u_1^2\delta) = \frac{1}{3}\ g\beta\ (T_W - T_o)\delta - \nu\ \frac{u_1}{\delta}$$

$$\frac{1}{30}\ (T_W - T_o)\ \frac{d}{dx}\ (u_1\delta) = 2\alpha\ (\frac{T_W - T_o}{\delta})$$

Solving these equations simultaneously employing the substitutions $u_1 = C_1\ x^{1/2}$ and $\delta = C_2\ x^{1/4}$ gives:

$$u_1 = 5.17\nu\ (0.952 + Pr)^{-1/2}\ (\frac{g\beta\ (T_W - T_o)}{\nu^2})^{1/2}\ x^{1/2} \tag{4.12}$$

From Equation (4.11) it can be seen that the maximum velocity in the boundary layer, u_m, is 0.148 u_1. Introducing this into Equation (4.12) gives:

$$u_m = 0.766\nu\ (0.952 + Pr)^{-1/2}\ (\frac{g\beta\ (T_W - T_o)}{\nu^2})^{1/2}\ x^{1/2} \tag{4.13}$$

For molten tin at an average melt temperature of 400 °C introduction of the appropriate fluid parameters (Table 6) yields the following expression for the maximum flow velocity in the boundary layer:

$$(u_m)_{400} = 0.25\ (T_W - T_o)^{1/2}\ x^{1/2} \tag{4.14}$$

The average velocity along a wall of height H would be:

$$\begin{aligned}(\bar{u}_m)_{400} &= 0.25\ (T_W - T_o)^{1/2}\ \frac{1}{H}\int_o^H x^{1/2}\ dx \\ &= 0.166\ (T_W - T_o)^{1/2}\ H^{1/2}\end{aligned} \tag{4.15}$$

The melt height for the system studied in Sections 2 and 3 was 0.64 cm. The temperature difference which created the bouyancy forces in the melt is obtained from Equation (4.3) and is $H\ \bar{G}_L$. Thus the average maximum velocity resulting from a horizontal temperature gradient between the vertical walls at the ends of the melt would be:

$$(\bar{u}_m)_{400} = 0.106\ \bar{G}_L^{\ 1/2} \tag{4.16}$$

In Figure 76, the line from Figure 46 is plotted along with the modified Eckert and Drake solution given in Equation (4.16). Although the calculated velocities are of the same order of magnitude as the experimentally determined values, the linear dependence of flow velocity on temperature gradient is not satisfied by this solution. Furthermore, when the value of $(\bar{u}_m)_{300}$ is calculated, the predicted ratio $(\bar{u}_m)_{300}/(\bar{u}_m)_{400}$ is 0.99 whereas experimentally, Figure 43, this ratio is 0.78.

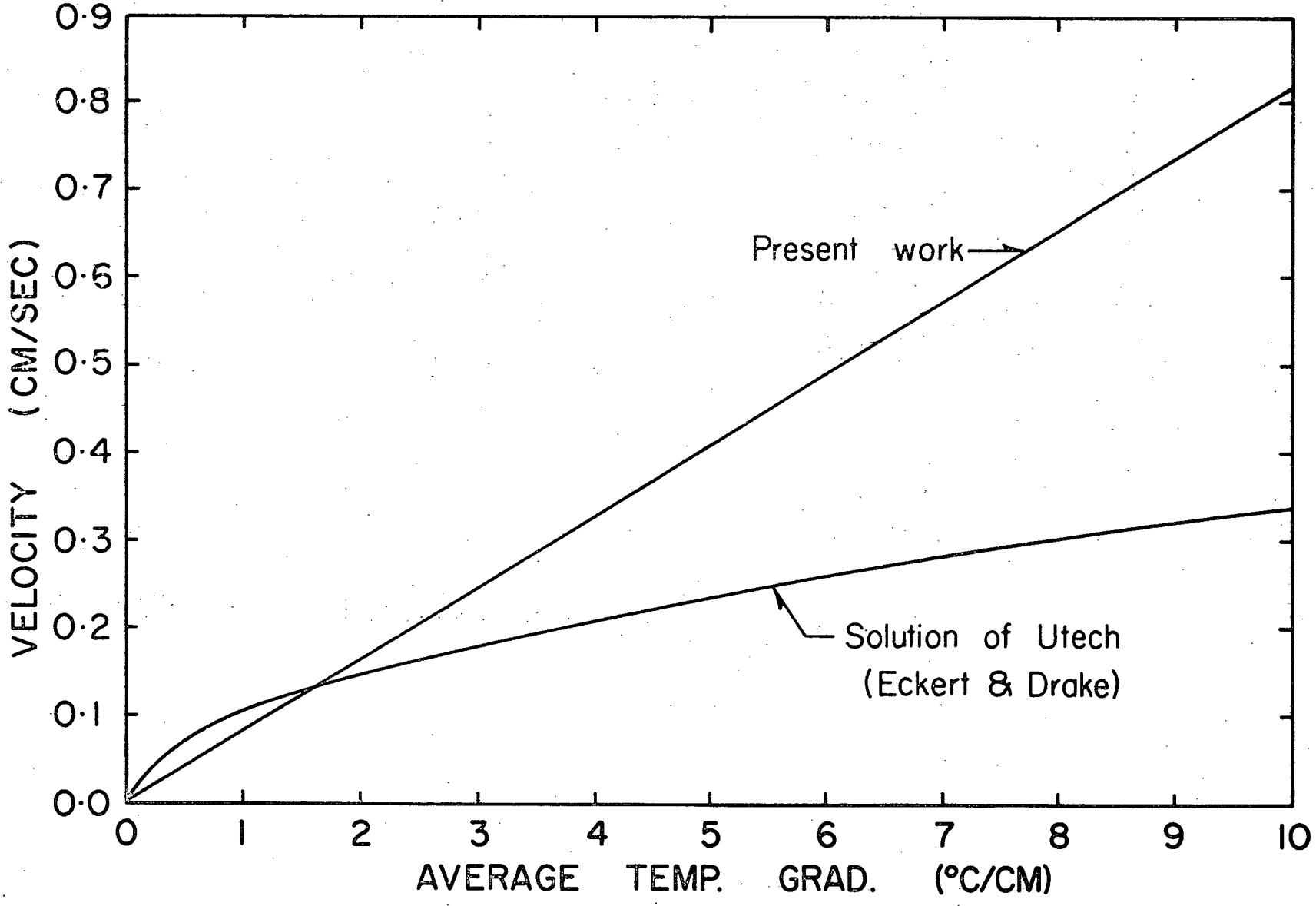

Figure 76. Comparison of the results of the present investigation with the prediction of the solution of Utech.

4.2.2. Solution of Cole[5]

The solution used by Cole to calculate u_m was the Eckert and Drake analysis modified to include the latent heat of solidification λ and the growth rate R in the heat flow Equation (4.9). Assuming the velocity and temperature distributions were those given by Equations (4.10) and (4.11) (except Cole made $u_1 = u_m$), the differential equations which have to be solved simultaneously are then:

$$\frac{1}{105} \frac{d}{dx} (u_m^2 \delta) = \frac{1}{3} g\beta (T_W - T_o) \delta - \nu \frac{u_m}{\delta} \tag{4.17}$$

$$\frac{T_W - T_o}{40} \frac{d}{dx} (u_m \delta) = \alpha \left(\frac{T_W - T_o}{\delta}\right) + \frac{R}{2} \left(\frac{\lambda}{c_p} - (T_W - T_o)\right) \tag{4.18}$$

Employing the substitutions $u_m = A_1 x^{1/2}$, $\delta = A_2 x^{1/4}$ Cole obtained a relation for u_m, which for the case of R = 0 (no solid present or a stationary solid-liquid interface) becomes[22]:

$$u_m = 4.2 \left(\frac{g\beta}{.63 + Pr} \right)^{1/2} (H\Delta T)^{1/2} \tag{4.19}$$

If the appropriate fluid parameters from Table 6 are inserted, and as before ΔT is taken to be $H \bar{G}_L$, then Equation (4.19) becomes:

$$(\bar{u}_m)_{400} = 0.715 \bar{G}_L^{1/2} \tag{4.20}$$

The Cole analysis has the same parabolic dependence of $\bar{u}_m$ on

temperature gradient $\bar{G}_L$ as the Eckert and Drake relation of Equation (4.16) but the calculated value of $\bar{u}_m$ from Equation (4.20) is approximately an order of magnitude larger than that calculated from Equation (4.16). Since Cole's solution is essentially the Eckert and Drake solution with the addition of terms accounting for the latent heat of solidification and the growth rate R, Equation (4.20) should be identical to Equation (4.16) when no solidification or melting (R = 0) is occurring. Examination of Cole's analysis reveals the following error. Cole assumed the velocity profile was:

$$u = u_m \frac{y}{\delta} \left(1 - \frac{y}{\delta}\right)^2 \qquad (4.21)$$

and eventually obtained a solution for u_m, the maximum velocity parallel to the interface. By differentiating Equation (4.21) and setting $du/dy = 0$, one can obtain the value of y for which $u = u_m$. This value is $1/3\delta$ and substituting this into Equation (4.21) yields:

$$u_m = 0.148\ u_m$$

Clearly then, Cole's calculated values of u_m will be too large by a factor of 6.85. When this correction is applied to Equation (4.20) the result is:

$$(\bar{u}_m)_{400} = 0.106\ \bar{G}_L^{1/2}$$

which agrees with the Eckert and Drake relation.

In view of the lack of agreement between the Eckert and Drake type of solution and the results obtained during this investigation, it becomes necessary to examine more carefully the assumptions involved in

deriving the velocity relationship predicted by Equation (4.16). One of the major assumptions of this analysis is that fully developed boundary layer flow exists along the vertical wall. Thus, corner effects can be neglected and the integrated boundary layer Equations (4.8) and (4.9) results as a simplification of the governing equations of thermal convection, namely:

Momentum equation in the x-direction

$$\frac{\partial u}{\partial t} + u \frac{\partial u}{\partial x} + v \frac{\partial u}{\partial y} = - g\beta\Delta T - \frac{1}{\rho} \frac{\partial p'}{\partial x} + \nu (\nabla^2 u) \qquad (4.22)$$

Momentum equation in the y-direction

$$\frac{\partial v}{\partial t} + u \frac{\partial v}{\partial x} + v \frac{\partial v}{\partial y} = - \frac{1}{\rho} \frac{\partial p'}{\partial y} + \nu (\nabla^2 v) \qquad (4.23)$$

Energy equation

$$\frac{\partial T}{\partial t} + u \frac{\partial T}{\partial x} + v \frac{\partial T}{\partial y} = \alpha (\nabla^2 T) \qquad (4.24)$$

Continuity equation

$$\frac{\partial u}{\partial x} + \frac{\partial v}{\partial y} = 0 \qquad (4.25)$$

where: x is the distance in the vertical direction

u is the velocity in the vertical direction

y is the distance in the horizontal direction

v is the velocity in the horizontal direction

p' is the pressure deviation from the initial static pressure.

The assumptions used in obtaining the above equations are:

(1) All fluid properties, with the exception of the density changes which give rise to the buoyancy forces, are constant for a given average melt temperature.

(2) The temperature difference across the melt is small compared with $1/\beta$.

(3) The viscous dissipation is neglected.

(4) Compressibility effects are neglected.

Purely analytical attempts to solve the flow and heat transfer characteristics of convection are severely handicapped by the complexity of the governing equations.

The integral boundary layer solution just discussed is limited by a minimum height to length ratio of the cell. Since this solution and the results of the present investigation are not in agreement it must be concluded that the height to length ratios employed herein were outside the range of applicability of the integral boundary layer solution.

Approximate solutions of the governing equations have been developed by Batchelor[23] and Poots[24]. Both solutions use non-dimensional forms of the governing equations. These non-dimensional forms are obtained by using the following dimensionless parameters:

$$X = \frac{x}{L}, \qquad Y = \frac{y}{L}$$

$$u = \frac{\alpha}{L}\frac{\partial \Psi}{\partial Y} \qquad v = -\frac{\alpha}{L}\frac{\partial \Psi}{\partial X} \qquad (4.26)$$

$$\Theta = \frac{T - T_o}{T_1 - T_o} \qquad \zeta = -\nabla^2 \Psi$$

where T_1 and T_o are the temperature of the vertical walls, Ψ is defined as the dimensionless stream function and ζ is defined as the dimensionless vorticity. Substituting the relationships in (4.26) into Equations (4.22) to (4.25) and eliminating the pressure terms by differentiating (4.22) with respect to Y and (4.23) with respect to X results in:

$$\frac{1}{Pr}\left(\frac{\partial \zeta}{\partial X}\frac{\partial \Psi}{\partial Y} - \frac{\partial \Psi}{\partial X}\frac{\partial \zeta}{\partial Y}\right) = Ra\,\frac{\partial \Theta}{\partial Y} + \nabla^2 \zeta \qquad (4.27)$$

$$\frac{\partial \Theta}{\partial X}\frac{\partial \Psi}{\partial Y} - \frac{\partial \Theta}{\partial Y}\frac{\partial \Psi}{\partial X} = \nabla^2 \Theta \qquad (4.28)$$

In obtaining Equations (4.27) and (4.28) all the time derivatives ($\partial/\partial t$) have been equated to zero since only the steady state solution is of interest. The boundary conditions in dimensionless form are:

$$X = 0,\ X = \frac{H}{L} \qquad \Psi = \frac{\partial \Psi}{\partial X} = 0$$

$$\Theta = Y$$

$$Y = 0 \qquad \Psi = \frac{\partial \Psi}{\partial Y} = 0 \qquad \Theta = 0$$

$$Y = 1 \qquad \Psi = \frac{\partial \Psi}{\partial Y} = 0 \qquad \Theta = 1 \qquad (4.29)$$

4.2.3. Solution of Batchelor[23]

Batchelor developed series solution for Θ and Ψ by expanding them in power series of the Rayleigh number, namely:

$$\Theta(X,Y) = Y + Ra\ \Theta_1(X,Y) + Ra^2\ \Theta_2(X,Y) + \ldots\ldots \qquad (4.30)$$

$$\Psi(X,Y) = Ra\Psi_1(X,Y) + Ra^2\Psi_2(X,Y) + \ldots\ldots \qquad (4.31)$$

These series can be substituted into Equations (4.27) and (4.28) and upon equating coefficients of like powers of the Rayleigh number equations describing Θ_1, Θ_2, Ψ_1 and Ψ_2 can be obtained. For values of Rayleigh less than 10^3 and for H/L ratios close to unity the value of Ψ_1 can be approximated by:

$$\Psi_1 = \frac{2}{3}\left(1 + \left(\frac{H}{L}\right)^{4}\right)^{-1} X^2 \left(\frac{H}{L} - X\right)^2 Y^2 (1 - Y)^2 \qquad (4.32)$$

Thus, under these conditions, and assuming that series (4.31) converges suffiently rapidly, the solution for the stream function can be written as:

$$\Psi = Ra\Psi_1(X,Y) \qquad (4.33)$$

The flow velocities can be obtained directly from Equation (4.33) with the use of the velocity relationships in Equation (4.26).

Before continuing with the development of the Batchelor solution, it is convenient to briefly discuss the solutions of Poots[24] and Stewart[17].

4.2.4. Solution of Poots[24]

Employing the dimensionless forms of the two-dimensional governing equations, Poots obtained approximate solutions for Θ and Ψ by expanding them as series of orthogonal polynomials. The general conclusions of this investigation were that:

(1) The solution of Poots was in agreement with the Batchelor solution up to Rayleigh equals 10^3.

(2) The labour involved in obtaining Poots' solutions for Rayleigh greater than 10^4 and H/L greater than 4 was made prohibitive by the slow convergence of the series solutions.

4.2.5. Solution of Stewart[17]

Stewart, employing a radioactive tracer technique, measured flow velocities associated with natural convection of liquid metal contained in a cell with a height to length ratio of unity. During this investigation the Rayleigh number ranged from 10^4 to 10^6. These values of Rayleigh are well outside the range in which the solutions of Batchelor and Poots may be applied. In order to analyse his experimental results, Stewart developed a finite difference solution of the governing equations.

The solution was based on the work of Wilkes[25] and Samuels and Churchill[26]. It was necessary to modify these solutions since the Wilkes analysis became unstable at large values of Rayleigh, and the results of Samuels and Churchill did not apply as their solution was for a system with a vertically applied temperature gradient whereas Stewart worked with a horizontal difference in temperature.

The finite difference numerical technique used by Stewart for the solution of a dimensionless form of the governing equations (slightly different form than that used by Batchelor) was the implicit alternating direction technique. Stewart found that the solution obtained for the flow velocity was in excellent agreement with the solution of Batchelor up to Grashof equals 10^5 (Rayleigh approximately 10^3). For Grashof greater than 10^5 Stewarts solution deviated from the Batchelor solution and then approached the Eckert and Drake boundary layer solution for values of Grashof of the order of 10^9.

During the course of the present investigation the values of Grashof (for an average melt temperature of 400 °C), as defined by Equation 4.3, was:

$$(Gr)_{400} = 4800\ \overline{G}_L \qquad (4.34)$$

and

$$(Ra)_{400} = 43.7\ \overline{G}_L \qquad (4.35)$$

The maximum value of $\overline{G}_L$ for which velocity measurements were made was less than 10 °C/cm. Therefore, from Equations (4.34) and (4.35) it becomes apparent that the conditions studied during this investigation fall well

within the range in which there is good agreement between the solutions of Batchelor, Poots and Stewart. Since the solution of Batchelor is by far the simplest of the three it is appropriate to investigate it further in the hopes of finding a suitable analysis for the experimental result of this investigation.

4.3. Modification of the Batchelor Solution

It will be shown below that the solution of Batchelor can be modified and extended so as to adequately describe the results of this investigation. As stated in Section 4.2.3. an approximate solution for the stream function is given by:

$$\Psi = \frac{2}{3} \text{Ra } A\ (X)\ Y^2\ (1-Y)^2 \qquad (4.36)$$

where $$A(X) = \left(1 + \left(\frac{H}{L}\right)^4\right)^{-1} X^2 \left(\frac{H}{L} - X\right)^2$$

Although the experimental values of Rayleigh lie within the range for which this approximation is useful, the experimental values of H/L are much less than unity. However, Batchelor states that it is unlikely that the convergence of the series would vary appreciably with the value of H/L. Furthermore, Carruthers[27] has suggested that Equation (4.36) is valid for flows in the neighbourhood of a vertical interface even for low values of the aspect ration H/L. Accordingly, the following the expression for the velocity parallel to the vertical wall is obtained:

$$u = \frac{\alpha}{L} \frac{\partial \Psi}{\partial Y} \tag{4.26}$$

$$= \frac{2\alpha Ra}{3\ L} A(X)\ (4Y^3 - 6Y^2 + 2Y) \tag{4.37}$$

If it is further assumed that Equation (4.36) is also valid for flow parallel to the much longer horizonal boundaries, then the longitudinal flow velocity as defined by;

$$v = -\frac{\alpha}{L} \frac{\partial \Psi}{\partial X} \tag{4.26}$$

is given by the expression:

$$v = -\frac{\alpha}{L} \frac{2}{3} Ra\ Y^2(1-Y)^2\left(1 + \left(\frac{H}{L}\right)^4\right)^{-1}\left(4X^3 - 6\frac{HX^2}{L} + 2\left(\frac{H}{L}\right)^2 X\right) \tag{4.38}$$

The Rayleigh number, as obtained by nondimensionlizing the governing equations, is:

$$Ra = \frac{g\beta L^3 \Delta T}{\alpha \nu}$$

The aspect ratios employed during this investigation were:

$$0.013 < \frac{H}{L} < 0.024$$

Therefore, $(H/L)^4 << 1$ and the $(1 + (H/L)^4)^{-1}$ term in Equation (4.38) reduces to unity where upon one obtains the following expression describing the dependence of longitudinal flow velocity on liquid metal

properties, melt geometry, temperature gradient between the hot and cold ends of the melt and position in the melt:

$$v = \frac{2\,g\beta L^3}{3\nu}\ \bar{G}_L\ Y^2(1-Y)^2\left(4X^3 - 6\,\frac{H}{L}\,X^2 + 2\,\left(\frac{H}{L}\right)^2 X\right) \qquad (4.39)$$

At first appearance, Equation (4.39) predicts a strong dependence of flow velocity on melt length L. However, when the last group of terms in Equation (4.39) is altered such that the variation of flow velocity with vertical position in the melt is described by a new variable XL/H*, the following appears:

$$4X^3 - 6\,\frac{H}{L}\,X^2 + 2\,\left(\frac{H}{L}\right)^2 X = \left(\frac{H}{L}\right)^3\left(4\left(\frac{XL}{H}\right)^3 - 6\,\left(\frac{XL}{H}\right)^2 + 2\left(\frac{XL}{H}\right)\right) \qquad (4.40)$$

Substitution of the right hand side of Equation (4.40) into Equation (4.39) yields the following expression:

$$v = \frac{2\,g\beta H^3}{3\nu}\,\bar{G}_L\,Y^2(1-Y)^2\left(4\left(\frac{XL}{H}\right)^3 - 6\,\left(\frac{XL}{H}\right)^2 + 2\,\frac{XL}{H}\right) \qquad (4.41)$$

The expression $4(XL/H)^3 - 6(XL/H)^2 + 2XL/H$ describes the variation of longitudinal flow velocity with vertical position in the melt. This velocity dependence on position is shown in Figure 77, and is consistent with the results of the autoradiography experiments which

---

* Since X = x/L (by Equations (4.26)) the new variable XL/H is x/H, that is, XL/H is the dimensionless distance in the vertical direction whose magnitude ranges from 0 to 1.

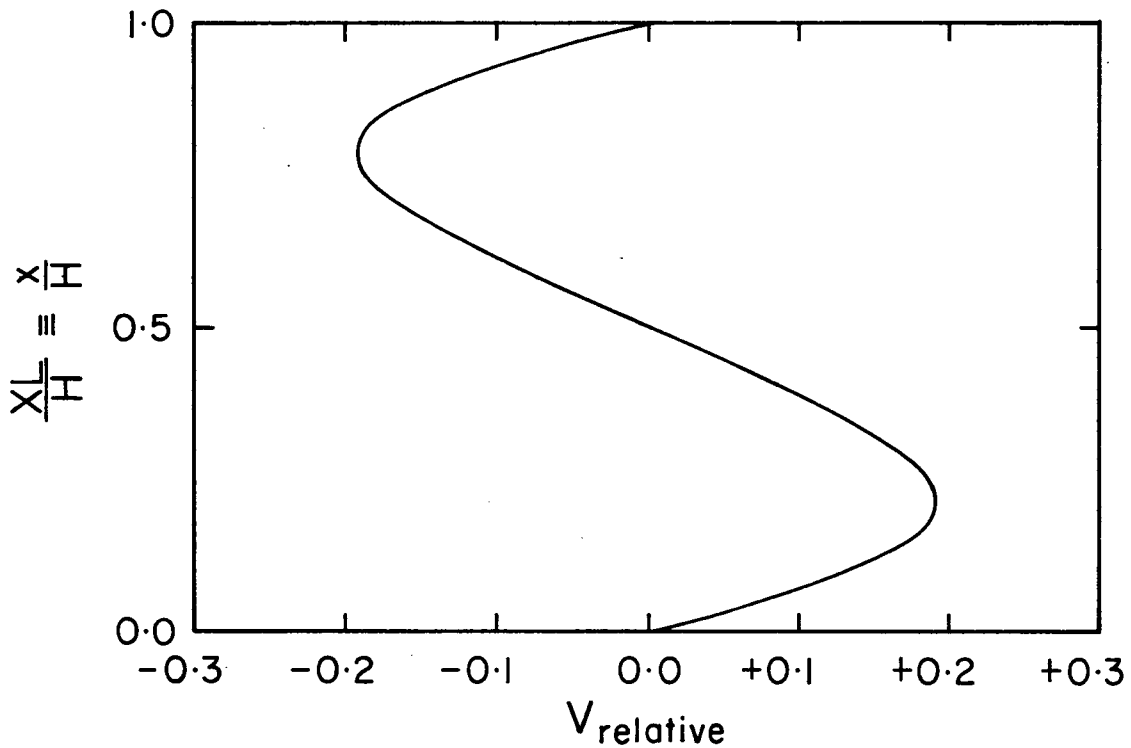

Figure 77. The variation of longitudinal flow velocity with vertical position in the melt.

show that the regions of more predominant flow exist close to the top and bottom of the melt.

The velocity measured by the tracer monitoring technique employed during this investigation would be expected to be very close to the maximum velocity in the boundary layers. The maximum velocity occurs at XL/H = 0.212 (and 0.788). Thus the expected maximum longitudinal flow velocity will be given by:

$$v = 0.128 \frac{g\beta H^3}{\nu} \overline{G}_L \quad Y^2(1-Y)^2 \qquad (4.42)$$

Equation (4.42) still contains the flow velocity dependence on position along the melt with v being 0 at the vertical walls and reaching a maximum at Y = 0.5 (half way along the melt). This maximum value of v is given by:

$$v = 0.008 \frac{g\beta H^3}{\nu} \overline{G}_L \qquad (4.43)$$

The integrated average value of v between Y = 0 and Y = 1 is given by:

$$v = 0.0043 \frac{g\beta H^3}{\nu} \overline{G}_L \qquad (4.44)$$

Comparison of the experimental results with the predictions of Equations (4.43) and (4.44) appear below.

4.4. Comparison of Theoretical Predictions and Experimental Results

4.4.1. Variation of Flow Velocity with Average Temperature Gradient Across the Melt

When the appropriate fluid parameters from Table 6 are inserted into Equations (4.43) and (4.44), the theoretically expected average and maximum flow velocities (at an average melt temperature of 400°C and melt height of 0.64 cm) are given by:

$$(v_m)_{400} = 0.113\ \bar{G}_L \qquad (4.43(b))$$

$$(v_a)_{400} = 0.061\ \bar{G}_L$$

The experimentally determined relation (from Figure 46);

$$v_{400} = 0.082\ \bar{G}_L$$

falls midway between the predicted average and maximum velocities of Equations (4.43(b)) and (4.44(b)).

4.4.2. Variation of Flow Velocity with Total Melt Length

Experimentally it has been determined that the flow velocity is independent of total melt length provided the average horizontal temperature gradient remains constant. As can be seen by inspection of Equations (4.43) and (4.44), this experimental observation is in agreement with the predictions of the modified Batchelor solution.

4.4.3. Variation of Flow Velocity with Average Melt Temperature

From Figure 43 the experimentally measured ratio of the

velocity at an average melt temperature of 300°C and 400°C is:

$$\frac{v_{300}}{v_{400}} = 0.78$$

Equations (4.43) and (4.44) predict that this ratio should be 0.84. Since Figure 43 was constructed with only three data points, and the overall experimental accuracy is believed to be ± 10% (or better),it is the opinion of this author that the theoretical and experimental values of flow velocity dependence on average melt temperature are in good agreement.

4.5. Summary

Although Batchelor's solution of free thermal convection in rectangular enclosures of high aspect ratio is not generally applied to low aspect ratio enclosures, the modified Batchelor solution appearing above does adequately describe the experimental results obtained in this investigation. There is very good agreement between this solution and the observed dependence of flow on total melt length and average melt temperature. Equations (4.43) and (4.44) both predict the observed linear dependence between flow velocity and the average horizontal temperature gradient across the melt. Furthermore, the magnitude of the predicted average and maximum velocity of longitudinal flow is in reasonably good agreement with the results of the present investigation.

Since the solutions of Batchelor and Stewart are in good agreement (over the range of Grashof and Rayleigh numbers employed

here), it is reasonable to expect that Stewart's more elaborate finite difference solution could have been used to analyse the results of this investigation. However, the solutions used by Cole and Utech clearly do not describe the flow in a long horizontal rod of liquid metal for the experimental conditions employed herein.

5 - CONCLUSIONS

A radioactive tracer technique has been developed to examine the nature of fluid flow in liquid tin contained in a long horizontal covered boat. Extensive tests have shown that the tracer introduction and monitoring techniques employed allow accurate and reproducible measurement of the flow velocities. Further experimentation has revealed the appearance of the flow patterns which occur in the melt. The most significant findings of this investigation are summarized below:

(1) An extremely small horizontal gradient, apparently any non-zero gradient, provides sufficient driving force for thermal convective flow.

(2) Laminar flow arising from thermal convection will not cause mass transfer through a region of zero horizontal temperature gradient.

(3) The flow velocities observed are the result of the presence of buoyancy forces created by a temperature gradient between the hot and cold ends of the melt. These velocities are not dependent on electromagnetic stirring effects.

(4) For the covered horizontal rod configuration investigated herein the flow velocity is linearly dependent on the average temperature gradient across the melt (and not on local horizontal temperature gradients).

(5) The flow velocity increases with increasing average melt temperature.

(6) Although the flow velocities measured were less than 1 cm/second, they are large relative to the slow grow rates commonly employed in unidirectional solidification experiments and, therefore, must be considered significant.

(7) The flow pattern occurring in the molten tin is a laminar unicellular longitudinal flow upon which is superimposed a transverse double cell flow. The transverse flow does not contribute significantly to the longitudinal flow velocity.

(8) The transverse flow observed would be expected to be a contributing factor to the preferential breakdown of solid-liquid interface morphology near the melt container.

(9) When the solution of Batchelor is extended and modified, there is good agreement between this solution and the results of the present investigation.

6 - SUGGESTIONS FOR FUTURE WORK

Employing the tracer introduction and monitoring techniques developed in this investigation, the experiments listed below could be performed in order to provide additional information on the nature of fluid flow in horizontal rods of liquid metal:

(1) Examination of the dependence of flow velocity on temperature gradient in uncovered melts.

(2) Examination of the dependence of flow velocity on melt depth.

(3) Examination of the variation of flow velocity with different cross sectional geometries.

(4) Examination of the effect on flow velocity of introducing a moving solid-liquid interface in both pure metal and alloy systems.

(5) A quantitative evaluation of the dependence of the effective distribution coefficient on flow velocity.

PART II - FLUID FLOW DURING SOLIDIFICATION - ITS EFFECT ON GRAIN STRUCTURE AND MACROSEGREGATION

1 - INTRODUCTION

1.1. Grain Structure

Fluid flow of residual liquid metal during ingot solidification is necessary (under normal conditions) if the columnar to equiaxed transition (CET) is to occur. The reduction of temperature gradients in the liquid ahead of the solid-liquid interface is hastened by increasing the convective mixing (free or forced). Since lowering of temperatures in the melt will allow nuclei (whatever their source be[31-34]) to survive and grow, increased fluid flow will promote an earlier CET. Grain structure manipulation can, therefore, be accomplished by controlling the liquid flow during solidification. Flow control may be accomplished in the following ways:

(1) Magnetic fields can be used to enhance or reduce fluid motion. Since metals are electrical conductors they are forced to move in the presence of a rotating magnetic field[35], or in a constant magnetic field if a d.c. current is passed through the liquid metal[36]. Reduction of convection occurs in a fixed magnetic field since there will be a retarding force to the motion of a conductor through the field[11,37,38].

(2) Motion of the mold during solidification can be used to control casting grain structure. The effect of steady-state mold rotation has been studied extensively by Cole and Bolling[39,40]. Wojciechowski and Chalmers[41], as well as Cole and Bolling, have examined the effect on grain structure of oscillating the mold during solidification.

Vertical reciprocation of semi-continuous D.C. cast aluminum ingots has also proved effective in producing finer grained ingots[42].

(3) The use of ultra-sonic energy to effect grain nucleation is another mode of grain structure control. Whether it should be classed as a form of mechanical mixing is still controversial[43,44].

1.2. Macrosegregation

Various forms of macrosegregation occur as a result of convection. Normal segregation has been discussed in Part I, Section 1. Back-flow along interdendritic channels (caused by volume changes on freezing), of normally segregated residual liquid, is generally accepted as the mechanism for inverse segregation[45].

Solute convection cutting across dendrites is believed to be responsible for 'A' type segregates in ingots and for the formation of 'freckles' in unidirectionally solidified castings. Support of this theory is provided by observation of solidification in ammonium chloride-water systems[46.47].

Suppression of convection (by magnetic fields) eliminates temperature fluctuations which would otherwise cause banding[37], and also changes the macrosegregation[11].

Until recently, differences in macrosegregation arising from the rotating and oscillating modes of ingot solidification had not been studied. The remainder of Part II will discuss the investigation by the author and fellow graduate student M.J. Stewart on macrossegregation arising from these various solidification techniques. The study will be presented here in the same form as it appeared in Metallurgical Transactions[48]. The thesis of M.J. Stewart[17] contains a similar section.

2 - MACROSEGREGATION IN CASTINGS ROTATED AND OSCILLATED DURING SOLIDIFICATION

2.1. Introduction

Castings which have a small equiaxed grain structure are considered to be more homogeneous and to have better mechanical properties than equivalent castings with a partially columnar structure. One way of controlling the grain structure is by mechanically mixing the residual liquid during solidification. This can be done by moving the mould. Constant rotation of a cylindrical mould, radially cooled, will suppress the columnar to equiaxed transition (CET); oscillation of the mould will promote an earlier CET; and a stationary mould will have a structure between the rotation and oscillation cases[39,40]. The control of grain structure by mechanical mixing of the liquid during casting may cause macrosegregation - - (a function of the kind and extent of liquid mixing). In addition, rotational forces might influence solute transport in the liquid if there is a large density difference between solute and solvent. If macrosegregation is enhanced by liquid mixing this could be detrimental to casting quality.

The purpose of the present investigation is to determine the extent of macrosegregation in stationary, rotated, and oscillated castings, and relate the results to the cast structure.

2.2. Experiment

The macrosegregation in the castings was determined by a radioactive tracer technique. The alloy used was Al-3 wt.% Ag made up of 99.99% Al and 99.8% Ag. The ingots were cylindrical, 3¼ inches in diameter and approximately 6 inches high. The casting apparatus used, Figure 78, enabled the casting of Al-Ag alloys to be made in stationary, rotating, or oscillating moulds. Melting was done in a graphite crucible in a resistance furnace. The alloy was superheated to approximately 800 °C and immediately prior to casting, a small amount of radioactive Ag^{110} was added into the melt. The castings were all poured at 750 °C (90 °C superheat) into stainless steel moulds, water cooled before and during casting. A graphite hot top was used to keep the heat transfer from the upper surface to a minimum. Three casting conditions were used: stationary mould, rotated mould at 126 rpm, and an oscillated mould. The oscillation was a rotation of 126 rmp with the direction of rotation being reversed every five seconds.

The casting microstructure was determined by sectioning and etching of the castings parallel and perpendicular to the cylindrical axis. Etching was done in a Modified Tucker etch (HCL, HNO_3, HF, and H_2O in a 2:2:1:15 ratio) and the etching products were washed off immediately with concentrated nitric acid.

To measure the macrosegregation in the ingot, the most expedient procedure, as commonly used, is to measure the solute concentration of cuttings taken at various points in the ingot by drilling. This is satisfactory if there is no microsegregation and no short range variations in the macrosegregation, which is rarely the case. To improve

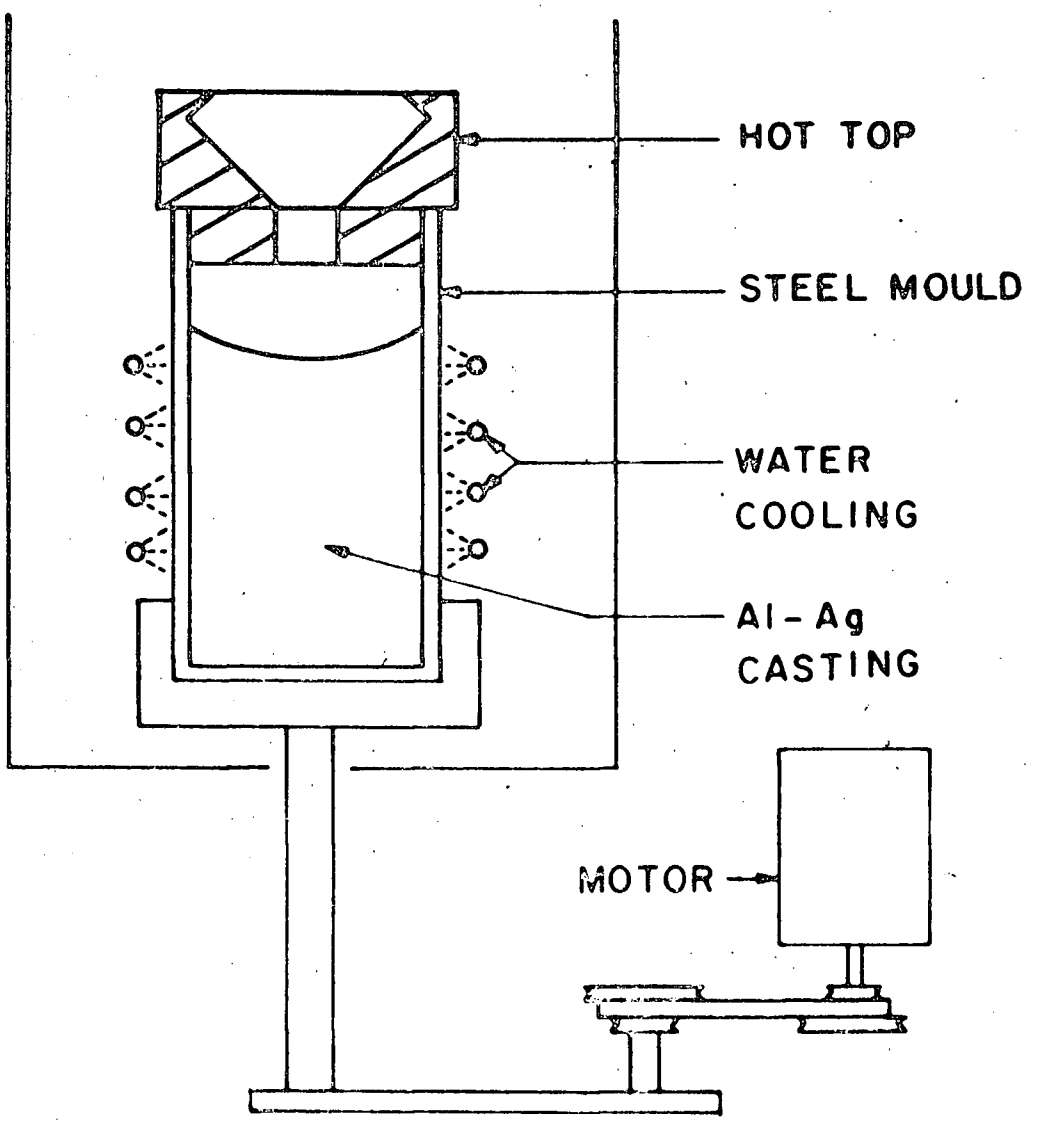

Figure 78. The experimental apparatus used for producing the stationary, rotated, and oscillated castings of Al - 3 wt. % Ag.

the averaging process, more drillings and analyses could be made, or alternatively a layer of the casting can be machined off and samples taken from this. Finally, the entire casting can be machined and the concentration of all the casting by sections can be measured. The time and effort involved increases very greatly from the first to final process listed above. Accordingly, all four procedures were used initially to determine their accuracy and reproducibility for the present castings. Four methods of sampling were employed to determine the degree of radial macrosegregation.

(a) Holes of 1/4 inch diameter were drilled through the casting in 1/4 inch steps in the radial direction. A fixed weight of solid turnings was packed into a standard container. The activity of the radioactive silver present in each sample was then measured with a scintillation well counter.

(b) Holes of 1/4 inch diameter were drilled as in method (a) except 1/8 inch steps were used. The analysis was the same as method (a).

(c) The castings were mounted in a lathe and 0.030 inch thick concentric cylinders one inch long were progressively removed. From each cut a random five gram sample was taken and the activity of the sample measured in a scintillation well counter under conditions of fixed geometry.

(d) The castings were machined as in (c) except the cut was 0.050 inches thick. All the material removed in each cut was dissolved in a concentrated solution of nitric acid

containing a small amount of mercury in solution. The solutions were then made up to either 250 or 500 ml. by adding water. A 10 ml. sample was taken from each solution and the activity of each sample measured.

In evaluating the results the concentration of silver is taken to be proportional to the measured activity. Ag^{110} is a strong gamma emitter and aluminum a weak absorber. As a result, small geometrical differences in samples counted in (a), (b) and (c) techniques should be negligible.

Autoradiography was used to show qualitatively the macrosegregation in the ingots. Since the energy of the radiation is high and the sample absorption is low the autoradiograph will represent the activity of a large distance into the ingot. Therefore to obtain reasonable resolution thin sections are required. Thin discs perpendicular to the cylindrical axis were prepared by machining and polishing the discs to a thickness of 0.020 inches.

2.3. Results

Vertical sections of castings which were stationary, rotating, and oscillating during solidification are shown in Figures 79(a), 79(b) and 79(c) respectively. The stationary casting has a small equiaxed region in the centre, the rotated casting has a columnar zone to the centre of the casting, and the oscillated casting has a large region, in agreement with previous observations. The equiaxed grains in the oscillated ingot are clearly shown to have grown dendritically in Figure 80, taken at higher magnification.

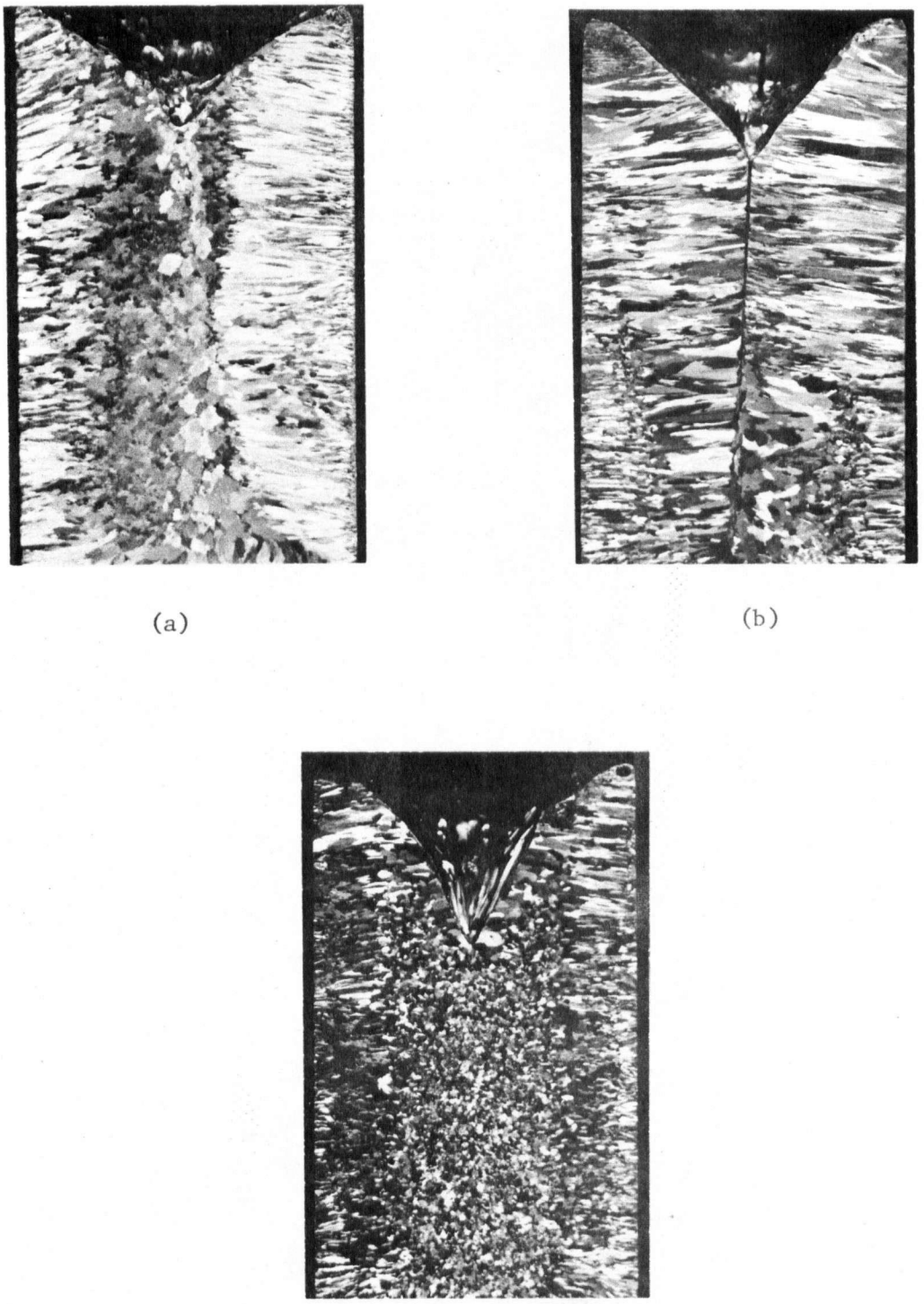

(a)

(b)

(c)

Figure 79. Representative ingots cast in (a) stationary, (b) rotating, and (c) oscillating moulds. x 2/3

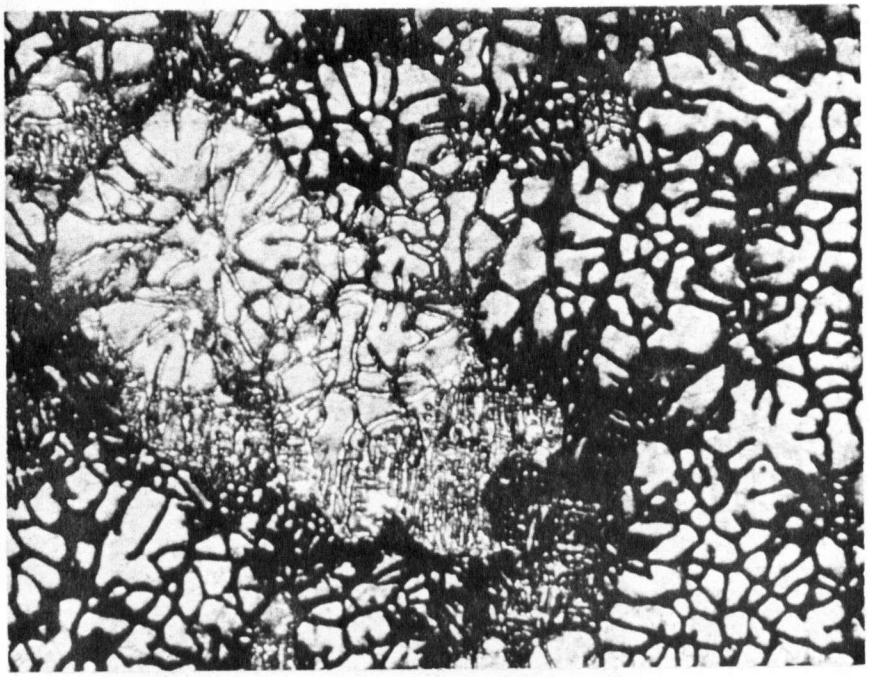

Figure 80. Equiaxed grains in the central region of the oscillated casting, magnification 40 times.

(a)

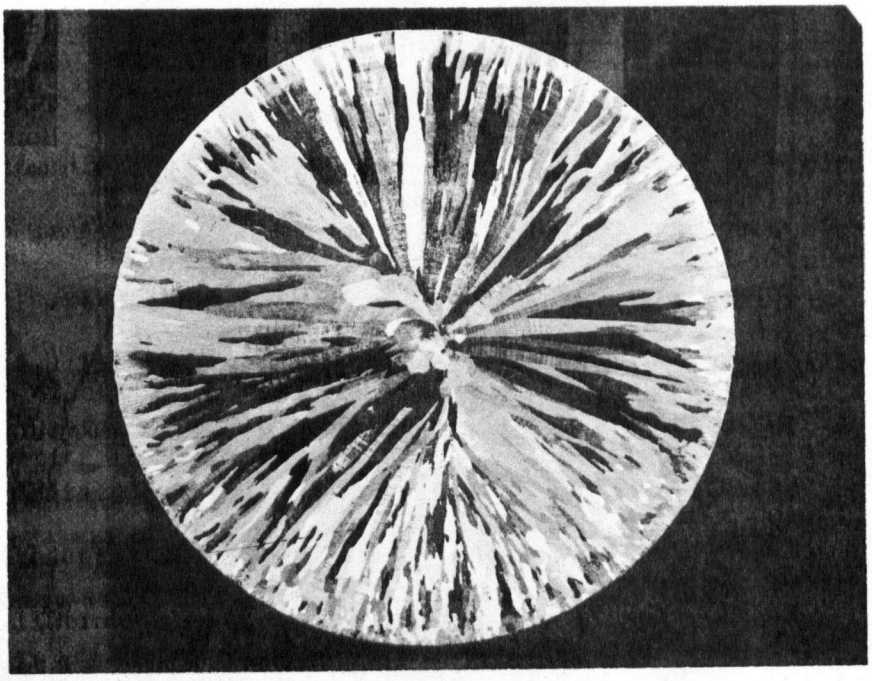

Figure 81. Representative ingot cast in a (a) stationary mould, actual size.

(b)

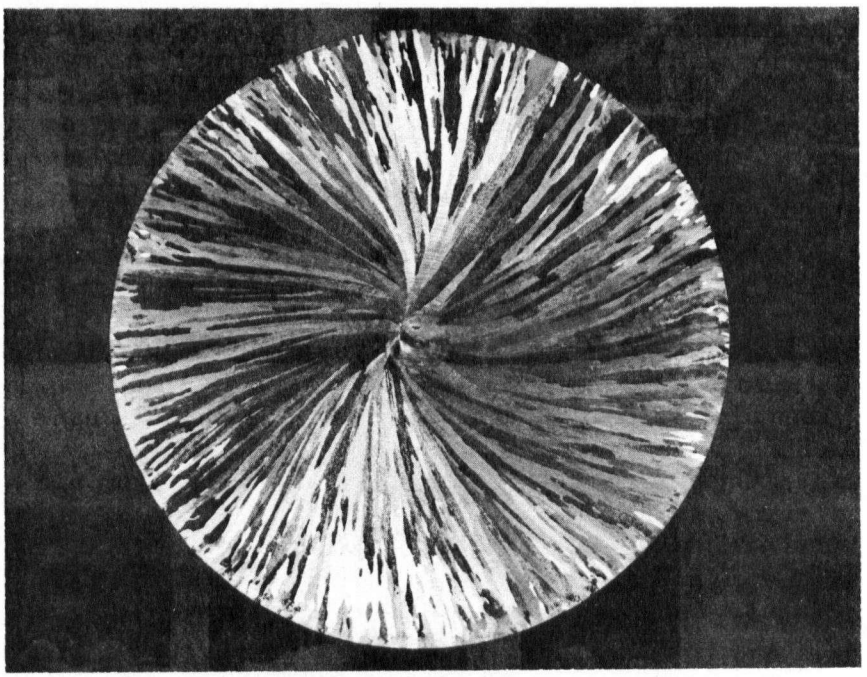

(c)

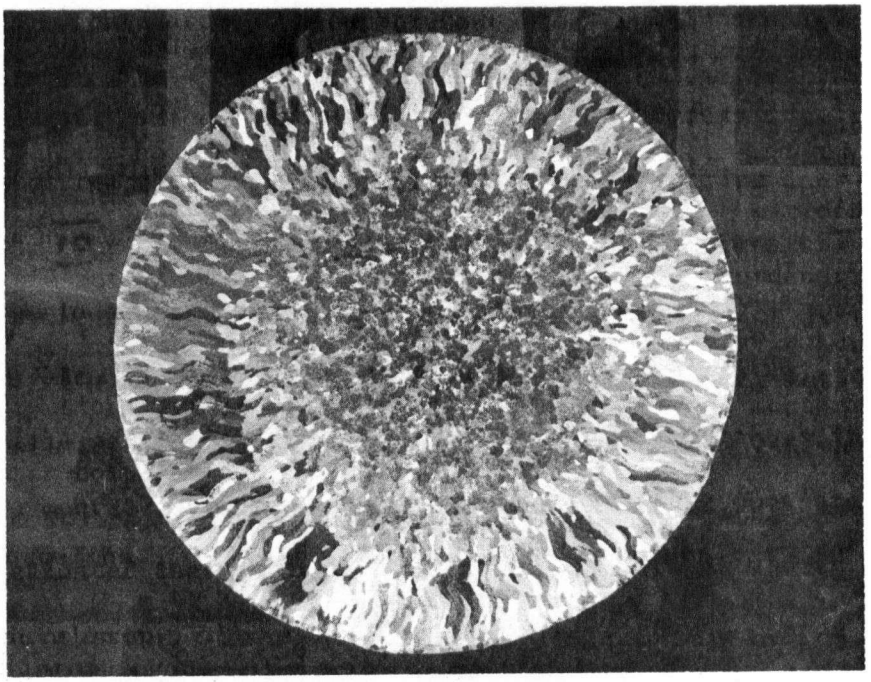

Figure 81. - Continued. Representative ingots cast in (b) rotating and (c) oscillating moulds, actual size.

The structures obtained on etched cross sections of the ingots (Figures 81(a), 81(b), and 81(c)) show the effect of the applied fluid motion on the columnar zone. In Figure 81(a) of the stationary cast ingot the columnar region is in a radial direction with all the grains growing perpendicular to the mould wall. The columnar region for the rotated ingot (Figure 81(b)) shows a spiral shape with the initial columnar grains growing non-perpendicular to the mould walls. These grains are growing towards the oncoming fluid in the liquid pool. In the oscillated ingot (Figure 81(c)) the direction of the columnar zone changes when the mould rotation is reversed so that they always grow into the flow. A similar observation has been made by Roth and Schippen[49]. In both the rotated and oscillated ingot there is a renucleation of the columnar grains to achieve the curved effects. There were no grains observed which curved or had a kink, indicating that the crystallographic growth orientation was always maintained.

The solute concentration of Ag in a stationary casting using the four sampling techniques described is shown in Figure 82. Comparing the four sets of points it is evident that the different techniques have various degrees of scatter associated with them. For the drilled holes with 1/4 inch steps (Figure 82(a)) the macrosegregation appears cyclic from the outer mould wall to the centreline. The experimental accuracy of the points plotted is such that they are a true representation of the concentration of the sample measured in the scintillation counter. Thus the scatter must be due to a change in the concentration along the drill hole. To test if this cyclic behaviour is genuine the 1/8 inch step hole method is shown in Figure 82(b).

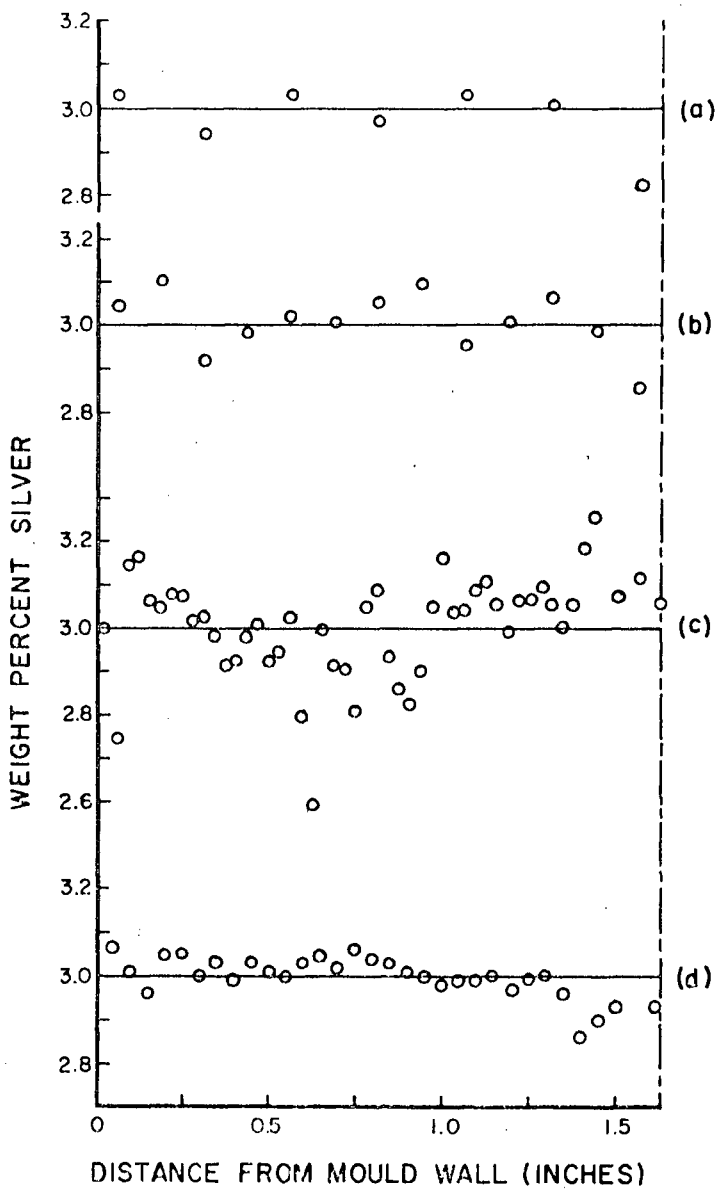

Figure 82. The radial silver distribution in a stationary casting; (a) 1/4 inch drill holes in 1/4 inch steps, (b) 1/4 inch drill holes in 1/8 inch steps, (c) 0.030 inch lathe turnings, (d) 0.050 inch lathe turnings dissolved in acid.

Again the points show a cyclic behaviour, but the cycle period is different for the two cases. Thus microsegregation along the drill hole must be the cause of the cycling. The plot for the solid lathe turnings (Figure 82(c))shows an extensive scatter between points. This large scatter could be caused by the microsegregation, by the selection of the material taken from the whole sample, or by not having a sufficiently constant sample geometry due to the nature of the lathe turnings. The final method of dissolving the turnings of the entire sample gave the results of Figure 82(d), which shows much less scatter than the other methods. In this case the counting geometry is not a problem as the liquid is contained in standard tube and the liquid counted is a true average of the sample composition. This method gave reproducible results and was used for all the subsequent macrosegregation measurements.

The radial macrosegregation in the three types of ingots is shown in Figure 83. Three sets of data were obtained for the radial macrosegregation, one from the central region of one group of castings, and the other two from near the top and bottom of a second similar group of castings. All the results for a particular type of casting were very similar.

The silver concentration in the stationary and rotated ingots, shown in Figures 83(a) and 83(b), is essentially constant indicating little macrosegregation, except for a small drop in concentration at the centreline of the casting. There is no effect on the macrosegregation due to the difference in density of the silver and aluminum in the rotated casting. In the oscillated case macrosegregation is present, with an initial rise in the silver concentration up to a peak. The concentration then decreases to the centreline of the casting

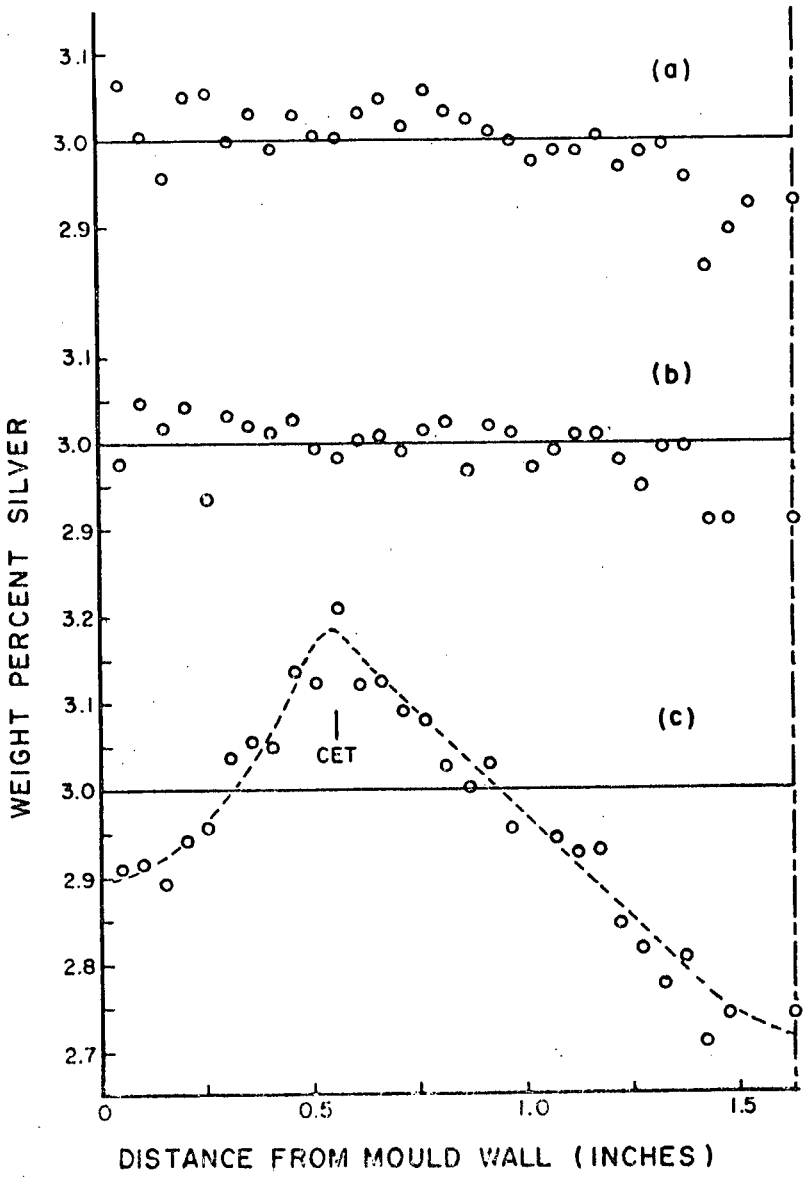

Figure 83. The radial silver distribution in (a) stationary, (b) rotated, and (c) oscillated ingots using method (d) of Figure 82.

to a value over 0.25% Ag below the C_o value. The position of the CET is shown on the curve; this position corresponds to the CET in Figure 83(c). The results show that the CET corresponds to the maximum silver concentration.

An autoradiograph of the oscillated ingot (Figure 84) shows the macrosegregation qualitatively. The lighter areas towards the centre of the ingot represent silver depleted areas which correspond to the quantitative measurements (Figure 83(c)). Due to this mottled effect in the silver distribution it can easily be seen that the drill hole methods of analysis could give spurious results, as can any analysis that does not include the total radial sample.

2.4. Discussion

The cast structure associated with stationary, rotated, and oscillated castings are similar to those reported by Cole and Bolling[39] and others and will not be discussed here. Two points will be considered.

(1) The relation of the observed macrosegregation with the cast structure.

(2) The shape of the solute curves.

Conditions for the CET are met much earlier in the oscillated casting than in either the rotated or stationary casting. This is believed due to the lowering of the temperature gradient in the molten region (oscillation causes extensive mixing) thus allowing "nuclei", produced by large shear forces at the interface, to survive and grow.

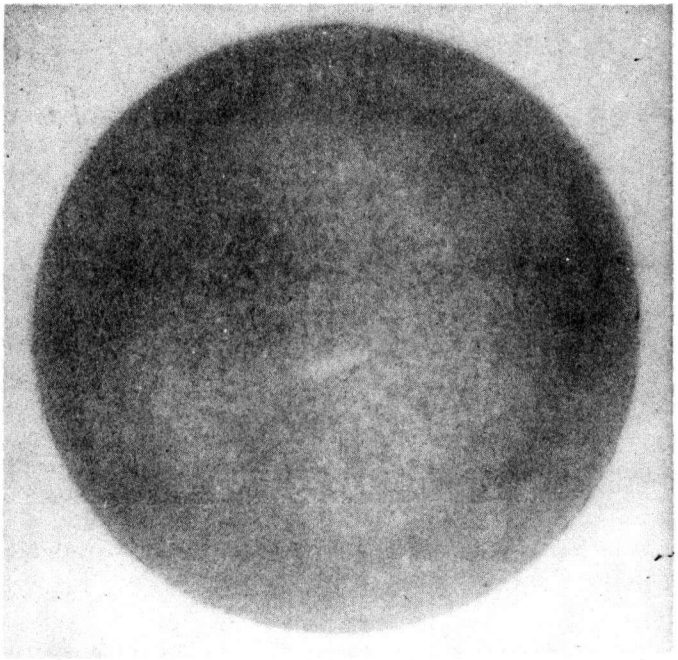

Figure 84. An autoradiograph of the cross-section of the oscillated ingot showing the silver distribution in the casting. Actual size.

During rotation reversal these large shear forces will cause remelting and/or breaking off of dendrite fragments[34,41] which can act as "nuclei". These can easily be swept into the central region of the liquid pool by the violent turbulent flow occurring as a result of oscillation. Observation of this flow in a rheoscopic liquid shows the existence of a turbulent wave generated at the interface and rapidly moving to the centre. If the mould is rotated at a constant speed the temperature gradient will remain high[39] and no shear forces will be present at the interface. Therefore, no nuclei will be produced and the CET will be suppressed, as observed. For the stationary ingot natural convection will yield low shear forces at the interface and the temperature gradient will be of some intermediate value.

The lack of macrosegregation in the rotated and stationary ingots can be attributed to the lack of significant fluid flow in the interdendritic region. Without fluid flow there will be no net solute flux from the interface region, and therefore, no macrosegregation.

For the oscillated casting high shear forces in the vicinity of the solid-liquid interface will produce more extensive interdendritic flow. This flow will sweep solute rich liquid out of the mushy zone. The solute distribution near the mould wall will then tend to conform to the equation for complete mixing:

$$C_s = kC_o(1-g)^{k-1}$$

where C_s is the solid solute composition, k the distribution coefficient, C_o the average initial solute composition and g the fraction solidified. When the rotation is reversed a turbulent wave is produced which will

transport this solute towards the centre of the solidifying ingot.

During columnar growth the solute distribution will therefore be as shown in Figure 85(a). When the CET is imminent the distribution will be that shown in Figure 85(b). The initial part of the curve corresponds to a complete mixing situation up to the peak. Beyond the peak the composition gradually decreases towards the centre due to the incomplete mixing of the solute rich liquid generated at the interface. Concurrent with this solute movement is the reduction of the temperature gradient which, until the CET occurs, does not allow survival of nuclei. (At every rotation reversal high shear forces and temperature fluctuations, due to turbulence, will produce a large number of dendrite fragments). When the temperature gradient is sufficiently low these fragments will be able to survive and grow and be swept by the turbulent wave throughout the remaining liquid. Since these fragments are of composition less than C_o the overall composition in this region will be reduced as shown in Figure 85(c). Also, due to the lowering of the temperature gradient the mushy zone will be increased in length. The mass and composition of dendrite fragments necessary to cause this reduction in composition (Figure 85(b) - Figure 85(c)) is calculated in the Appendix, Section 2.6. The solute distribution profile of Figure 85(c) will be that of an ingot oscillated during solidification. The macrosegregation predicted above was observed in the oscillated ingot, Figure 83(c).

2.5. Conclusion

The present investigation has shown that no significant

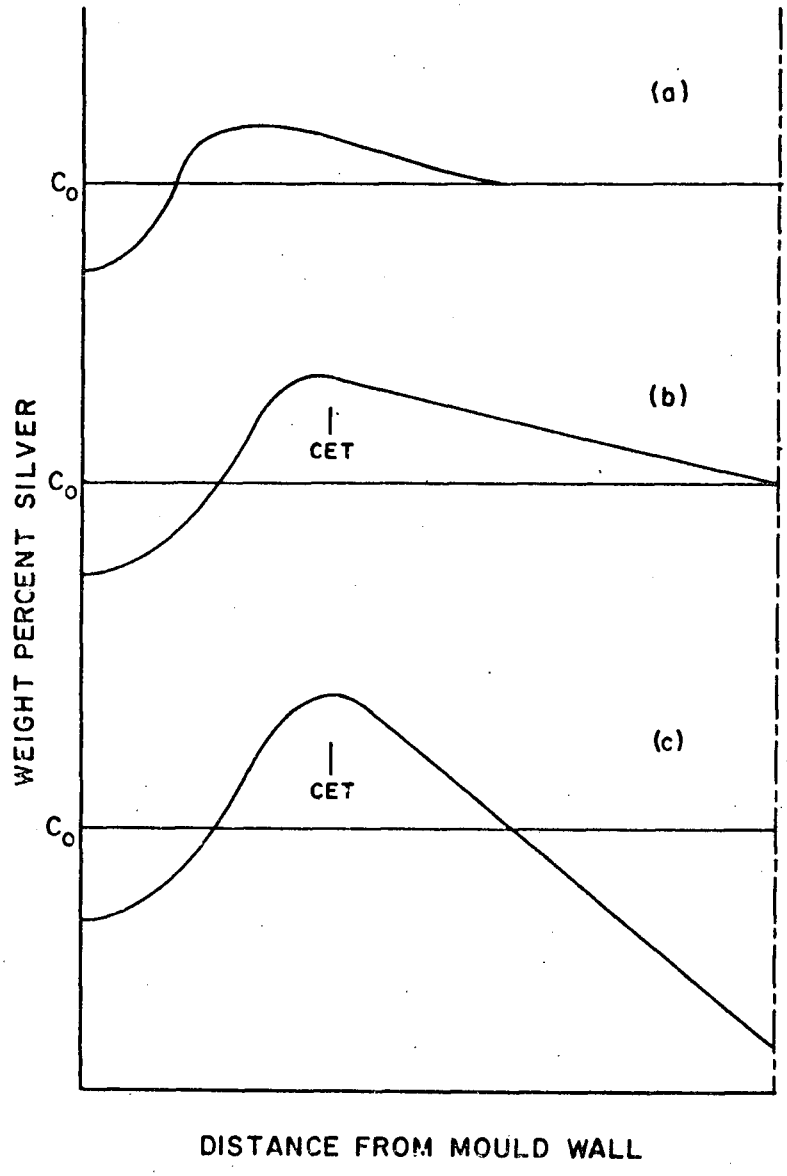

Figure 85. The development of the radial macrosegregation in an oscillated ingot, (a) prior to the time of the CET, (b) at the time of the CET, and (c) the final silver distribution in the casting.

macrosegregation accompanies solidification in stationary or rotated moulds for the system examined. This implies that the large density difference between the solvent (Al) and solute (Ag) has no effect on the radial solute distribution. However, appreciable macrosegregation is associated with the oscillation mode of solidification. The initial rise is attributed to solute mixing in the liquid interfacial region due tothe turbulent flow. The maximum concentration is associated with the columnar to equiaxed transition. The solute depletion in the centre of the casting is caused by small grains of low solute concentration being swept, by the turbulent waves, from the mushy zone to the ingot centre.

2.6. Appendix to Section 2

The model proposed for macrosegregation in the oscillated ingot assumes sufficient dendrite fragments are swept into the central liquid zone, to give the change in the distribution between Figure 85(b) and 85(c). The following analysis is an approximate calculation for the mass of fragments which is required.

Assume V_E is the volume of the central liquid region just prior to the CET. The average composition in this volume after total solidification assuming a linear distribution profile in this region and C_o = 3.0 wt % Ag, is given by:

$$\overline{C} = \frac{\int_o^R 2\pi\ r\ C(r)dr}{\int_o^R 2\pi\ rdr}$$

where C(r) is composition as a function of radius and R is radius of CET. From Figure 83(c), $C(r) = \frac{.48}{R}\ r + 2.70$, therefore $\overline{C}$ = 3.02 wt % Ag.

Comparing Figures 85(b) and 85(c) an estimate of the average composition in V_E just prior to the CET can be made ($C(r) = \frac{.15}{R} r + 3.00$) and is equal to 3.10 wt % Ag.

Assuming the composition of dendrite fragments swept into the central region is $\alpha k_o C_o$, where α is a factor to account for the increase in solute concentration in the dendrite branches as solidification progresses, assumed to be 1.5, k_o is 0.25 for the alloy under consideration. Therefore:

$$\alpha k_o C_o = (1.5)(0.25)(3.0)$$
$$= 1.12 \text{ wt \% Ag}$$

Let v be the volume of dendrite fragments swept into the central molten region (V_E) at the time of the CET. The resulting change in the average concentration in V_E can then be used to solve for v.

Therefore: $3.10\ V_E + 1.12\ v = 3.02\ (V_E + v)$

Therefore: $v = 0.04\ V_E$

This calculation shows that a small amount of solid fragments is required relative to the total liquid volume to cause the decrease in concentration observed. The large mushy zone, due to the low thermal gradient, and the large interdendritic flow, due to the turbulence produced during the rotation reversal, should result in this small volume of fragments being made available to cause the observed effect.

BIBLIOGRAPHY

1. W.G. Pfann, Zone Melting, John Wiley & Sons, New York, 1958.
2. B. Chalmers,Principles of Solidification, John Wiley & Sons, New York, 1964.
3. C. Wagner, Trans. AIME, 1954, 200, p.154.
4. F. Weinberg, TMS-AIME, 1963, 227, p.231.
5. G.S. Cole and W.C. Winegard, J. Inst. Met. 1965, 7, p.153.
6. K.A. Jackson and B. Chalmers, Private communication in Reference 5.
7. G.F. Bolling and J.R. Kramer, ibid.
8. A. Müller and M. Wiehelm, Z. Naturf., 1964, A, 19, p.254.
9. H.P. Utech, Sc.D. Thesis, Dept. of Metallurgy, M.I.T.
10. E. Eckert and R.M. Drake, Heat and Mass Transfer, McGraw-Hill, 1959.
11. H.P. Utech, W.S. Brower and J.G. Early, "Crystal Growth", Proceedings of an International Conference on Crystal Growth, Boston, 20-24, June, 1966, p.201.
12. D.T.J. Hurle, Phil. Mag., 1966, 13, #122, p.305.
13. K.G. Davis and P. Fryzuk, TMS-AIME, 1965, 233, p.1796.
14. J.R. Carruthers and W.C. Winegard, Can. Met. Quart. 6, p.223.
15. J.R. Carruthers, Ph.D. Thesis, Dept. of Metallurgy,University of Toronto, 1966.
16. M.J. Stewart and F. Weinberg (to be published).
17. M.J. Stewart, Ph.D. Thesis, Dept. of Metallurgy, University of British Columbia, 1970.
18. G.S. Cole, Ford Motor Co. Report, "Transport Process and Fluid Flow in Solidification", December 9, 1969.
19. D.R. Oliver, Chem. Eng. Sc., 1962, 17, p.335.
20. C.S. Cole, Ph.D. Thesis, Dept. of Metallurgy, University of Toronto, 1963.
21. H.J. Merks, Appl. Sci. Research, 1958, [A], Vol.8, p.100.

22. G.S. Cole, TMS-AIME, 1967, Vol.239, p.1287.

23. G.K. Batchelor, Quart. Appl. Math., 12, 1954, p.209.

24. G. Poots, Quart. Mech. Appl. Math., 11, 1958, p.257.

25. J. O. Wilkes, Ph.D. Thesis, University of Michigan, Ann Arbour, Michigan, 1963.

26. M.R. Samuels and W. Churchill, A.I.Ch.E.J., 13, 1967, p.77.

27. J.R. Carruthers, J. Crystal Growth, 2, 1968, p 1.

28. W.R. Martini and S.W. Churchill, A.I.Ch.E.J., 6, 1960, p.251.

29. S. Weinbaum, J. Fluid Mech. 18, 1964, p.809.

30. J.W. Elder. J. Fluid Mech, 23, part 1, p.77.

31. W.C. Winegard and B. Chalmers, TASM, 1954, 216, p.1214.

32. B. Chalmers, J. Australian Inst. Metals, 1963, 8, p.255.

33. R.T. Southin, TMS-AIME, 1967, 239, p.220.

34. K.A. Jackson, J.D. Hunt, D.E. Uhlman and T.P. Seward III, TMS-AIME, 1966, 236, p.149.

35. W.C. Johnson and W.A. Tiller, Westinghouse Research Report, "Fluid Flow Control During Solidification Part I", December 15, 1959.

36. G.S. Cole and G.F. Bolling, TMS-AIME, 1966, 236, p.1366.

37. H.P. Utech and M.C. Flemings, "Crystal Growth" Proceedings of an International Conference on Crystal Growth, Boston, 20-24, June, 1966, p.659.

38. D.R. Uhlman, T.P. Seward III and B. Chalmers, TMS-AIME, 1966, 236, p.527.

39. G.S. Cole and G.F. Bolling, Ford Motor Co. report "Enforced Fluid Motion and the Control of Grain Structures in Metal Casting", March 15, 1967.

40. G.S. Cole and G.F. Bolling, Ford Motor Co. report, "Manipulation of Structure and Properties", October 30, 1969.

41. S. Wojciechowski and B. Chalmers, TMS-AIME, 1968, 242, p.690.

42. N. Bryson, Alcan Research, Kingston Ont., private discussion.

43. R.T. Southin, J. Inst. Met., 1966, 94, p.401.

44. D.H. Lane, J.W. Cunningham and W.A. Tiller, TMS-AIME, 1960, 218, p.985.

45. J.S. Kirkaldy and W.V. Youdelis, TMS-AIME, 1958, 212, p.833.

46. R.J. MacDonald and J.D. Hunt, TMS-AIME, 1969, 245, p.1993.

47. S.M. Copley, A.F. Giamei, S.M. Johnson and M.F. Hornbecker, Met. Trans., 1970, 1, p.2193.

48. M.J. Stewart, L.C. MacAulay and F. Weinberg, Met. Trans., January 1971.

49. W. Rother and M. Schippen, Z. Metallk, 47, 1956, p.78.

50. J. Kohl, R.D. Zentner, and H.R. Lukens, Radioisotope Applications Eng. D. Van Nostrand Company, Princeton, N.J., 1961.

51. H. Thresh, Draft Manuscript of"The Viscosity of Liquid Tin, Lead and Tin-Lead Alloys", Submitted to TMS-AIME, Feb. 1969.

52. R.N. Lyon, Liquid Metals Handbook, The Committee on the Basic Properties of Liquid Metals, Office of Naval Research, Dept. of the Navy, 1954.

53. H.R. Thresh, A.F. Crawley and D.W.G. White, TSM-AIME, 1968, 242, p.819.